Assessing the impacts of ocean acidification, global warming and terrestrial runoff on the cross-shelf variability of coral calcification in the central Great Barrier Reef

Juan Pablo D'Olivo Cordero

A thesis submitted for the degree of Doctor of Philosophy
The Australian National University
August 2013

Declaration

The work presented in this thesis was carried out while I was a full-time student at the Research School of Earth Sciences, at the Australian National University. Except where mentioned in the text the research described is my own. No part of this thesis has been submitted to any other university or similar institution.

Juan Pablo D'Olivo Cordero

Acknowledgments

This work would have not been completed without the help of many others.

Foremost I would like to express my gratitude to my supervisor Malcolm McCulloch who gave me the opportunity to undertake this research, and whose patience, motivation, enthusiasm, and immense knowledge have been invaluable to me. I am equally thankful to my co-supervisor Steve Eggins whose dedication and enthusiasm are gratefully appreciated. His stimulating suggestions and insightful comments truly helped me enrich this work.

Graham Mortimer and Les Kinsley provided invaluable technical support. Graham played a key role in the development of the methodology for PTIMS B isotopes analysis as well as other laboratory techniques, and always had the time and patience for all my questions and requests. Les kindly provided the guidelines and technical assistance for solution ICP-MS, LA-ICP-MS and TIMS analysis, always solving every eventuality. My sincere thanks also go to Chantal Alibert for showing a complete selfless interest in my project and engaging in very stimulating discussions. Julie Trotter was behind the logistics of the 2009 coral sampling fieldwork and kindly provided the equation for seawater *p*H estimates from *Porites* corals $\delta^{11}B$ data.

I had the pleasure to work alongside fellow PhD student Junk-Ok Kang, having almost parallel projects was truly helpful, continuously providing mutual advice, and sharing ideas (and doubts). Jung-Ok also developed the method used to measure coral density. Jennie Mallela was of great help in many ways and made an excellent companion and collaborator during the collection of water samples in February 2009 and coral samples in July 2009. Susan Alford who kindly took the time to review and correct my thesis, her comments greatly improved this manuscript. Benjamin Walther collaborated in the production of LA-ICP-MS data. Martin Wille helped with the boron concentration measurements of water samples and was always willing to give a hand. My thanks also go to the entire administrative assistant staff especially Robyn Petch and Susanne Hutchinson for making everything run smoothly; your work behind curtains does not go unnoticed. Outside RSES, I would like to thank Michael Kindsford and Mark O'Callaghan (JCU) who have continuously collaborated collecting coral samples from the inner-shelf reefs. Stephen Lewis (JCU) was directly involved in the collection of plume water samples during the floods of 2007 and 2009, and provided salinity and Ba data for these samples.

My friend Heidi Minter, who more than a close friend became my adoptive family in Australia. My housemates and good friends Pedro, Erik and Robert. My officemates Andrea, Kelly, Aimée, Rebecca and Hector whom suffered from my mess and randomness with no complaints! Not forgetting the fantastic friends and fellow PhD. students at RSES Seann, Cassian, Julie, Luna, Magda, Rogério, Clemens, Sasha, Irina (and of course Alisa) amongst so many others. Finally to the great football family at ANU, having a run provided a much needed exercise and distraction.

This thesis is dedicated to my family:
To my dad, Juan Carlos, for being a constant source of inspiration and support. To my mom Ana Silvia, for always believing in me and encouraging me to pursuit more. Thanks to both for raising me with a love of science, I could not have asked for better role models. To my brother Guillermo, it is you whom I have missed the most during all

these years. To Margarita thanks for being by my side, supporting me through all these years, especially during the tough times.

And most especially to my little angel Juan Sebastian, thanks for lighting up my life (and highlighting all my papers).

This study was supported by funding from the Australian National University, the Research School of Earth Science and the ARC Centre of Excellence in Coral Reef Studies in funding awarded to Professor McCulloch. The Secretaria de Educación Publica (SEP) provided a complementary scholarship during the final stage of my studies.

Contents

List of Figures

List of Tables

Abstract

Ocean acidification and thermal stress due to anthropogenic greenhouse gas emissions present significant, potentially interacting, threats to the future of coral reefs. Coastal reef environments, as in the case of the Great Barrier Reef (GBR), can also be exposed to terrestrial stressors. This thesis evaluates the combined effects of ocean acidification, rising temperatures and river inputs on the calcification of *Porites* corals along a transect across-shelf the central GBR, north of Townsville. Calcification rates were obtained for 41 long-lived *Porites* corals from 7 reefs, in an inshore to offshore transect across the central GBR. The boron isotope composition ($\delta^{11}B$) of selected cores was used to reconstruct annual and sub-annual changes in seawater *p*H in inner-shelf and mid-shelf environments. These unique seawater *p*H records are integrated with sea-surface temperature, river discharge and rainfall records to assess the nature and cause of seasonal, interannual, decadal and long-term (~50 years) trends in coral calcification.

Significant across-shelf differences in the temporal variability and long-term evolution of coral calcification are documented and can be related to local and global-scale changes in environmental conditions and water quality. Corals in the mid-shelf and outer-reef regions of the GBR exhibit an increase in calcification of 10.9±1.1% (±1 S.E.) and 11.1±3.9% respectively since ~1950 which are associated with the rise in sea-surface temperatures. However, calcification rates of mid-shelf corals show a decline of 3.3±0.9% over the recent period (1990-2008). This may indicate that a thermal optimum for calcification has been reached. Calcification rates in inner-shelf reefs over 1930-2008 display a long term trend of decreasing calcification of 4.6±1.3%. The interannual-decadal component of variation is modulated by wet and dry periods, particularly during the last ~40 years. The negative effects of bleaching on coral growth are evident in inshore reefs, and are particularly strong during 1998, with a significant recovery occurring after 3 years. This translates to constant calcification rates of 1.1±2.0% for the inner-shelf reefs over 1990-2008. These results highlight the need to consider regional differences in environmental factors when assessing and predicting changes in the GBR.

Sub-annual and annual variation in the $\delta^{11}B$ of inner-shelf corals record seasonal and interannual seawater *p*H changes of up to 0.5 *p*H units. This variability is overlain on a long-term decrease of 0.02 *p*H units per decade, consistent with estimates of surface seawater acidification due to rising atmosphere CO_2 levels. Sub-annual low $\delta^{11}B$ (*p*H)

values occur in summer and partly reflect the effects of higher temperatures and increased calcification (a source of CO_2). Higher $\delta^{11}B$ (*p*H) values are observed in wet years when nutrients supplied by river run-off promote extensive phytoplankton blooms that take up CO_2 and increase seawater *p*H. Decreased calcification of inner-shelf corals during large flood events, despite higher *p*H conditions, may reflect increased shading, turbidity, sedimentation and/or competition for carbon. The complex interactions between processes that can affect coral calcification, particularly in coastal zones, need to be considered when predicting the future of coral reefs in warmer and more acidic oceans.

1. General introduction, project overview and literature review

1.1. General introduction

Coral reefs are unique and diverse marine ecosystems that are built on the calcium carbonate skeletons and cement secreted by corals, calcareous algae and other reef-dwellers (Kleypas et al. 2001; Buddemeier et al. 2004). Coral reefs provide nursery habitat, shelter and food for many organisms as well as contribute to the efficient recycling of nutrients (Buddemeier et al. 2004; Lough 2008b). Coral reefs are also a source of biochemical compounds and construction materials and provide important services to human society; including fisheries, tourist industries and coastal habitations (Hoegh-Guldberg et al. 2007). Global warming due to rising greenhouse gases and the closely linked effect of ocean acidification, as well as overexploitation by anthropogenic activities (overfishing, increased nutrient and sediment loading, pollution, direct destruction, and habitat modification), are threatening the future of coral reefs (Done 1999; Buddemeier et al. 2004; Hoegh-Guldberg et al. 2007; Lough 2008b). It has been predicted that under current scenarios coral reefs will undergo a phase shift towards seaweed dominated ecosystems, reduced biodiversity and accretion processes will fail to outcompete erosion (Hoegh-Guldberg et al. 2007; Lough 2008b; Hughes et al. 2010; Andersson and Gledhill 2013). In the Great Barrier Reef (GBR) coral reefs have grown adjacent to the continental land mass where they are affected by terrestrial runoff (Furnas 2003), particularly inner-shelf reefs. Agricultural and urban development have modified river catchments and resulted in increased nutrient, pesticide and sediment fluxes to the GBR (McCulloch et al. 2003; Brodie et al. 2010a). In fact terrestrial pollution and its link to outbreak of crown of thorns starfish together with fishing and climate change are considered the main stressors to the GBR (see Brodie and Waterhouse 2012). These localized changes overlay the global scale changes due to ocean warming and acidification. Predicting the future of coral reefs in the GBR and elsewhere requires knowledge of the interactions between these global and local changes. The synergistic effect of multiple stressors could exacerbate the effect of a single stressor and produce threshold responses (Knowlton 2001; Manzello 2010). For example the reduction in aragonite saturation state is feared will reduce the calcification rates in corals which in

turn could increase their vulnerability to storm damage (Done 1999). The increase in frequency of storms and other extreme events, like coral bleaching, are believed to in turn reduce calcification rates and cause mass mortality leading coral communities to a degraded state (Done 1999; Baker et al. 2008).

Scleractinian corals record changes in calcification rates and past environmental conditions in the form of growth bands and geochemical proxies that are incorporated into their carbonate skeleton. The information of growth bands provides important information on coral calcification and its relationship to environmental parameters (Lough 2008a; Lough and Cooper 2011). The geochemical proxies have been extensively used as tracers for sea surface temperature (SST) and salinity changes in the ocean (see reviews by Cohen and McConnaughey 2003; Corrège 2006a). One relatively novel proxy is $\delta^{11}B$ which has been used to reconstruct seawater *p*H (Pelejero et al. 2005; Wei et al. 2009). The combined information from growth parameters and the $\delta^{11}B$ proxy obtained from *Porites* corals in the central GBR will be explored further in this study. This information not only extends our knowledge of past environmental variability, but can also be used to develop models for future predictions of the sustainability of coral reef systems.

1.2. Project scope and aims

The primary goal of this study was to contribute to the understanding of how coral growth has responded to the combined effects of increased temperatures, ocean acidification and decrease in water quality on the central GBR during the last ~80 years. This is divided into two subordinated goals: (1) to test if the temporal changes in coral growth of *Porites* coral colonies are spatially consistent across an inner-shelf to outer-shelf transect in the central GBR. This transect represents a transition from a sheltered, more turbid, and terrestrial-influenced environment (inner-shelf) to more exposed, less turbid, oceanic waters at the edge of the continental shelf (outer shelf; Lough and Barnes 2000). (2) Apply the $\delta^{11}B$ paleo-proxy to *Porites* coral colonies from inshore and mid-shelf environments to reconstruct seawater *p*H. Particularly looking at how the *p*H is affected in the inner-shelf environment that during flood events receives the terrestrial influx of fresh water, sediments and nutrients. The obtained calcification data and reconstructed seawater *p*H

were compared to assess how these two parameters relate to each other in the inner-shelf and mid-shelf reefs of the central GBR.

This thesis is organized as follows:

- Chapter 1 provides a summary of the current state of the literature on ocean acidification and the use of corals as a source of environmental information from calcification rates and the $\delta^{11}B$ proxy.
- Chapter 2 includes a description of the study area for the central GBR and collection of coral samples. A description of the instrumental rainfall, river run-off and temperature data is also included.
- Chapter 3 includes LA-ICP-MS data for the well-known environmental proxies for temperature and river discharge (e.g. Sr/Ca, U/Ca, Ba/Ca) applied to inner-shelf coral samples. These results are compared to previously reported data. A specific objective here was to updated previously reported Ba/Ca data for the inner-shelf area. Differences between records indicate possible local differences (e.g. island mass effects) or vital effects.
- In Chapter 4 temporal changes in coral growth parameters annual extension, density and calcification rates are described of 41 coral cores for the last ~80 years. The data is compared in relation to cross-shelf environmental variability and put into context of previous studies.
- Chapter 5 presents a reconstruction and interpretation of changes in surface seaw*a*ter *p*H during the last ~50 years in the central GBR based on the $\delta^{11}B$ paleoproxy measured in 3 coral core records. A model explaining the reconstructed changes in seaw*a*ter *p*H and coral calcification in relation to environmental and biological process is postulated.

1.3. Literature review: Coral calcification and ocean acidification

The future of corals reefs is believed to be at risk from anthropogenic activities associated with increased ocean temperature, reduced seawater *p*H and environmental degradation. Of these, coral bleaching associated with thermal stress and increased ocean acidification have recently received particular attention from the scientific community as it is believed that they could severely affect the process of calcification of scleractinan corals. This review

starts by describing how the growth history of corals can be retrieved from information stored in the coral skeleton. Also included is a description on how environmental gradients relate to spatial and temporal changes observed in coral growth. This is followed by describing the changes in seawater carbonate chemistry that lead to ocean acidification and how these changes could affect coral calcification. Finally, the scientific basis for the use of the $\delta^{11}B$ seawater *p*H proxy in coral samples is given.

1.3.1. Coral calcification as a source of environmental information

Most reef building corals are colonial, hermatypic organisms that belong to the order Scleractinia, and are characterized by the precipitation of an aragonitic exoskeleton. The coral colonies comprise interconnected anemone-like polyps that reside in a skeletal framework formed by individual corallites. The corallite architecture forms a central tube structure (collumnella), a series of radiating vertical plates (septa) and surrounding walls (theca), which together form the housing for the polyps (Veron 2000). The living tissue only occupies the top few millimeters of the skeleton, and it is here that biomineralization takes place. As the coral grows it precipitates new layers of skeleton leaving the old skeleton unoccupied. Given that many of the organisms that inhabit reefs depend on the coral structures, understanding the changes in coral growth rate is arguably a key parameter for evaluating the health of the coral reef ecosystem (De'ath et al. 2009; Tanzil et al. 2009).

Coral growth occurs by vertical extension through the deposition of new material at the surface of the coral combined with the slow thickening of the underlying material within the tissue layer (Barnes and Lough 1993). Corals grow continuously throughout the year but changes in the environmental conditions affect their calcification rates. Massive coral colonies typically form of a series of alternating layers (bands) of low and high density in the skeleton, which usually represent seasonal variations. These annual/seasonal density patterns in massive corals were first identified by Knutson et al. (1972), and since then have been used extensively as markers to assign the chronology to coral records. Having a precise chronology is essential for accurately reconstructing past environmental conditions. If the collection date of coral is known counting back well displayed pairs of high and low density bands allows establishing a precise chronology (Lough and Cooper 2011).

Massive coral colonies are long-lived (up to hundreds of years) and as they growth a wide range of different proxies are incorporated into their skeleton, making corals excellent recorders of environmental variability (e.g. see reviews by Druffel 1997; Henderson 2002; Cole 2003; Felis and Patzold 2004; Corrège 2006a). This environmental information can be stored as changes in the growth parameters, as luminescent bands or as variations in the isotopic and elemental composition of the skeleton. The majority of recent studies on massive corals are based on geochemical analysis while the information from growth bands in corals has been mainly relegated to assist establishing the chronology and selecting transects for the geochemical analysis (Lough 2008a; Lough and Cooper 2011). However, several studies have demonstrated that coral growth records can be very useful sources of environmental information (e.g. Dodge and Lang 1983; Lough and Barnes 1990b; Scoffin et al. 1992; Draschba et al. 2000; Lough and Barnes 2000; Carricart-Ganivet et al. 2007; Lough 2008a; De'ath et al. 2009; Tanzil et al. 2009; Helmle et al. 2011; reviewed by Lough and Cooper 2011). Linking the changes in annual coral growth to changes in the environmental variables is an aim in sclerochronology; however, individual environmental variables typically explain only a fraction of the variability in coral growth (Helmle et al. 2011).

Some of the most basic information that can be obtained from coral growth bands is the rate of linear extension (cm yr^{-1}) and the coral skeletal density (g cm^{-3}). The product of linear extension and density can then be used to determine calcification rates (g cm^{-2} yr^{-1}). Linear extension rate in massive *Porites* is usually directly related to changes in calcification rate while these parameters are inversely related to density changes (Scoffin et al. 1992; Lough and Barnes 2000; Lough 2008a).

1.3.1.1. Chronology and linear extension

Of the growth parameters, linear extension rates (also referred as annual extension or growth rate) is the easiest to measure and most frequently reported in the literature (Lough and Barnes 1990b,2000; Lough and Cooper 2011). Since changes in calcification rates of *Porites* corals are explained mainly by linear extension this variable by itself makes a good description of coral calcification (Lough 2011a). Linear extension can be obtained by several methods, including direct measurements of density bands from X-rays, gamma and

X-ray densitometry profiles, computerized tomography (CT) scans, luminescent bands or seasonally driven changes in element composition ratios.

Density bands can be observed by X-radiographic examinations of sections (usually 5 -10 mm in thickness) of coral cut along the growth axis (Weber et al. 1975). This method has been the most commonly used for dating coral records, but the complex three dimensional architecture of corals and changes in growth direction can produce artifacts in the X-rays, such as multiple bands or ambiguous banding patterns, that can cause difficulties with the chronology assignment (Lough and Barnes 1992; Hendy et al. 2003). Gamma densitometry and CT densitometry have been also been used to obtain the growth information stored in the density bands (e.g. Lough and Barnes 1990b; Bosscher 1993; Lough and Barnes 2000; Cantin et al. 2010).

In some coral records, luminescent bands can be observed under UV light. Two types of luminescent bands are described in massive *Porites* corals; intense narrow luminescent lines associated with terrestrial run-off and faint luminescent bands associated with the annual density bands (Barnes and Taylor 2001; Barnes et al. 2003; Barnes and Taylor 2005). In the Great Barrier Reef (GBR) the timing and intensity of the narrow luminescent lines is often correlated to rainfall and river runoff (Isdale 1984; Lough et al. 2002; Barnes et al. 2003; Hendy et al. 2003; Lough 2007). These bands tend to be more common in coastal corals that are subject to the effects of river discharge (Isdale 1984), with the expression of the luminescent bands reducing with distance from the coast (Barnes et al. 2003; Lough 2002; Lough 2011a). No significant difference was found in the luminescent parameters along a depth transect, from 5 to 15-20 m, in corals from a mid-shelf reef of the central GBR (Carricart-Ganivet et al. 2007). The origin of these luminescent bands is still debated. Initially they were associated with higher concentrations of fulvic acids from terrestrial river input (Boto and Isdale 1985), but later work suggests the luminescent bands could be associated to regions of lower skeletal density (Barnes and Taylor 2001). In a subsequent study by Barnes and Taylor (2005) they concluded that the high intensity luminescent lines cannot originate simply by changes in density but more likely related to changes in crystal size and packing, differences in crystal chemistry, or with a combination of these possibilities.

Finally, the geochemical and isotopic composition of some elements in the coral skeleton (e.g. B, Ba, Sr, Mg, U, $\delta^{18}O$) commonly shows strong seasonal variation in response to environmental factors such as temperature or salinity (Cole 2003). Therefore, counting the number of density or luminescent bands, or geochemical cycles can be used to obtain the growth chronology for a coral, while measuring the distance between equivalent parts of these bands or cycles can be used to obtain the extension rate (Lough and Cooper 2011).

1.3.1.2. Measurements of coral density

Two different concepts of coral skeletal density are described in the literature, 'micro-density' and 'bulk-density' (Barnes and Devereux 1988; Bucher et al. 1998). Bulk density relates to the variations in thickness and spacing of the principal components of the skeletal meso-architecture (essentially the septa, thecae and dissepiments) in a given volume (Barnes and Devereux 1988; Risk and Sammarco 1991; Le Tissier et al. 1994). Micro-density refers to the arrangement and organization (packing) of calcium carbonate acicular crystals, which are the most fundamental architectural unit of the coral skeleton (Barnes and Devereux 1988; Bucher et al. 1998). The variation in the annual density band of *Porites* corals are associated with changes in the meso-architecture, which is the density measurement most frequently reported in literature (Barnes and Devereux 1988).

Two methods are described by Barnes and Devereux (1988) to measure density that preserve the meso-scale variations of the skeleton. These are direct measurements of the volume (e.g. calipers) and the gamma densitometry method. Other methods include the use of X-ray densitometry (Buddemeier 1974; Buddemeier et al. 1974; Dodge and Brass 1984; Chalker et al. 1985; Dodge et al. 1992; Carricart-Ganivet and Barnes 2007) and CT densitometry (Logan and Anderson 1991; Bosscher 1993; Bessat and Buigues 2001; Cantin et al. 2010). Other methods destroy the meso-scale variations (e.g. density of powdered coral skeleton) or are not affected by it (e.g. water displacement) and therefore provide estimates of the micro-density (Barnes and Devereux 1988). The bulk density can be measured by the water displacement method by not allowing the voids in the skeleton to fill with the weighting medium (e.g. Bucher et al. 1998). Unless indicated otherwise the water displacement term will be used here after to refer to estimates of the bulk density.

1.3.1.3. Densitometry methods

One of the main advantages of densitometry methods is that it provides a continuous scan of the skeleton at high spatial resolution. High and low density bands can be identified from this profile providing a high resolution measurement of the density variations. If the timing of the density bands is known (i.e. they are annual) then a chronology can be derived and linear extension measured. The gamma densitometry method measures the attenuation of a beam of gamma photons across the thickness of a coral slice and the beam is continuously scanned along the slice providing a density profile (Lough and Cooper 2011). This method has been extensively used in the literature (Chalker and Barnes 1990; Lough and Barnes 1990a,b,1992,1997; Draschba et al. 2000; Lough and Barnes 2000; Cooper et al. 2008); however, it is dependent on having access to specialized technology.

Another common densitometry method used to measure density variations along the growth axis is the x-radiograph film densitometry (Buddemeier 1974; Buddemeier et al. 1974; Dodge and Brass 1984; Chalker et al. 1985; Dodge et al. 1992; Carricart-Ganivet and Barnes 2007). This is an inexpensive method; however, it is sensitive to intensity heterogeneity of the X-rays that require careful correction. This is caused by the heel effect and spherical spreading (inverse square law; Carricart-Ganivet and Barnes 2007; Duprey et al. 2012). Furthermore, this method requires calibration against external standards whose absolute density values are obtained from direct measurement of the density, e.g. the water displacement technique (Carricart-Ganivet and Barnes 2007). Both of these densitometry methods assume the thickness of the coral slab to be constant. Another issue that can potentially affect these densitometry methods results from the complex three dimensional structures of *Porites* corals. Slices not following the growth axis and variations in corallite orientation can alter banding patterns and result in density bands not being equally well displayed (Lough and Barnes 1990b,1992; Le Tissier et al. 1994). Densitometry transects are typically only a few mm wide and susceptible to variations in corallite orientation. Several tracks are often required to be analysed to obtain a representative average as considerable variability is observed even between tracks only 12 mm apart (Lough and Barnes 1990a,b). Besides the conventional X-rays the medical X-ray CT scanning of corals has also been used successfully to measure variations in density (Logan and Anderson 1991; Bosscher 1993; Bessat and Buigues 2001). This method is non-destructive allowing

coral cores or full colonies to be analysed without slicing them. This permits selection of the best track to measure the density variations, as well as providing information to select the optimum plane for sectioning (Bosscher 1993; Cantin et al. 2010).

1.3.1.4. Direct measurements of density

Direct measurements of the density are herein referred to those measurements in which density is obtained from the product of the weight and volume of sections or blocks cut out from a slice of coral skeleton. Obtaining the volume can be complicated as often coral samples do not have regular geometries, thus limiting the use of callipers or other similar techniques. The measurement of the volume of removed sections of coral has been archived by callipers (Allison et al. 1996), mercury displacement (Dustan 1975; Highsmith 1979), frozen material (Carricart-Ganivet et al. 2000) or more typically by water displacement (Jokiel et al. 1978; Brown et al. 1990; Risk and Sammarco 1991; Scoffin et al. 1992; Bucher et al. 1998; Edinger et al. 2000; Smith et al. 2007; Manzello 2010). These methods provide a direct measurement of the density over a larger area and do not require access to specialized technology, compared to densitometry methods. However, like all methods it is first necessary to carefully establish the chronology of the coral slice using the information obtained from luminescent bands, density bands or geochemical composition of the skeleton. One limitation of these direct methods is that samples are analysed in blocks encompassing several years and hence density is averaged over this period. The water displacement method has, however, been used to measure density of samples with an annual resolution (Brown et al. 1990) or even sub-annual resolution (Barnes and Devereux 1988). Applying this method at high resolution can be labour intensive, especially for large number of samples.

In the present study the water displacement method was used to estimate the temporal variation in density from pieces of coral skeleton (typically 0.7 cm × 2.5 cm × ~5cm in size) cut continuously from 41 long cores (~50cm in length; see Chapter 4). This is the first time this method has been used on such large scale. The data obtained were found to be very useful to extract the common variability in different cores and to describe the long-term variations in density. This method provides an inexpensive alternative that only requires basic laboratory setup and, therefore, can be easily implemented. In the majority of

the geochemical studies for corals information on the growth parameters is not included or is only used as a mean to establish a chronology (Lough 2008a; Lough and Cooper 2011). The availability of this relatively straightforward method could encourage researchers to include coral growth information.

1.3.1.5. Growth parameters from different massive Porites species

Massive heads of *Porites* in the GBR are represented by five species *P. australensis, P. lobata, P. lutea, P. mayensi* and *P. solida* (Lough and Barnes 2000; Veron 2000). The genera *Porites* is characterized by a simple meso-architecture in which the vertical and horizontal components are less differentiated than in the skeletons of other genera (Barnes and Devereux 1988). This makes the precise and exact identification of massive *Porites* a challenging task. This difficulty is increased when working with cores because of the small surface available for examination, and because often this surface ends up being damaged during coring (Barnes and Lough 1992). Nonetheless, it has been shown that the five species of massive *Porites* found in the GBR show similar growth characteristics, only *Porites solida* shows a significantly higher density (Lough et al. 1999).. Combining the growth records from different species of *Porites* has been a common practice in several studies (e.g. Lough and Barnes 2000; Cooper et al. 2008; Lough 2008a; De'ath et al. 2009; Carricart-Ganivet et al. 2012).

1.3.2. Spatial and temporal variations in coral growth parameters

1.3.2.1. Latitudinal variations of coral growth and sea surface temperature

The distribution of scleractinian corals is geographically constrained to latitudinal and depth limits imposed by environmental parameter such as temperature, aragonite saturation state, water quality, light and salinity levels (Isdale 1981; Kleypas et al. 1999; Grigg 2006). Growth parameters in massive corals usually show variations along environmental gradients (Smith et al. 2007). Growth parameters of *Porites lobata* corals from Hawaii exhibit a latitudinal gradient, with an increase in density, and reduction in linear extension and calcification towards higher latitudes (Grigg 1982). Average linear extension and calcification rates of *Porites* corals from the GBR increase with the higher SST's towards

lower latitudes (Lough and Barnes 2000). Corals from Thailand, Hawaii, the Arabian Gulf and Papua New Guinea were found to adjust to the same linear relationship of ~3 mm yr^{-1} per °C for linear extension and ~0.3g cm^{-2} yr^{-1} per °C for calcification (Lough and Barnes 2000; Lough 2008a). This spatial relationship of linear extension and calcification of *Porites* corals with temperature shows a stronger correlation with annual minimum SST than with annual maximum SST or annual average SST (Lough and Barnes 2000). Similar dependence of coral growth rates have been observed and results have been reported for other species of corals with a temperature sensitivity of linear extension for the Indo-Pacific corals *Platygyra* of 0.9 mm yr^{-1} per °C (Weber and White 1974) and for the Caribbean coral *Montastrea annularis* 0.94 mm yr^{-1} per °C (Weber and White 1977). A subsequent study on *Montastrea annularis* in the Caribbean indicates the relationship with temperature to be the opposite with an increase in density and decrease in linear extension associated with higher temperature (Carricart-Ganivet 2004).

1.3.2.2. Across shelf variability

In the GBR the largest environmental differences in coral communities occurs across-shelf (Lough and Cooper 2011) rather than latitudinally along the length of the GBR. This strong across-shelf gradient is the result of the transition from a terrigenous influenced environment close to the coast to near oceanic conditions in the outer shelf. A marked cross shelf variation exists with water properties such as turbidity decreasing towards the outer-shelf (Done 1982). Inner-shelf reefs are characterized by high sediment loads, poor illumination, and high variability in salinity, mainly related to the periodic decrease in salinity, silt input and nutrient enrichment, as a result of the discharge from rivers (Wolanski and Jones 1981). The diversity of reefs is influenced by this across-shelf environmental gradient resulting in a higher diversity in the protected mid-shelf environment and decreases in outer and inner-shelf reefs (Done 1982). The skeletal growth of *Porites* corals from the GBR is also influenced by this across-shelf gradient. Growth rates tend to show larger variability close to the coast and slower and more consistent rates towards the outer-shelf. These patterns are the result of the largest environmental variability close to the coast (Isdale 1981). In a pioneer study Isdale (1983) found linear extension increased closer to the coast, while in a subsequent study by Risk and Sammarco (1991) density show the opposite trend, i.e, increased with distance from shore. In a more

comprehensive study by Lough and Barnes (1992), later expanded by Lough et al. (1999), they demonstrated that linear extension and calcification increased towards the coast while density showed the opposite trend. Furthermore, Lough et al. (1999) found that the inshore to offshore pattern was not evident in the south section of GBR; a reduction in tissue thickness related to upwelling nutrient enrichment in this area is given as a possible explanation for this.

Other regions also show similar differences in near-shore and offshore environments. Higher concentration of suspended particulate matter (SPM) in Indonesia (Tomascik and Sander 1985) and a decrease in water quality in the Mayotte Island, in the south Indian Ocean (Priess et al. 1995), have been linked to reduced extension rates of *Porites* spp. corals. In *Porites* corals from Thailand linear extension rate decreased, bulk density increased while calcification showed no apparent change linked to a gradient of increasing hydraulic energy (Scoffin et al. 1992). In the Gulf of Mexico density and calcification rates of *Montastrea annularis* corals decreased along a gradient towards higher turbidity and sediment load, while linear extension showed the inverse trend (Carricart-Ganivet and Merino 2001). The growth of *Montastrea annularis* in Barbados was found to vary along a gradient of SPM (Tomascik and Sander 1985). Coral growth was found to increase with SPM until a certain maximum concentration, after this, coral growth is reduced due to smothering, reduced light levels and reduced zooxanthellae photosynthesis (Tomascik and Sander 1985).

1.3.2.3. Depth

Environmental gradients can occur between regions or reefs and even within the different zones of a reef or within the same zone of a reef with depth. In fact any factor that affects light levels will have an impact on the rates of coral calcification and reef development (Done 2011; Veron 2011). There have been several studies that report a decrease in linear extension with depth in massive corals around the world. Buddemeier (1974) reported a decrease in linear extension with depth for *Porites lutea*, collected from the Eniwetok Atoll. Rosenfeld et al. (2003) reported a significant decrease in linear extension in a colony of *Porites lutea* from the Gulf of Aqaba after it was transplanted from a depth of 6 m to a depth of 40 m. Grigg (2006) found a growth optimum depth of 6 m and a critical limit of

30-50 m for *Porites lobata* from Hawaii. Growth rates for *Montastrea annularis* corals have also been shown to decrease as depth increases. Hubbard and Scaturo (1985) found that *Montastrea annularis* on St. Croix clustered into two groups; the first one including corals at <12 m and the second those at >18-20 m, with the later showing lower growth rates. This marked decrease is associated by the authors to a 'light compensation depth' that affects photosynthetically driven calcification and suggests that coral growth rates at this site is mainly controlled by water depth, light level, turbidity and sedimentation rate. Bosscher and Meesters (1993) found a similar decrease of growth rate with depth in *Montastrea annularis* from Curacao that is related to the exponential decrease in light that is explained by a photosynthetic hyperbolic tangent function, with a light saturation depth at ~15 m. Other studies report similar reductions in growth rates of *Montastrea annularis* occurring at 18 m depth in St. Croix (Baker and Weber 1975; Dodge and Brass 1984) and at 15 m depth in Jamaica (Dustan 1975).

A discrepancy occurs for *Porites* corals from the central mid-shelf GBR where no significant trend in growth rate was observed between 0 and 20 meters (Carricart-Ganivet et al. 2007). Al-Rousan (2012) showed that the decrease in extension rate with depth for *Porites* corals from the Gulf of Aqaba is almost exponential, with similar values in extension rates observed in the first 12 m and significantly decreasing at greater depths. This could suggest that the light compensation depth for *Porites* corals from the mid-shelf Rib Reef in the central GBR occurs below 20 m. The combination in light intensity, temperature and nutrients, amongst other variables (e.g. wave intensity) at specific locations most likely explains the differences in the light compensation depth observed between studies.

1.3.2.4. ***Temporal variability***

Of particular interest is the temporal response of coral growth as this provides a perspective against which to assess environmental changes (Bessat and Buigues 2001). For the GBR Lough and Barnes (2000) reported an increase of 4% in the calcification rates of massive *Porites* between the two 50 year periods of 1880–1929 and 1930-1979, following a corresponding increase in SST. Furthermore, these authors identify that this temporal response of calcification varies with latitude over the 20-year periods between 1903–1922

and 1979–1998. They estimate an increase in calcification of 5% on the northern part of the GBR, 12% on the central GBR and 20% on the south GBR (up to 50% south to the GBR) based on the relationship between average calcification and SST. In a subsequent study Cooper et al. (2008) documented a decrease in calcification of 15% over the 17 year period of 1982 to 2008 for two inshore regions in the northern GBR. This recent decrease in calcification was generalized to the whole GBR by De'ath et al. (2009); the suggested causes for this decrease are associated with thermal stress and ocean acidification. In their study Cooper et al. (2008) describe that the temporal relationship of coral calcification and linear extension with temperature is not linear with an optimum value for coral growth of 26.5°C. Shi et al. (2012) also report a nonlinear relationship with temperature. This indicates that after a maximum temperature threshold value is crossed coral growth can be significantly reduced.

The widespread response of decreased calcification in the GBR reported by De'ath et al. (2009) is yet to be tested as the results from Lough and Barnes (2000) and Lough (2008a) suggest that the response of growth in *Porites* corals in the GBR shows important latitudinal and across-shelf variability. The study of Lough (2008a) was focused on growth changes over the period of 1960 to 2005 for three reefs from the central GBR, one inshore reef, one mid-shelf reef and one offshore reef. The author report a decrease in calcification for the inner and outer-shelf reefs; however, no significant change for the mid-shelf reef of Rib. Carricart-Ganivet et al. (2012) report an inverse relationship of linear extension and temperature for *Porites* from Rib Reef in the central GBR (1989-2002) and for *Montastrea annularis* corals from the Caribbean (1985-2009). Based on these results Carricart-Ganivet et al. (2012) suggests that the temperature threshold values for coral growth may have already been crossed at these locations.

In the central Red Sea linear extension of *Diplostrea heliopora* corals increases as a response to the warming of the oceans; however, in the last decade (1998-2008), the warmest period, a decrease of 30% is observed (Cantin et al. 2010). The authors suggest that the thermal limit for these corals could have been crossed in 1998 as an explanation for this decline. An increase of calcification following the rise in temperature is described by Bessat and Buigues (2001) on *Porites* spp. for the period 1800–1990 in Moorea, French Polynesia. Tanzil et al. (2009) reported a decrease of ~21% in linear extension and 24% in

calcification between 1986 and 2005 for *Porites lutea* corals from Thailand. It is important to note that this is a discrete comparison between two short periods (December 1984–November 1986 and December 2003–November 2005 and, therefore, highly subject to interannual variability and not necessarily representative of a long term trend. Coral calcification in *Porites* corals from the Meiji Reef in the southern South China Sea show a moderate increase in calcification rates associated with the rise in temperature during the 20th century (Shi et al. 2012). A study on massive *Porites* corals form reefs along an 11° latitudinal range in the southeast Indian Ocean off Western Australia show no widespread decrease during the 20th century but rather significant regional differences (Cooper et al. 2012). *Montastrea faveolata* corals of the Florida Keys show that over 1937-1996 extension increased, density decreased and calcification remained stable, while the most recent decade was not significantly different than decadal averages over the preceding 50 years for extension and calcification (Helmle et al. 2011). In the western Caribbean Sea a decrease in linear extension linked to temperature changes was observed for the corals in *Siderastrea sidereal* corals for the forereef but no significant change was observed in the backreef and nearshore (Castillo et al. 2012).

1.3.2.5. Effects of ocean acidification on calcifying organisms

The process of ocean acidification is detailed in section 1.3.3 and the associated changes in the ocean chemistry are described in section 1.3.4. The general effects of ocean acidification on calcifying organisms are summarized in section 1.3.5. The effects of ocean acidification on corals at a physiological level are described in section 1.3.6, while the effects at the community level of the reef are provide in section 1.3.7.

1.3.2.6. Anthropogenic pollution

The natural reef environment is also disturbed by human influences such as anthropogenic pollutants. Toxic substances from sewage pollution may induce metabolic changes in corals, decrease rates of growth and reproduction, or reduce viability of corals (reviewed by Loya and Rinkevich 1980; Dodge and Brass 1984; Guzman et al. 1994). In Barbados reduced growth rates is observed in *Montastrea annularis* corals exposed to a variety of anthropogenic pollutants including discharge from a rum refinery effluent outlet (Runnalls

and Coleman 2003). Pollution from crude oil is also reported to have detrimental effects on coral reefs. Effects in corals from the Caribbean include reduced growth rates, direct damage to tissues, thinning of cell layers and disruption of cell structure, damage to tactile stimuli and normal feeding mechanisms, excessive mucus secretion leading to enhanced bacterial growth and eventual coral destruction (Dodge and Brass 1984; Guzman et al. 1994). After a major oil spill on reefs of Panama concentrations of hydrocarbons in reef sediments were significantly positively correlated with amounts of coral injury and significantly negatively correlated with coral growth, with no signs of recovery 5 years after the spill (Guzman et al. 1994). Furthermore, the use of crude-oil emulsifiers is believed to enhance the toxic effects of spilt oil (Loya and Rinkevich 1980). Increased coastal activities, construction and urbanization during the 1960's in the Jordanian Gulf of Aqaba is linked to significant enrichment in heavy metals and reduction in skeletal extension rates of *Porites* corals (Al-Rousan et al. 2007). A decrease in water quality recorded in the coral skeleton as heavy metals is associated with a decrease in growth rates, species number, abundance and diversity in corals from Hong Kong (Scott 1990). Guzman et al. (2008) found a gradual decline in coral growth linked to increased runoff and sedimentation to coastal areas resulting from the construction and operation of the Panama Canal.

1.3.2.7. Storms and wave energy

Wave energy and storm frequency is one of the main factors controlling coral growth and reef development (Dollar 1982). There is a typical energy gradient that creates a reef zonation based on reef structure and coral community structure (Done 1983). In the Indo-Pacific massive *Porites* are more common in the most sheltered environments of the backreef and fringing coral reefs (Dollar 1982; Done 1983; Veron 2000). However, the variability of coral growth within zones in a reef is not well documented. Smith et al. (2007) observed that transplanted coral colonies from the back reef and the forereef consistently had higher skeletal growth rates, lower bulk densities, and higher calcification rates on the back reef than on the forereef. Coral growth for massive *Porites* spp. show a threshold response to water flow (this is an increase in growth followed by a marked decrease after an optimum flow value is crossed), whereas growth of the branching coral *Porites irregularis* increased linearly with flow rate (Goldenheim and Edmunds 2011). In

Belize storms cause breakage and scouring of corals at depths of up to 26 m, which according to Highsmith et al. (1980) appears to prevent coral reefs from reaching a mature state characterized by low calcification and growth rates. Furthermore, these authors predict that long-term reef calcification and growth rates are highest on reefs periodically disturbed by storms of intermediate intensity. Coral growth and reef accretion in Oahu, Hawaii, show that coral growth (linear extension) at optimal depths is comparable along a gradient in wave energy at all stations, but significant reef accretion occurs only at wave sheltered stations (Grigg 1998).

1.3.3. CO_2 in the ocean

Since the beginning of the industrial revolution there has been an increase in the atmospheric CO_2 concentrations, from 280 to 394 ppmv, produced mainly by the combustion of fossil fuel, cement production, agriculture and deforestation (Royal Society 2005; most recent CO_2 values available from http://scrippsco2.ucsd.edu/, 2013; IPCC 2007). The present-day rapidly rising level of ~394 ppmv, represents an increase of 114 ppmv over the last 200 yrs. This is already high in comparison to values observed during the previous 800,000 yrs when the atmospheric CO_2 concentrations oscillated between ~180 ppmv (ice ages) and ~280 ppmv (interglacials; Lüthi et al. 2008; Tyrrell 2008). In a more recent study Hönisch et al. (2012) suggest that current acidification of ocean related to the increase in atmospheric CO_2 is occurring at least 10 times faster than during the Paleocene–Eocene Thermal Maximum. This indicates that the actual rate of change may be unprecedented over the last ~300 million years. Unless emissions are reduced, atmospheric CO_2 levels are predicted to continue to rise to between 730 ppmv and 1000 ppmv by 2100 at a rate of about 1% yr^{-1} (Royal Society 2005; Kleypas et al. 2006; IPCC 2007). This rate of increase is close to 100 times faster than any changes that have occurred during the previous 650,000 years prior to the industrial revolution (Fabricius 2008).

Containing about 38000 Gt C, the oceans are the largest labile reservoir of carbon, accounting for 95% of the carbon in the oceanic, atmospheric and terrestrial biosphere systems (Royal Society 2005; Kleypas et al. 2006). The oceans are a very important component of the carbon cycle actively exchanging large quantities of CO_2 with the atmosphere and providing an annual oceanic sink of 2.4±0.5 $PgCyr^{-1}$ for 2010 (Peters et al.

2011), with annual rates of CO_2 uptake increasing with time (Le Quéré et al. 2009). This exchange is governed by Henry's law of gases; the increase in atmospheric CO_2 results in an increase of the CO_2 concentration in the oceans. Of the anthropogenic CO_2 emissions released into the atmosphere, only about 40-50% continues to reside in the atmosphere, with approximately 20-30% being taken up by the terrestrial biosphere and the remainder 20-30% absorbed by dissolution into the oceans (Sabine et al. 2004; Canadell et al. 2007; Le Quéré et al. 2009; Peters et al. 2011). Due to the slow exchange of waters between the surface and deep ocean, most of the carbon absorbed by the ocean is in the surface ocean layer (Tyrrell 2008), with 30% at depths shallower than 200 m and around 50% in the first 400 m (Sabine et al. 2004).

The increase in atmospheric CO_2 and other greenhouse gases is responsible for a rise in global surface temperatures due to an enhanced greenhouse effect. The CO_2 uptake by the oceans reduces the concentration of the greenhouse CO_2 gas in the atmosphere and, therefore, the magnitude of global warming. However, this is at the cost of changing the chemistry of seawater, resulting in ocean acidification and a reduction in the carbonate ion concentration (Orr et al. 2005; Kleypas et al. 2006). The resulting changes in seawater inorganic carbon equilibrium are perhaps the most direct and predictable consequence of increased atmospheric CO_2 (Kleypas and Langdon 2000; Doney et al. 2009). The CO_2 absorbed by the oceans over the last 200 years has already reduced the *p*H of the global surface ocean by ~0.1 *p*H units, which is equivalent to a 30% increase in $[H^+]$ (Royal Society 2005). Depending on future emissions scenarios, it is predicted that by 2100 surface ocean *p*H will have decreased on average by between 0.14 and 0.4 units (Haugan and Drange 1996; Orr et al. 2005; IPCC 2007). These changes in ocean chemistry are likely to affect the organisms that inhabit the oceans especially aragonite calcifying organisms like scleractinian corals (Kleypas 1999; Langdon et al. 2000; Hoegh-Guldberg et al. 2007).

1.3.4. The Carbonate system in the Ocean

At modern seawater *p*H (8.0 to 8.2), dissolved CO_2 in the ocean exists mainly as three species: $CO_{2(aq)}$, HCO_3^- (bicarbonate) and CO_3^{2-} (carbonate ion). Collectively, the sum of these three species is known as dissolved inorganic carbon (DIC). A fourth species, H_2CO_3

(carbonic acid), is short-lived and its trace concentration is usually included with CO_2. Aqueous $CO_{2(aq)}$ represents around 1% of the total DIC, and of the two electrically charged forms, HCO_3^- is the most abundant, making up around 90% of the total, with the remaining 9% existing as CO_3^{2-}. The distribution between the three predominant carbon species varies as a function of seawater *p*H (Figure 1-1), and is temperature, salinity and pressure dependent.

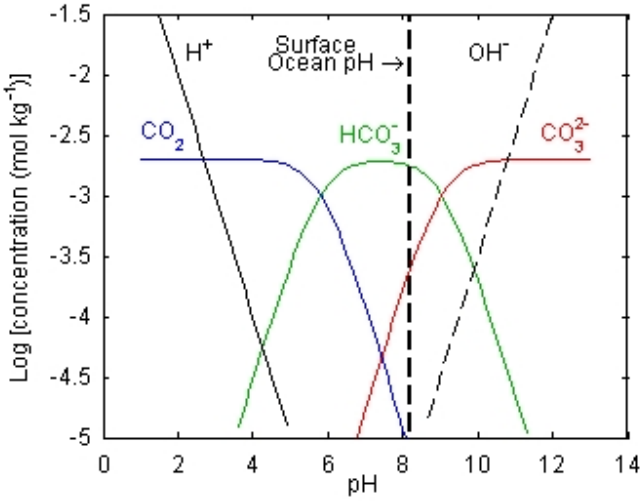

Figure 1-1. *Bjerrum plot showing concentrations of the major dissolved forms of inorganic carbon in seawater. DIC = 2000 µmol kg^{-1}, temperature T=15°C, salinity S=35, and pressure P = 1 atm (after Zeebe and Wolf-Gladrow 2001).*

When CO_2 is dissolved into the ocean it reacts quite rapidly (milliseconds) with seawater to initially form H_2CO_3. This is followed by even faster reactions in which this weak acid dissociates and releases protons (H^+) to form HCO_3^- and CO_3^{2-} (Zeebe and Wolf-Gladrow 2001). As $[H^+]$ increases with the formation of HCO_3^-, some of the CO_3^{2-} ions react with the H^+ to become HCO_3^-. Hence the net effect of increasing CO_2 in the atmosphere is to increase the oceanic concentrations of H^+, HCO_3^-, $CO_{2(aq)}$ and H_2CO_3, and to reduce the concentration of CO_3^{2-}. Based on present day conditions, models indicate that even if CO_2 emissions stabilize, atmospheric CO_2 levels will rise to double preindustrial levels by the end of the century if not sooner (Kleypas and Langdon 2000). This will decrease the $\left[CO_3^{2-}\right]$ from ~9% to ~6%, representing a significant overall decrease of ~30% relative to current values (Kleypas and Langdon 2000).

Because a large part of the released H^+ reacts with CO_3^{2-} to form HCO_3^-, the changes in *p*H related to the dissolution of CO_2 are relatively small; this is referred as the carbonate buffer effects (Royal Society 2005). However, as this process consumes some of the CO_3^{2-} ions, the oceans eventually become under-saturated with respect to CO_3^{2-} ions and deposited $CaCO_3$ starts to dissolve. The solubility of $CaCO_3$ increases with decreasing temperature and increasing pressure, thereby making cold- deep carbonate deposits the most susceptible to dissolution. The depth at which seawater $CaCO_3$ in seawater dissolves is known as the saturation horizon (Royal Society 2005).

Calcium carbonate predominantly exists as two polymorphs: aragonite, with an orthorhombic symmetry, and calcite, with trigonal symmetry. The saturation state (Ω) of seawater with respect to the calcite or aragonite polymorphs is given by the product of the concentrations of the carbonate ions and calcium, at the *in situ* temperature, salinity, and pressure, divided by the stoichiometric solubility product of calcite or aragonite (K_{sp}^*):

$$\Omega = \frac{\left[CO_3^{2-}\right] \cdot \left[Ca^{2+}\right]}{K_{sp}^*}$$

For $\Omega>1$, seawater is supersaturated with the mineral phase; $\Omega<1$ indicates under-saturated conditions, and where Ω is equal to one saturation is reached; so the saturation horizon is defined where $\Omega = 1$. The structural differences between calcite and aragonite make the latter more soluble, that is, aragonite has lower saturation state Ω values (Tyrrell 2008).

$[Ca^{2+}]$ is conservative in seawater and can be considered almost constant. Therefore the saturation state of carbonates in seawater is mainly controlled by the variations in $\left[CO_3^{2-}\right]$, and in turn, atmospheric CO_2 (Feely et al. 2004). In tropical regions, surface waters are supersaturated with respect to all the mineral phases of $CaCO_3$, with aragonite saturation state (Ω_{arag}) values currently around 3 to 4 (Kleypas 1999). The tropical oceans are likely to remain supersaturated with respect to aragonite with future atmospheric CO_2 emissions, but the saturation state values will be significantly reduced. A number of studies (e.g. Kleypas 1999; Royal Society 2005; Hoegh-Guldberg et al. 2007; Erez et al. 2011) predict that this

will negatively affect the calcification rates for calcifying organisms like corals, and inhibit their ability to compete with non-calcifying organisms. However, as discussed in the next section there are still large uncertainties on the response of corals to ocean acidification.

1.3.5. Effects of increased CO_2 on corals

The decrease in Ω_{arag} and seawater *p*H associated with the increase in dissolved CO_2 in the ocean has received much attention in recent years for its potentially negative effect on coral calcification (Kleypas 1999; Kleypas et al. 2006; Hoegh-Guldberg et al. 2007; Holcomb et al. 2010; Manzello 2010). As described, changes in ocean chemistry due to increasing atmospheric CO_2 levels are predictable; however, the response of calcifying marine organisms and ecosystems to these changes is poorly understood and difficult to predict (Kleypas and Hoegh-Guldberg 2008; Vézina and Hoegh-Guldberg 2008). It is generally believed that there will be negative impacts on numerous marine taxa (Doney et al. 2009), with calcifying organisms considered to be especially at risk (Orr et al. 2005; Fabry et al. 2008). As a consequence, corals and coral reef ecosystems are of particular concern as their existence depends on the massive and complex calcium carbonate structures deposited by calcifying organisms such as scleractinian corals and coralline algae. Precipitation of the calcium carbonate skeleton can be described in a simple form by the equilibrium reaction:

$$Ca^{2+} + CO_3^{2-} \Leftrightarrow CaCO_3$$
$$Ca^{2+} + 2HCO_3^{-} \Leftrightarrow H_2O + CO_2 + CaCO_3$$

The decrease in Ω_{arag} resulting from the reduction in $\left[CO_3^{2-}\right]$ is expected to result in a reduction in calcification rates and/or a reduction in the larval output (Kleypas 1999; Langdon et al. 2000; Hoegh-Guldberg et al. 2007), as well as limiting cementation and stimulating bioerosion (Manzello et al. 2008). The model of Silverman et al. (2009) predicts that when atmospheric pCO_2 levels reach 560 ppmv, net calcification of coral reefs will approach zero; beyond this level reefs will start dissolving. Any significant reduction of calcification rates could inhibit the ability of scleractinian corals to compete with other organisms like algae and sponges that can result in an ecological "regime shift" (Kleypas and Yates 2009).

As described in section 1.3.2.4 a reduction in calcification rates has been observed in a number of studies during last ~20 yrs in corals from the GBR (Cooper et al. 2008; De'ath et al. 2009), Thailand (Tanzil et al. 2009), the Red Sea (Cantin et al. 2010) and the Arabian Gulf (Lough et al. 2003). Increased thermal stress and decreased saturation state both being suggested as the plausible causes for this apparent decline (Cooper et al. 2008; Lough 2008a; De'ath et al. 2009). *In situ* studies show a decrease in calcification of corals along natural gradients of higher CO_2, and lower Ω_{arag} and seawater *p*H (Crook et al. 2013). However, experimental studies have revealed widely varying calcification responses of different organisms to higher CO_2 and lower Ω_{arag} (Doney et al. 2009; Ries et al. 2009). Tropical and temperate scleractinian corals are no exception as their response to acidic conditions and low Ω_{arag} varies between different experimental studies from a relatively linear decrease to either no response or to a nonlinear decrease (Marubini and Atkinson 1999; Marubini et al. 2001; Langdon and Atkinson 2005; Schneider and Erez 2006; Cohen et al. 2009; Holcomb et al. 2010; Jury et al. 2010; Ries et al. 2010; Comeau et al. 2013a; Comeau et al. 2013b). Three reasons have been proposed for the variety of responses observed. The first explanation is that corals exert control over their *p*H at the site of calcification (Al-Horani et al. 2003; Cohen and Holcomb 2009; Krief et al. 2010; Ries 2011; Trotter et al. 2011; Venn et al. 2011; McCulloch et al. 2012a). The second is that depending on nutrient levels, the extra dissolved inorganic carbon from CO_2 dissolution can result in either a positive or negative response of calcification depending on the balance between the negative effect on saturation state and the positive effect on gross carbon fixation (Holcomb et al. 2010). And finally it has been argue that the negative effect of declining $\left[CO_3^{2-}\right]$ on the calcification can be partly mitigated by the use of HCO_3^- for calcification (Comeau et al. 2013a).

As corals elevate their *p*H at the site of calcification this could help them overcome environmental changes in the carbonate chemistry. It follows that the response in coral calcification to changes in the seawater carbonate chemistry will largely depend on the strength of internal *p*H control at the calcifying fluid (Ries 2011). Data from coral $\delta^{11}B$ suggest that corals maintain a high internal *p*H at a constant offset to the external *p*H (Krief et al. 2010; Trotter et al. 2011). In a recent study McCulloch et al. (2012a) demonstrated that due to the up-regulation of *p*H at the site of calcification internal changes are approximately one-half of those in ambient seawater. This has recently been confirmed by

an *in vivo* experiment that showed a more gradual change of *p*H at the site of calcification relative to the surrounding seawater, leading to an increase in gradient at lower pH between the site of calcification and seawater (Venn et al. 2013). However, results from Ries et al. (2010) indicate that the response of coral calcification to reduced pH and Ω_{arag} may not be linear. Therefore, at the early stages of ocean acidification the response in calcification may be weak, but after a pCO_2 threshold level is crossed the negative effects on calcification changes could be more abrupt and severe (Ries et al. 2010). Given the general lack of field-based carbonate chemistry data it is not yet possible to make a proper assessment of the impacts of ocean acidification on coral calcification.

1.3.6. Physiological effects of CO_2 on calcification

Understanding how coral calcification occurs is critical for predicting the response of corals to ocean acidification (Kleypas et al. 2006). Unfortunately, there are still gaps in our knowledge as to how calcification occurs at a physiological level (Allemand et al. 2004). Calcification is a complex process that is mediated by the coral from a medium that is isolated from external seawater. The basic coral unit, the polyp, is a double-walled sack with each wall composed of double-sided layers of cells, an ectodermal and an endodermal layer (Figure 1-2; Cohen and McConnaughey 2003; Allemand et al. 2004). The aragonite skeleton is precipitated in a fluid filled space between the calcioblastic ectoderm. The chemistry of this fluid is controlled by the calcioblastic ectoderm. The calcification process involves synthesis/secretion of an organic matrix and transport of Ca^{2+} and dissolved inorganic carbon to the site of calcification (Allemand et al. 2004). Experimental studies indicate that scleractinian corals elevate their internal *p*H and Ω_{arag} at the site of calcification to facilitate the precipitation of their carbonate skeletons (Al-Horani et al. 2003; Ries 2011; Venn et al. 2011). Two mechanisms have been proposed to elevate the *p*H and Ω_{arag} at the site of calcification: (1) the enzyme carbonic anhydrase catalyzes the hydration of CO_2 and formation of HCO_3^- (Allemand et al. 2004) but the associated production of protons would then reduce the CO_3^{2-} concentration; (2) Ca^{2+} is transported to the site of calcification via Ca^{2+}-ATPase and accompanied by the removal of H^+ (McConnaughey and Whelan 1997; Allemand et al. 2004). With the later mechanism, removal of H^+ increases *p*H within the site of calcification and promotes diffusion of CO_2

across the calcioblastic ectoderm increasing both Ω_{arag} and DIC (Cohen and McConnaughey 2003). The control of *p*H by removal of H^+ from the calcification site helps to explain how corals can tolerate and calcify at low *p*H conditions (Cohen and Holcomb 2009), and could provide insight into the response of corals to changes in seawater carbonate chemistry.

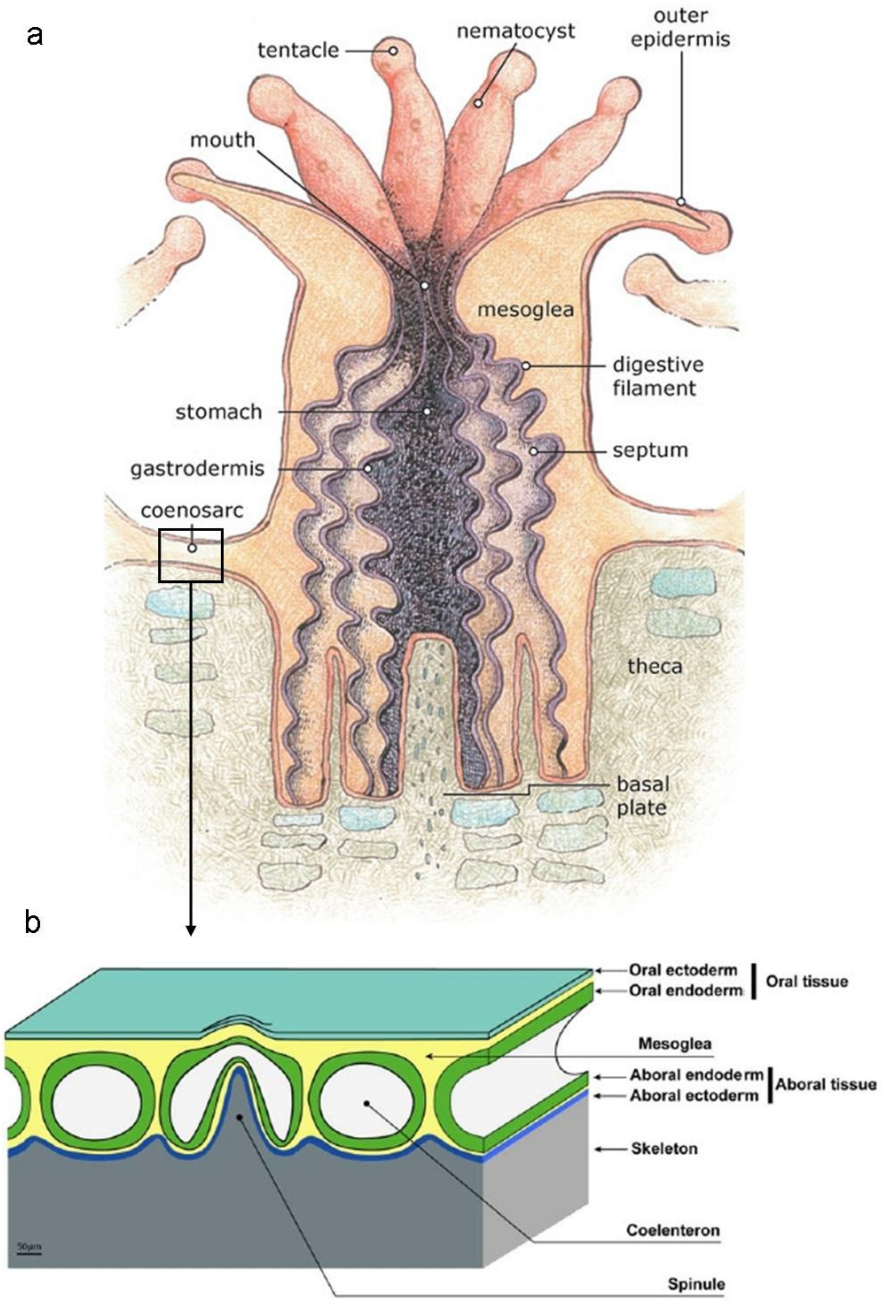

Figure 1-2. *(a) Anatomy of a typical coral polyp (http://coralreef.noaa.gov; Gini Kennedy). (b) Schematic of the coral tissue showing the ectodermal and endodermal layers separated by the mesoglea (modified from Allemand et al. 2004).*

Calcification by corals and photosynthesis by the zooxanthellae are physiologically linked processes, as evidenced by coral calcification rates being usually three times higher in the day than at night (Gattuso et al. 1999a). However, details of the relationship between calcification and photosynthesis remain controversial with several links proposed (Cohen and McConnaughey 2003; Allemand et al. 2004). Photosynthesis is a primary source of ATP required for energy dependent processes like calcium transport to the site of calcification (Al-Horani et al. 2003) and may further stimulate calcification by supplying food (Muscatine 1990) and oxygen in support of coral respiration (Rinkevich and Loya 1984). Furthermore, modification of the DIC equilibrium by photosynthesis could promote carbonate precipitation by lowering the pCO_2 in the coral tissue (Goreau 1959). Alternatively, it has been postulated that excess H^+ produced by calcification could be neutralized by the OH^- produced by the zooxanthellae (Allemand et al. 2004). It has also been proposed that photosynthesis contributes to the synthesis of the organic matrix into which aragonite crystal are deposited (Gautret et al. 1997; Cuif et al. 1999).

Marubini and Davies (1996) suggested that photosynthesis and calcification compete for a limited source of DIC, so that under nutrient-rich conditions the algae population increases and calcification decreases. However, Holcomb et al. (2010) found that under high nutrient and high CO_2 conditions, the excess DIC can alleviate the competition between photosynthesis and calcification. In this sense, some of the negative effects on coral calcification caused by ocean acidification could be reduced by the accompanying increase in DIC. It follows that the response of calcification to changes in CO_2 depends on multiple factors, including the Ω_{arag}, light, temperature, DIC, nutrient levels (Holcomb et al. 2010), as well as factors that influence the internal pH control at the site of calcification (Cohen and Holcomb 2009; Ries et al. 2009; Ries 2011; Trotter et al. 2011).

1.3.7. Effects of elevated CO_2 on coral reef communities

In addition to physiological changes of the coral and zooxanthellae, there is also the community level response to increased CO_2. This can be especially important in semi-isolated environments (e.g. enclosed lagoons) and/or highly productive areas where biological processes actively modify the seawater chemistry (e.g. Hinga 2002; Andersson et al. 2005; Bates et al. 2010; Anthony et al. 2011; Drupp et al. 2011). Little is known about

the impact of ocean acidification in coastal environments, where organisms are subject to natural variations as large as one *p*H unit on both seasonal and daily timescales (Hinga 2002). Reconstructed seawater *p*H from coral $\delta^{11}B$ suggests that there is significant sub-annual, interannual, and also decadal variability of around 0.3 *p*H units in the coral reef systems that have been studied to date (Pelejero et al. 2005; Wei et al. 2009). These variations are significantly larger than the long-term trend in surface ocean *p*H (i.e. -0.020 *p*H units per decade) and also the open ocean seasonal variability of 0.1 *p*H units (Pelejero et al. 2010). Coral reef metabolism influences the seawater chemistry and is controlled by the balance between calcification-dissolution and production-respiration (Gattuso et al. 1995; Bates et al. 2010). Respiration of organic matter and calcification shifts seawater *p*H to lower values through the generation of CO_2, whereas photosynthesis removes CO_2, shifting the equilibrium towards higher *p*H values. Changes in seawater *p*H are mainly the result of the uptake and release of CO_2, but are also affected by the metabolic uptake and release of nutrients. For instance, assimilation of NO_3^- increases the alkalinity and *p*H whereas assimilation of NH_4^+ has the opposite effect (Gattuso et al. 1999b). The magnitude of metabolically driven changes in *p*H also depends on the rate of equilibration with the atmosphere (Hinga 2002), and with the action of waves and wind promoting faster exchange.

1.3.8. Coastal environments and the effect of river plumes on carbonate chemistry: the Burdekin River

The GBR is the world's largest coral reef ecosystem. It extends along the continental shelf of the northeastern Australia margin for a distance of 2300 km, and includes 3,244 catalogued reefs that cover an estimated area of 20,000 km^2 or 10% of the continental shelf (Hopley 1982; Furnas 2003). The majority of these reefs are freestanding platform reefs that are located in the outer waters of the continental shelf generally immersed in low nutrient, clear oceanic waters (Furnas 2003; Hopley et al. 2007). However, about 900 reefs are fringing reefs, proximal to the mainland or islands near the coastline (Hopley et al. 1989; Furnas 2003; Devlin and Brodie 2005) and subject to a range of terrestrial influences. The northern part of the GBR has the highest reef density and compromises a sequence of ribbon reefs, and, as the shelf is narrow, most of these reefs are influenced by terrestrial runoff. The central area, categorized as "Dry tropics", has the lowest reef density of the

GBR and is affected by the largest river discharge (Devlin et al. 2001; Devlin and Brodie 2005). Broad widely distributed patch reefs characterize the southern GBR, where the shelf widens to 200 km and the majority of reefs are well separated from land, making them less susceptible to terrestrial influences (Furnas and Mitchell 1997).

The continental drainage basins draining into the GBR between the tip of Cape York and Fraser Island have an aggregate area of 425,000 km^2 (Furnas and Mitchell 2001). This study focuses on reefs from the central GBR, which are mainly affected by the Herbert River and Burdekin River basins. The Burdekin River has the second largest drainage area (covering 130,000 km^2) and largest mean annual flow (9.7 billion m^3 yr^{-1}) in the GBR Marine Park with annual discharge reaching up to 50 km^3 during the biggest flood events (King et al. 2001; Furnas 2003). The Burdekin River episodically floods to some degree in most years, but the duration and intensity of the flood events, and therefore river runoff, are characterized by high year-to-year and decadal variability (Furnas 2003; Lough 2007).

Most of the river discharge (70%) occurs during the wet-season in the form of flood events limited to the Austral summer (December-March), with the peak in river discharge following discrete storms or cyclonic events (Furnas and Mitchell 2001; King et al. 2001; Lough et al. 2002; Furnas 2003). After the wet season little or no freshwater discharge occurs (Devlin and Brodie 2005). The discharge from the river forms a low salinity buoyant plume (usually 10-20 m thick) which can extend for hundreds of kilometers along the coast (Figure 1-3 and Figure 1-4) and can last up to several weeks (Devlin et al. 2001). The plume is progressively dispersed (usually drifting in a northward direction) and mixed by the winds and currents (King et al. 2001; Furnas 2003). As some inner-shelf reefs and mid-shelf reefs are periodically exposed to these low salinity waters, their habitants are susceptible to major river runoff events. River runoff is the main input of terrestrial material and contaminants on the GBR (Devlin et al. 2001; Brodie et al. 2012b); this is reflected in higher concentrations of dissolved nutrients, particulate matter and plankton biomass near the coast (Furnas 2003). In the case of the Burdekin River 98% of the nutrient load is discharged during flood events (Brodie et al. 2010b). Despite being short lived, monitoring of the water quality (e.g. suspended particulate matter and chlorophyll level) indicates that most flood plume events can have impacts that last far longer than the duration of the plume intrusion (Devlin et al. 2001; Devlin et al. 2008). As the plume

waters are transported away from the river mouth SPM decreases while dissolved nutrients remain high; the combination of increased light and dissolved nutrients leads to an increase in phytoplankton mass (Devlin et al. 2008). The levels of chlorophyll-a (an indicator of phytoplankton biomass) are higher in waters of the central and south GBR adjacent to catchments with agricultural development compared to those less disturbed catchments typical of the northern regions of the GBR (Brodie et al. 2007).

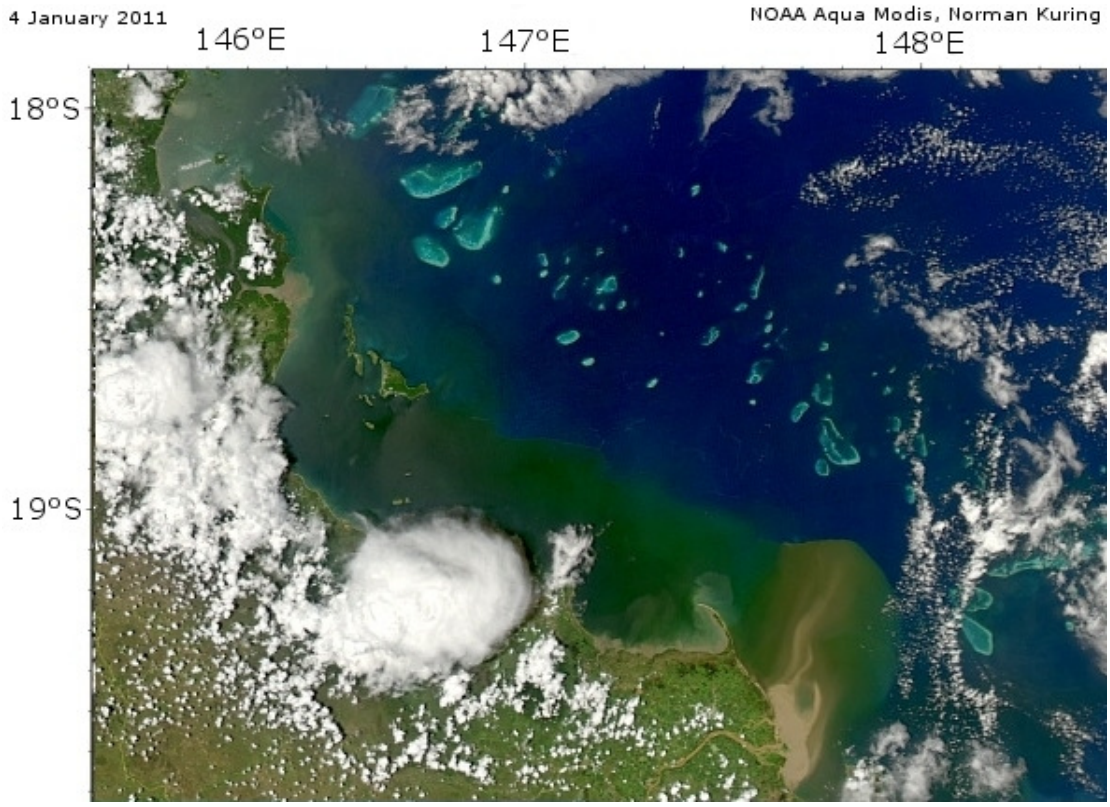

Figure 1-3. *Satellite image from the 2011 flood event showing the Burdekin River plume.*

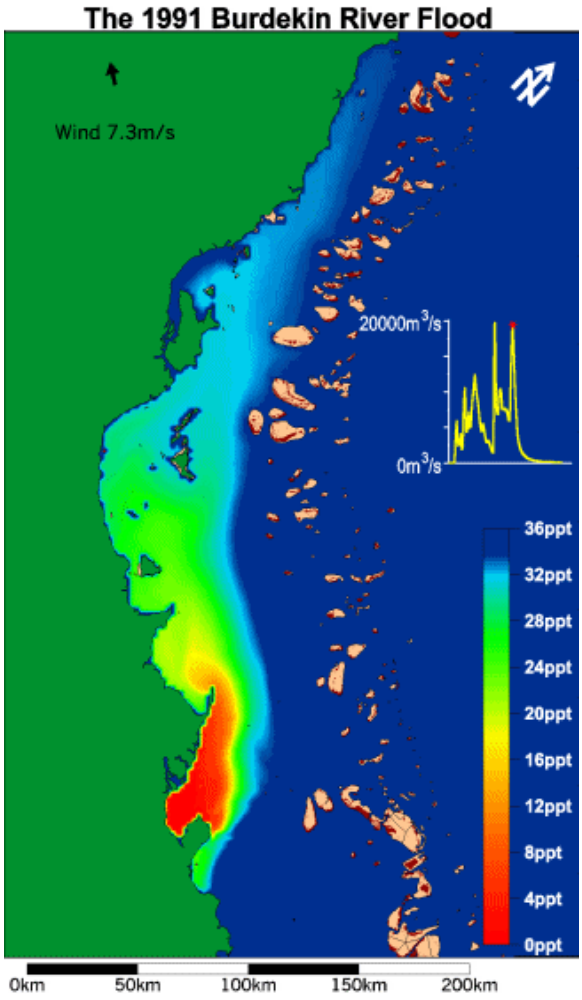

Figure 1-4. *Salinity map of the simulation for the 1991 strong flood of the Burdekin River after 63 days of flooding (after King et al. 2002).*

Changing land-use practices since the arrival of European settlers has produced an increase in discharge of terrestrial material from the Burdekin River into the GBR (Furnas 2003; McCulloch et al. 2003; Lewis et al. 2007). Because river plumes are generally acidic (lower *p*H) relative to the ocean waters, this could affect the development of coastal calcifying organisms (i.e. corals, shellfish). Salisbury et al. (2008) have suggested that a reduction in Ω in the Gulf of Maine to levels around 1.5 during river discharge events is a potential threat to shellfish of that area. These authors also estimated Ω from salinity for several rivers plumes of the world (Figure 1-5). Based on their modeling and considering that salinity values close to the inner-shelf reefs off the coast from Townsville can be as low as 24 ppt during large Burdekin flood events (King et al. 2001; Figure 1-4) Ω_{arag} could be reduced to values close to 3 for these reefs. This is below the limit of ~3.2 suggested for coral reef development (Kleypas 1999; Hoegh-Guldberg et al. 2007). Salisbury et al. (2008)

suggest that the potential effect of low Ω of river plumes on calcifying organisms could be exacerbated as atmospheric CO_2 increases and the patterns of river discharge change. It follows that the episodic discharge of acidic waters from rivers to inner-shelf corals of the GBR could be adding to the stress caused by global acidification.

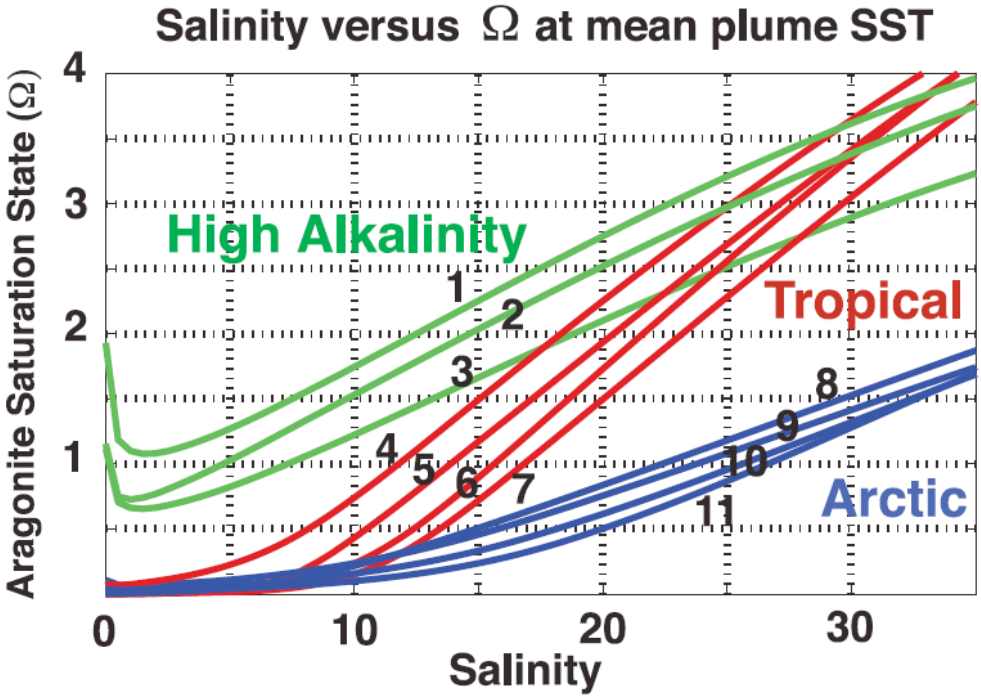

***Figure 1-5**. Estimated Ω_{arag} vs. salinity for several major world river 1, Mississippi; 2, Yangtze;3, Nile; 4, Congo; 5, Amazon; 6, Mekong; 7, Orinoco; 8, Yenisey; 9, Amur; 10, MacKenzie; 11, Ob. The different colors are used to denote the strong grouping of rivers by alkalinity and latitude (after Salisbury et al. 2008).*

1.3.9. Boron isotopes in marine carbonates

1.3.10. Past changes from $\delta^{11}B$ as a seawater pH paleo-proxy

To make predictions about the impact of future increases in atmospheric pCO_2 and accompanying acidification of the surface ocean, it is important to determine the baseline natural variability. Unfortunately, *p*H measurements are sparse to non-existent and long time-series in the Pacific are limited to the HOTS open ocean station in Hawaii (Dore et al. 2009). The longest time-series for seawater carbonate parameters in the GBR comes from Heron Island where monitoring commenced in 2009 (http://www.pmel.noaa.gov/co2/) Interest in boron isotope ($\delta^{11}B$) composition of marine carbonates has grown in recent

years, as a means of constraining past changes in the global carbon cycle and atmospheric CO_2 (e.g. Hönisch et al. 2003; Pelejero et al. 2005; Wei et al. 2009). The $\delta^{11}B$ composition of different biogenic carbonates has been used to estimate changes in *p*H of the ocean. This technique has been applied to foraminifera (Spivack et al. 1993; Sanyal et al. 1997; Foster 2008; Hönisch et al. 2009; Rae et al. 2011; Henehan et al. 2013). Its application to corals has been evaluated by Hönisch et al. (2004), Reynaud et al. (2004) and Trotter et al. (2011), and has been successfully used for seawater *p*H reconstructions using massive *Porites* corals by Pelejero et al. (2005), Liu et al. (2009), Wei et al. (2009), Douville et al. (2010) and Shinjo et al. (2013). Reported [B] in corals vary from ~40 to 80 ppm with a typical value of 50 ppm, about 5 times higher than in foraminifera (Vengosh et al. 1991; Hemming and Hanson 1992; Gaillardet and Allègre 1995). The high [B] found in coral skeletons, in addition to their fast and continuous growth rates, makes corals ideal for reconstructing past *p*H changes in seawater (Hemming et al. 1998)

The $\delta^{11}B$ seawater *p*H paleo-proxy relies on the preferential incorporation in marine carbonates of the isotopically lighter $B(OH)_4^-$ over the $B(OH)_3$ species and the *p*H control on the relative species concentration and isotopic distribution (Hemming and Hanson 1992; Hönisch et al. 2004). Because changes in seawater *p*H depend on the HCO_3^-/CO_2 ratio, and the HCO_3^- content of seawater is essentially constant, at least on short timescales ($<10^6$ year), the changes in $\delta^{11}B$ composition can be interpreted as reflecting variations in the atmospheric pCO_2 (Hemming et al. 1998). Accordingly, reconstructions of past seawater *p*H variations can help to better understand the effects and implications of increased atmospheric pCO_2 in the oceans. In the same way the information from this proxy can contribute to a better understanding of the effects of ocean acidification on corals reefs.

1.3.10.1. <u>Boron in seawater</u>

Dissolved B in seawater comprises two dominant species: boric acid $B(OH)_3$ and the borate anion $B(OH)_4^-$ (Hershey et al. 1986). At low concentrations, the distribution of these aqueous B species is related to *p*H though the equilibrium reaction:

$$B(OH)_3 + H_2O \leftrightarrow B(OH)_4^- + H^+ \text{ (Hemming and Hanson 1992).}$$

The relative proportion of the two species is dependent on *p*H according to the relationship:

$$\frac{\left[B(OH)_4^-\right]\left[H^+\right]}{\left[B(OH)_3\right]} = 10^{-pK_B}$$ (Gaillardet and Allègre 1995)

with the dissociation constant of boric acid (pK_B) defined by a value of 8.597 at T=25 and S=35 (Dickson 1990). At low *p*H, virtually all B in seawater exists as the $B(OH)_3$ species; at high *p*H B dominantly occurs as the $B(OH)_4^-$ species (see Figure 1-6). In seawater at a typical modern *p*H of 8.2, ~80% of the B is present as $B(OH)_3$ and ~20% as $B(OH)_4^-$ (Hemming and Honisch 2007).

Boron has two stable isotopes, ^{10}B and ^{11}B, with abundances of 19.82% and 80.18%, respectively (Barth 1993; Coplen et al. 2002). Variations in natural samples are given in conventional δ notation, such that:

$$\delta^{11}B(‰) = \left[\left(R_{sample} / R_{standard}\right) - 1\right] \times 10^3$$

(relative to NBS SRM-951 standard), where R = $^{11}B/^{10}B$ (Barth 1993). The $^{11}B/^{10}B$ ratio of the NBS SRM-951 standard is certified as 4.04362±0.000137 (2σ) for the Positive Thermal Ionization (PTI) methods (Catanzaro et al. 1970). The isotopic exchange reaction between the two B species is given by the equilibrium reaction:

$$^{10}B(OH)_3 + {}^{11}B(OH)_4^- \leftrightarrow {}^{11}B(OH)_3 + {}^{10}B(OH)_4^-$$

for which the originally determined fractionation factor $\alpha_{(B3\text{-}B4)}$ = 1.0193 at 25°C (Kakihana et al. 1977). The borate anion $B(OH)_4^-$ is therefore enriched in ^{10}B relative to boric acid (Kakihana et al. 1977). This isotopic offset between the B species is the result of differences in the number and modes of vibrational energies (Kakihana et al. 1977). After analyzing most of the experimental data to date, Barth (1993) concluded that the isotopic exchange between B species, mainly $^{10}B(OH)_4^-$ and $^{11}B(OH)_3$, controls the B isotopic fractionation and isotopic variations in nature (Kakihana et al. 1977; Palmer et al. 1987; Spivack and Edmond 1987; Vengosh et al. 1991). The fractionation factor has recently been theoretically recalculated: $\alpha_{(B3\text{-}B4)} \geq 1.030$ (Zeebe 2005) and $\alpha_{(B3\text{-}B4)}$=1.026-1.028 (Rustad et al. 2010), and experimentally determined: $\alpha_{(B3\text{-}B4)}$ = 1.0272±0.0006 (Klochko et al. 2006).

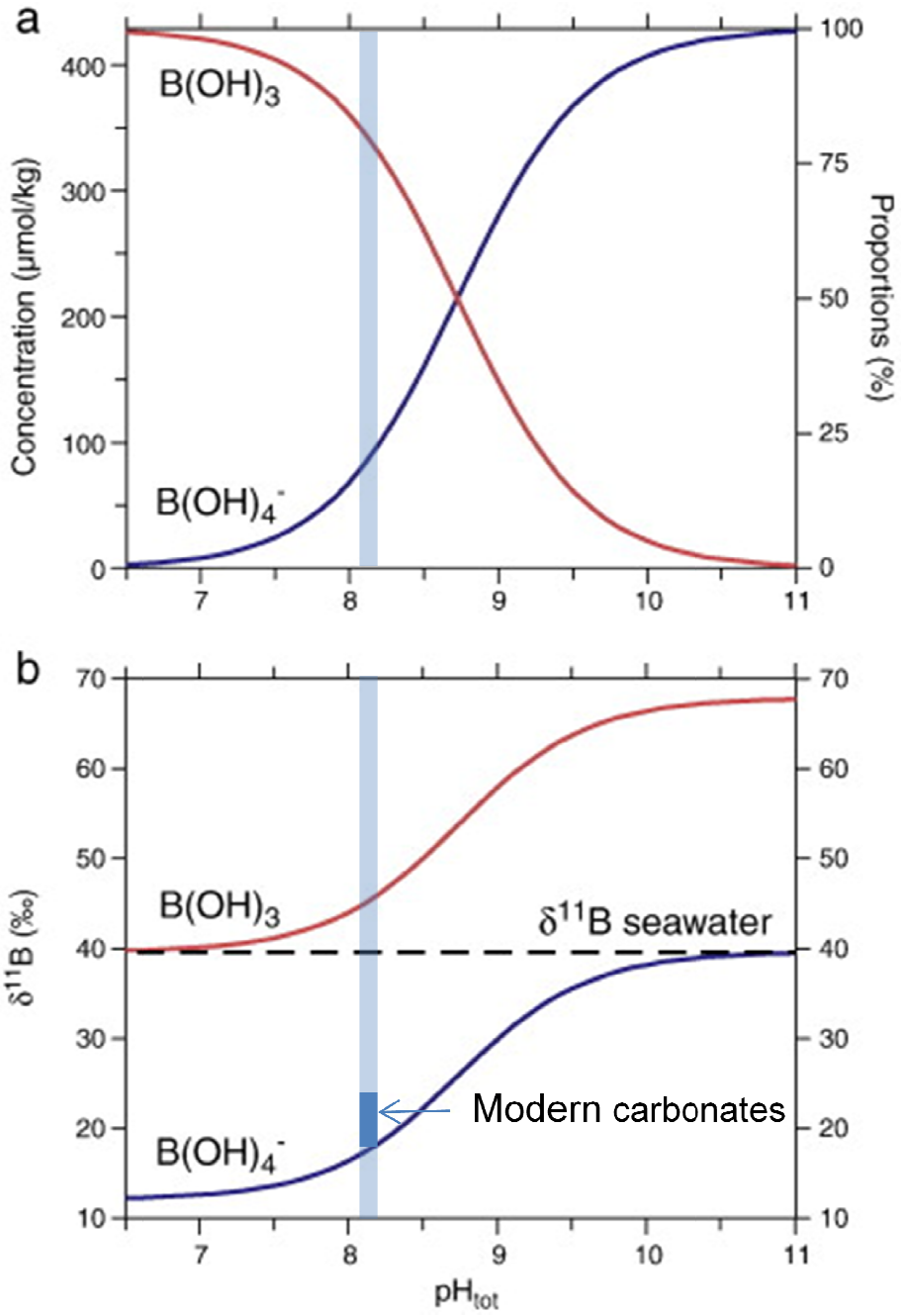

Figure 1-6. *(a) Bjerrum plot for the concentration of B species vs seawater pH. (b) Boron isotopic composition of individual aqueous species vs pH calculated from the fractionation factor from (Klochko et al. 2006) with the typical values found in modern marine carbonates (after Rae et al. 2011). Values at approximately present day ocean pH of 8.2 are highlighted (blue line). The isotopic composition of the individual B species vs. pH is calculated from the proportion of species and the isotope exchange reaction (Vengosh et al. 1991; Hemming and Hanson 1992).*

Seawater is enriched in ^{11}B by 40‰ relative to continental material and has a $\delta^{11}B$ of +39.5‰ relative to NBS SRM 951 (Spivack and Edmond 1987; Foster 2008). This heavy

isotopic composition results from the isotopic fractionation between B species, and the preferential adsorption onto detrital clays, secondary minerals formed during the low-temperature alteration of oceanic crust, and carbonates minerals (Palmer et al. 1987; Barth 1993). Because the dominantly adsorbed species on active surfaces are the negatively tetrahedral charged species, the marine environment becomes enriched in the isotopically heavier trigonal species (Barth 1993).

1.3.10.2. Boron in marine carbonates

The $\delta^{11}B$ of marine carbonates is typically ~24‰, which is similar to the $B(OH)_4^-$ composition of seawater (Hemming and Hanson 1992; Gaillardet and Allègre 1995). The low $\delta^{11}B$ values found in marine carbonates strongly implies the preferential incorporation of $B(OH)_4^-$ (Hemming and Hanson 1992; Barth 1993).

^{11}B MAS NMR spectroscopy of synthetic aragonite and of aragonitic coral samples indicates the presence of tetrahedrically coordinated BO_4 groups in aragonite (Sen et al. 1994). This is consistent with B being structurally incorporated rather than present in fluid inclusions or trace mineral phases (Sen et al. 1994). Experimental results further indicate that the composition of the synthetic minerals is identical to the $\delta^{11}B$ of the $B(OH)_4^-$ species in the parent solution (Hemming et al. 1995). Since the $\delta^{11}B$ composition of the precipitated mineral increases with *p*H, it is then expected that the incorporation and isotopic fractionation in the aragonite will be strongly correlated to *p*H (Hemming et al. 1995).

Experimental studies show that the increase of total [B] in the parent fluid results in an increase of the bulk [B] in precipitated calcium carbonates (Kitano et al. 1978; Hemming et al. 1995). Boron is incorporated at two to five times higher concentrations in aragonite than calcite for a given fluid [B] (Kitano et al. 1978; Hemming et al. 1995), consistent with differences in substitution site size coordination between calcite and aragonite. ^{11}B MAS NMR spectroscopy (Sen et al. 1994) and synthetic growth of aragonite and calcite under controlled laboratory conditions (Hemming et al. 1995) suggests that B in calcite is present principally in trigonal coordination, whereas tetrahedrally coordinated species dominate in aragonite. If $B(OH)_4^-$ is the predominant species that interacts with carbonate surfaces a

change in coordination of B is necessary for incorporation into calcite, whereas no such change is required for incorporation into aragonite. This change in coordination should be energetically or kinetically hindered and reflected in the partitioning behavior. This is consistent with observations that B is preferentially incorporated in aragonite relative to calcite and with the $\delta^{11}B$ of these carbonates (Hemming et al. 1995). More recent MAS NMR experiments by Klochko et al. (2009) suggest that in addition to the tetrahedral species some of the ^{11}B enriched trigonal species may be incorporated into the carbonate lattice. This would explain the enrichment in ^{11}B observed in biogenic carbonates (Klochko et al. 2009) in respect to re-calculated α values of Klochko et al. (2006). This supports previous hypotheses for the enrichment in ^{11}B observed in marine carbonates, modifications of the *p*H at the site of calcification, and B partitioning in carbonates during mineralization (Klochko et al. 2006).

The incorporation of B as $B(OH)_4^-$ into carbonate has been suggested to occur via substitution of the CO_3^{2-} group in the carbonate lattice by HBO_3^{2-} (Vengosh et al. 1991; Hemming and Hanson 1992). The HBO_3^{2-} species has been favored because its size and charge characteristics are most similar to the carbonate ion (Hemming and Hanson 1992). The trigonal coordination observed in calcite is consistent with the postulated HBO_3^{2-} species, but inconsistent with NMR observations on aragonite of BO_4 groups (Sen et al. 1994). Klochko et al. (2009) report similar relative proportion of boron species in two coral aragonites and one foraminiferal calcite, with BO_3 and BO_4 groups representing roughly 36–46% and 54–64%, respectively. These authors propose a three stage-model of B incorporation into carbonates. This model incorporates the formation of transition $B(OH)_2CO_3^-$ isomers described by Tossell (2006) that break down to simpler forms and coordination of BO_3 and BO_4 as they are incorporated into the carbonate structure. This could help explain the detection of BO_3 groups by NMR (Klochko et al. 2009).

If the incorporation of B (as HBO_3^{2-}) occurs by substitution of CO_3 a thermodynamic coefficient for B partitioning between the solution and the precipitated solid can be defined as:

$$\left(\frac{Ca(HBO_3)}{CaCO_3}\right)_{solid} = K_D\left(\frac{[B(OH_4^-)]}{[HCO_3^-]}\right)_{seawater}$$ (Gaillardet and Allègre 1995)

This suggests that the [B] of marine carbonates depends on variations of $B(OH)_4^-$ and HCO_3^- in the seawater, and therefore on pH and the total inorganic carbon ($\sum CO_2$) content of seawater (Gaillardet and Allègre 1995).

1.3.11. Factors affecting B isotope distribution and incorporation in corals

1.3.11.1. Boron composition of seawater

Boron has a concentration of 4.5 ppm and isotopic composition of 39.6‰ at S = 35 and T = 25°C (Spivack and Edmond 1987; Hemming and Hanson 1992; Lemarchand et al. 2000; Foster et al. 2010). Boron flux estimates indicate a residence time in the oceans of 14 Myr (Lemarchand et al. 2000), this is around 7 Myr less than the previous value of 21 Myr reported by Spivack et al. (1993). However, given the analytical uncertainties, the $\delta^{11}B$ of the oceans can only be considered constant over the last 3 Myr (Lemarchand et al. 2000). This indicates that during this time interval the variations in marine carbonates can be interpreted as changes in the isotope fractionation between seawater and precipitated carbonate minerals due to changes in seawater *p*H (Spivack et al. 1993).

1.3.11.2. Kinetic fractionation of B isotopes

If only $B(OH)_4^-$ is absorbed onto the growing crystal surfaces of the aragonite skeletons of corals, kinetic fraction might occur because the lighter $^{10}B(OH)_4^-$ molecules are adsorbed more readily than the heavier $^{11}B(OH)_4^-$. This requires growing layers of $CaCO_3$ to form fast enough to bury the light B beneath subsequent layers before further exchange can take place. Alternatively, if the exchange with dissolved B occurs and is sufficiently rapid, no kinetic isotopic effects are expected. Zeebe et al. (2001) have evaluated the kinetic isotopic

effects during calcification as a function of the time scale for crystal growth and the time scale for equilibration between the dissolved B species. Given that relaxation times calculated for B compounds are around 100 μs and that the time for crystal layer growth ranges from 0.5 s to 13 h, it was calculated that kinetic isotope fractionation effects are unlikely (Zeebe et al. 2001), and that the $\delta^{11}B$ of the carbonates should be independent of growth rates.

1.3.11.3. Vital effects in the incorporation of B into the coral skeleton

One of the main concerns when working with geochemical tracers in biogenic carbonates is the possible existence of biological effects on the incorporation of the tracers into the mineral structure (de Villiers et al. 1995; Meibom 2003; Weiner and Dove 2003; Cohen and Gaetani 2010). Hönisch et al. (2004) assessed the effects of light and feeding rate on corals, and found that $\delta^{13}C$ isotope and $\delta^{11}B$ isotope compositions do not show a clear relationship with these parameters. However, Al-Horani et al. (2003) found *p*H and $[Ca^{2+}]$ variations in the calcifying fluid, caused by illumination during the diurnal cycles, which suggest a coupling between the photosynthetic activity of the zooxanthellae and calcification. In considering these and their own results, Hönisch et al. (2004) suggest that once photosynthesis exceeds a threshold value and stimulates Ca^{2+}-ATPase activity, the enzyme system works at a constant rate, independent of light-level and photosynthetic rate. Hönisch et al. (2004) further suggest that the boron isotope composition in biogenic carbonate responds to external changes in seawater *p*H, supporting the use of $\delta^{11}B$ in corals as a proxy for *p*H changes in seawater.

Reynaud et al. (2004) studied the effect of temperature on the $\delta^{11}B$ of the coral skeleton by culturing *Acropora* sp. corals under two different temperatures (25 and 28°C) and pCO_2 conditions (~440 and ~720 ppmv). They observed a *p*H effect, but no temperature effect on the coral $\delta^{11}B$ composition. Based on similarity of the $\delta^{11}B$ values found in corals and seawater $^{11}B(OH)_4^-$ $^{11}B(OH)_4^-$, these authors further suggest that corals do not significantly modify ambient seawater *p*H at the site of calcification These observations do not agree with the models for coral calcification by Cohen and McConnaughey (2003) and Allemand et al. (2004) or the experimental results from Al-Horani et al. (2003), Ries (2011) and Venn

et al. (2011), however, they can be reconciled if a different α value (e.g. Klochko et al. 2006) is used. The use of the correct α value is critical as it affects both the absolute calculated *p*H value and amplitude of variation (Reynaud et al. 2004; Wei et al. 2009; Trotter et al. 2011).

In order to precipitate aragonite, the Ω_{arag} should be greater than one. Corals grow aragonite skeletons hundreds of times faster than the rate at which inorganic aragonite precipitate from seawater with a *p*H of 8. It has been suggested that this reflects an increase in the Ω_{arag} up to a value of ~25 (Cohen and McConnaughey 2003; Ries 2011). This increase can be obtained by increasing the concentration of [Ca^{2+}] and/or [CO_3^{2-}] at the site of calcification (Cohen and McConnaughey 2003). Using microelectrodes beneath the subcalcioblatic layer Al-Horani et al. (2003) suggested that the *p*H at the calcification site is significantly elevated, with observed *p*H values of 8.13 during the night and 9.28 during the day. Following a similar procedure Ries (2011) reported an increase of 1.9 *p*H units at the site of calcification at a seawater *p*H of ~8.17. More recent values obtained by live tissue imaging *p*H-sensitive dyes suggest that a seawater *p*H of ~8.0 internal *p*H at the site of calcification is elevated by ~0.5 and ~0.2 *p*H units during light and dark conditions, respectively (Venn et al. 2011) and in average by 0.4 *p*H units Venn et al. (2013).

Models for elevating *p*H at the site of calcification and allowing the precipitation of aragonite at rates hundreds of times higher than from seawater *p*H, suggest that this can be achieved by importing Ca^{2+} to the site of calcification and removal of protons via the Ca^{2+}ATPase (Cohen and McConnaughey 2003; Allemand et al. 2004). Although the increase in [Ca^{2+}] is too small to significantly accelerate calcification, proton removal from the calcification site converts HCO_3^- to CO_3^{2-}, and increases the Ω_{arag} significantly. According to Cohen and McConnaughey (2003), a proton gradient of one *p*H unit can produce a 100-fold increase in the [CO_3^{2-}] at the calcifying site. Accordingly, it is expected to find higher $\delta^{11}B$ values in the calcifying fluid.

The $\delta^{11}B$ curves in corals seem to mimic the shape of the theoretical curve for borate in seawater. Hönisch et al. (2004) noted a constant negative offset in the $\delta^{11}B$ compositions of

corals relative to the theoretical $B(OH)_4^-$ curve of Kakihana et al. (1977). Krief et al. (2010) subsequently showed this offset to be much greater when referenced to the recalibrated $B(OH)_4^-$ curve of Klochko et al. (2006), which is characterized by a steeper slope and lower values. This was confirmed by Trotter et al. (2011) who showed that all $\delta^{11}B$ data available from corals shows an offset to more positive $\delta^{11}B$ when compared to the Klochko et al. (2006) borate curve (Figure 1-7). This has been interpreted as a fractionation effect related to physiological processes known as 'vital effects' (Trotter et al. 2011). This offset can be reconciled if a process occurs that enriches the skeleton in the heavier isotope or if the *p*H is increased at the site of calcification (Krief et al. 2010). In the case of corals this has been attributed to the elevation of the internal *p*H at the site of calcification (Krief et al. 2010; Trotter et al. 2011; McCulloch et al. 2012a) in agreement with the *p*H observations. This ability of corals to up-regulate their *p*H at the site of calcification may help them mitigate the effects of ocean acidification (McCulloch et al. 2012a; Venn et al. 2013)

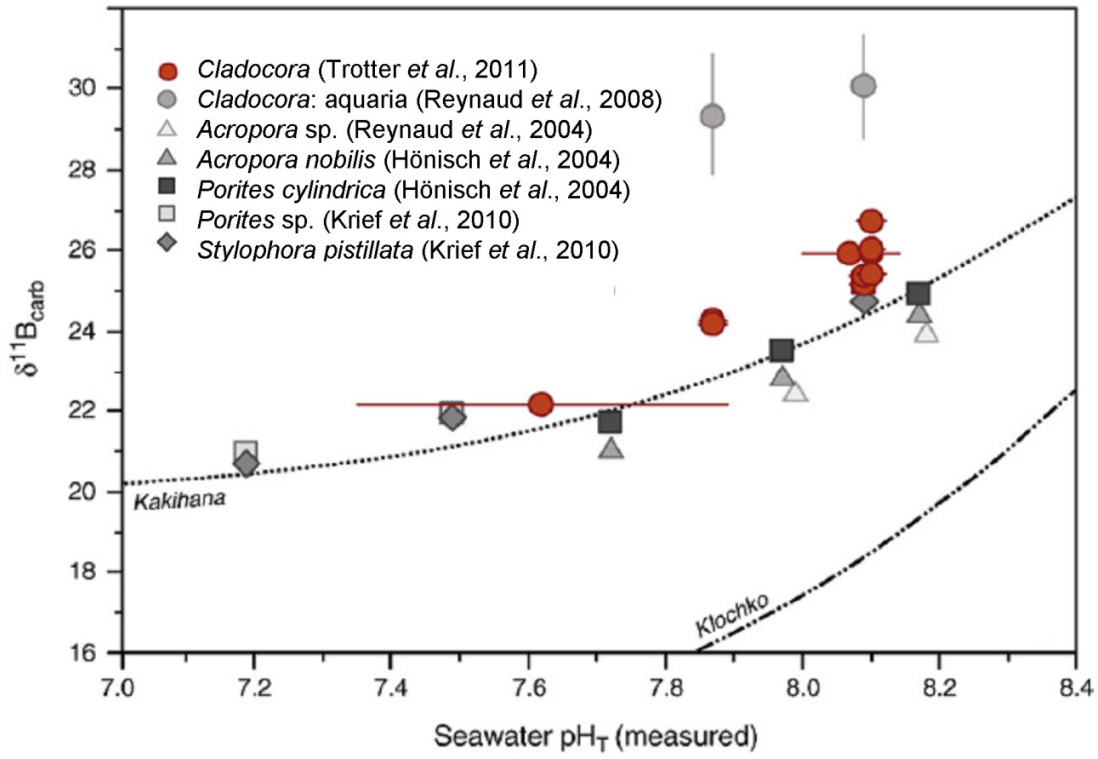

Figure 1-7. *Comparison of $\delta^{11}B$ for a suite of corals from the literature relative to seawater pH_T and borate reference curves. Error bars at ±1 SD (after Trotter et al. 2011).*

Ries (2011) proposed two scenarios to maintain the elevated *p*H at the site of calcification. In the first, a fixed amount of H^+ is removed while the ratio between the internal *p*H at the site of calcification and seawater *p*H varies. In the second, the internal *p*H at the site of calcification is maintained at a fixed ratio to the external seawater *p*H and therefore the amount of H^+ removed from the site of calcification varies. Experimental results for the coral *Astrangia poculata* seem to agree with this second scenario (Ries 2011). This is also consistent with the model proposed by Marubini et al. (2001) that the *p*H of the calcifying fluid is proportional to external seawater *p*H, and with studies that show that the $\delta^{11}B$ composition of *Porites* and other scleractinian corals varies with changes in seawater *p*H (Hönisch et al. 2004; Krief et al. 2010; Trotter et al. 2011; McCulloch et al. 2012a). In their recent work Venn et al. (2013) confirmed that the internal *p*H at the site of calcification follows the external changes in seawater *p*H. Trotter et al. (2011) proposed an approach to quantify the fractionation resulting from physiological processes that can be used to estimate seawater *p*H from $\delta^{11}B$ measured in corals. Trotter et al. (2011) specifically use the α value from Klochko et al. (2006) and adjust the pK_B to the ambient seawater temperature and salinity of each sample to calculate the *p*H. The internal *p*H at the site of calcification is then adjusted using specific calibration equations based on the difference between the estimated seawater *p*H from $\delta^{11}B$ measured in coral and measured seawater *p*H.

1.3.12. Summary

In general this review has highlighted the wide range of factors controlling coral growth. A variety of responses are observed in studies of coral growth parameters and their relationship to environmental parameters. A number of studies show decreasing trends in coral growth in recent times, but other studies show no significant change, slight increase or mixed response. Despite differences a general pattern emerges with higher nutrients, temperature and levels of light linked to an increase in linear extension and a decrease in density of massive corals. However, apparent threshold levels exist for these environmental parameters after which the rates of calcification are reduced. Increased pollution, wave energy and terrigenous influences (associated with reduced salinity, and increased sedimentation, turbidity and nutrient concentration) are generally related to a decrease in coral growth. The specific environmental settings, differences between species and regional

adaptability are suggested as a possible explanation for some of the differences between studies. There is general consensus in the literature that as oceans continue to become more acidic this will have negative effects on corals particularly on the calcification process; however, it is possible that the negative effects will be attenuated by the corals up-regulation of their internal *p*H at the site of calcification. The calcification history of corals is stored in the skeleton as density or luminescent bands. Corals also incorporate a wide number of geochemical proxies, including $\delta^{11}B$ which can be used to reconstruct seawater *p*H. Together this information can potentially be used both to reconstruct past environmental information and as an indicator of how coral calcification is affected by changes in the environment.

2. Study area and general methodology

2.1. Study area and settings of the central GBR

This study focuses on the region of the central GBR located between longitude 146.2-147.4°E and latitude 18.10–19.5°S. As described in section 1.3.8 this area of the central GBR is subject to periodic terrestrial runoff, principally from the Burdekin River generating buoyant freshwater plumes that are transported along the coast (Wolanski and Jones 1981). The currents result from the predominately south-east wind regime (Brodie et al. 2007) and the Coriolis force causes river plumes to travel northward from Cape Upstart near the Burdekin River mouth to Innisfall located 250 km north (Wolanski and Jones 1981). As a result the effects from the plumes are usually constrained to the area close to the coast but occasionally can extend 100 km offshore (Devlin et al. 2001; King et al. 2001). The effect of the river plumes are reflected as luminescent bands in the skeletons of massive corals (Isdale 1984), with the intensity of the luminescent bands directly related to the magnitude of the river flow (Lough et al. 2002; Lough 2007). There is also an inflow from the Coral Sea that occurs around the central GBR, which allows upwelled water from the deeper continental slope on the outer GBR to spread quickly across the GBR shelf and may protect coral reefs by preventing river plumes from spreading onto the outer shelf (Brinkman et al. 2002). Overall the cross-shelf flows are weaker than south-north currents; as a result inner-shelf waters are somewhat isolated from the outer shelf (Brodie et al. 2007). Advective processes appear to be more significant than tidal flushing by the ocean and classical estuarine circulation in the lagoon, even in flood conditions (Wolanski and Jones 1981).

The seasonal climate in the GBR and adjacent land area is dominated by the south-easterly trade wind circulation and the Australian summer monsoon westerly circulation (Sturman and Tapper 1996; Lough 2007). This effectively divides the year in two seasons a warm/wet summer from October to March and cool/dry winter from April to September, Based on this seasonality the year can be more properly defined from October-September (Lough 2007). The wet season is dominated by monsoonal rainfall, which brings ~80% of the annual rainfall and occasional tropical cyclone activity (Wolanski and Jones 1981). Over the past 100 years no significant change in either rainfall or river discharge is

observed towards wetter or drier conditions but is characterized by considerable interannual and decadal variability (Lough 2001; Lough 2007). Interannual and decadal variability in rainfall and river discharge is modulated by El Niño–Southern Oscillation (ENSO) events and the Pacific Decadal Oscillation (Lough 1994; Lough 2007). Annual river runoff of the Burdekin River can vary between 3% and 300% of the mean annual value of 9.7 x10 m^3 (Wolanski and Jones 1981). El-Niño (La-Niña) years are associated with weaker (stronger) summer monsoon circulation, which results in reduced (increased) rainfall, river flow and tropical cyclone activity (Lough 2001; Lough 2007).

Sea surface temperature (SST) shows well defined seasonal cycles (Furnas and Mitchell 1997). The annual range of variability in SST at the outer-shelf Myrmidon Reef is 4.8°C with a daily mean average reaching a minimum of 24°C in August and a maximum of 29°C in February with significant cross-shelf gradients (Lough 2001). Temperature is a major control of biological productivity and nutrient cycling in the GBR (Furnas and Mitchell 1997). The major effects of ENSO on GBR are observed during La Niña events through an increase in freshwater inputs, reduced surface radiation and enhanced tropical cyclone activity (Lough 1994). Lough (1999) describes El Niño events as characterized by a two phase evolution of SST anomalies, with an intensification of seasonal variability; i.e. colder winters and warmer summers. The high variability that occurs between El Niño events indicates that the typical pattern may not be observed in any individual event (Lough 2001). Redondo-Rodriguez et al. (2012) found that 'classic' ENSO events have a strong signature in the atmospheric circulation but are not consistently associated with summer SST anomalies in the northern GBR. In contrast, these authors found El Niño Modoki to be associated with negative summer SST anomalies in the northern GBR, and anomalous warming during La Niña Modoki, with no relationship found in the southern GBR. An El Niño Modoki event is characterized by maximum warming in the central equatorial Pacific associated rather than in the eastern equatorial Pacific, as during a 'classic' El Niño event (Ashok et al. 2007). Since the beginning of the 20th century temperatures have steadily increased in the central GBR, with annual SST increasing by 0.5°C, maximum SST by 0.3°C and minimum SST by 0.8°C (Furnas and Mitchell 1997).

The shelf in the GBR is relatively shallow, gradually deepening to 40 to 60 meters toward the shelf edge. Much of the lagoon, defined as the channel between inland and the mid-

shelf, is less than 50 m in depth (Wolanski 2001; Steinberg 2007). In the central region (18°S) the shelf widens to 110 km and slopes to a depth of around 100 meters (Steinberg 2007). In this study the reefs are divided into inner, mid and outer-shelf reefs according to three distinct shelf-parallel regions or zones coinciding with percentage distance from shore, water depth and surface sediment facies (Belperio 1983; Belperio and Searle 1988; Lough et al. 2002). The inner-shelf zone is located within 0-26% of the distance across the shelf, encompasses depths from 0-20 meters and is dominated by muddy terrigenous sediments. The mid-shelf zone is located within 26-100% of the distance from shore, with water depths of 20-40 m and is characterized by a mix of carbonate and siliciclastic sediments of terrigenous origin. The outer-shelf zone is located 60-100% of the distance from shore, has a water depth 40-100 m and is dominated by carbonate sediment (Mathews et al. 2007). The main reef matrix is located in the area between 30 km from the coast and the shelf break and consists of widely scattered reefs with deep passages (>40 m) between them (Wolanski and Pickard 1985).

In the inner-shelf region, coral reefs are subject to relatively large temperature variations and degraded water quality due to frequent flood events; in comparison, the mid-shelf region is a more stable and sheltered environment, affected by only some large river flood events (Lough et al. 2002; Furnas 2003). Outer-shelf reefs are subject to a more energetic physical environment and periodic shelf-break upwelling (Furnas and Mitchell 1996; Berkelmans et al. 2010). For example, during Tropical Cyclone Ingrid (2005) wave heights were three times higher on the outer-shelf than on inner-shelf areas (Fabricius et al. 2008). Wave action is the main mechanism for sediment re-suspension; non-cyclonic wave re-suspension is only significant in the inner-shelf area, seldom occurring in the mid-shelf. According to Orpin and Ridd (2012) exposure times and concentrations of suspended sediment carried by river plumes are an order of magnitude lower at the reefs compared to wave resuspension.

2.2. Reefs studied

This study focuses on seven corals reefs including the inner-shelf reefs of Magnetic Island, Havannah Island and Pandora, the mid-shelf reefs of Davies, Wheeler and Rib and the outer-shelf reef of Myrmidon. These reefs were selected to provide a description of the

inshore to offshore gradient (Figure 2-1), with inner-shelf reefs directly under the path of influence of the Burdekin River flood plumes. This across-shelf gradient is one of the two main environmental gradients in the GBR with the other one being the latitudinal changes (Lough and Barnes 2000).

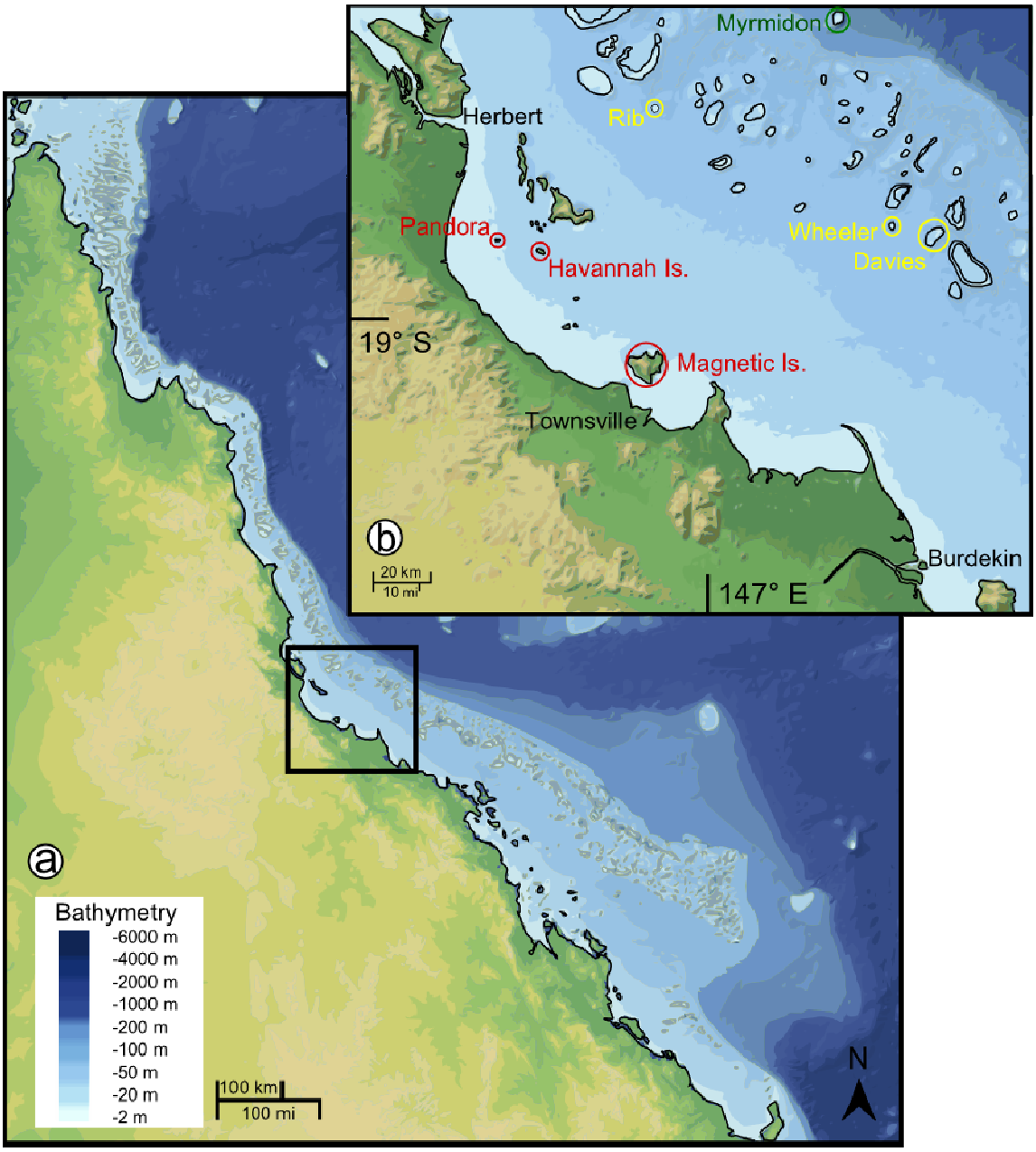

Figure 2-1. *(a) Bathymetric map of the GBR (modified from http://h.e-atlas.org.au/, 2012) depicting (b) the locations of reefs sampled within the central GBR, inner-shelf reefs of Havannah Is. and Pandora circled in red; these reefs lie in the pathway of the Burdekin river flood plumes. The mid-shelf reefs of Rib, Wheeler and Davies are circled in yellow, and the outer-shelf reef of Myrmidon is circled in green.*

Inner-shelf reefs

Havannah Island Reef (Figure 2-2a) is a fringing reef with an area of ~1.5 km^2 and is located at 18°50'S 146°32'E, 23 km from the coast. The island has been continuously monitored for the last 20 years as part of the AIMS Long Term Monitoring Program (AIMS LTMP, 2013). Median reef-wide live coral cover increased from moderate levels in 1987 (11-30%) to high (41-50%) levels by 1997. Coral cover levels collapsed in 1998 due to mortality from extensive coral bleaching. Since then the median live hard coral cover has remained low with a 0-5%.median live reef-wide coral recorded in 2011, lower than the 23% mean average for the GBR. Low level bleaching was observed in 2011(AIMS LTMP, 2013). Pandora Reef (Figure 2-2b) is a small planar reef with no lagoon that covers an area of 0.6 km^2 located at 18°48'S 146°25'E; this is approximately 15 km from the coast and about 7 km away from Havannah Is. Pandora coral cover reached a maximum of 58% in 1994 and decreased 20% as result a of the 1998 bleaching event. Levels steadily recovered to 50% in 2009, but reduced to 36% as a result of damage caused by Tropical Cyclone Yasi in February 2011 (AIMS LTMP, 2013). These reefs are inside the ≤20 m coastal area. This coastal area and reefs are impacted approximately annually by flood plumes, mainly from the Burdekin River, but also from the Herbert River and other minor local rivers. During flood events salinity lowers to values around 31-32 ppt and can drop to values of around 24 during extreme flooding events (King et al. 2001).

Magnetic Is. is a high continental island with an area of 52 km^2 situated in Cleveland Bay 8 km from the city of Townsville (Bull 1982). This island is influenced by the Burdekin and Ross Rivers and salinities in the range of 17 to 36 have been reported for Nelly Bay on the south east side (Collins 1978). This area has a semi-diurnal tidal regime with diurnal inequality (Bull 1982), which are tides characterized by unequal heights for successive high or low waters, or in both pairs of tides. For Townsville Harbor, the mean spring tide range is 2.5 m and the mean neap range is 0.8 m (Morrisey 1980). This area is catalogued as 'No Outbreak' which indicates that Crown-of-Thorns (COTS) outbreaks have never been recorded (AIMS LTMP, 2013). Intrusion of cold water resulting from upwelling can also occasionally affect this area (Berkelmans et al. 2010).

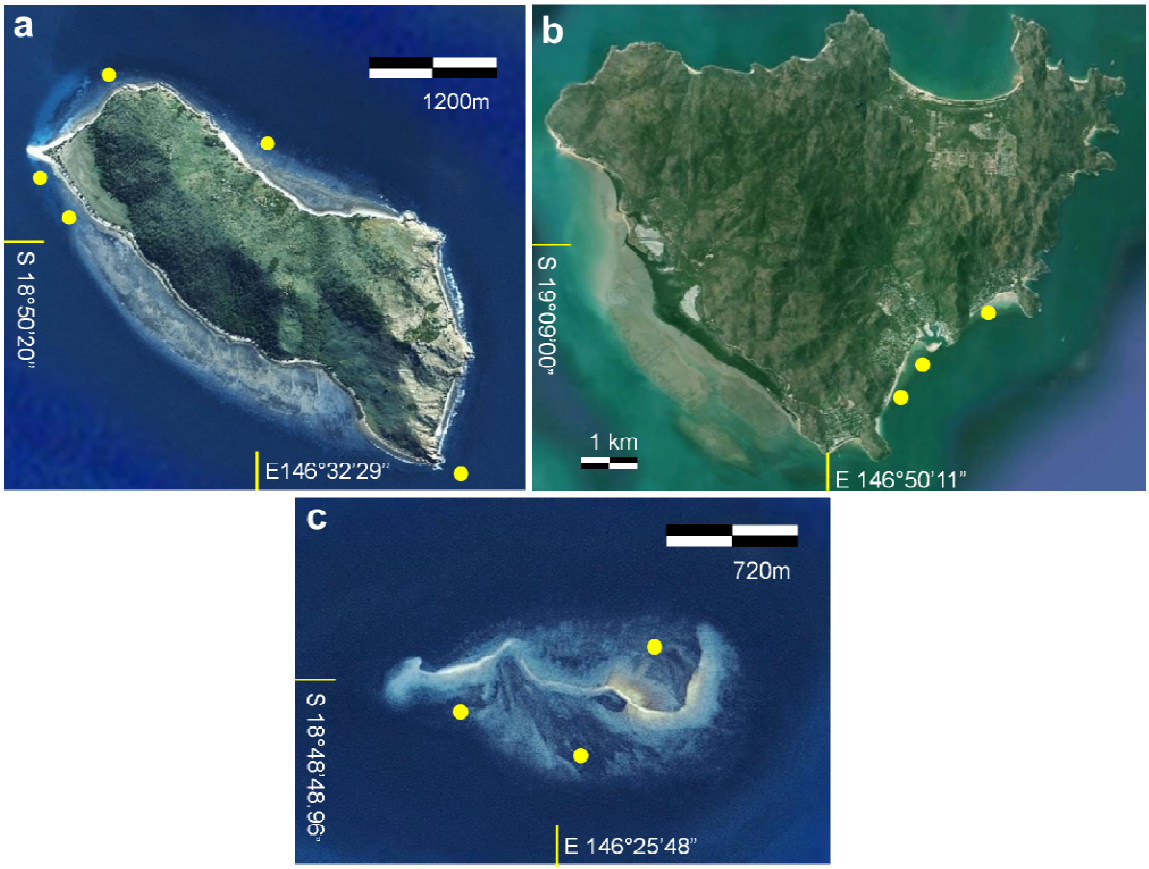

Figure 2-2. *Satellite images from Google Earth showing (a) Havannah Island, (b) Magnetic Island and (c) Pandora Reef. Yellow dots mark coral samples sites.*

Mid-shelf reefs

Davies Reef (Figure 2-3a) is an elliptical lagoonal reef 5.5 km long and 2.5 km wide that is located 70 km from the coast at 18°49'S 147°38'E. Coral cover has fluctuated around 30% since 2002. In 2011 coral cover decreased to 18%, the lowest cover recorded at Davies Reef since intensive surveys began, as a result of damage caused by Tropical Cyclone Yasi (AIMS LTMP, 2013). In 2011 Davies Reef was classified as recovering from COTS outbreaks, which have been documented in 1990-1993, 1997-1998 and 2002-2005 (AIMS LTMP, 2013). Coral cover is dominated by branching corals (mostly dead) with occasional *Porites* spp. heads. Wheeler Reef (Figure 2-3b) is a circular planar reef about 1 km in diameter that is located approximately 14 km north of Davies Reef and 70 km away from the coast (18°48'S 147°31'E). It has very little algae cover and high coral cover dominated by *Acropora* spp. with abundant *Porites* spp. colonies and members of many other genera. COTS outbreaks were last recorded in 1988 when coral cover dropped to 8% and since then coral cover has recovered reaching 50% in the latest survey in 2007 (AIMS LTMP, 2013).

Rib Reef (Figure 2-3c) is a crescentic reef, 2 km in diameter, that is located at 18°29'S 146°52'E, about 56 km from the coast. This reef had a live hard coral cover of 11% in 2007-8 (AIMS LTMP, 2011) and is dominated by *Acropora* spp. corals, with a few *Porites* spp. and *Diploastrea heliopora* colonies, and with considerable algae cover. Since monitoring began in 1994 coral cover reached a peak in 1996 with 66%. Since then levels have decreased due to tropical cyclone damage and COTS outbreaks with an 8% coral cover documented in 2012. These mid-shelf reefs receive no influence from river plumes except during exceptional floods, such as the 1974 event (King et al. 2001).

Outer-shelf reefs

Myrmidon Reef (Figure 2-3d) is an irregular shaped planar reef with an area of 6.2 km^{-2}, that is located on the outer edge of the GBR at 18°16'S 147°23'E, around 110 km from the coast. This isolated reef had a live hard coral cover of 24% in 2006-7, and is located close to the continental shelf, where it receives minimal if any influence from coastal processes and is dominated by oceanic conditions. This area is frequently subject to the effects of shelf-break upwelling (Wolanski and Pickard 1983; Berkelmans et al. 2010). This reef has been surveyed by AIMS LTMP since 1988, with COTS outbreaks only recorded in 1998 and in insufficient numbers to cause coral mortality. Algae have dominated the benthos since 2000 and covered 67% of the substrate in 2011. Coral cover reached a maximum of 39% in 1999. In 2002 bleaching caused an 11% decrease in coral cover and since then has continued to decrease with a coral cover of 20% in 2011 (AIMS LTMP, 2013).

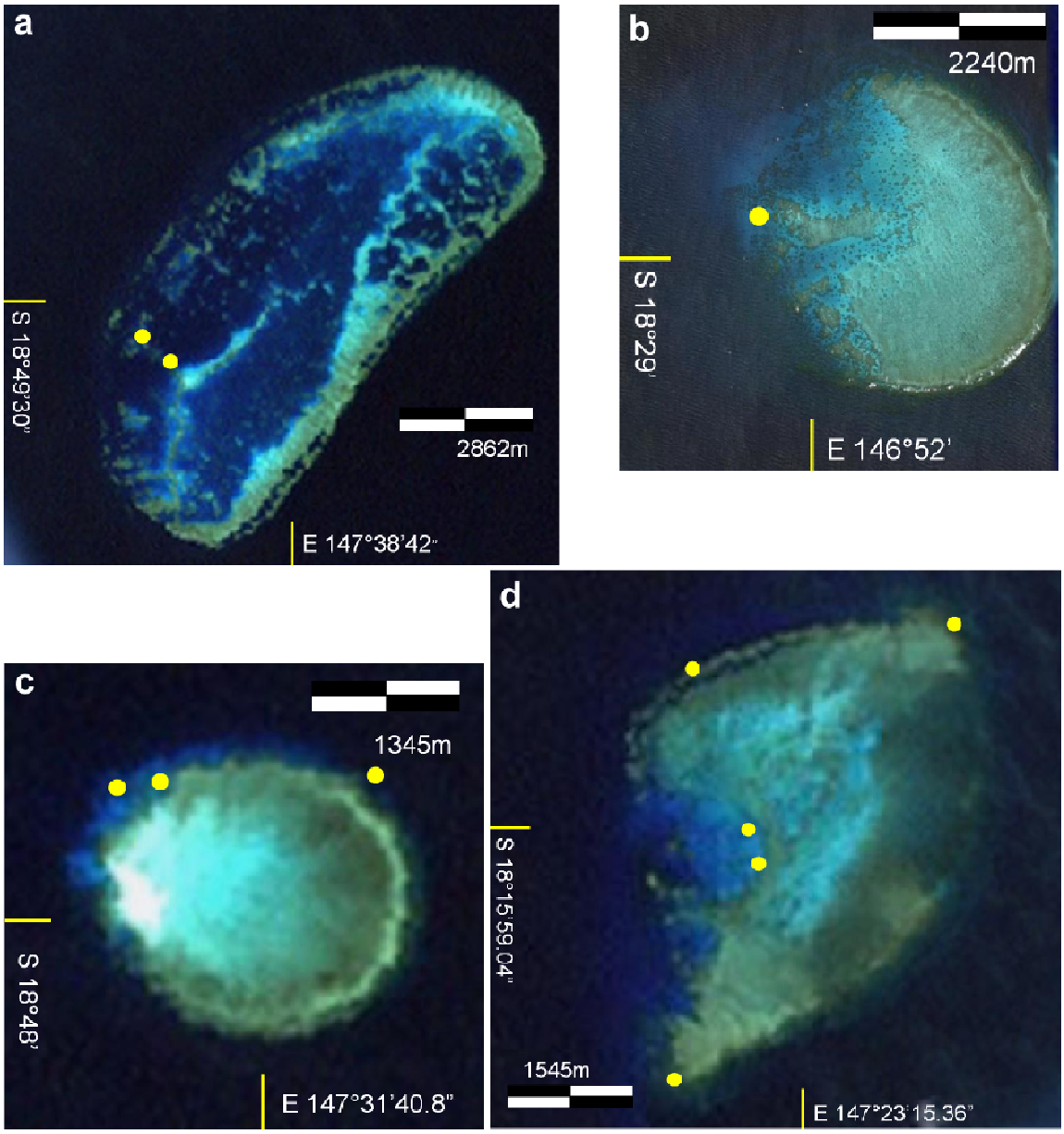

Figure 2-3. *Satellite images from Google Earth of the mid-reefs of (a) Davies, (b) Rib and (c) Wheeler and, the outer-shelf reef of (d) Myrmidon Reef. Yellow dots mark collection sites.*

2.3. Instrumental rainfall, river discharge and sea surface temperature records

Monthly rainfall data for Townsville were obtained from the Bureau of Meteorology (http://www.bom.gov.au/climate/data/, 2011), and monthly river discharge for the Burdekin and Herbert rivers as ML were obtained from the State of Queensland, Department of

Environment and Resource Management (DERM, http://watermonitoring.derm.qld.gov.au, 2011). *In situ* monthly SST were obtained from the Australian Institute of Marine Science (AIMS, http://data.aims.gov.au/, 2011), for the inner-shelf, mid-shelf and outer-shelf regions (Figure 2-4). For the inner-shelf SST data spanning from 1993 to 2008 were obtained by averaging temperature logger records at Pandora Reef, Havannah Is., Cleveland Bay, Pioneer Bay, Cattle Bay and Pelorous Is. Mid-shelf SST data were obtained from loggers from Kelso Reef, Davies Reef and John Brewer Reef and spans from 1992 to 1994 and 1996 to 2008. Outer-shelf SST data spanning from 1991 to 1992 and 1996 to 2004 were obtained from the temperature loggers at Myrmidon Reef. These periods only include complete years data (Oct-Sep) that is also covered by the coral data (see Chapter 4). For longer time periods (1930-2008) the extended reconstructed SST NOAA NCDCERSSTv3b (ERSSTv3b) monthly data from the Comprehensive Ocean-Atmosphere Data Set (COADS) with a spatial resolution of 2°×2° centred at 18°S and 147°E were used (http://iridl.ldeo.columbia.edu, 2011). Annual data is defined based on the water year (October–September) in Queensland (Lough 2007,2011a).

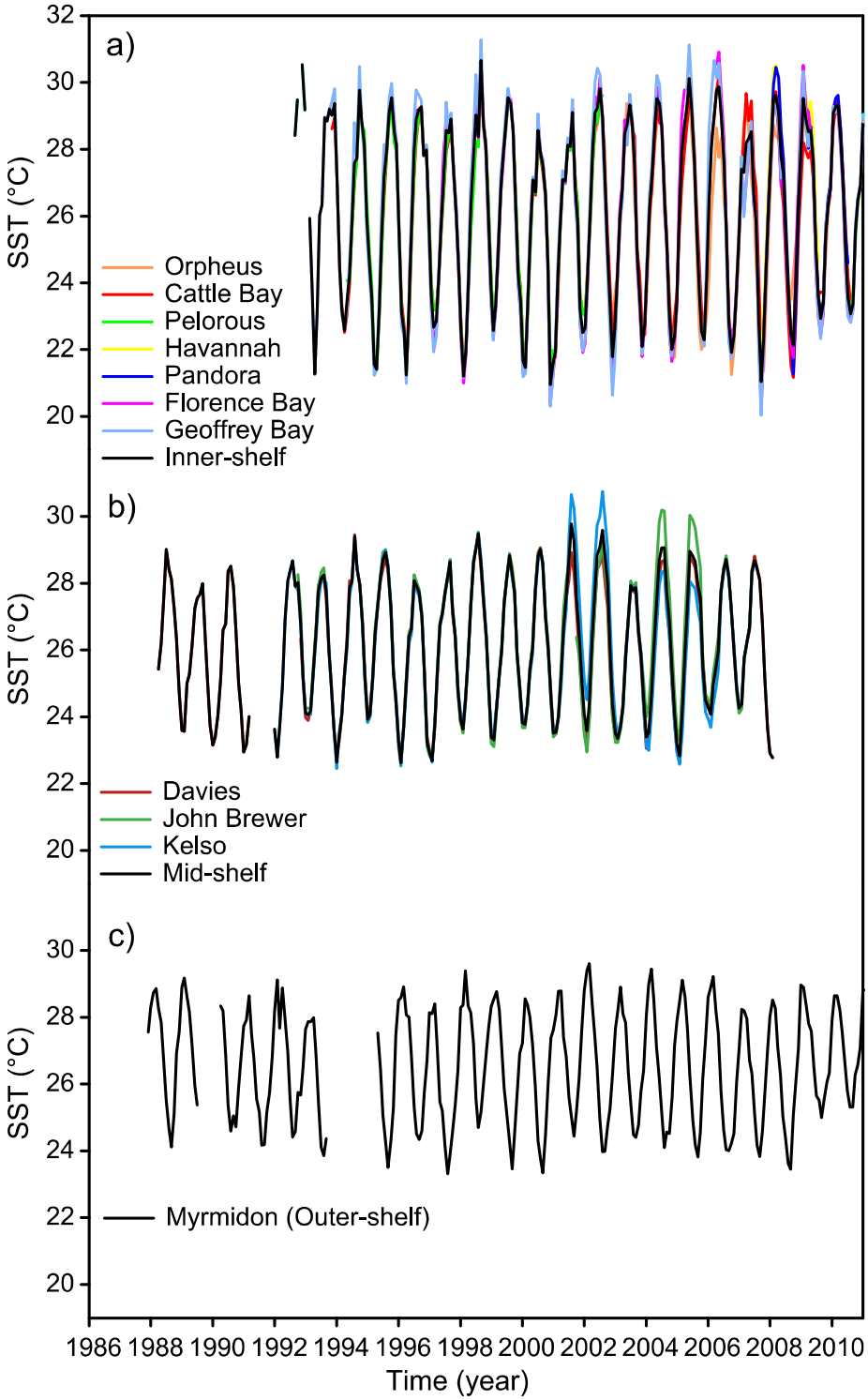

Figure 2-4. *(a) inner-shelf, (b) mid-shelf and (c) outer-shelf in situ monthly SST data loggers from AIMS. Also shown in black is the average of all data series.*

The *in situ* SST records show a decreased seasonal variation across the shelf in the central GBR (Table 2-1) with more stable temperatures occurring in the deeper waters close to the

Coral Sea (Wolanski 1994). Annual maximum SST values are typically 0.6°C higher in inner-shelf than outer-shelf areas; however, mean annual SST (~26.5°C) is around 0.4°C warmer in the latter. This is because the seasonal range is larger in the inner-shelf area (7°C) compared to the outer-shelf area (5°C) with the largest difference occurring in winter when inner-shelf waters are 1.7°C colder than the outer-shelf area. Seasonal SST variability in the mid-shelf is similar to the outer-shelf values, indicating that the coastal effects are significantly reduced in the mid-shelf region. The reconstructed SST (ERSSTv3b) fails to capture the full seasonal variability particularly underestimating winter SSTs. This difference is higher with the data loggers closer to the coast (Table 2-1). This indicates that important across-shelf SST differences exist in the central GBR that can only be resolved by the *in situ* data. However; the data from *in situ* data loggers is often of limited length or can have gaps in the data (Alibert et al. 2003).

Table 2-1. *Annual (October-September) average SST, maximum monthly SST, minimum monthly SST and annual SST range (max – min) for the in situ SST data from AIMS and the reconstructed SST* ERSSTv3b (2°x2°) *data from COADS over the period of 1995-2006.*

		SST (°C)							
Database	**Region**	**Mean**	**SD**	**Max**	**SD**	**Min**	**SD**	**Range**	**SD**
In situ SST (AIMS)	Inner-shelf	26.06	0.42	29.32	0.56	22.17	0.63	7.15	0.69
	Mid-shelf	26.04	0.45	28.96	0.39	23.29	0.48	5.44	0.39
	Outer-shelf	26.48	0.44	28.73	0.45	23.91	0.50	5.05	0.36
COADS	18°S 146°E	26.64	0.39	28.94	0.33	24.24	0.51	4.70	0.46

2.4. Methods

2.4.1. Coral core collection

This study is based on the analysis of 41 coral cores (Table 2-2) drilled from carefully selected *Porites* spp. colonies broadly representative of the seven reefs across the continental shelf of the central GBR shelf described (Figure 2-1). Before 1998 a hydraulic operated system was used to extract coral cores 70 mm in diameter and up to 550 mm in length. Later a more portable custom-built pneumatic system developed at ANU was used to extract 50 mm diameter cores and 550 mm in length. After the drilling operation the

coral colonies were cleaned of debris by creating water movement and the hole left in the colonies after core removal was sealed with concrete plugs. Full coral recovery from the coring procedure was incidentally documented in the 2009 coring campaign when an old cement plug was inadvertently hit while drilling on a coral colony at Magnetic Island.

Thirty nine of the 41 coral core samples were collected from colonies living at depths generally between ~3 and 11 meters. Small heads (<1.5m) and very shallow-water colonies (upper surface <2m above low-tide mark) were specifically avoided to preclude possible ontogenetic artifacts (Lough 2008a) and effects from shallow-water induced stress (e.g. Barnes and Taylor 1973). Two cores were however collected from colonies of only 60 cm height, from a water depth of 25.5 m from the fore-reef of Myrmidon Reef, but are treated separately. Samples were identified to the genus level, as no significant differences in the growth parameters of massive *Porites* are apparent at species level (Lough and Barnes 1992; Lough et al. 1999).

Twenty two coral cores were collected from the inner-shelf reefs of Pandora (10 cores), Havannah Is. (8 cores) and Magnetic Is. (4 cores). Of these, 17 correspond to cores collected between 2006 and 2009; three were collected between 1998 and 2002, and the remaining two in 1988. The effect of flood plumes is recorded in coral cores from these reefs as luminescent flood bands (Isdale 1984; Lough et al. 2002) as well as peaks in Ba/Ca values (Alibert et al. 2003; McCulloch et al. 2003). For the mid-shelf region 13 coral cores are included from Davies Reef (5 cores), Wheeler Reef (5 cores) and Rib Reef (3 cores). All 13 cores from the mid-shelf reefs were collected in 2009. The mid-shelf region of the central GBR is relatively broad and largely unaffected by flood plumes, as indicated by a general absence of luminescent bands (Lough et al. 2002) and associated Ba/Ca peaks (Fallon et al. 2003). The exception however is during major reef-wide flood events, such as occurred during 1968, 1974, 1991, where strong luminescent bands are apparent. Six outer-shelf cores were collected in 2005, cores from Myrmidon Reef are systematically shorter as *Porites* colonies in the GBR show a marked reduction in extension rate with distance from shore and depth (Isdale 1983; Lough and Barnes 1992; Lough 2008a).

Table 2-2. *Reef locations, sites and details of coral core samples.*

Region	Reef	Core code	Coring date	Latitude	Longitude	Colony height (m)	Depth from top (m)	Length (cm)	Age model
Inner-shelf	Magnetic Is	MAG88	1988	19.17S	146.85E	5	3-5	167	1871-1987
		MAG01	2001			3	3-5	33	1976-2000
		MAG09_1a	2009			2	2	106	1987-2008
		MAG09_2	2009			1.6	2.2	75	1962-2007
	Havannah Is	HAV01	1987	18.84S	146.54E	6	2.5	530	1784-1985
		HAV02	2002			4	5	45	1980-2001
		HAV06A_S3	2006			2-3	3-5	55	1966-2005
		HAV06 #5	2006			2-3	3-5	37	1975-2005
		HAV06#6	2006			2-3	3-5	51	1962-2004
		HAV08_1	2008			2-3	3-5	50	1953-2007
		HAV08_2	2008			2-3	3-5	65	1964-2007
		HAV09_3	2009			2.2	3.6	100	1932-2008
	Pandora	PAN98 C3	1998	18.81S	146.43E	2-3	3.2	55	1972-1997
		PAN02A	2002			2-3	3-5	53	1964-2001
		PAN06A	2006			2-3	3-5	53	1985-2005
		PAN06 9	2006			2-3	3-5	48	1982-2005
		PAN07 17	2007			2-3	3-5	37	1985-2006
		PAN08_1	2008			2-3	3-5	62	1965-2007
		PAN08_2	2008			2-3	3-5	46	1977-2007
		PAN09_1	2009			1.5	5.8	68	1953-2008
		PAN09_2	2009			1.5	3	38	1990-2008
		PAN09_3	2009			1.6	3	60	1976-2008
Mid-shelf	Davies	DAV09_1	2009	18.83S	147.63E	1.5	7	59	1982-2008
		DAV09_2	2009			3.5	6.5	47	1979-2008
		DAV09_4	2009			3	7.6	49	1975-2008
		DAV09_5_1	2009			3	3	50	1967-2008
		DAV09_5_2	2009			3	3	77	1947-2008
	Wheeler	WHE09_1	2009	18.80S	147.53E	2	5.5	52	1974-2008
		WHE09_2	2009			1.2	5.2	47	1972-2008
		WHE09_3	2009			2.5	4	54	1978-2008
		WHE09_4	2009			1.5	4	66	1959-2008
		WHE09_5	2009			4	7.4	49	1980-2008
	Rib	RI09_1_1	2009	18.48S	146.87E	4	4	100	1948-2008
		RIB09_2	2009			3	4	99	1952-2008
		RIB09_3	2009			2	5	97	1950-2008
Outer-shelf	Myrmidon	MYR05-272	2005	18.27S	147.38E	1	3.5	47	1981-2004
		MYR05-271	2005			3	4	80	1984-2004
		MYR05-S1	2005			0.7	16.5	30	1980-2004
		MYR05-S2	2005			2	11	47	1967-2004
		MYR05-S5a	2005			0.6	25.5	16	1966-2004
		MYR05-S5b	2005			0.6	25.5	20	1952-2004

After collection organic material was partly removed by submerging the top of the core in a solution of 30% H_2O_2 diluted with H_2O in an approximately 1 to 6 ratio for a few hours. This bleaching was mild enough that in some cases part of the characteristic brown colour associated with the tissue layer was still present after cleaning; this was done in order to prevent dissolution of the skeleton (Nagtegaal et al. 2012). Cores were then rinsed with freshwater and let to dry at ambient temperature, preferentially under direct sun light. Each coral core was cut into slices (~7 mm thick) along the plane of the vertical growth axis using a table saw fitted with a diamond coated masonry blade. Each slice was then ultrasonically cleaned in ultrapure (18.2 MΩ) MQ water and dried at ambient temperature. The slices were X-rayed and observed under UV illumination to reveal the density and luminescent annual banding, respectively.

X-rays were taken of all coral slices to reveal density variations using standard hospital X-ray equipment (Figure 2-5). The film is X-rayed at 50 KvP and 10 mA with a source to object distance of 1.25 m for 5 to 15 seconds. For the inner-shelf samples black and white photographs of the slices were taken under UV illumination to capture luminescent bands. In some cases the luminescent bands were traced directly from the slices onto overhead transparencies. Corals were selected for analysis based on their band quality as determined from X-ray images and/or luminescent annual banding; corals with irregular bands or heavily bioeroded were discarded. The 41 samples included were carefully selected from a collection of 45 cores; the other 4 cores were discarded for showing severe bioerosion or off-axis growth. Some of the corals selected included show bioerosion or off-axis growth at specific sections in the core; data from these sections is not included in the present study. The low number of samples rejected may be a result of a careful selection of samples in the field.

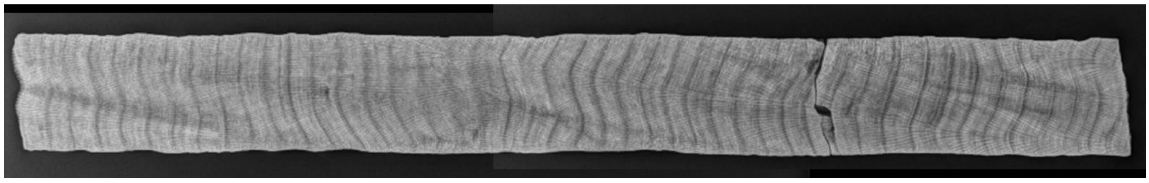

Figure 2-5. *X-ray negative of a slice of a Porites spp. coral from Havannah Is. showing the annual density banding pattern.*

3. Geochemical data from LA-ICP-MS in coral records

3.1. Introduction

Instrumental records of past environmental changes in the ocean are temporally and spatially limited. Various natural proxies have been exploited to fill this knowledge gap; in particular the use of geochemical changes in coral skeletons have been used to reconstruct past changes in the tropical oceans (Smith et al. 1979; Beck et al. 1992; Alibert and McCulloch 1997; Wei et al. 2000; Hendy et al. 2002; Marshall and McCulloch 2002; McCulloch et al. 2003; Corrège 2006a,b). Corals are particularly useful as paleoclimate recorders because they are widely distributed in the tropical oceans and can be accurately dated, forming continuous records that contain a broad array of geochemical tracers for temperature, salinity, *p*H and upwelling (Gagan et al. 2000; Corrège 2006a).

During the process of calcification various geochemical tracers of environmental information are incorporated and stored in the coral skeletons. These include $\delta^{18}O$, $\delta^{13}C$ and $\delta^{11}B$ and various minor and trace elements, such as Sr, Mg, U, B, Ba, Mn, Sr, Pb, Y, Zn, Cd. The elemental ratios Sr/Ca, U/Ca, Mg/Ca and B/Ca have been used to reconstruct SST variations (Smith et al. 1979; Min et al. 1995; Shen and Dunbar 1995; Mitsuguchi et al. 1996; Alibert and McCulloch 1997; Hendy et al. 2002; Fallon et al. 2003). Ba/Ca has been used to reconstruct land use changes, sediment fluxes, fluvial discharge and upwelling (McCulloch et al. 2003; Sinclair and McCulloch 2004; Fleitmann et al. 2007; Lewis et al. 2007; Alibert and Kinsley 2008; Carilli et al. 2009a; Carriquiry and Horta-Puga 2010). Other ocean upwelling indicators include Cd/Ca and Mn/Ca (Shen et al. 1987; Shen et al. 1991), with Mn/Ca also being described as an indicator of productivity (Alibert et al. 2003) and to local disturbances associated to infrastructure development (Lewis et al. 2012).

Despite the potential for corals to serve as paleoenvironmental indicators a wide response in the climatic interpretation of corals has been observed ranging from: (1) no relationship with environmental variables, (2) temporally variable significance to (3) a significant and stable relationship (Quinn and Sampson 2002; Lough 2004; Sinclair 2005). A reduced

relationship with a given environmental variable can relate to errors in the assignment of the age of the coral, the introduction of non-climatic variability by growth, the effect of other environmental variables or true local variability in the environmental variable not observed in the instrumental data (Quinn and Sampson 2002; Lough 2004; Sinclair 2005; Lewis et al. 2012). Furthermore, the process of incorporation of major elements into the coral skeleton is still not fully understood (Corrège 2006a; Jones et al. 2009). For example in the case of the Sr/Ca ratio some non-temperature-related artefacts have been noted (de Villiers et al. 1995; Cohen et al. 2002; Gaetani and Cohen 2006). Early marine diagenesis can produce secondary calcite, which has significantly lower and more variable Sr/Ca values (Sayani et al. 2011), and secondary aragonite, which has higher Sr/Ca values that can translate into 4-5°C cooler SST (Müller et al. 2001). Thermal stress, caused by either low or high temperatures can produce lower Sr/Ca values due to the breakdown of the biological control on Sr/Ca fractionation (Marshall and McCulloch 2002). Analysis along the maximum growth axis, ensuring that coral skeleton has no diagenetic alteration and replication are some of the tools to reduce potential biases (Marshall and McCulloch 2002; Lough 2004; Sayani et al. 2011).

The emphasis here is on the Sr/Ca and Ba/Ca ratios, as they are established proxies for temperature and riverine input to the central GBR, respectably. Particular attention has been given to updating previous inner-shelf Ba/Ca reconstructions (McCulloch et al. 2003) and using these to obtain more detailed information of the effects of river run-off directly at the reef, as compared to inference based on river discharge or inland river discharge measured at the river mouth or rainfall measured inland. Sr/Ca data was generated in an attempt to obtain *in situ* SST information that would extend the available instrumental *in situ* SST time series that extend back only to the early 1990's. This is important as the reconstructed SST data available (e.g. COADS) lacks the spatial resolution necessary to resolve the across shelf variability in the central GBR.

3.2. LA-ICP-MS Methodology

From the core collection described in section 2.4.1 (Table 2-2) three inner-shelf coral records, one collected in 2006 (from Havannah Is.) and two in 2008 (one from Havannah Is and one from Pandora Reef) were selected for geochemical analysis by LA-ICP-MS. These

cores were selected because they had clear density bands and were the most recent material available at that time. Core collection and slicing procedures are described in section 2.4.1. Selected slices were cut into pieces 2.5cm wide and < 9.5cm long following the maximum growth axis for density and laser ablation inductively plasma mass spectrometry (LA-ICP-MS) measurements. The cut pieces were then cleaned in 18.2 MΩ ultrapure milli-Q water using an ultrasonic probe to remove any coral powder leftover from the sawing process. The ultrasonic probe was operated at a low output power to prevent damage to the microstructures of the coral skeleton. Cleaned pieces were then left to dry overnight in an oven set at a temperature <60°C.

One of the advantages of analysis by LA-ICP-MS is that it provides fine-scale details that are not readily captured with bulk sampling techniques (Alibert and Kinsley 2008). The cores were analyzed for Ca, Sr, U, Ba, B, Mg, Mn, Cd, and Li using the ANU HelEx laser ablation ArF excimer system (Compex 110i) coupled to an ICP-MS (Varian 820 MS). The analysis protocol follows that reported by Sinclair et al. (1998), (Sinclair 1999), Fallon et al. (1999), Alibert et al. (2003) and Jupiter et al. (2008). As these are "routine" analyses only a short description and discussion of the data is presented in the current study.

Ablation sampling was performed in an ANU HelEx laser ablation sample stage under a helium atmosphere. The stage is designed to hold two coral pieces 25 mm wide, 7 mm thick and up to 95 mm long. The coral pieces are placed in a sample stage, and scanned at 40 µm s^{-1} using 5 Hz pulse rate. A rectangular slit 400 µm wide (perpendicular to the growth axis) and 40 µm long (parallel to the growth axis) is used as the projection mask for the laser beam. The rectangular slit is used to ensure representative sampling of the complex coral structure (Fallon et al. 1999). Prior to analysis samples are cleaned by pre-ablating along the analysis track using a slit 500 µm wide and 50 µm long, a 10 Hz pulse rate and scanning at 100 µm s^{-1}. The analysis track is aligned prior to analysis along the maximum growth axis based on the density or luminescent banding orientation (see Chapter 4). Coral sample analyses are bracketed between measurements of a soda-lime glass standard (NIST 614) and an in-house coral standard from a coral from Davies Reef (Fallon et al. 1999). The background is measured for 60 seconds before every measurement and for 300 seconds at the beginning and end of each analytical run. All of the data reduction analyses were performed using an Excel software program developed at the Australian National

University (ANU)'s Research School of Earth Sciences (RSES) by L. Kinsley. Data reduction includes outlier removal, background subtraction, drift corrections based on the standard measurements, ratio calculations based on the Metal/^{43}Ca and smoothing of the data. Data was smoothed with an 8 point running average to remove the fine scale variability in the data that is difficult to use for environmental interpretation (Sinclair et al. 1998). Sr/Ca and ^{138}Ba/Ca and ^{137}Ba/Ca for the glass standard determined in 40 runs of LA-ICP-MS are included in Figure 3-1, relative standard deviation for the corresponding selected ratios are presented in Table 3-1.

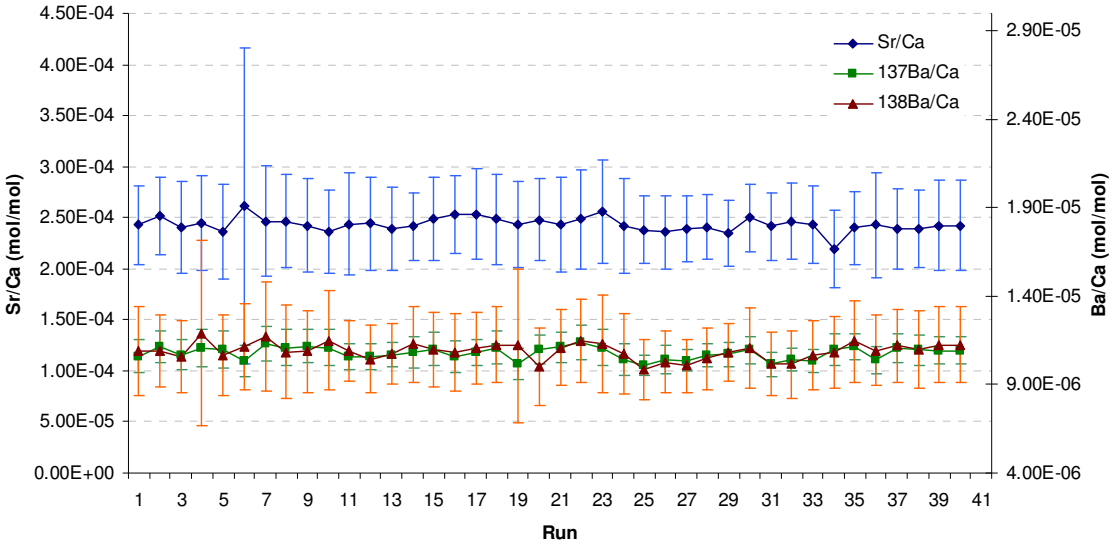

Figure 3-1. *Analyses of Sr/Ca and Ba/Ca in the NIST 614 SRM glasses in all the LA-ICP-MS runs. Error bars indicate standard deviation.*

***Table 3-1**. Analytical precision for LA-ICP-MS measurements indicated as relative standard deviation for the NIST 614 standard for 40 runs.*

Ratio	%RSD
$^{11}B/^{43}Ca$	5.99
$^{25}Mg/^{43}Ca$	5.88
$^{44}Ca/^{43}Ca$	1.00
$^{86}Sr/^{43}Ca$	2.62
$^{88}Sr/^{43}Ca$	2.01
$^{137}Ba/^{43}Ca$	2.48
$^{138}Ba/^{43}Ca$	3.46
$^{238}U/^{43}Ca$	3.25

3.3. Results

Seasonal cycles for the Sr/Ca, U/Ca and B/Ca occur in the inner-shelf corals, with Ba/Ca displaying distinct seasonal peaks (Figure 3-2). Age models based on these seasonal cycles were adjusted using the Analyseries program (Paillard et al. 1996). Minimum and maximum trace element/Ca ratio values were correlated to satellite SST COADS ERSSTv3b data. This time-series analysis software allows compensation for the summer-to-winter growth bias noted by Fallon et al. (1999) and simultaneous adjustments using several proxies; for this study Sr/Ca, B/Ca and Ba/Ca were used. As previously noted by (Sinclair et al. 1998), B/Ca ratios show the "cleanest" cyclic variations, however, the environmental significance of this variation remains uncertain. On the other hand Sr/Ca is predominantly controlled by temperature (Smith et al. 1979; Beck et al. 1992; Alibert and McCulloch 1997; Marshall and McCulloch 2002; Fallon et al. 2003), and therefore was used as the primary seasonal temperature cycle proxy to generate the age model.

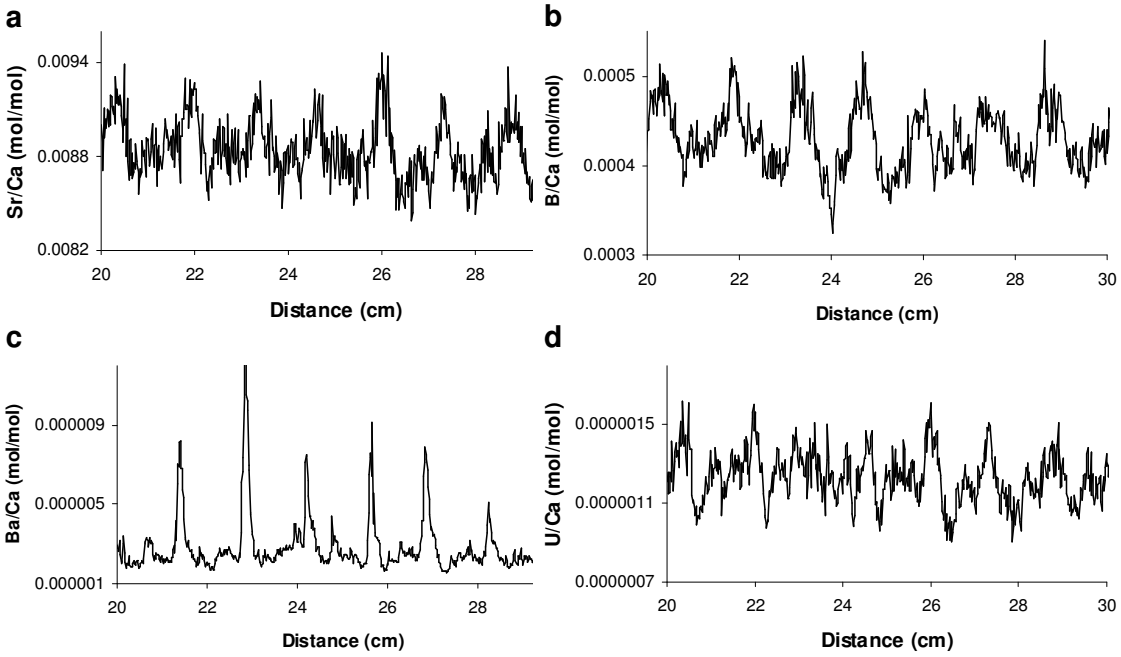

Figure 3-2. *Section of the trace elements profiles after applying an 8 point smoothing (a) Sr/Ca, (b) B/Ca, (c) Ba/Ca and (d) U/Ca plotted against distance for the HAV06_A S3 coral.*

The distance between peaks in the trace elements profiles for Sr/Ca, B/Ca and Ba/Ca can be used to calculate the linear extension rates. In the case of the inner-shelf corals Ba peaks are highly correlated with river flood events (McCulloch et al. 2003). The timing of flood events is well known, allowing the precise measurement of the amount of linear coral growth between different flood events. Similar linear extension data can be obtained using this approach compared to the more conventional methods like X-rays and UV luminescence (Figure 3-3 and Table 3-2). A detailed description of the X-rays and UV luminescence linear extension methods here employed is provided in Chapter 4.

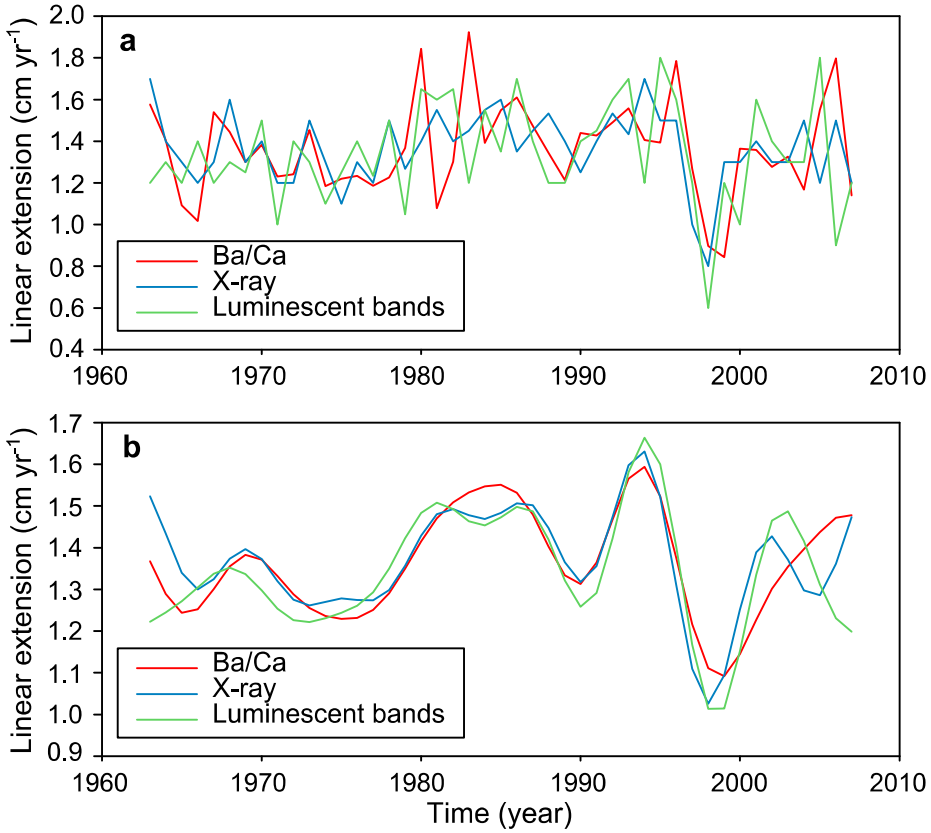

Figure 3-3. *(a)Annual linear extension rates obtained by measuring the distance between Ba/Ca peaks, density bands from X-rays and luminescence bands observed under UV light (black) for Havannah Is. inner-shelf core HAV08_2. (b) Smoothed versions of the annual time series after a low pass band filter of 8 years (0.125 Hz) was applied.*

Table 3-2. *Pearson product moment correlation coefficients (r) for the annual linear extension data of core HAV08_2.*

	X-ray			UV luminescence		
	r	p	df	r	p	df
Ba/Ca	0.469	0.001	45	0.304	0.042	45
X-ray				0.364	0.014	45

The rescaled geochemical data were re-sampled at monthly resolution. The Sr/Ca monthly data obtained from the three inner-shelf corals is compared to satellite SST records in Figure 3-4. Sr/Ca series for the three corals usually follow the variations in temperature, except for some short periods where the Sr/Ca is offset from the SST data. These offsets are not consistent between the records, possibly due to variations between measurements or to different vital effects between the colonies. Possible reasons for differences in the measurements include different biases in the LA-ICP-MS data, or true differences in the skeleton composition.

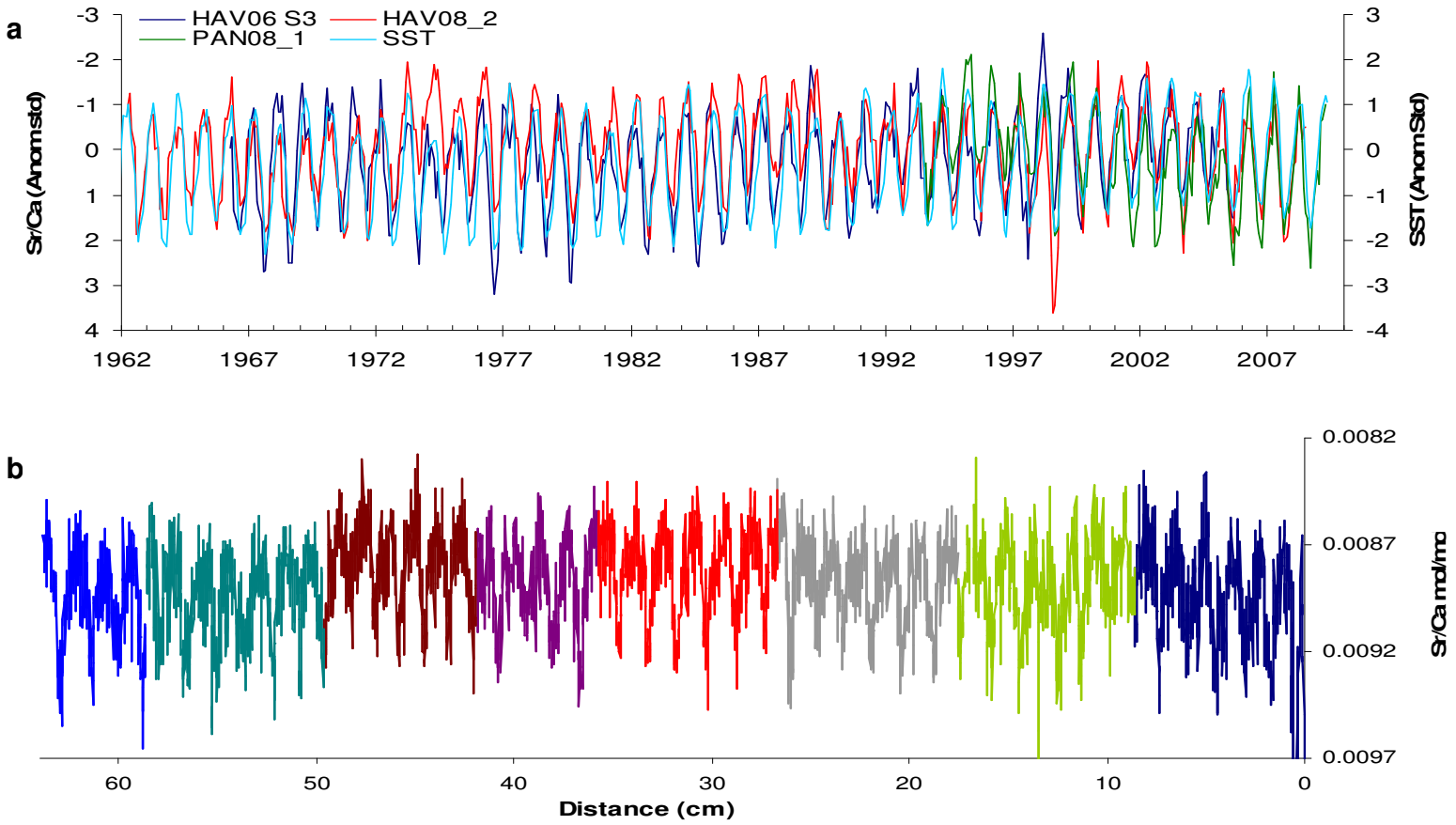

Figure 3-4. *(a) LA-ICP-MS Sr/Ca time series for the inner-shelf cores HAV08_2, HAV06_A S3, and PAN08_1 vs ERSSTv3b reconstructed SSTs. Data is presented as standardized anomalies to facilitate comparisons. (b)LA-ICP-MS Sr/Ca data for the individual sections of the coral core HAV08_2 coral core vs distance.*

Monthly Sr/Ca values are plotted against corresponding monthly *in situ* SST data for the common period for the all the data sets of 1993-2005 (Figure 3-5a). Regression lines were fitted to obtain Sr/Ca-temperature relationships for each of the three analyzed inner-shelf coralsFigure *3-5.*

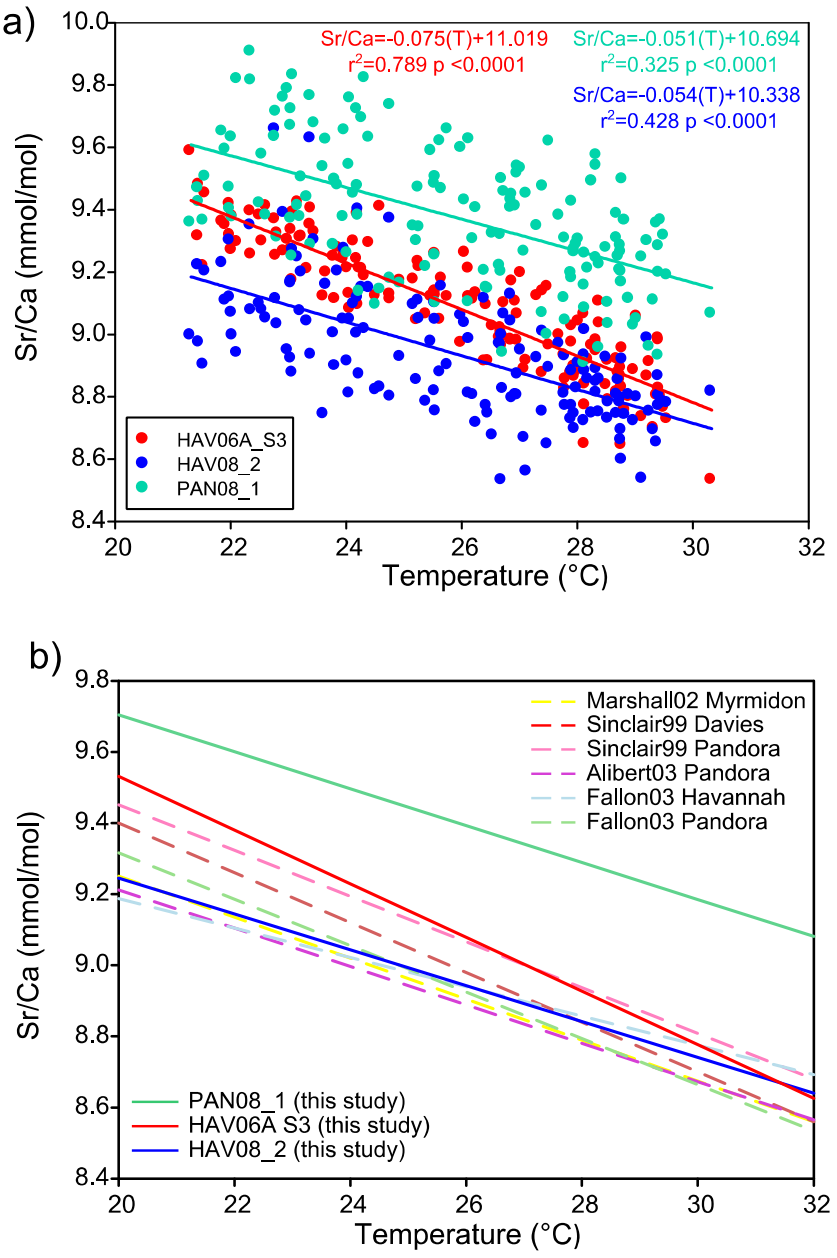

Figure 3-5. *(a) Linear regression of Sr/Ca vs in situ SST for inner-shelf corals from Havannah Is. and Pandora Reef. (b) Comparison of Sr/Ca-in situ SST calibrations obtained in this study to those previously obtained from central GBR reef of Havannah Is., Pandora Reef, Davies Reef and Myrmidon by Sinclair et al. (1998), Marshall and McCulloch (2002), Alibert et al. (2003) and Fallon et al. (2003).*

Each *Porites* coral core produces a unique Sr/Ca – temperature relationship with different slopes and y-intercept values, even for corals from the same reef (Figure 3-5b). This is consistent with previous studies which have concluded this to be the result of different 'vital effects' in individual colonies (Fallon et al. 2003). The two calibration curves for the Havannah Is. corals show y-intercept values that are consistent with previously reported data (Figure 3-5), whereas PAN08_1 is offset to significantly higher Sr/Ca values and displays a poorer correlation with SST (Table 3-3). Similar offsets have been previously reported for corals from the same region (Gagan et al. 2000; Fallon et al. 2003) and warrant further investigation.

The Sr/Ca correlations with monthly SST data are shown in Table 3-3 and are similar to those previously reported from LA-ICP-MS studies (Sinclair et al. 1998; Fallon et al. 1999; Fallon et al. 2003). The correlations between the Sr/Ca data and the SST from ERSSTv3b are very similar to the ones based on just the *in situ* SST data (AIMS). This correlation validates the use of the satellite-derived data to assign the age model and to calibrate geochemical signals over the period not covered by *in situ* data.

Table 3-3. *Monthly Sr/Ca vs SST Pearson product moment correlation coefficients for three inner-shelf corals (all correlations are statistically significant at 95%, p<0.0001).*

	in situ SST		ERSSTv3b SST	
Coral	Period	r	Period	r
HAV06 S3	1993-2005	0.888	1966-2005	0.883
HAV08_2	1993-2005	0.657	1962-2008	0.632
PAN08_1	1993-2005	0.57	1993-2008	0.608

However, when mean annual coral Sr/Ca is compared with mean annual ERSSTv3b data only core HAV06 S3 shows correlations that are statically significant ($r=0.65$ $p<0.0001$ $n=40$). For HAV08_2 $r=0.071$ $p=0.636$ $n=47$ and PAN08_1 $r=0.047$ $p=0.876$ $n=16$. The lack of agreement with the other two corals suggests that either these corals are not faithful environmental recorders or indicate a potential error associated with the methodology (e.g. analytical bias between measured coral sections).

To check for offsets due to errors in the measurements, selected coral sections were re-analyzed along a parallel track. The majority of the repeat analyses show a good

reproducibility but others show offsets between runs. Figure 3-6 shows Sr/Ca analyses along parallel tracks for two adjacent sections of PAN08_2. There is a good reproducibility of the annual cycles in all pieces, but a clear offset is observed between the different analyses of the first section, which could account for a difference of up to ~0.4°C. This could be related to heterogeneity of the standard used to correct the samples or true differences in the coral skeleton along the analyzed parallel tracks. Further testing is beyond the scope of the present study but is required to explore this hypothesis, including the analysis of multiple tracks when possible. It is worth noting that the corals analysed here all possess regular growth rates.

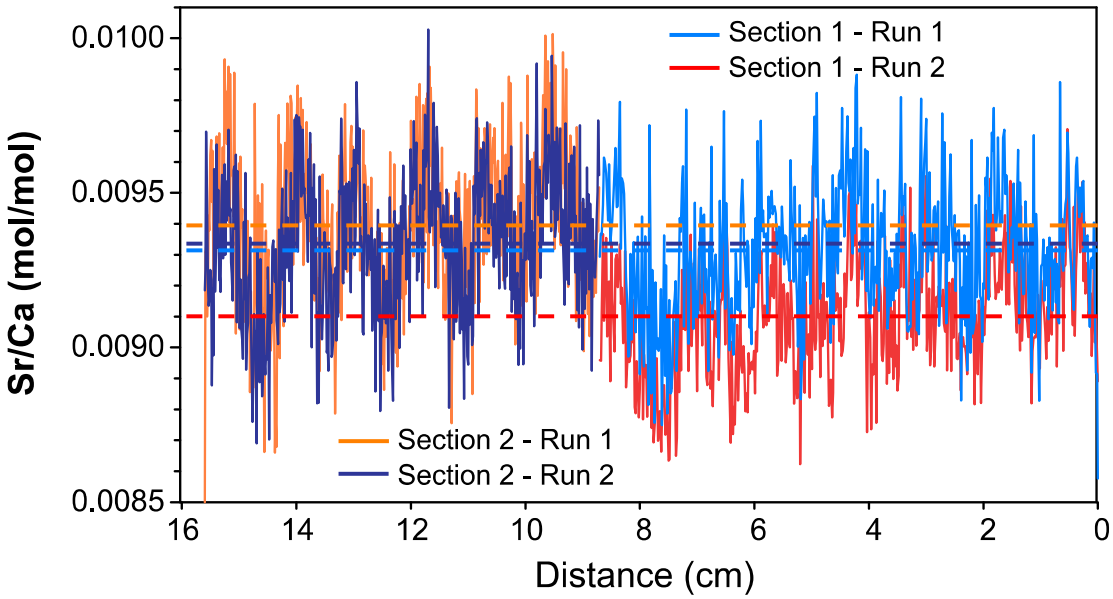

***Figure 3-6**. Sr/Ca profile along parallel track for two continuous sections of coral PAN08_2. The dashed lines are the mean values for the corresponding section.*

Monthly Ba/Ca data for inner-shelf corals were compared with previous results obtained by McCulloch et al. (2003) and are shown in Figure 3-7. All records show a pattern with distinctive peaks during late summer that coincide with the timing of seasonal river runoff. There is excellent agreement between the PAN08_1, and the Havannah Is. record (HAV01) reported by McCulloch et al. (2003) with both having similar average baselines. The two new Ba/Ca records from Havannah Is. show lower Ba/Ca baseline (Table 3-4) values than the PAN08_1 core and previously reported inner-shelf corals with typical values of ~4×10^{-6} mol/mol (Fallon 2000; McCulloch et al. 2003). The baseline Ba/Ca level observed in these

two Havannah records is very similar to the value of ~2 × 10^{-6} mol/mol found in mid-shelf and outer-shelf reefs (Fallon 2000).

Table 3-4. *Ba/Ca baselines for individual coral cores (±SD) over the common period of 1970-1998 (1982-1998 for PAN08_1). Record HAV01 obtained from McCulloch et al. (2003).*

Sample	Ba/Ca × 10^6 (mol/mol) ±1SD
PAN08_1	4.2±0.5
HAV08_1	2.6±0.5
HAV06 S3	3±0.5
HAV01	4.3±0.6

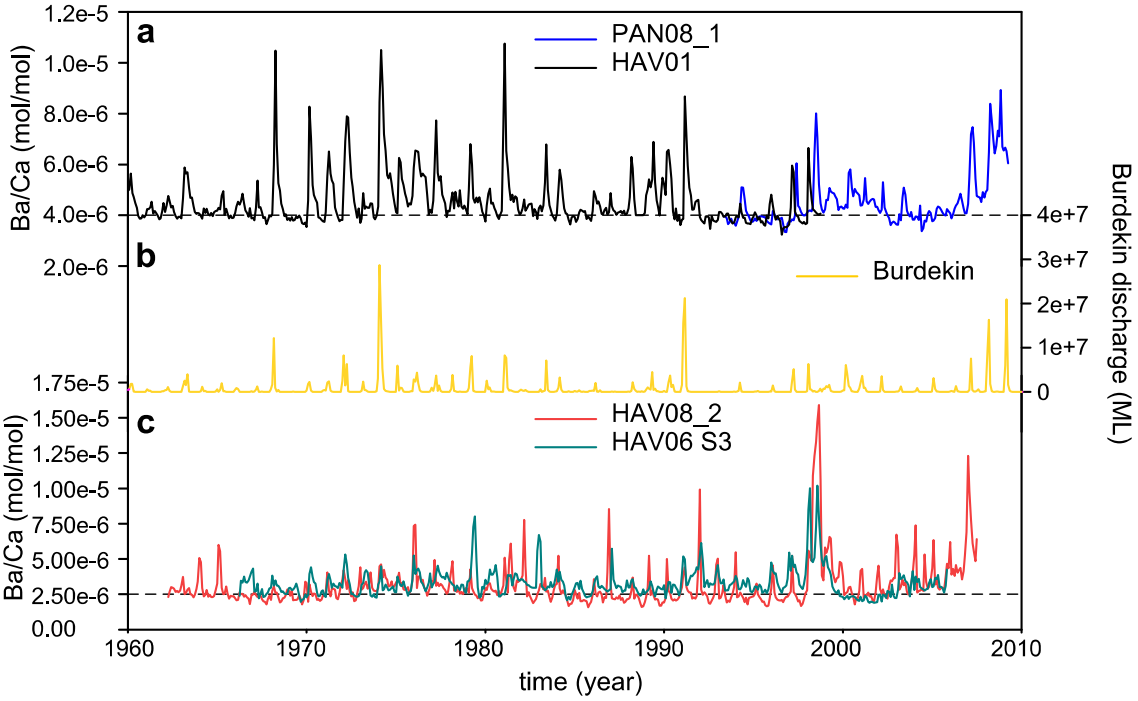

Figure 3-7. *Monthly time-series for: (a) high Ba/Ca baseline coral records, (b) discharge for the Burdekin River and (c) low Ba/Ca baseline coral records. Record HAV01 obtained from McCulloch et al. (2003).The dash line is used as a general reference for the different baseline values.*

All four records show a very large peak around 1998 that coincides with the timing of the '1998' severe bleaching event (Figure 3-7). Disruption of environmental proxies during bleaching events has been previously observed in coral geochemical records (Marshall and McCulloch 2002; Abram et al. 2003; Wei et al. 2009). Another feature of the three new coral records is the recent increase in baseline Ba/Ca values during the most recent period (since ~2002). This increase persists for several years (at least 2 or 3 cm from the core top) and is unlikely due to presence of the tissue layer, as this usually only covers the first ~0.5 cm. Disturbance of these Ba/Ca results due to hydrogen peroxide cleaning of the core as shown by (Sinclair 2005) is unlikely. If this increase in coral Ba/Ca is a true environmental

signal it could reflect an increase of Ba or terrestrial material delivered to the reef due to changing land use practices, as no change in river discharge or rainfall levels is evident since 2002 (Figure 3-7b).

Annual Ba/Ca for four corals and a master (average) Ba/Ca chronology generated from the normalized data of core PAN08_1 and HAV01 are compared to runoff data from the Burdekin River in Table 3-5. The HAV01 record reported by McCulloch et al. (2003) and the PAN08 from this study are significantly correlated with runoff, the two other records are not significantly correlated with river runoff. Based on the correlations with river run-off and rainfall only cores HAV01 and PAN08 were combined to obtain the master Ba/Ca chronology. Chronological errors are unlikely to be responsible for the differences observed between records as luminescent bands were used to cross-date and validate the age model (see Chapter 3).

***Table 3-5**. Pearson correlation coefficients for annual coral Ba/Ca time-series with rainfall at Townsville and river runoff data from the Burdekin River and Herbert River (non-significant correlations indicated in gray). Record HAV01 was obtained from McCulloch et al. (2003). The master chronology was obtained from combining records PAN08_1 and HAV01. Correlations cover the period 1993-2007 for PAN08_1, 1962-2007 for core HAV08_2 1966-2005 for core HAV06_S3 and 1958-1998 for HAV01,*

	Correlations Ba/Ca								
	Rainfall (Townsville)			**Burdekin River**			**Herbert River**		
Record	**r**	**p**	**df**	**r**	**P**	**df**	**r**	**p**	**df**
PAN08_1	0.619	0.014	15	0.774	**0.001**	15	0.697	0.004	15
HAV08_2	0.337	0.022	46	0.066	0.662	46	0.180	0.231	46
HAV06 S3	0.289	0.071	40	0.129	0.428	40	0.187	0.247	40
HAV01	0.587	**<0.001**	77	0.811	**<0.001**	77	0.675	**<0.001**	77
Master	**0.581**	**<0.001**	**86**	**0.800**	**<0.001**	**86**	**0.670**	**<0.001**	**86**

Anomalously low baseline Ba/Ca values and lower correlations between Ba/Ca and river discharge are observed in two of the Havannah Is. coral records. A difference in the Ba/Ca baseline of corals from the inner-shelf region of the central GBR was also noted by Lewis et al. (2007). These authors found a temporal variation in the baseline Ba/Ca value of a coral from Magnetic Island the later showing lower baseline values than reported by McCulloch et al. (2003) and similar to the ones reported here. To test if the incorporation of Ba is related in some way to the skeletal growth rate, the individual Ba/Ca average baseline

levels were compared against the average growth parameters of each core. However, no significant correlation was found ($p<0.05$). The possibility that these cores correspond to different species of *Porites* with different 'vital effects' affecting the Ba incorporation could not be tested as sampled colonies were not identified to the species level. The exact reasons as to why some corals are more reliable recorders of environmental changes than others remain unclear. This could be partly related to the presence of anomalous Ba spikes within some records and to possible local micro environment differences.

Anomalous Ba spikes that are not related to river discharge could cause a loss of correlation with river/rainfall data. Such anomalous Ba spikes have been previously reported (Hart and Cohen 1996; Tudhope et al. 1996; Fallon 2000; Sinclair 2005; Lewis et al. 2012) but the cause of their occurrence is not fully understood. Unique oceanographic conditions have been called upon to explain differences in the Ba signal between nearby locations (Tudhope et al. 1996). Varying magnitude of correlation of some Ba/Ca records with Burdekin River discharge could relate to the variable nature of flood events, as the propagation of the flood plume not only depends upon the volume of flood water but also on the wind intensity and direction (Devlin et al. 2001). Luminescent lines for big flood events (e.g. 1968, 1974, 1991) are present in all cores indicating that fresh water reached the corals, even for flood events for which there is no Ba/Ca spike in some of the cores. However, the Ba/Ca signal recorded by the coral will depend not only on the transport of flood plume waters to the reef, but also on how much Ba is delivered by the plume waters. This can be affected by the distribution of rainfall within the catchment and with the amount of sediment material accumulated inland (e.g during drought-breaking floods; McCulloch et al, 2003). Re-suspension of sediments by wave and wind mixing could also influence the relationship between Ba/Ca and river discharge and in the case of Havannah Is., mass effects could generate local environmental differences. Topography generates secondary currents that form convergence zones and eddies that affect mixing, nutrient and sediments distribution (Hamner and Hauri 1981; Wolanski and Hamner 1988). In this way, the location of the colony with respect to the reef could modify the Ba/Ca signal recorded. Other factors that could complicate the interpretation of Ba/Ca ratios in corals include barite trapping following phytoplankton blooms, decaying blooms of *Trichodesmium*, physiological perturbations associated with coral spawning and events that cause sediment resuspension such as dredging (Esslemont et al. 2004; Sinclair 2005).

On a decadal time scale the master chronology Ba/Ca (HAV01 and PAN08_1) shows good agreement with the discharge and rainfall instrumental data with clear dry and wet periods observed over 1920-2008 (Figure 3-8). Wet periods characterize the 1950's and 1970's as well as the early 1990's and 2000's, and dry periods in the 1960's and mid 1980's, 1990's and 2000's (Lough 2007).

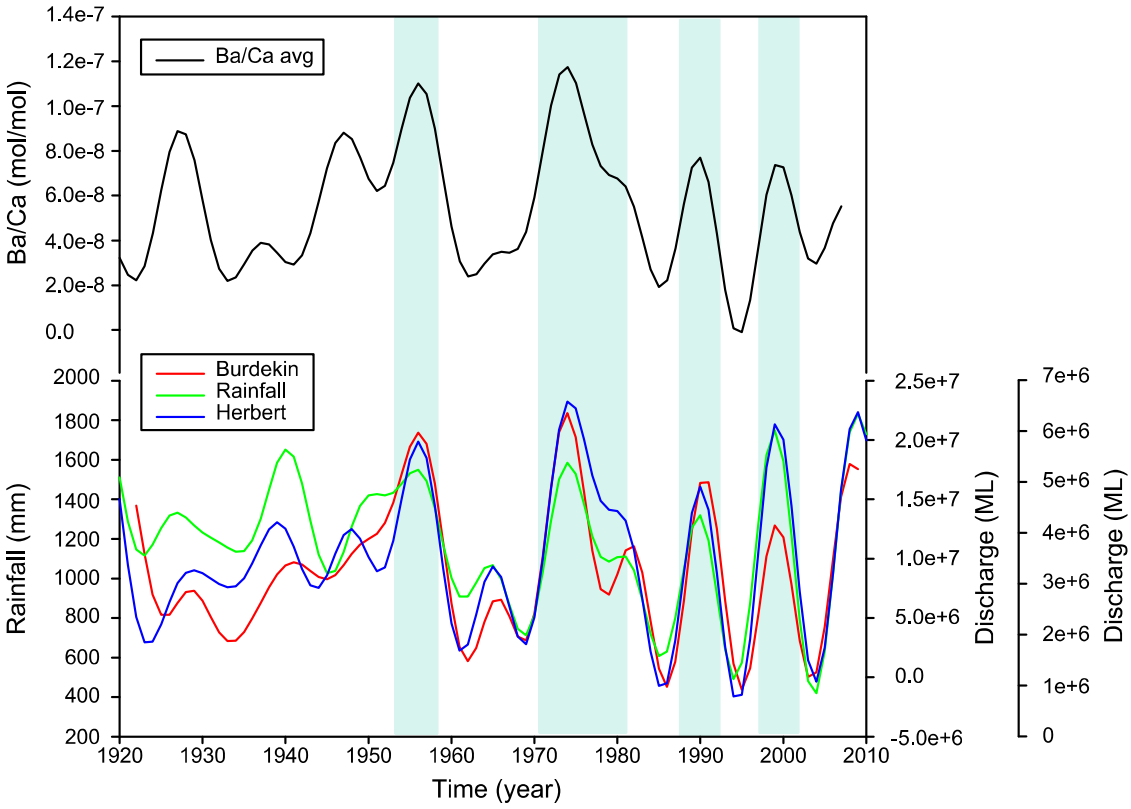

Figure 3-8. *Smoothed low pass band filter of 8 years (0.125 Hz) applied to highlight low frequency variability present in the master coral Ba/Ca, rainfall and river run-off (Burdekin and Herbert) time-series. Blue vertical bars highlight wet periods.*

The wavelet analysis (Figure 3-9) indicates that over the period 1920-2008 the Ba/Ca is characterized by interannual and decadal modes of variability. The last ~30 years (~1980-2008) are characterized by a reduction of the interannual and decadal variability and are dominated by a decadal mode of variability. This could indicate a 'switch' in the mode of variability observed in the Ba/Ca. This might relate to the increase in variability of rainfall and river flow in north-eastern Australia reported by Lough (2011b), who also notes that and that the most recent period has witnessed more frequent wet and dry extremes.

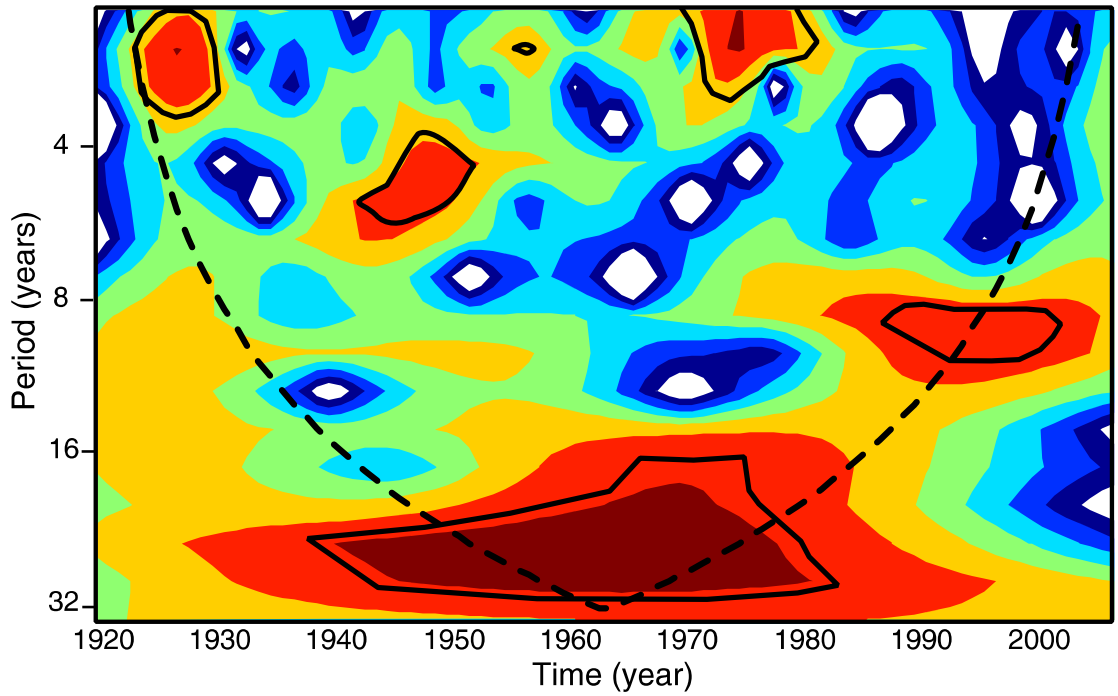

Figure 3-9. *Morlet wavelet analysis for the annual master Ba/Ca time series. The thick contour encloses regions of greater than 95% confidence for a red-noise process with a lag-1 coefficient of 0.11. The region below the dashed line indicates the 'cone-of-influence', where zero padding has reduced the variance. Wavelet software provided by C. Torrence and G. Compo, and is available at http://atoc.colorado.edu/research/wavelets/.*

3.4. Summary

Trace elements were analyzed by LA-ICP-MS in three inshore cores from the central GBR. Annual Sr/Ca was significantly correlated with SST for only one of the three cores analyzed, for this reason the Sr/Ca data was not used to extend the *in situ* SST records at this study site. However, core PAN08_1 was successfully used to update the Ba/Ca record published by McCulloch et al. (2003), but again two out of three cores here analyzed show anomalies and therefore have not been included in the master chronology used to reconstruct terrestrial runoff. The fact that not all records show the same or equally good correlations with environmental parameters highlights the importance of a multi-core approach and the validation of proxy records against instrumental records for paleo-climate reconstructions (Hendy 2003; Lough 2004; Jones et al. 2009). The reason for the lack of correlations with environmental parameters of some coral records remains uncertain and requires further analysis including assessment of the potential differences between species and local effects.

4. Coral Calcification in the Central Great Barrier Reef: Assessing the Impacts of River Runoff and Climate Change

4.1. Introduction

Coral reefs are in decline with clear evidence for major reductions in coral cover on a global scale (e.g. Gardner et al. 2003; Hughes et al. 2011; De'ath et al. 2012). Although clearly linked to anthropogenic disturbances, the identification of specific causes and their interactive effects remains unclear, with a combination of factors being likely. These range from the global effects of climate change with increasing stress and episodic bleaching caused by unusually high seawater temperatures (Hoegh-Guldberg et al. 2007), a progressive slow-down in the rates of calcification due to CO_2 driven ocean acidification (Ries et al. 2010; McCulloch et al. 2012a; Venn et al; 2013), to more local impacts. The latter include a range of effects such as overfishing, increased levels of nutrients, tropical cyclones, degraded water quality and associated effects such as disease and crown of thorn outbreaks (McCulloch et al. 2003; Cooper et al. 2008; Lough 2008a; De'ath et al. 2009, 2012; Brodie et al. 2010b). Discriminating between a range of spatial and temporal possible causative factors for reduced coral cover remains an important challenge that provides a rationale for ongoing efforts to improve local environmental conditions, essential for the overall maintenance of coral reef systems in the face of ever increasing global threats posed by climate change and ocean acidification (e.g. Buddemeier et al. 2004; Wei et al. 2009; McCulloch et al. 2012a).

In the Great Barrier Reef (GBR) an important long-term indicator of the impacts of environmental changes and reef health generally has been constraints provided by coral growth records from long-lived massive *Porites* (Lough and Barnes 2000; Lough 2008a; De'ath et al. 2009). For the key parameter of coral calcification, a significant decline of 14.2% from 1990 to 2005 (i.e. ~9% per decade) has most recently been reported for the GBR by De'ath et al. (2009). This study is based on an update of the original findings of Lough and Barnes (2000), and is notable for the large magnitude of recent declines, which

is a reversal from the previously reported increase in calcification between the 50 year periods of 1880–1929 and 1930-1979 (Lough and Barnes 2000). The large-scale declines in calcification reported by De'ath et al. (2009), if sustained and typical of the whole GBR, would have severe consequences for the GBR generally, and may for example be an important factor driving the rapid declines in coral cover of ~30% observed since ~1980 (Hughes et al. 2011; De'ath et al. 2012). This in addition to COTS and tropical cyclones which according to De'ath et al. (2012) are the primary drivers of the decline in hard coral cover on the GBR.

Although the De'ath et al. (2009) study examines a large number of records (328) from *Porites* heads, more than one-half (~170) of these are from only 5 reefs and the majority from the inshore rather than the main mid-outer reefs of the GBR. Thus whether major changes in calcification inferred by De'ath et al. (2009) reflect those of the inner reef rather than the whole GBR remains uncertain. The more recent period (1990-2005) emphasized in the De'ath et al. (2009) study is also characterized by intense 1998 and 2002 bleaching events in the GBR (Berkelmans et al. 2004). Although coral bleaching events are typically short-lived they can have significant longer-term effects on both coral cover as well as calcification with recovery usually only being observed after a few years, (typically 2-3 years), but in highly stressed sites up to 8-10 years (Suzuki et al. 2003; Carilli et al. 2009b; Gilmour et al. 2013). Thus the large magnitude of the more recent (post 1990) changes in calcification reported by De'ath et al. (2009) may also reflect short-term fluctuations in calcification caused by the effects of the very intense 1998 bleaching event.

Here temporal and spatial changes in coral growth (density, linear extension rate and calcification rates) from an independently collected set of cores obtained from relatively long-lived (>100 years) *Porites* colonies are documented. Cores were sampled from 7 reefs in a transect that is broadly representative of a strong inshore to offshore environmental gradient across the central portion of the GBR (Figure 2-1). The inshore reefs are episodically impacted by flood plumes, with increased sediment flux and degraded water quality resulting from a range of land-based activities such as grazing, agriculture, mining and land clearing in river catchments (Furnas 2003; McCulloch et al. 2003; Lewis et al. 2007; Brodie et al. 2010b). The mid-reef, although occasionally affected by extremely large flood plumes, is generally subject to low local anthropogenic pressure, while the outer reef

is removed from land-based effects and only subject to major oceanic influences. Details of the coral samples and study area are provided in Chapter 2. Specific aims of this study are thus to independently document changes in coral calcification over 1930-2008 (inner-shelf) 1947-2008 (mid-shelf) and 1952-2004 (outer-shelf), including the periods during and after the large-scale mass-coral bleaching events of 1998 and 2002 (Berkelmans et al. 2004). Importantly, by comparing the inner-, mid- and outer-shelf reefs this study attempts to discriminate between the impacts from local, mainly inshore changes in water quality from land-based effects, versus larger regional-scale impacts due to rising ocean temperatures, episodic bleaching, as well as the all-pervasive effects of CO_2 driven ocean acidification.

4.2. Material and Methods

4.2.1. Sample analysis

This study includes coral growth parameters for the forty one coral cores collected from seven reefs across the central GBR shelf described in Chapter 2. To describe the growth characteristics of the corals studied, two parameters were measured, the linear extension rate (cm yr^{-1}), and the density (g $CaCO_3$ cm^{-3}). The calcification rate (g $CaCO_3$ $cm^{-2}yr^{-1}$) was obtained from the product of the extension rate and density.

4.2.2. Sclerochronology

4.2.2.1. Linear extension and chronology

Annual linear extension rates were determined by measuring the distance between the start of successive high-density bands or between the start of annual luminescent bands. These measures correspond to the mean coral growth from one summer to the next (Isdale 1981,1984; Lough and Barnes 1990a,b,1992). Particular care was taken to follow the maximum growth axis. To avoid reporting incomplete years of growth the most recent data are reported for the first complete annual band that completely cleared the tissue layer. The linear extension measurements for one core typically consist of 2 or 3 parallel tracks following the growth axis. In sections where only one track could be followed through the maximum growth axis or when bands showed a consistent perpendicular angle along the width of the core only one track was measured. The luminescent lines or density bands

were traced onto an acetate transparency film directly from the skeleton exposed to UV light or from printout images of UV light or X-rays. The distance between density or luminescent bands was measured from these transparencies or from digital images with the aid of image analysis software Coral XDS (NOVA Southeastern University, 2010). Results from direct measurements (made using a ruler) and with the aid of the software for sections of cores WHE09_1, WHE09_2, WHE09_4 and DAV09_2a show a correlation coefficients of r=0.9 n=23, r= 0.8 n=38, r=0.9 n=18 and r=0.8 n=29, respectively, for which the *t-test* indicates no significant differences (p=0.8, p=0.8, p=0.48 and p=0.54, respectively).

Lough and Barnes (1992) report a larger variability in the width and intensity of annual density bands in inner-shelf corals from Pandora Reef compared with mid-shelf corals from Rib Reef and outer-shelf corals from Myrmidon Reef. This enhanced variability complicates the identification of the density bands in inner-shelf corals, and as an alternative, luminescent bands can be used to measure linear extension when density bands are not clear (Allison et al. 1996; Lough 2011a). Using the luminescent bands can also reduce the uncertainty of assigning an age model as it allows cores to be visually cross-dated based on characteristic flood events (see Lough and Barnes 1990a) and therefore prevent dating errors associated with partial, missing or double density bands (Castillo et al. 2011). Furthermore, as measurements of luminescent bands are made along the surface of the corals they are less susceptible to being affected by the complex 3-D skeletal characteristics of *Porites* corals (Lough 2011a). Whilst comparable data sets can in principle be obtained from either methods (described in section 4.2.2.3); when present, luminescent bands are generally clearer and much better defined than the density bands. In the present study the chronology and linear extension measurements for all the inner-shelf corals were obtained from the luminescent bands. The information from X-ray negatives was used to assist in establishing the age model, ensuring the correct chronology was assigned. An example of the luminescent bands observed in inner-shelf corals from Havannah Is. and Pandora Reef is presented in Figure 4-1.

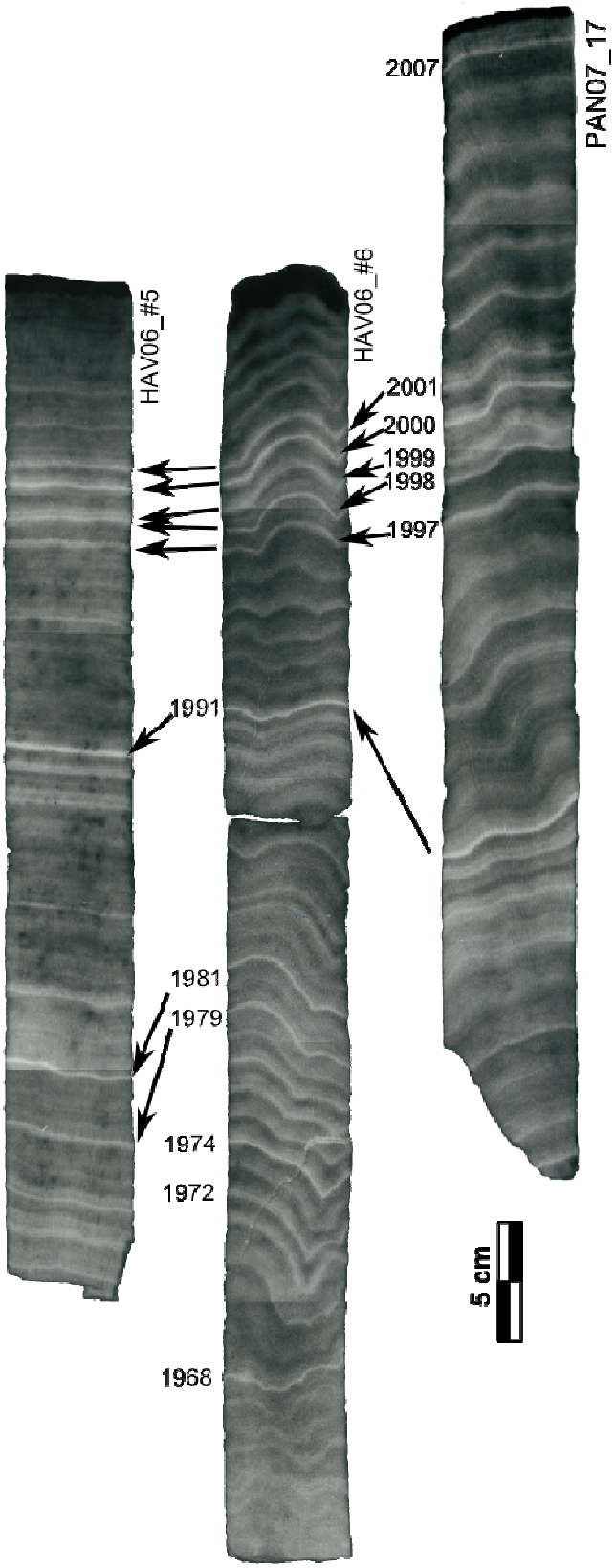

Figure 4-1. *Black and white images of luminescent bands photographed under UV lighting for three inner-shelf corals from Havannah Is. and Pandora Reef, the high intensity bands relate to episodes of high river discharge.*

Because density bands in corals from the mid-shelf region are obvious and luminescent bands are not always present (Lough and Barnes 1992), linear extension for corals from this region was based on the information from X-rays. Where present, luminescent lines linked to specific flood events (e.g. 1968, 1972, 1974, 1979, 1981, 1991 and 2009) were used to ensure chronological control. No clear evidence for luminescent bands was observed in the outer-shelf corals from Myrmidon Reef, a result of the minimal influence of terrestrial processes in this area (Lough et al. 2002). The age model and linear extension measurements for corals from Myrmidon Reef are based on the information obtained from X-rays alone. The uncertainty in the chronology was greater for corals from Myrmidon Reef, a result of the slow growing and curvature typical of corals from this reef that can cause distortions on the X-rays (Lough and Barnes 1992).

4.2.2.2. Data interpolation

An uncertainty in the timing of the formation of luminescent band exists associated with interannual variations in the timing in peak river run-off (Lough and Barnes 1990a). For the Burdekin River monthly peak river discharge is normally distributed with 92% of the flood events occurring between January and March, and a modal value of 42% in February (Figure 4-2). To account for this variability the exact month in which peak river discharge occurred for each year was included in the age model and incorporated into the derivation of linear extension data obtained from luminescent bands. For example, in the case of the luminescent band corresponding to the year 1970 the assigned date of the original chronology was 1970.083 as the peak in river discharge occurred in January. The linear extension time series generated were then resampled to an annual resolution using linear interpolation.

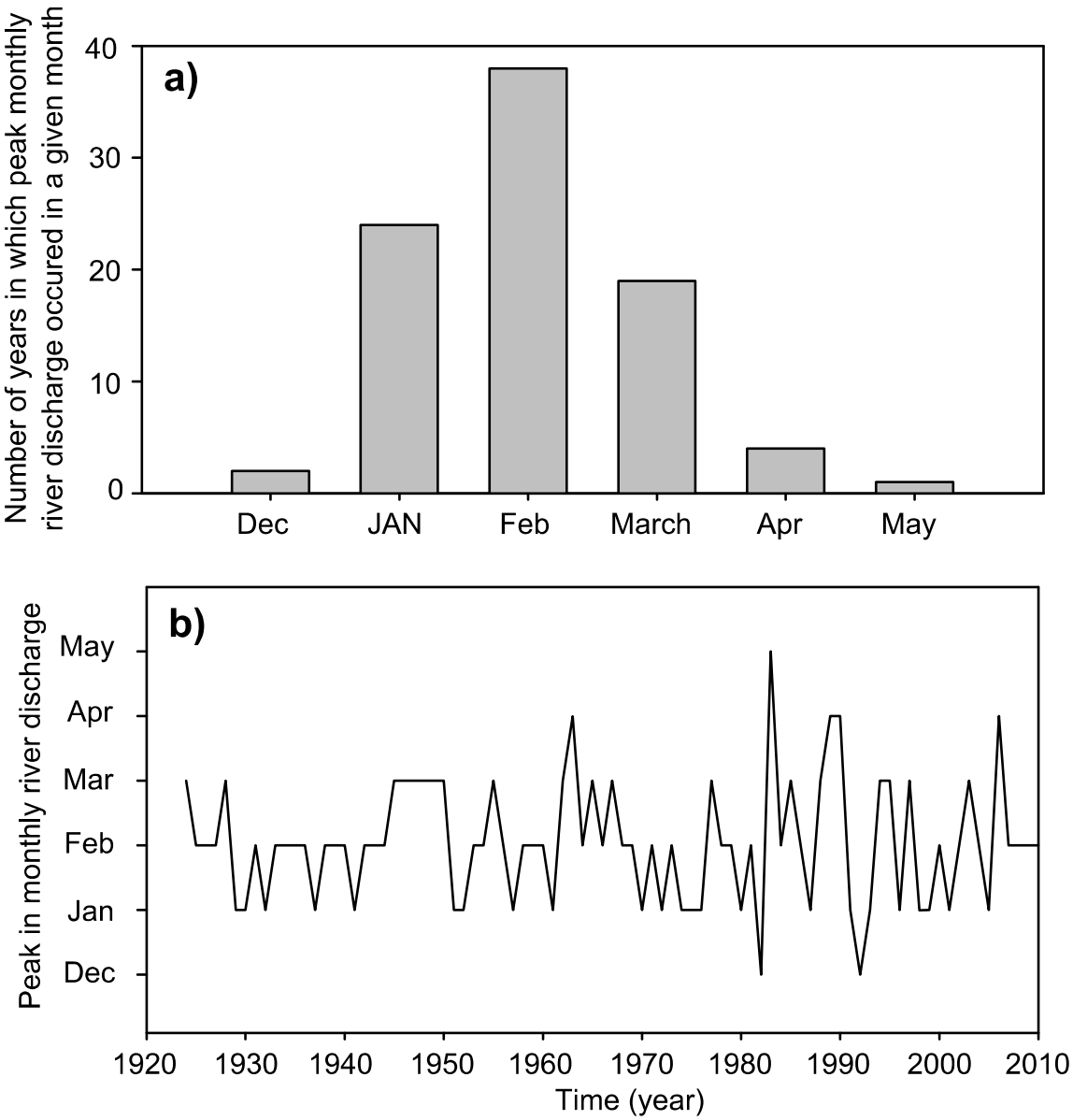

Figure 4-2. *(a) Distribution of the number of years in which peak monthly discharge for the Burdekin River occurred during a given month over the period of 1924 to 2010. (b) Temporal variation in the timing of peak monthly river discharge from 1924 to 2010.*

A similar variability exists for the timing of the formation of the density bands, which for *Porites* corals in the GBR is reported to be on average 3 months, but up to 8 months (Barnes and Lough 1993). Applying a similar correction to the timing of density bands is not possible as their formation is probably affected by a combination of several environmental parameters (e.g. temperature and light). The variations in the timing of the luminescent and density bands could affect the absolute annual extension rate and density

values however; the effect on the long term changes is reduced as any offset from one year is usually compensated in the next year.

4.2.2.3. Comparison between X-ray and UV luminescence linear extension data

The two main methods used to measure linear extension in this study, from X-rays and UV-luminescence, were compared to test if they produce similar information. The annual linear extension rates obtained from X-rays and UV luminescence were compared for four inner-shelf corals: HAV08_1, HAV08_2, PAN08_1 and PAN08_2, all of which present regular density bands (Figure 4-3). Correlations between the two methods over the common period of 1975-2006 were statistically significant for cores HAV08_1 and HAV08_2 from Havannah Is. ($r=0.6$; $p<0.0001$ in both cases) and not insignificantly correlated for cores PAN08_1 and PAN08_2 from Pandora Reef ($r=0.2$ and $r=0.1$ respectively). Despite differences in the annual values between the two methods similar long-term variability is observed, which becomes more evident after applying a Gaussian low band pass filter of 0.125 Hz to the data (Figure 4-4). The agreement between methods is again more evident for the two cores from Havannah Is. (HAV08_1 and HAV08_2) and not evident for the two cores from Pandora, particularly core PAN08_2. A visual inspection of the X-rays indicates that PAN08_2 has the least clear density bands of the four corals.

Figure 4-3. *X-ray negatives for 4 slices of Porites sp. corals from the inner-shelf reefs of Havannah Is. (HAV08_1 and HAV08_2) and Pandora Reef (PAN08_1 and PAN08_2) showing the annual density banding pattern.*

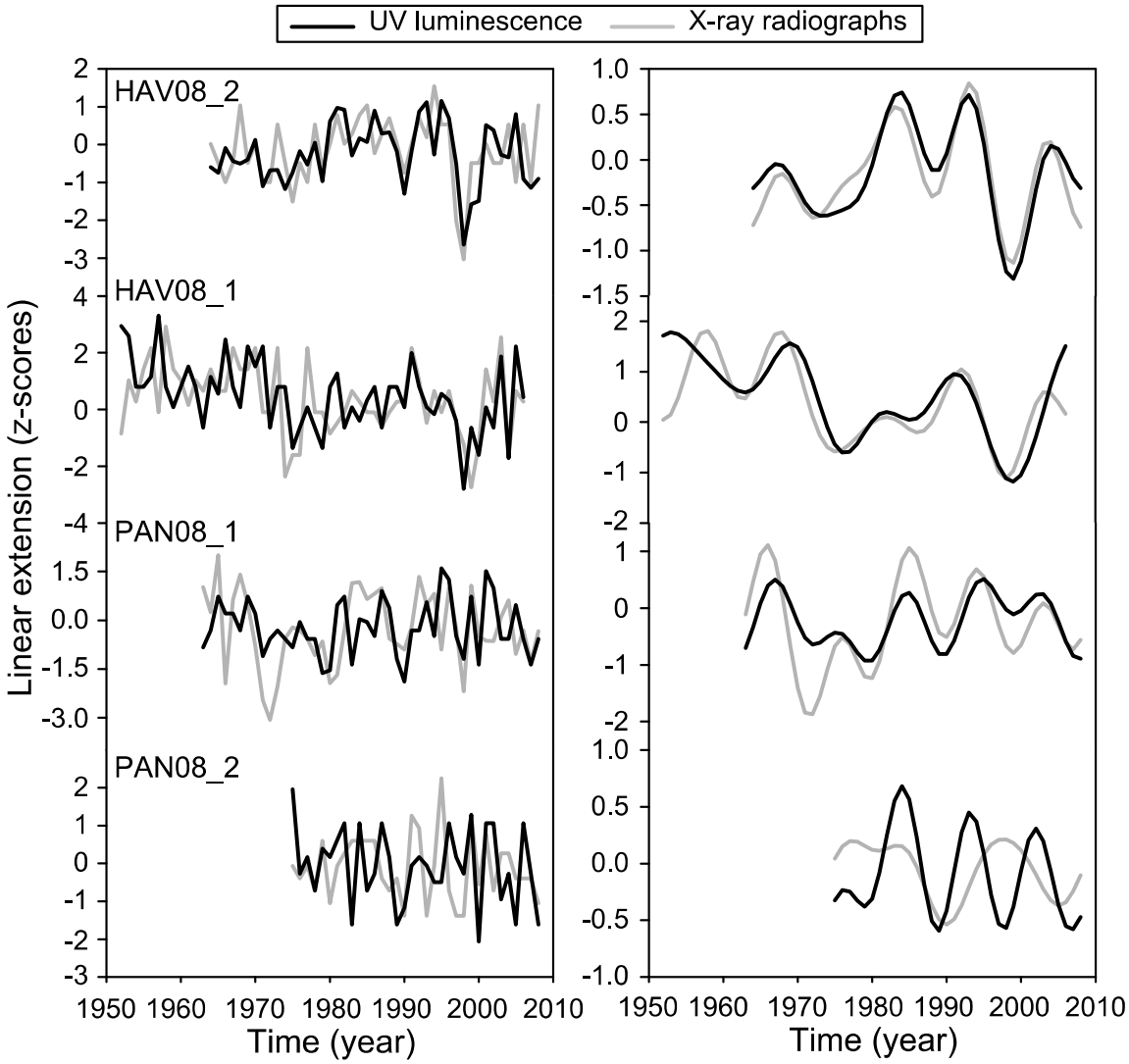

Figure 4-4. *(left) Annual linear extension rates obtained from X-rays (gray) and UV light (black) for four inner-shelf cores. (right) Smoothed versions of the annual time series after a low pass band filter of 8 years was applied. The data were normalized by subtracting the mean and divided by the standard deviation from each series.*

Master chronologies for each method were obtained from the normalized data of the four corals records (Figure 4-5) and give a correlation between methods of r=0.5 (p=0.006) calculated over the common period for the four coral records of 1975-2006 (r=0.3, p=0.018 over 1953-2008). The similarities between methods is again more evident after the data is smoothed using a low pass filter of 0.125 Hz to remove the interannual variability. The difference between the two methods increases as the number of cores is reduced towards the early part of the record. Reproducibility between tracks measured in a single coral slab by the same method is found to vary significantly between different cores, with correlations coefficients (r) varying between 0.3 and 0.9 for the UV luminescence data (with an average

r of 0.6 for 23 tracks) and 0.0 to 0.8 for the X-ray method (with an average r of 0.5 for 17 tracks). Therefore, at least part of the annual variability observed between methods is to be explained by variations on the tracks analysed. These results indicate that two different methods do not always produce comparable results; however this can be improved when several records are included.

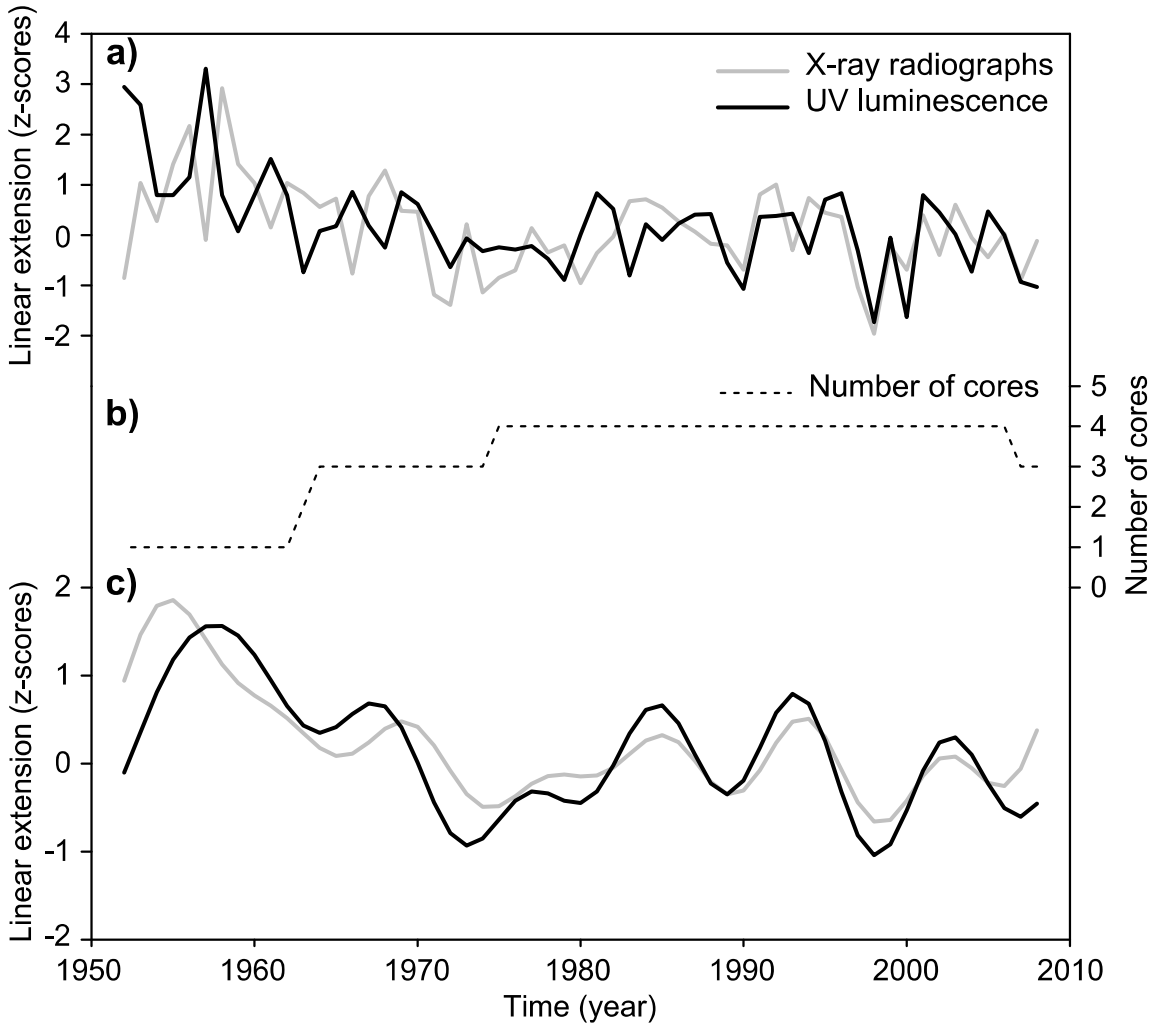

Figure 4-5. *(a) Master chronology for annual linear extension obtained from X-rays (gray) and UV light (black) for four inner-shelf cores presented in Fig. 4.3. (b) Number of cores through time. (c) Smoothed versions of the annual series in (a) after a low pass band filter of 8 years was applied.*

4.2.2.4. Coral density

Coral skeletal bulk density was measured using the water displacement method (Jokiel et al. 1978; Brown et al. 1990; Risk and Sammarco 1991; Scoffin et al. 1992; Bucher et al. 1998; Edinger et al. 2000; Smith et al. 2007; Manzello 2010) applied to pieces of coral cut

out from a single slab of all cores. Care was taken to ensure that the pieces followed the maximum growth axis. Pieces were cut similarly to those used for coral laser ablation mass spectrometry analysis (e.g. Fallon et al. 2003), which are typically 0.7 cm thick, 2.5 cm wide and less than 9.5 cm long The length of the pieces used in this study have an average resolution of 5 years (±2 years SD, n=414). No major difference was observed between corals sampled with a 5 year or 10 year resolution (Jung-Ok Kang, pers. com., 2011).

Pieces were cut from the start of a high density or luminescent band in the case of the inner shelf corals, except when there was a natural break in the core. The pieces were ultrasonically cleaned three times and then dried at ~50°C. The weight of each piece was measured in air and in water using a Mettler B6 manual hanging balance with an accuracy of ±0.00002g. After obtaining the dry weight each piece was vacuum-sealed with plastic wrapping using a domestic system (Sunbeam VAC420). The plastic was heat-shrunk using a heat gun to ensure an air tight seal and cut as close as possible to the skeleton to minimize the amount of plastic used to cover the piece. The dry weight of each plastic wrapped piece of coral was then measured. The weight in water was obtained by suspending coral pieces in distilled water. For the weight in water, a watch glass in an aluminium frame was suspended from the hook underneath the balance using nylon monofilament (Figure 4-6). A plastic container was filled with deionized water to cover the watch glass. The plastic enclosed coral was placed onto the watch glass, taking care to ensure that it was completely submerged in water and that no air bubbles adhered. Special care was taken to avoid punctures in the plastic. When this occurs it is easily recognized while weighing in water because the weight of the coral piece will drift as water invades the sample. Water temperature was routinely measured to calculate the density of the water.

Water was prevented from filling the skeleton during the wet weighting to preserve the mesoscale variations associated with bulk density (Bucher et al., 1998); therefore, the method used here is equivalent to a direct measurement of the volume. One of the advantages of using the water displacement method to obtain the volume over the direct measurements (e.g. callipers) is that coral pieces with a simple or complicated geometry can be equally easily resolved. The difference between the weight in air and the weight in water is equivalent to the volume of each coral piece. Density (g cm^{-3}) was obtained from the ratio of the weight (g) in air and the volume (cm^3). A correction for the amount of

plastic used was considered in the calculations. The measurements involved in the calculation of bulk-density are:

ρ_w = density of water (1 g cm^{-3} at 20°C)

DW_c = dry weight of the skeletal material unwrapped

DW_{cp} = dry weight of the skeletal material wrapped in plastic

$DW_p = DW_{cp} – DW_c$: dry weight of the plastic wrap

BW_{cp} = buoyant weight of the wrapped coral

$V_p = DW_p / \rho_p$: volume of the plastic

$V_t = (DW_{cp} – BW_{cp}) / \delta_w$: total volume (coral + plastic)

$V_c = V_t - V_p$: volume of the coral

$\rho_c = DW_c / V_c$: coral density

The formulae to obtain the density of the plastic (ρ_p) are: (the terms have the same meaning as above, where *a* refers to the acrylic instead of the coral)

$V_a = (DW_a - BW_a) / \delta_w$: volume of the acrylic

$\rho_a = DW_a / V_a$: density of the acrylic

$DW_p = DW_a – DW_{ap}$: weight of the plastic wrap

$V_p = (DW_{ap} – BW_{ap}) / \rho_w - V_a$

$\rho_p = DW_p / V_p$

A set of rectangular acrylic blocks, of known volume (measured using a caliper) were employed as standards to validate the method and calculate the density of the plastic used to cover the coral pieces. The reproducibility of the measured density of the acrylic standards and coral samples was 0.06% (n=35) and 0.55% (n=22), respectively.

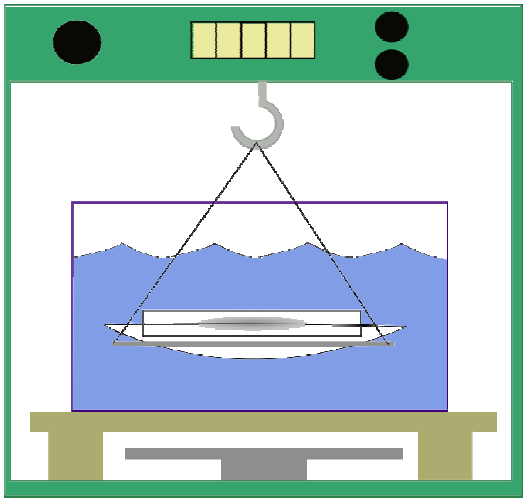

Figure 4-6. *Schematic of the system used to measure buoyant weights involved in the bulk density calculations.*

A density of 0.61 g cm^{-3} was calculated for the plastic used to cover the coral from the previous formulae. This value was used to correct the density estimates derived from the wet weight of coral pieces after calculating the amount of plastic used to cover each coral piece. The resulting density of the acrylic pieces measured with no plastic and the average value of acrylic pieces corrected for the density of the plastic cover are all in excellent agreement (Figure 4-7) with a mean density values of 1.186 g cm^{-3} and 1.188 g cm^{-3} respectively.

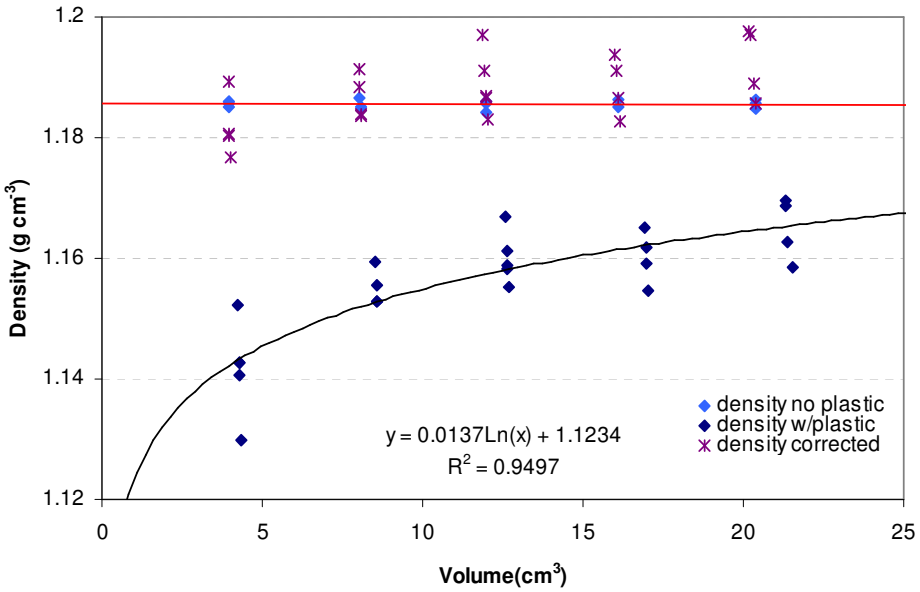

Figure 4-7. *Density vs volume for acrylic pieces used as standards.*

4.2.2.5. Data normalization

To obtain the coral growth master chronologies each coral record was scaled to the mean value using a normalization procedure (e.g. Dodge and Lang 1983). The procedure involved calculating the mean of the growth of each core over the common period of 1981-2002. This value was subtracted from the annual values of the corresponding core. This process equally weights all portions of the chronology. The average value for the period of 1981-2002 was calculated from the raw data for each region (inner-shelf, mid-shelf or outer-shelf) and added to the normalized annual values of each core. The scaling equation can be expressed as:

$$z_t = (x_t - \overline{x_c}) + \overline{x_R}$$

where x_t is a growth parameter at certain point of time, $\overline{x_c}$ is the mean value of the growth parameter over 1981-2002 for a given core and $\overline{x_R}$ is the average mean value for all the standardized cores from a specific region. Finally the resulting time series for each core were combined into a master chronology (Figure 4-8, Figure 4-9 and Figure 4-10). The data for the two corals from Myrmidon Reef collected at a depth of 25.5 m are included in the master chronology; however, all the data from this reef were scaled in respect to the median values calculated for the shallow corals. The cores collected before 1988 from Havannah Is. and Magnetic Is. and the data from AIMS were normalized with respect to the mean value over the period of 1962-1988. These data were then scaled using the mean value over the period of 1962-1988 calculated from the previously scaled records that extended to this same period. HAV01 and MAG88 correspond to cores also included in the AIMS dataset but were independently measured from replicate slabs of the same cores.

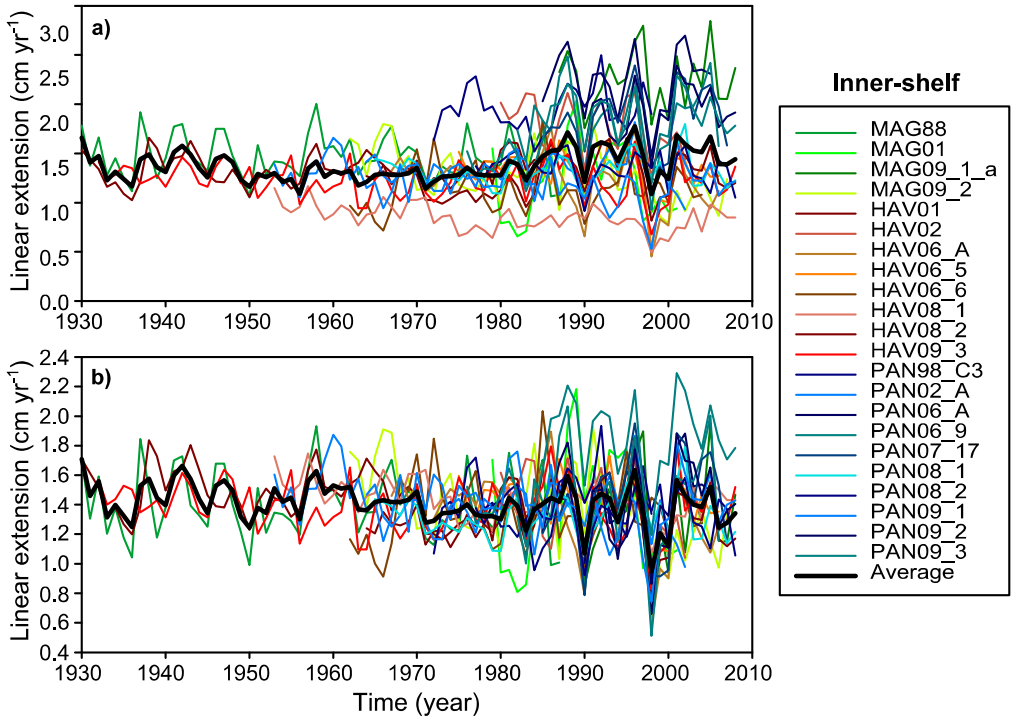

Figure 4-8. *Annual linear extension rates time-series for 22 coral cores from the inner-shelf reefs of Magnetic Is., Havannah Is. and Pandora in the central GBR presented as (a) raw data and (b) normalized data relative to 1981-2002 (see text). A master chronology is included for both datasets (black bold line).*

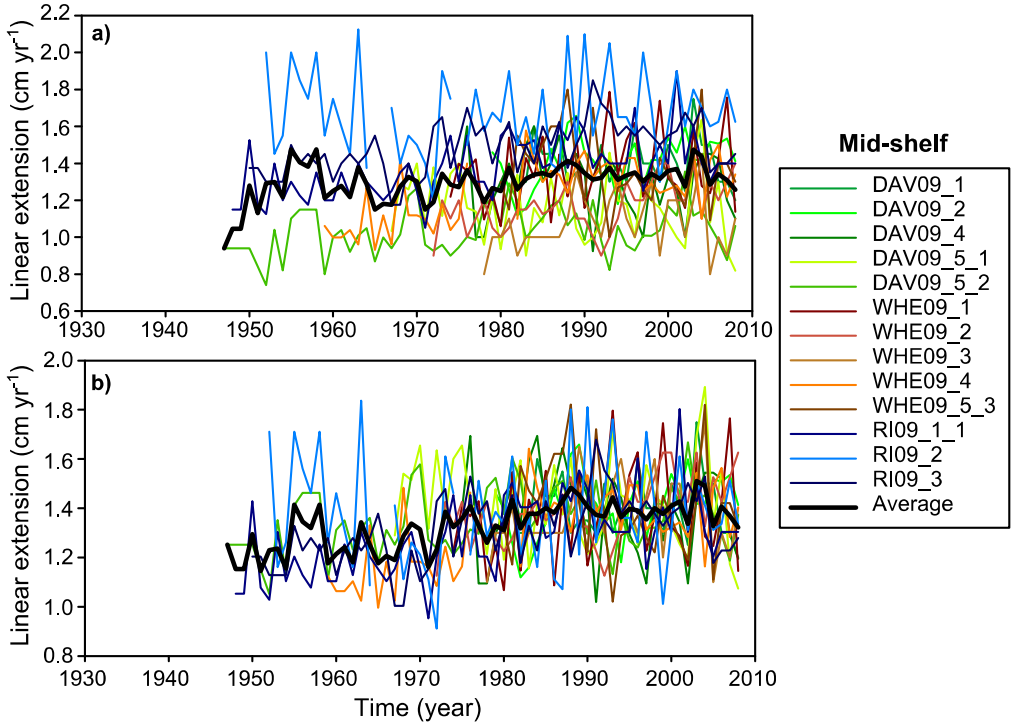

Figure 4-9. *Annual linear extension rate time-series for 13 corals cores from the mid-shelf reefs of Davies, Wheeler and Rib in the central GBR presented as (a) raw data and (b) normalized data relative to 1981-2002 (see text). A master chronology is included for both datasets (black bold line).*

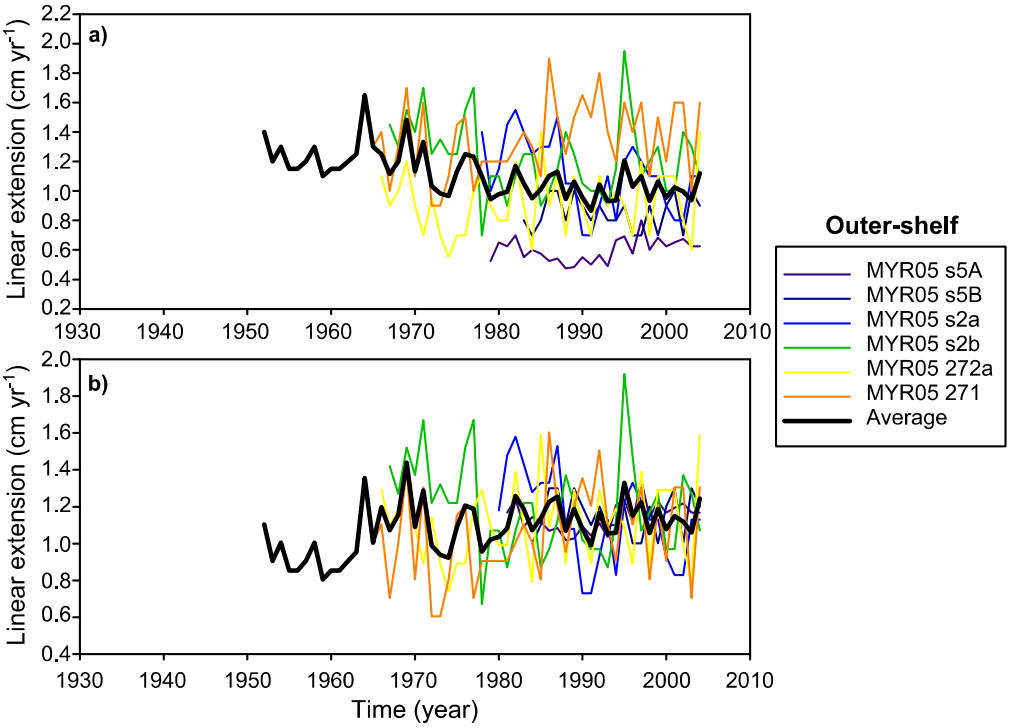

Figure 4-10. *Annual linear extension rates time-series for six corals cores from the outer-shelf reef of Myrmidon in the central GBR presented as (a) raw data and (b) normalized data relative to 1981-2002 (see text). A master chronology is included for both datasets (black bold line).*

4.3. Results

4.3.1. Cross-shelf variability in average coral growth parameters, 1981-2002

Average growth parameters were calculated for individual cores (n=41) of seven reefs (Table 2-2) from across the central GBR relative to a common reference period of 1981 to 2002 (Figure 4-11). The average linear extension rate is significantly correlated with calcification rates ($r=0.83$, $p<0.001$, $n=41$) and significantly inversely correlated with density ($r=-0.69$, $p<0.001$, $n=41$). Density shows no significant relationship with calcification ($r=0.18$, $p=0.257$, $n=41$).

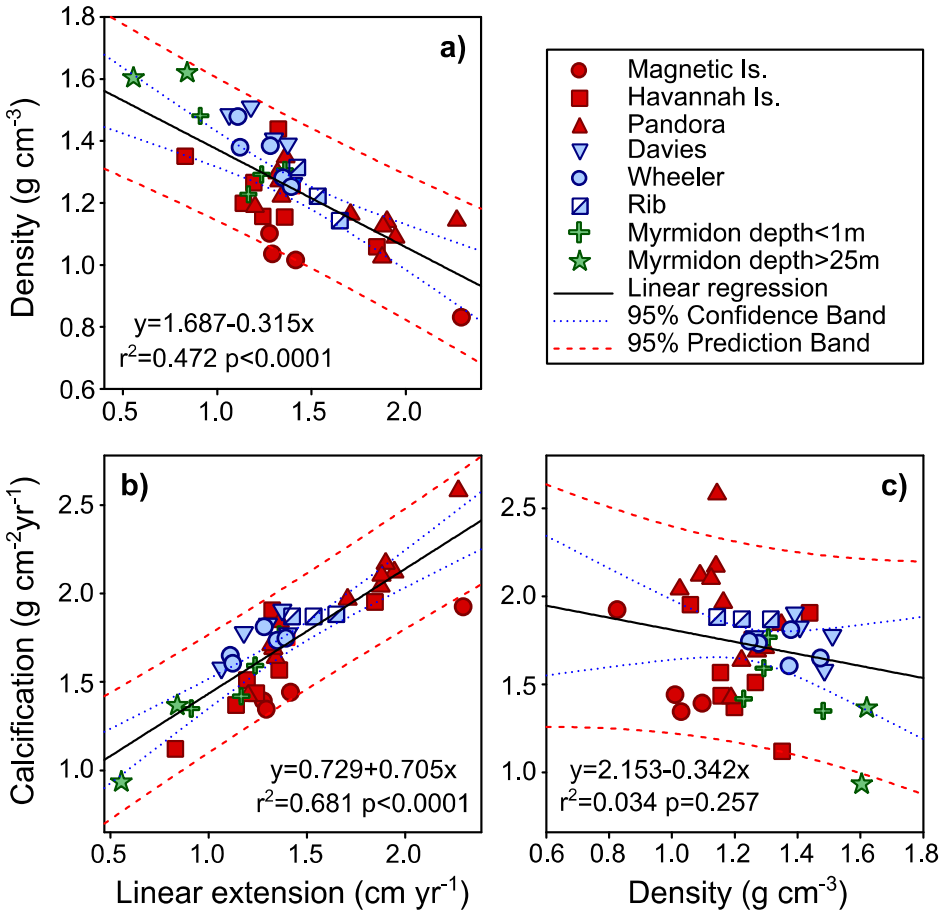

Figure 4-11. *Growth variables for 41 Porites colonies from the central GBR averaged over 1981-2002 for (a) linear extension vs, density, (b) linear extension vs. calcification and (c) density vs. calcification. Linear regressions and their significance are included. The confidence bands indicate the uncertainty associated to the regression lines, while the prediction bands relate to the distribution of values within the 95% probability. Colonies are grouped according to reef (see legend) and shelf location as inner-shelf (red), mid-shelf (blue) or outer-shelf (green).*

The inner-shelf colonies have the largest variability and highest linear extension rates and lower density values, but no significant linear relationships are observed for coral growth parameters versus distance across-shelf at the reef-scale (Figure 4-12). The outer-shelf deeper-water colonies have denser skeletons that calcify at a slower rate (Figure 4-12). Average annual calcification rates are approximately constant and do not show any clear across-shelf linear relationships (Figure 4-12c), although the mid-shelf reefs (Table 4-1) have slightly higher and less variable values. The lowest calcification rates were obtained from the deep-water outer-shelf Myrmidon Reef, and the inner-shelf corals from Havannah Is. and Magnetic Is. Differences between average linear extension, density and calcification were tested for corals in inner-shelf, mid-shelf and outer-shelf groupings (1 way ANOVA).

The shelf groups show differences in the mean density and calcification values that are statistically significant ($p<0.001$) but not for linear extension. Pairwise multiple comparisons (Holm-Sidak) indicate statistically significant differences were observed between the three groups for calcification, while no significant difference were observed between groups for linear extension. Density is significantly lower in the inner–shelf versus mid-shelf corals. The Myrmidon cores collected at 25.5 m depths were not included in these statistical comparisons.

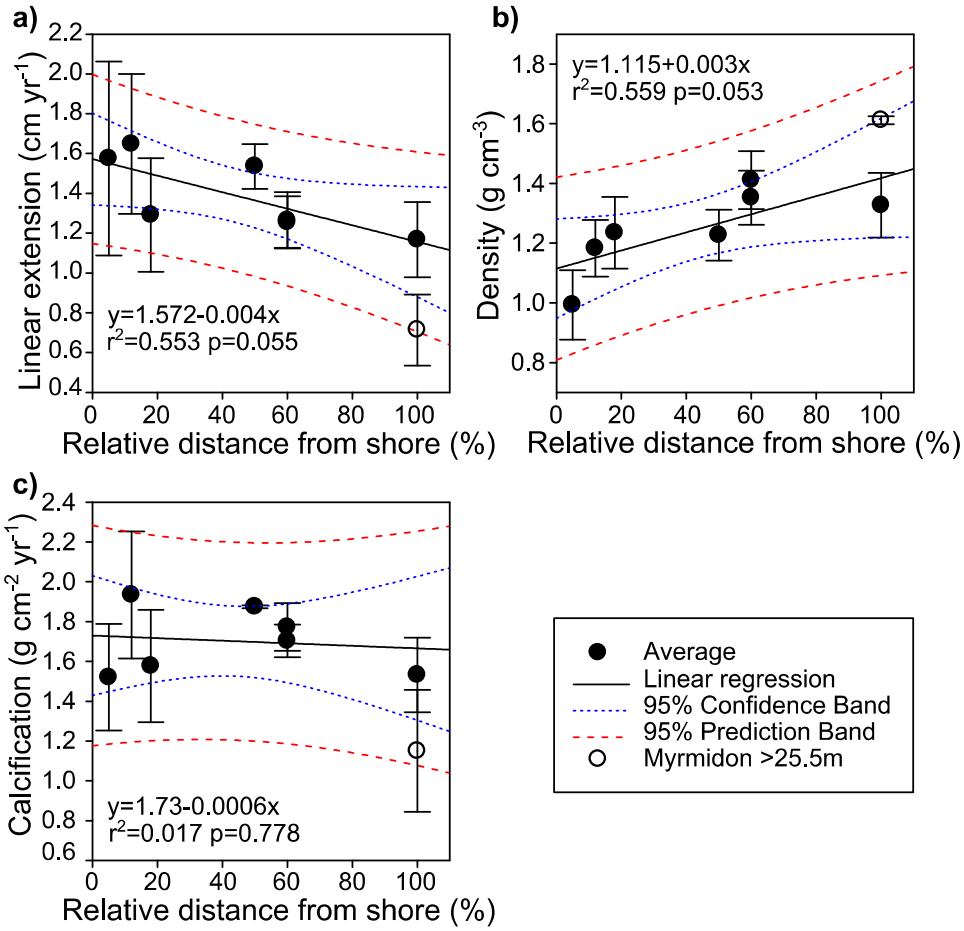

Figure 4-12. *Coral growth parameters: (a) linear extension rates, (b) density, and (c) calcification rates for individual reefs averaged over 1981-2002 plotted vs. distance across shelf expressed as a percentage of the width of the shelf (see Lough and Barnes 2000). The percentage distances to each reef correspond to: Magnetic Is. (5%), Pandora Reef (12%), Havannah Is. (18%), Rib Reef (50%), Davies Reef (60%), Wheeler Reef (60%) and Myrmidon Reef (100%). Error bars represent one standard deviation. The two fore reef corals from Myrmidon collected at 25.5m (open symbols) are not included in the linear fits and significance calculations. The confidence bands indicate the uncertainty associated to the regression lines, while the prediction bands relate to the distribution of values within the 95% probability..*

***Table 4-1**. Average growth characteristics for the 7 reefs based on the common period of 1981-2002 (±1 SD).*

Reef	Samples	Distance across shelf (%)	Linear Extension (cm yr^{-1})	Density (g cm^{-3})	Calcification (g cm^{-2} yr^{-1})
Magnetic Is.	4	5	1.58±0.49	0.99±0.11	1.52±0.27
Havannah Is.	8	18	1.30±0.29	1.23±0.11	1.58±0.29
Pandora	11	12	1.66±0.35	1.18±0.10	1.94±0.32
Davies	5	60	1.26±0.15	1.41±0.10	1.77±0.12
Wheeler	5	60	1.29±0.12	1.35±0.09	1.73±0.09
Rib	3	50	1.59±0.11	1.22±0.09	1.93±0.02
Myrmidon	4	100	1.17±0.20	1.31±0.12	1.53±0.18
Myrmidon (25m)	2	100	0.71±0.18	1.61±0.01	1.15±0.31

4.3.2. Co-variation between coral growth and environmental parameters

Over interdecadal timescales, annual linear extension rates for colonies in the inner-shelf of the central GBR are highly variable, ranging from ~0.85 cm yr^{-1} to 2.28 cm yr^{-1} (Figure 4-8; SD=0.38) and with standard deviations, from ~0.13 cm yr^{-1} to ~0.41 cm yr^{-1}. Annual linear extension rates are less variable in the mid-shelf (Figure 4-9; SD=0.18) and outer-shelf regions (Figure 4-10; SD=0.2 excluding the cores collected at a depth of 25.5 m). For the three regions there is a reduction in the number of cores in the earlier years. As described in section 4.2.2.5 each coral record was scaled using a normalization procedure that preserves original measurement units. The time overlap between the 5-year lengths of different corals pieces used for density measurements, results in a smoothed master chronology with a ~3 year resolution (Figure 4-13), but gives incompletely resolved interannual records. This approach however has the advantage of effectively averaging the relatively large seasonal fluctuations in density, capturing the main longer-term changes. Variations in annual calcification rate are in any case mainly controlled by annual extension rates in *Porites* (Lough and Barnes 1997).

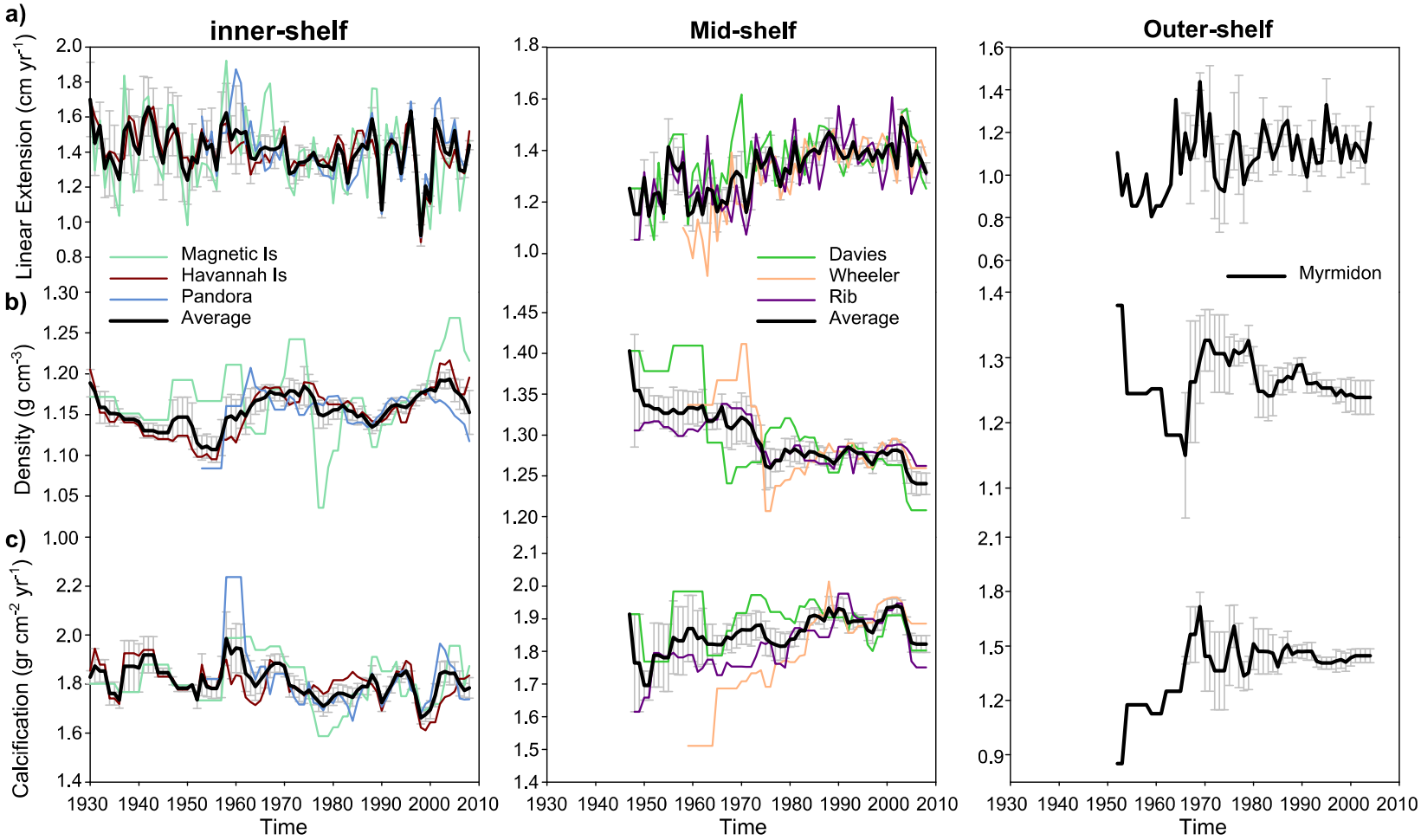

Figure 4-13. *Time-series of the growth parameters: (a) linear extension, (b) density and (c) calcification from the inner-shelf reefs of Havannah Is., Pandora Reef and Magnetic Is. (left), the mid-shelf reefs of Davies Reef, Wheeler Reef and Rib Reef (middle), and the outer-shelf Myrmidon Reef (right). The bold black line is the average for all colonies from each region; the gray bars represent the standard error (± SE).*

Time-series for density, calcification rate and annual linear extension rate were grouped according to their location on the shelf (Figure 4-13). In general there is good agreement between reefs from a given region (Table 4-2). Linear extension in the inner-shelf shows high interannual variations that are very similar within the three inner-shelf reefs (Figure 4-13). Particularly notable is the pronounced 2-3 years decrease in linear extension of almost 40% in the inner central GBR reef immediately following the 1998 bleaching event.

For the mid-shelf reefs for the period of 1947-2008 a general increase in linear extension and calcification is observed. A similar increase was observed in the more poorly represented outer-reef of Myrmidon. This reef shows a marked increase in calcification during the early part of the record (~1950-1970), but then remains approximately constant from 1980 to 2004. In the case of Myrmidon Reef, no significant difference was found in the master chronology by including the two cores collected at a depth 25.5 m ($r=0.97$, $p<0.001$).

Table 4-2. *Correlation coefficients (r), probabilities (p) and degrees of freedom (df) of growth parameter time-series (linear extension, density and calcification) between proximal reefs in the central GBR. Gray values indicate lack of statistical significance (95%). The df for the density and calcification time series were adjusted to allow for the reduced resolution of these time series.*

	Linear extension		Density		Calcification		Period	df
	r	p	r	p	r	p		
Inner-shelf								
Magnetic-Havannah	0.474	0.000	0.190	0.349	0.469	0.0149	1930-2008	77
Magnetic-Pandora	0.346	0.010	-0.111	0.654	0.515	0.0255	1953-2008	55
Havannah-Pandora	0.623	0.000	0.596	0.008	0.312	0.021	1953-2008	55
Mid-shelf								
Davies-Wheeler	0.465	0.001	0.191	0.463	-0.109	0.6771	1959-2008	49
Davies-Rib	0.356	0.005	0.396	0.078	0.118	0.6137	1948-2008	60
Wheeler-Rib	0.528	0.000	0.841	0.000	0.726	0.001	1959-2008	49
Outer- vs Mid-shelf								
Myrmidon-Davies	0.243	0.080	-0.100	0.693	-0.108	0.6697	1952-2004	52
Myrmidon-Wheeler	0.418	0.004	0.006	0.9826	0.532	0.0362	1959-2004	45
Myrmidon-Rib	0.111	0.430	0.096	0.7047	0.510	0.0306	1952-2004	52

To analyse the long-term interdecadal variability and assess the relationships to environmental parameters, the growth variables were smoothed with an 8-year low-pass filter (to remove the interannual variability). The smoothed time series were compared to similarly smoothed data of mean ERSSTv3b, rainfall at Townsville, and discharge for the

Burdekin River and Herbert River (Figure 4-14). The smoothed inner-shelf linear extension and calcification rate time-series show interdecadal variability from ~1960 to 2008 that matches the 'wet' and 'dry' periods observed in rainfall and river discharge. A significant inverse relationship of coral growth with rainfall is most evident in the last ~30 years (1969-2008; $r=-0.6$, $p<0.0001$, $n=40$), and is not significant before 1969 (1930-1968 $r=-0.2$, $p=0.239$, $n=39$). This pattern of interdecadal variability does not appear in the density time-series, and could relate to lower sampling resolution or indicate that density is less sensitive to these changes.

The smoothed time-series (Figure 4-14) of mid-shelf and outer-shelf annual coral calcification rates generally show a similar trend with SST over most of the record, consistent with enhanced calcification from warming. The exception is the most recent 5 year period (2003 to 2008) where there is a decrease in calcification in the mid-shelf mainly caused by a decrease in density (Figure 4-14). In contrast, in the inner-shelf, linear extension and calcification rates generally show the opposite long-term trend to SST, with linear extension and calcification decreasing with time, while SST has almost continuously increased.

On annual timescales linear extension rates for the inner-shelf, mid-shelf (1991-2008) and outer-shelf (1991-2004) regions are compared with annual *in situ* SST (maximum, minimum and average values), discharge from the Burdekin and Herbert rivers, and rainfall at Townsville in Figure 4-15. The *in situ* SST data (c.f. reconstructed SST) provide the necessary spatial resolution (tens of km) to resolve the variability between the three regions studied. The 1998 value is excluded from the linear regressions for the inner-shelf data as this is an outlier influenced by the strong El Niño event in that year. Linear extension was severely reduced in inner-shelf corals during this year with some *Porites* showing scaring and growth hiatuses (J.P. D'Olivo pers. obs.; Lough; 2008). Mid- and outer-shelf corals show no significant correlation (95% significance level) with any of the environmental parameters.

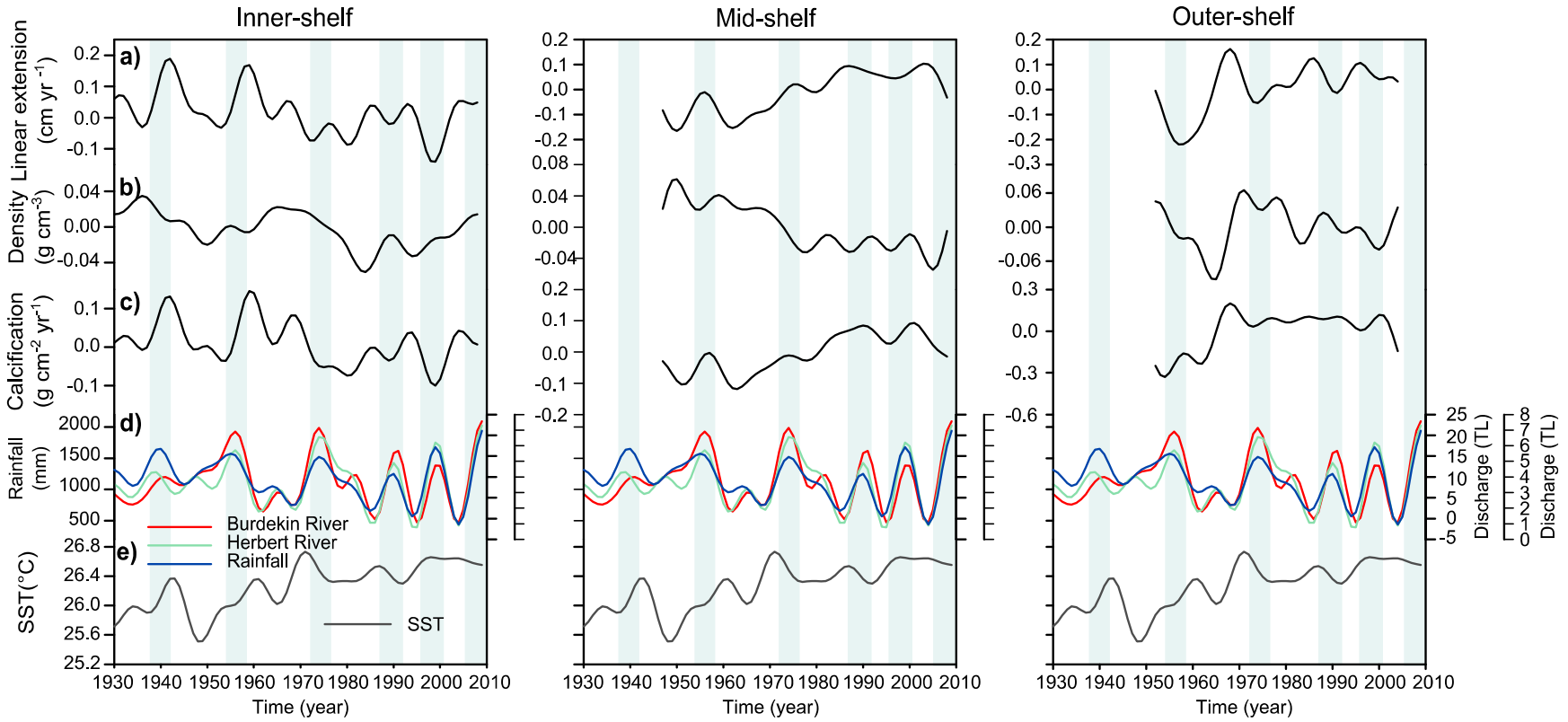

Figure 4-14. *Eight-year low pass filtered time series of the growth parameters: (a) linear extension, (b) density and (c) calcification. The data are grouped in inner-shelf, mid-shelf and outer-shelf and compared with (d) rainfall at Townsville, discharge at the Burdekin and Herbert rivers mouths, and (e) average SST from ERSSTv3b NOAA 2°×2°. The shaded areas highlight the wet and high discharge periods.*

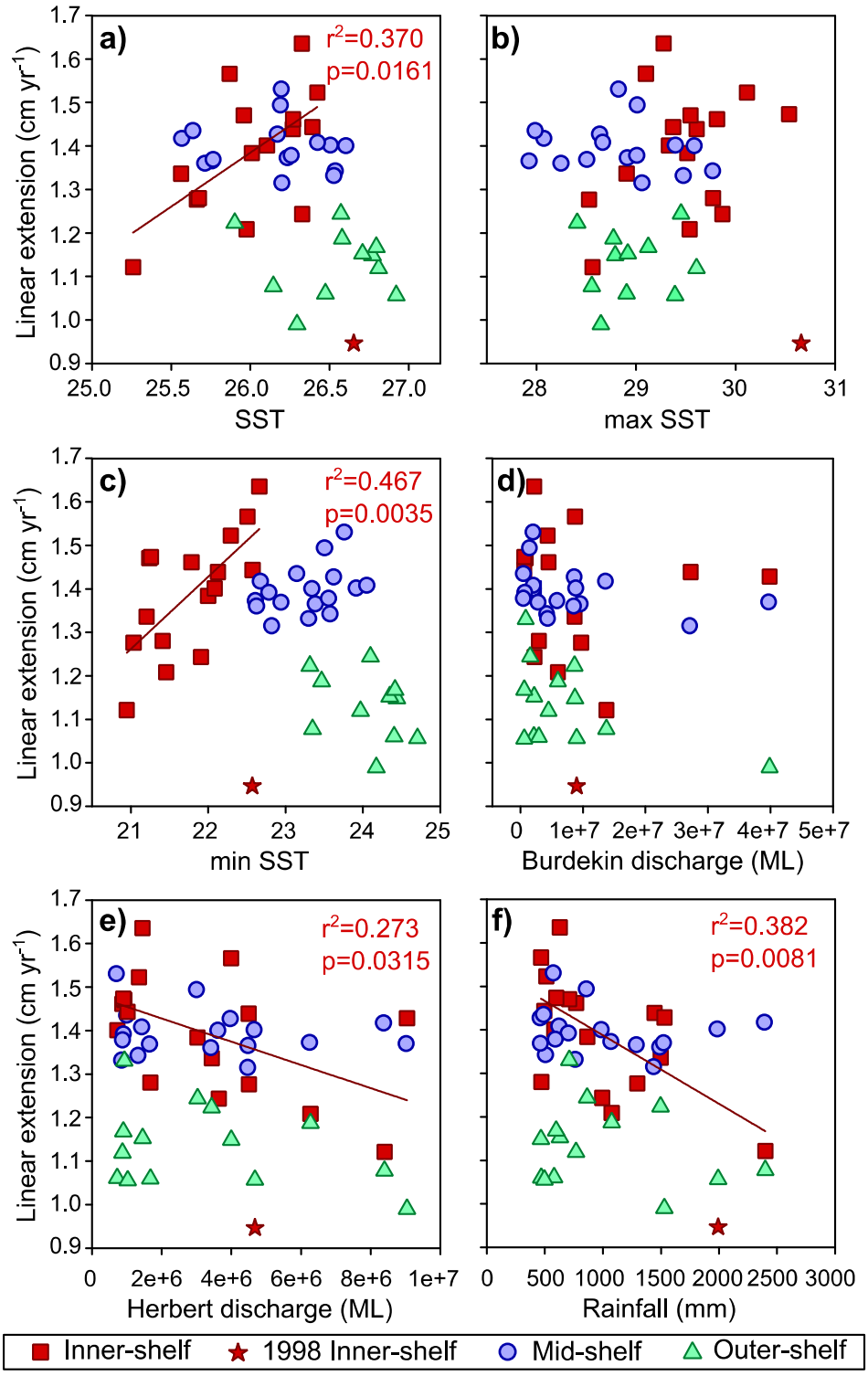

Figure 4-15. *Scatter plots based on annual time-series of composite coral linear extension rates vs.: (a) average annual in situ SST, (b) maximum annual in situ SST, (c) minimum annual in situ SST, (d) Burdekin River discharge, (e) Herbert River discharge, and (f) rainfall at Townsville over the period 1991-2008 (1991-2004 for the outer-shelf). Gaps in the in situ SST data occur in 1991-1992 for the inner-shelf, 1995 for the mid-shelf and 1993-1995 for the outer-shelf region. Regression lines for each region and their corresponding coefficient of determination indicated only when statistical significance exists. The calcification data for 1998 were not included in the linear fits for the inner-shelf data (see text).*

The inner-shelf in contrast, shows significant correlations of annual linear-extension rates with annual average SST, minimum SST, rainfall and discharge from the Herbert

River. It should be noted that while the river discharge correlates significantly with rainfall at Townsville (Table 4-3), the latter is a local indicator, whereas river discharge integrates variability in rainfall and runoff over the entire catchment. Furthermore, although the Herbert River is located closer to the studied inner-shelf reefs, it is expected to have a smaller effect on these reefs compared to the Burdekin River because of the much greater river discharge volumes and the predominant northward transport of the flood plumes from the latter (King et al. 2001; Furnas 2003; Wooldridge et al. 2006).

Table 4-3. *Correlation coefficients (r) between annual rainfall at Townsville (mm) and annual discharge data (ML) from the Burdekin River and Herbert River (1930-2008).*

	Burdekin			Herbert		
	r	p-value	df	r	p-value	df
Herbert	0.73	<0.0001	78			
Rainfall	0.59	<0.0001	78	0.62	<0.0001	78

4.3.3. Comparisons with AIMS coral calcification data

Coral growth data from this study are compared with measured growth data from 151 *Porites* cores from 100 individual colonies reported by De'ath et al. (2009) from the same central region of the GBR, which corresponds to 46% of the total number of samples reported by these authors. Part of the AIMS data set is available at National Oceanographic and Atmospheric Administration Paleoclimatology Data Center (www.ncdc.noaa.gov/paleo/) with the complete updated data set provided by J. Lough (pers. com., 2013). These data have recently been re-assessed by J. Lough (pers. com., 2013) with 40 of the 151 cores here included (26.5%) containing incomplete years in the uppermost (i.e. youngest) portion of the cores (see Figure 4-16). Incomplete years are those in which the density band from the most recent year was still being formed at the time of collection (J. Lough pers. com., 2013) but nevertheless originally included as a full year. This has the effect of reducing the calcification rate mainly as a result of an abridged extension rate in the final year (Figure 4-16 and Figure 4-17). Further scrutiny of the De'ath et al. (2009) data set undertaken here also revealed other possible anomalous end-of-year records in the most recent sections (Figure 4-17 and Figure 4-18). In addition 51 pairs of cores collected from the same colonies that were considered as individual samples in the De'ath et al. (2009) study are averaged here as single records. The revised AIMS data set is referred to herein as AIMS09, with the aberrant data identified by J. Lough (pers. com. 2013) removed and duplicate records averaged.

Both the original and modified data sets for central GBR from De'ath et al. (2009) are described in Table 4-4.

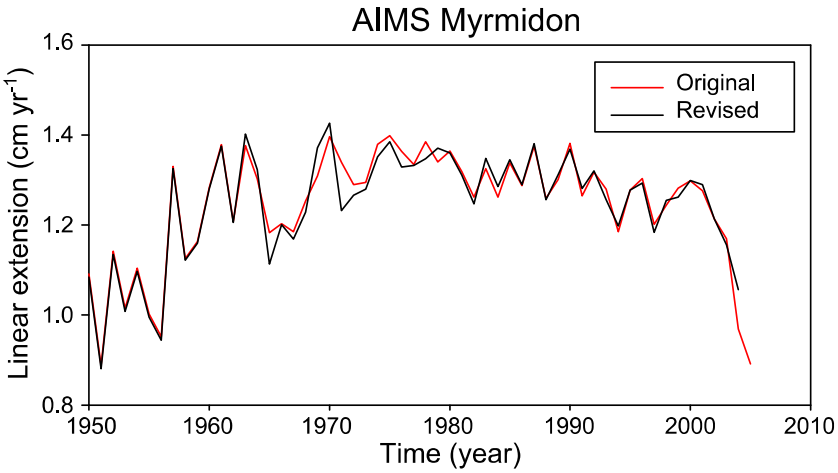

Figure 4-16. *Average annual linear extension rate time-series for AIMS coral cores from the outer-shelf showing the original data and corrected AIMS09 data for incomplete years removed and combining duplicate cores from single colonies.*

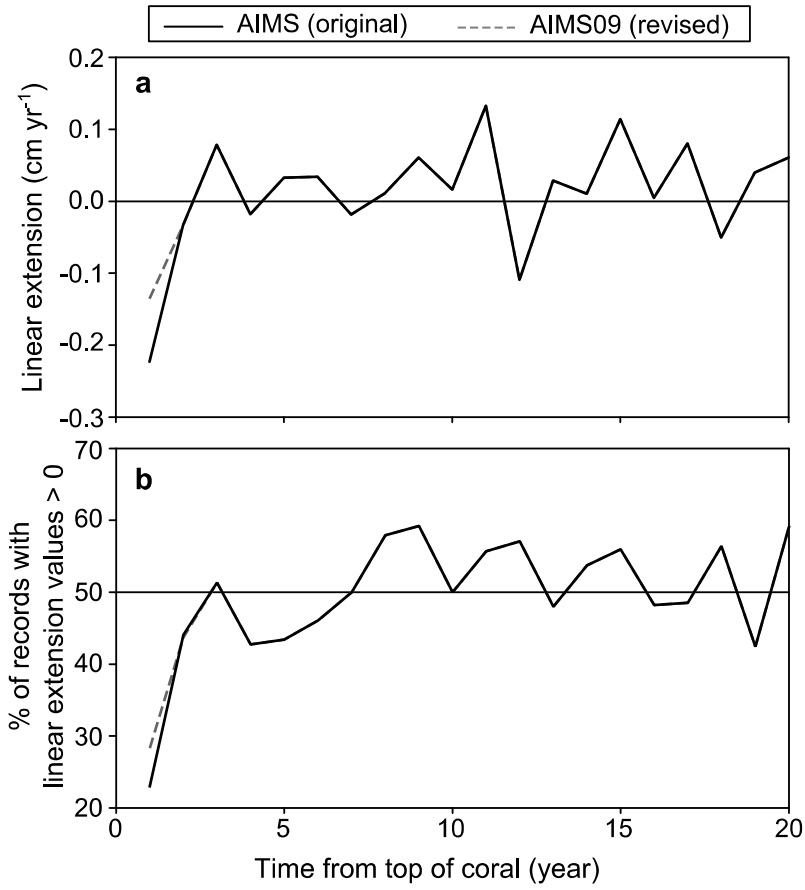

Figure 4-17. *(a) Time series of the normalized (reference period 1981-2002) annual linear extension rates for the De'ath et al. (2009) and revised AIMS09 datasets for the central GBR data and (b) percentage of cores with linear extension rates values above the average (1981-2002). The most recent year from each core was set as Year 1, regardless of the actual dates of collection, the latter ranging from 1983 to 2005. The low linear extension values and large number of cores with low values in the most recent year is indicative of artefacts generated from the inclusion of incomplete end of year records.*

Table 4-4. *Number of cores included from the AIMS dataset according to region. Original number of cores from the central GBR as reported by De'ath et al. (2009). Number of cores including incomplete years removed by J. Lough (personal communication 2013). Number of cores after combining pairs of cores obtained from the same colony*

	Original number of cores	Cores with incomplete years	Number of cores after combining pairs
Inner-shelf	64	20	42
Mid-shelf	48	6	33
Outer-shelf	39	14	25
Total	151	40	100

For the inner-shelf central GBR region the original AIMS dataset includes 64 cores, but after combining duplicate cores from the same colonies reduces to 42 inner-shelf records from Pandora Reef (n=28), Magnetic Is. (n=18) and Havannah Is. (n=1). For the mid-shelf region 49 cores are included but after combining duplicate cores results in 33 mid-shelf records from Rib Reef (n=28), Kelso Reef (n=2), Wheeler Reef (n=1), Lodestone Reef (n=1) and Yankee Reef (n=1). The outer-shelf includes 39 cores from 25 colonies, all from Myrmidon Reef. The coverage of the AIMS data is thus similar to this study, but is strongly biased towards collections from just 4 reefs (Magnetic Island, Pandora, Rib, and Myrmidon reefs). For consistency the most recent year was removed from those paired cores for which an incomplete year was removed by J. Lough (2013) from one core but not the corresponding pair.

Despite the issues of incomplete final year records affecting the AIMS data, over multi-decadal (i.e. 1930-2004) timescales, there is generally good agreement in the long-term average calcification parameters determined with the AIMS09 data-set and this study (Figure 4-18). This is illustrated by comparing linear trends from the long-term (i.e. 1930-1952 to 2004-2008) data sets of both studies (Table 4-5). For the mid-reef of the central GBR good agreement is observed between the studies with similar increases in linear extension (~15±3%; ±SE) and an overall increase in calcification from 1947 to 2008 of 8.8±1.1% (this study) compared to 4.7±2.3% from 1930 to 2004 for the AIMS09 dataset. For the inner reef although both data sets show similar (within errors) long-term decrease in extension rates (~7.7±3%), the AIMS09 also shows a decrease in density (-4.4±0.6%) and hence a more pronounced decline in calcification. In contrast data from this study show the often reported inverse correlation between these parameters (e.g. Scoffin et al. 1992; Lough and Barnes 2000), i.e. an increase in density (3.2±0.6%) with declining extension rate, but both studies still show overall long-term declining rates of calcification.

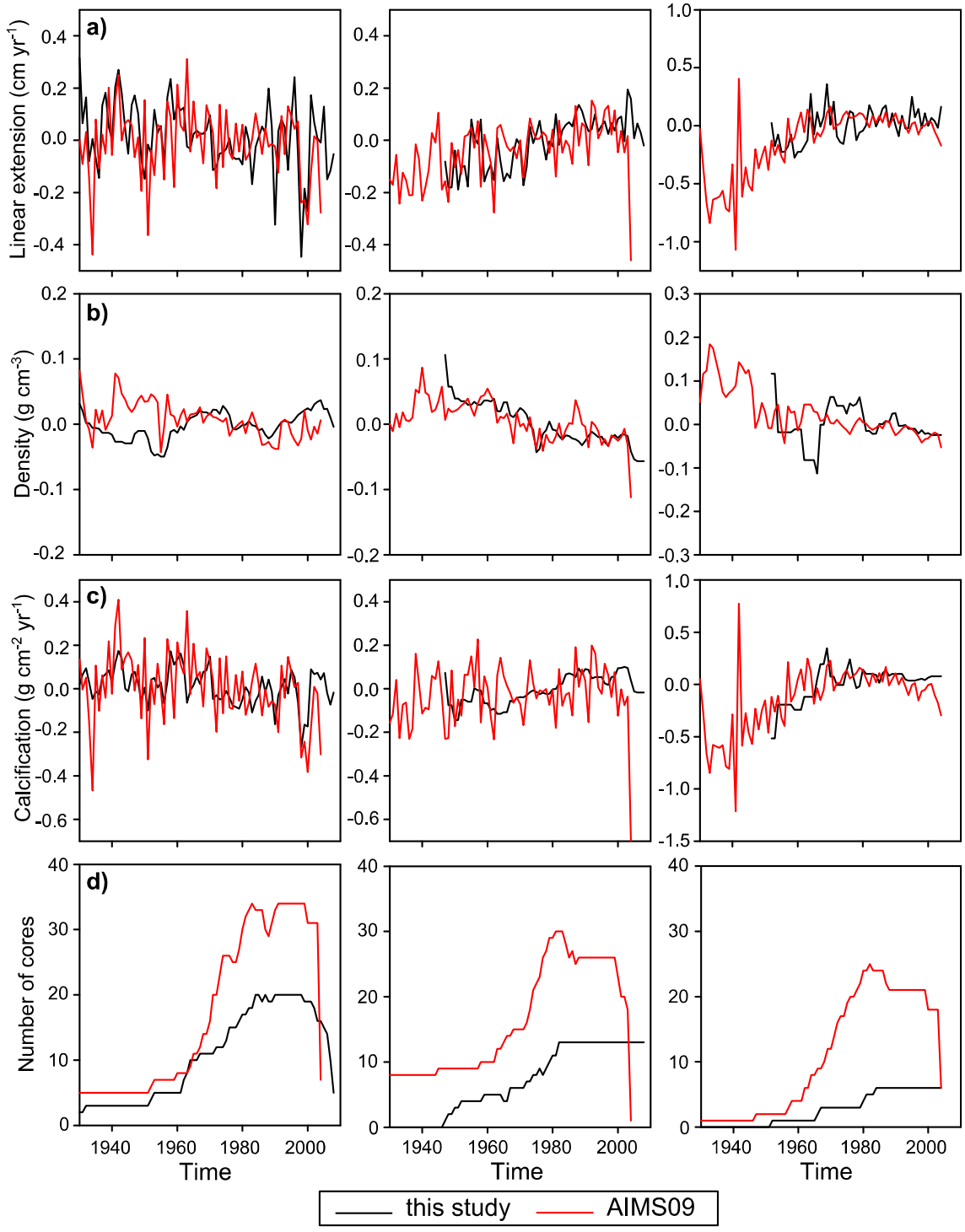

Figure 4-18. *Annual and ~5 year time-series for the normalized growth parameters; (a) linear extension, (b) density and (c) calcification obtained in this study and AIMS09 (De'ath et al. 2009). (d) Number of colonies included in each data set. The data are grouped as inner-shelf (left), mid-shelf (middle) and outer-shelf (right). The anomalously low values in the final years particularly for the inner-shelf and mid-shelf in linear extension and hence calcification for the AIMS09 data is indicative of artefacts generated by inclusion of records with incomplete end-of -year (see text and Figure 4-17).*

Correlations between the respective long-term data sets (normalized to the average of the records from each region) also show reasonable agreement. For example, for the parameter of annual linear extension, there is a significant correlation between this study and AIMS09 for long-term records from the inner-shelf (r=0.33, n=75, p=0.004), mid-shelf (r=0.38, n=57, p=0.004) and outer-shelf (r=0.29, n=53, p=0.038). There is also excellent agreement in duration and magnitude of the impact on coral growth rates of the 1998 stress event for both studies, with the main disparity being the aberrant final end-year record (Figure 4-18) in AIMS09. In contrast, for the recent period from 1990 to 2008, data from this study show recovery from the 1998 bleaching event, with inner reefs having approximately constant calcification (1.1±2.0%), while the mid-shelf reefs show a decline of 3.3±0.9%. The recent values from this study are in marked contrast to the 14.2% reef-wide declines for the GBR, reported by De'ath et al. (2009) over 1990-2005.

Table 4-5. *Percentage change (±SE) calculated from linear trends obtained for the periods of 1930-2008* and 1990-2008 for the three growth parameters (linear extension, density and calcification) for this study and AIMS09 dataset. Gray values indicate the lack of statistical significance (p<0.05).*

	This study(ANU)					
	1930-2008*			1990-2008		
Region	Lin. Ext.	Density	Calc.	Lin. Ext.	Density	Calc.
Inner	-9.5±2.3	3.2±0.6	-4.6±1.3	2.1±4.1	3.1±0.7	1.1±2.0
Mid	16.3±2.2	-6.6±0.6	10.9±1.1	-0.3±2.6	-2.6±0.7	-3.3±0.9
Outer	13±5	-3.3±1.4	11.1±3.9	6.2±6.4	-2.9±1.1	-0.7±1.9

	AIMS		
	1930-2004		
Region	Lin. Ext.	Density	Calc.
Inner	-5.8±2.9	-4.5±0.6	-11.4±2.4
Mid	13.6±2.1	-4.4±0.6	4.7±2.3
Outer	8.3±4.3	-7.2±1.0	6.2±4.0

* Trends for the mid-shelf data from this study include the period from 1947 to 2008 and for the outer-shelf from 1952 to 2004.

4.4. Discussion

4.4.1. Spatial variability in coral calcification across the central GBR

Although subject to large variability, there is a gradient of increasing extension and decreasing density from offshore to inshore across the central GBR (Figure 4-12). This is similar to trends reported previously by Lough and Barnes (2000), who attributed their results to reduced light and increased sedimentation rates with proximity to the

coast. Similar trends are found in the southern Gulf of Mexico (Carricart-Ganivet and Merino 2001). In the GBR outer-shelf, corals are subject to more physically energetic environments, extend more slowly and form denser stronger skeletons, possibly an adaptation to minimize physical damage by storms (Fabricius et al. 2008) or to greater wave energy. Corals from inner-shelf reefs which are subject to the effects of terrestrial runoff have higher linear extension rates at the expense of growing weaker (less dense) skeletons. Higher extension rates may help corals compete for resources, light and space (Carricart-Ganivet et al. 2012) or reflect growth induced effects of higher levels of nutrients. This indicates that on average *Porites* corals attempt to maintain near-constant calcification by offsetting increased (decreased) linear extension with decreased (increased) density, suggesting that maintenance of coral calcification is an energetically limited process (Cohen and Holcomb 2009). The clearest example of this relationship is the comparison of the growth parameters of the deep-water (25.5m) cores from Myrmidon fore-reef, which exhibit the highest densities, and lowest rates of linear extension (Table 4-1 and Figure 4-12). Depth has also been shown to have an effect on the growth of *Montastrea annularis* corals from the Caribbean with corals extending slower and forming denser skeletons with increasing depth (e.g. Bosscher and Meesters 1993). In the case of the central GBR no significant effect on the coral growth of *Porites* corals was observed up to depths of 20 m (Carricart-Ganivet et al. 2007).

4.4.2. Longer-term drivers of coral calcification in the central GBR

The correlation between inner-shelf coral linear extension and minimum SST (Figure 4-15) is consistent with the spatial relationships between average growth rates and average environmental conditions found by Lough and Barnes (2000). Minimum temperatures generally show larger variations in the inner-shelf compared to elsewhere in the central GBR (Table 2-1). It is therefore not surprising that linear extension for the inner-shelf shows a significant correlation with minimum rather than maximum temperature (Figure 4-15), as coral growth is more sensitive to changes at the lower temperature limits (Jokiel and Coles 1977). The average linear extension rate of inner-shelf corals is also inversely correlated with local rainfall and discharge from the Herbert River although, no significant relationship is observed with discharge from the Burdekin River. This could indicate that smaller localised terrestrial runoff has a stronger or more consistent effect in the reefs studied rather than the large flood plumes from the Burdekin River.

The interannual to decadal variability that characterizes the linear extension and calcification rates of the inner-shelf, however probably relates both to variations in SST and the effects of terrestrial runoff (Figure 4-14). Rainfall and river discharge do not show a significant long-term change in the region, although have become more variable since the late nineteenth century compared to earlier periods, possibly as a result of global warming (Lough 2007). Sedimentation and turbidity from terrestrial runoff in the inner-shelf of the GBR have also increased following European settlement and extensive land clearing in the late 19th century (Furnas 2003; McCulloch et al. 2003; Brodie et al. 2010). The chronic exposure of corals to elevated levels of nutrients and sediments has been linked to reduced coral calcification (e.g. Marubini and Davies 1996; Marubini and Atkinson 1999; Anthony and Fabricius 2000; Carricart-Ganivet and Merino 2001; reviewed by Fabricius 2005; Silverman et al. 2007); however, a number of studies have also shown no change or higher calcification rates with increased nutrient levels (e.g. Koop et al. 2001; reviewed by Fabricius 2005; Holcomb et al. 2010). These observations are thus consistent with higher suspended particulate matter levels providing energy for coral growth, until a maximum concentration is reached, after which a reduction in coral growth occurs due to smothering, reduced light levels and reduced zooxanthellae photosynthesis (Tomascik and Sander 1985).

The strengthening of the inverse relationship between terrestrial runoff and coral calcification over the recent period 1969-2008 therefore probably relates to an overall decrease in water quality reflecting a combination of increasingly degraded catchments and greater variability in rainfall and river discharge (Furnas 2003; Lough 2007; Brodie et al. 2010b; Lough 2011b). These observations therefore suggest that locally derived nutrients may now be directly affecting coral calcification in parts of the inner-GBR, and can have severe consequences when associated with periods of additional stress, such as occurred during the 1998 bleaching event (see section 4.4.3).

In contrast, the mid-shelf corals exhibit reduced interannual and decadal variability of coral growth parameters, probably due to the smaller seasonally driven range in SST and reduced terrestrial runoff effects compared to the inshore reefs. The long-term increase of ~0.8°C in SST over 1947-2008 is paralleled by increasing calcification and linear extension rates of mid-shelf and outer-shelf corals (Figure 4-13 and Figure 4-14). This positive temperature effect on calcification (c.f. McCulloch et al. 2012a) has so far

dominated and masked any negative effects from ocean acidification. However it is noted that in the last 5 years of the records from this study (i.e. 2003-2008) there is a decrease in calcification for the mid-shelf reefs primarily due to a decrease in density rather than extension rate as is usually the case (e.g. during 1998 bleaching). Whether this is a sustained change has yet to be confirmed, but if so, may indicate a changed regime where the negative effects of CO_2 driven climate change (e.g. ocean acidification; Wei et al. 2009; McCulloch et al. 2012) are becoming pre-eminent.

It is also noted that the long-term increase in calcification in the mid-shelf and to a lesser extent the outer-shelf corals is not necessarily a positive outcome, as it is also accompanied by a decrease in density which could make these corals more susceptible to damage from tropical cyclones and storms. A similar scenario is proposed by Carricart-Ganivet et al. (2012) for the Gulf of Mexico, with a reduction of density in *Montastrea* spp. predicted to increase the susceptibility to both physical and biological breakdown.

4.4.3. Stress and bleaching event of 1998

Although the 1998 bleaching was widespread throughout the GBR (Berkelmans and Oliver, 1999), in the central region, it is only the inner-reefs where effects are clearly evident in the *Porites* growth records (Figure 4-13 and Figure 4-18). This agrees with an aerial survey conducted during the 1998 bleaching event that found a higher percentage of reefs bleached and greater severity of bleaching on the inshore reefs compared to mid-shelf and outer reefs (Berkelmans and Oliver 1999). Based on the currently available records of coral growth, the 1998 event and the resultant decrease in calcification associated with it, appear to be unprecedented in both its severity and the extended duration for recovery. It is not until ~2002 that inshore extension rates and hence calcification, recovered to the pre-1998 bleaching levels. In the early 1930's there is a similar prolonged (2-3 years) decrease in extension rates of ~20%, but this is not as extreme as the ~35% decrease 1998 event. Whether this can be attributed to the effects of bleaching cannot be determined and would require high resolution Sr/Ca derived SSTs studies of the type undertaken by Marshall and McCulloch (2002) for the 1998 bleaching event. The other notable event for which there is no obvious explanation is in 1990, where there is an abrupt but short-lived (<1 year) decline in inshore extension rates of ~30%. Unlike the effects of the 1998 event, in 1990 there is no evidence for

anomalously high temperatures or bleaching, with only the timing of the flood event being unusual as the peak in the wet season occurred around April, two months later than is typical.

The abrupt reduction in calcification and long lasting effects of the 1998 bleaching event were also noted by Marshall and McCulloch (2002) and Suzuki et al. (2003) in corals from Pandora Reef as well as elsewhere in the GBR (Lough 2008a). The spatial patterns and intensity of the 1998 bleaching event are unmatched with the severity only being approached by the 2002 bleaching event (Berkelmans et al. 2004). However, in 2002 there are no signs in *Porites* growth records from this study for significant decreases in coral growth as occurred in 1998. Higher thermal stress (quantified as degree heating days) and surface irradiance observed in 2002 compared to 1998 led Maynard et al. (2008) to suggest that thermal adaptation must be responsible for the reduced bleaching in 2002. It is worth noting that the highest value recorded for monthly average maximum *in situ* SST from the inner-shelf corresponds to February 1998 when values reached ~30.3°C whereas in 2002 maximum temperatures remained below 30°C.

Thus, in addition to the extremely high thermal stress encountered by corals in inner-shelf reefs during 1998 other factors may have led to the high levels of intense bleaching. Additional stress due to nutrient and sediment loading observed in the rainfall and river runoff data (Furnas, 2003) prior to the 1998 bleaching event could have been a major additional factor, with low salinity waters still being present during the early stages of bleaching. This is consistent with coral fitness and resilience to episodic events being reduced as a result of the compounded effects of local anthropogenic stressors (e.g. Hughes et al. 2003).

4.4.4. Current state of the GBR

Long-term 1947-2008 (1952-2004) changes in linear extension for the mid-shelf (outer-shelf) corals of the central GBR are dominated by an overall increase of 2.7±0.4% (2.1±1.0%) per decade, consistent with enhanced rates of extension from the kinetic effects of higher temperature (McCulloch et al. 2012a). However, this is partially offset by significant declines in density of -1.1±0.6% (-0.6±0.3%) per decade resulting in only a modest increase in calcification of 1.4±0.2% (2.1±0.8%) per decade. Although this

study is only based on the findings from *Porites* cores, if ubiquitous across coral species, of the mid- and outer-shelf of the GBR, lower density skeletons could make corals more vulnerable to tropical cyclone damage, particularly delicate branching corals. This may be account for the finding of cyclone damage now being the major cause (48%) for declining coral cover in the GBR (De'ath et al. 2012).

For the inner GBR, for the period from 1930 to 2008, a different pattern emerges. A persistent long-term decline in calcification (-1.2±0.3% per decade) is accompanied by little o no change in density. This together with large interannual variations in extension rates implies a marked negative influence of river runoff. The long-term declines in coral growth found here for the inner-shelf is also consistent with the decreased coral cover data reported for the same Townsville region, by Sweatman et al. (2011). Sweatman et al. (2011) and Sweatman and Syms (2011) note that the large reduction (20-28%) in coral cover inferred for the GBR during the last 20 years, is mainly due to pronounced declines in 6 inner reefs, compared to the total of 29 sub-regions studied.

Furthermore, as already discussed the inner-GBR appears to exhibit a relatively high sensitivity to bleaching, particularly during the 1998 event when high temperatures were preceded by a major river runoff event. This now provides supporting field-based evidence from the inner-GBR reefs for strong negative interactive effects between degraded water quality and sensitivity to bleaching during extreme warming events (see Wooldridge 2009). It is also noted that these negative interactive impacts on calcification are occurring despite the larger natural variations in inshore seasonal SST, compared to mid-shelf, indicating that degraded water quality is more than offsetting any potential beneficial effect from adaptation to a large SST seasonal cycle. Thus local factors rather than long-term climate change appears to be the dominant driver causing the rapid declines in coral cover of ~30% observed since ~1980 (Hughes et al. 2011; De'ath et al. 2012).

For the most recent period from 1990 to 2008 the central GBR has overall maintained approximately constant rates of calcification (Table 4-5). The updated data (2008) document a significant recovery of coral growth for inner-shelf corals following the 1998 bleaching event, but offset by a moderate (3.3±0.9%) decrease in calcification for the mid-shelf reefs. Whilst the findings from this study are in marked contrast to the much more extreme (14.2%) reef-wide declines in calcification reported by De'ath et al.

(2009), they nevertheless give grounds for concern. As already noted, the inner reefs of the GBR show significant long-term trends of decreased coral calcification that can be attributed to degraded water quality, and during periods of thermal stress results in increased susceptibility to coral bleaching. Although the more distal mid-shelf and outer-shelf corals reefs areas are in better health, pronounced recent downturns in calcification maybe indicative of a transition from positive temperature enhancement of calcification to decreased rates due to thermal stress and/or the negative effects of ocean acidification (McCulloch et al. 2012a). It is thus clear that regional assessments provide an informative description of the changes in coral growth in the GBR, and importantly insights into their causes and thereby strategies for mitigation. Importantly these types of studies can help to identify those areas of the GBR for which direct local action will have beneficial outcomes. This has important management implications, re-enforcing the ongoing need to improve water quality in the inshore reefs, by for example remediating disturbed river catchments and minimizing/limiting impacts from large-scale coastal developments.

5. The influence of coastal processes on seawater *p*H in coral reefs across the central Great Barrier Reef

5.1. Introduction

In the last decade there has been an increased concern about the effects of CO_2 uptake by the ocean, particularly on calcifying organisms, including reef forming corals. Experimental data indicates that the increase in CO_2 will cause a reduction on the calcification rates of marine organisms (Ries et al. 2010). However, the response of coral calcification during the early stages of reduced *p*H and Ω_{arag} remains a topic of debate as results vary significantly between studies (Langdon et al. 2000; Marubini et al. 2008; Cohen and Holcomb 2009; Ries et al. 2009; Ries 2011; McCulloch et al. 2012a; McCulloch et al. 2012b). Predicting the calcification response of corals in natural reef environments is further complicated as calcification is influenced by other physical and chemical variables including temperature and nutrients (see section 1.3.2). This is further complicated as the combination of these factors vary between different oceanic provinces (Falter et al. 2012).

Long-term changes in calcification rates of corals from the GBR have been suggested to be associated with thermal stress and ocean acidification (Cooper et al. 2008; Lough 2008a; De'ath et al. 2009). One of the limiting factors in linking the long-term response of corals calcifications to environmental changes results from a lack of field data; this is particularly true for seawater chemistry parameters including seawater *p*H measurements (Cooper et al. 2008). *In situ* measurements in the central GBR reveal that the Davies Reef flat, a mid-shelf reef, are highly variable over diel and seasonal timescales with *p*H (total scale) ranging from 7.92 to 8.17, pCO_2 ranging from 272 to 542 µatm, and Ω_{arag} ranging from 2.9 to 4.1 (Albright et al. 2013). Shaw (2012) observed that on a seasonal scale seawater *p*H on the reef flat of Lady Elliot Island, the southernmost island of the GBR, inversely varies with temperature and reports a seasonal range of ~0.06 units, the later established from 2-week sampling periods between seasons. On spatial scales Gagliano et al. (2010) reports a variability of 0.1 *p*H units between micro-regions within a reef (Magnetic Is.) and up to

0.39 *p*H units when comparing micro-regions of two reefs, Magnetic Is (sampled in April 2008) and Lizard Is. (sampled in December 2007), separated by 100's of kilometres in the GBR. However, all of these studies represent discrete measurements and are, therefore, difficult to relate to long-term temporal changes in seawater *p*H in coral reef communities of the GBR.

Along with rising temperatures and reduction of seawater *p*H, inner-shelf coral reefs of the GBR are also being exposed to increasing terrestrial influences from grazing, agriculture, mining and land clearing that is causing a decrease in water quality (McCulloch et al. 2003; Lewis et al. 2007; Brodie et al. 2010b). Known impacts include the promotion of intense and extensive phytoplankton blooms, an increase in macro-algae abundance, and affects on the biodiversity, cover and recruitment of corals (Devlin and Brodie 2005; Brodie et al. 2010b). Increased productivity during phytoplankton blooms can cause seawater *p*H to rise significantly (Hinga 2002). Nutrient-enhanced photosynthetic activity has been shown to amplify the seasonal *p*H cycle by more than 0.5 *p*H units in experiments on marine enclosures in Narragansett Bay, Rhode Island (Frithsen et al. 1985) and to increase seawater *p*H by 0.7 units in the Peruvian coastal upwelling zone (Simpson and Zirino 1980). It is not known to what extent terrestrial runoff and the associated phytoplankton blooms influence seawater *p*H in the GBR partially because of the lack in seawater *p*H observations.

On multi-decadal timescales, measurements of $\delta^{11}B$ have been applied to coral skeletons to reconstruct changes in seawater *p*H. Pelejero et al. (2005) found a significant decadal component in $\delta^{11}B$ reconstructed seawater *p*H that was linked to the Inter-decadal Pacific Oscillation through the effect of wind strength on flushing of the Flinders Reef lagoon in the Coral Sea. An interannual trend of decreasing seawater *p*H of ~0.2-0.4 units was observed by Wei et al. (2009) since the 1940's at Arlington Reef, a mid-shelf coral reef from the northern GBR. In the northwestern Pacific the $\delta^{11}B$ signal in a *Porites* coral from Guam was used to reconstruct a ~0.05–0.08 *p*H units decrease for surface seawater *p*H since the mid-20th century (Shinjo et al. 2013).

In this chapter the $\delta^{11}B$ proxy is applied to coral samples obtained from cores of massive *Porites* heads collected from two inner-shelf and one mid-shelf reefs of the central GBR.

The $\delta^{11}B$ data is used to reconstruct the interannual variability in surface seawater *p*H over the past ~50 years in this part of the GBR. These results are complemented with measurements of coral calcification from multiple long cores collected from massive *Porites* heads along an inner-shelf to outer-shelf transect north of Townsville described in Chapter 4. This provides a comparison between the dynamic environment of the inner-shelf reefs, which are subject to terrestrial and anthropogenic influences compared to the mid-shelf reefs characterized by more stable conditions, and less exposed to terrestrial runoff and pollutants (Lough 2001; Furnas 2003; Brodie et al. 2012a). Particular focus is placed on changes that have occurred in inner-shelf reefs, which are subject to episodic inputs of acidic fresh water, sediments and nutrients from river runoff from the Burdekin and Herbert Rivers. The sub-annual and interannual variability of the $\delta^{11}B$ proxy provides unique information on how the seawater *p*H varies in a natural coastal system and how these changes relate to those observed in coral calcification.

5.2. Material and methods

Boron isotope ratios of coral and water samples were analyzed by positive thermal ionization mass spectrometer (PTIMS) method using a Finnigan TRITON at ANU RSES. The PTIMS mode was used in preference to the negative TIMS (NTIMS) because the latter produces poorer analytical precision due to mass fractionation and isotopic interference Lemarchand et al. (2002). The analytical method for $\delta^{11}B$ is based on previous methods by Wei et al. (2009) and refined by G. Mortimer (RSES ANU). The B separation procedure is based on the method of Lemarchand et al. (2002) adapted to calcium carbonate samples and involves removal of organic matter and purification by three-step column chemistry involving the B-specific resin, Amberlite IRA 743. B isotope measurements are accomplished by simultaneous analysis of the $Cs_2{}^{11}BO_2^+$ and $Cs_2{}^{10}BO_2^+$ species at masses 308 and 309, respectively, using a double Faraday cup fixed in the H4 cup position.

5.2.1. Sample preparation for $\delta^{11}B$ analysis

Three cores taken from massive *Porites* coral collected from the central GBR were selected from the core collection described in Table 2-2 for detailed (annual resolution) $\delta^{11}B$ analysis; these were PAN02 and HAV06 S3 from the inner-shelf reefs of Pandora Reef and

Havannah Is., and core RIB09_3 from the mid-shelf reef of Rib Reef. These cores were selected based on availability (i.e. the more recent inner-shelf material was not available at the time the sample preparation started) and because these showed clear regular annual density banding. Samples representing annual growth increments, i.e. from the beginning of each high density band (for mid-shelf corals) or luminescent band (for inner-shelf corals), were milled along the maximum growth axis of slabs from the selected cores using a 5 mm drill bit. In addition, higher resolution sampling was undertaken in 2 mm increments using a 5 mm drill bit from cores HAV09_3 (Havannah Is.) and RIB09_3. The high-resolution samples were collected from two periods, 1997 to 2000 and from 1990 to 1992, which span the record Burdekin River flood of 1991 and the 1998 bleaching event. The 2 mm sampling interval provides a temporal resolution of between 2 and 3 months, based on measured extensions rates of between 1.3-1.6 cm yr^{-1}.

About 20 mg of coral powder (sufficient to recover approximately 1 μg of B) was weighed from each milled sample and placed in a 1.7 ml microcentrifuge tube containing ~0.5 ml of 30% H_2O_2 to remove organic matter. The tubes were placed in an ultrasonic bath for a couple of minutes and then left to react for 2 to 3 days with occasional agitation. The tubes were then centrifuged and the supernatant was removed. The samples were then repeatedly rinsed with ultra-pure Milli-Q water, centrifuged again and the supernatant removed, this step being repeated three times. The coral powder was dissolved in 3 M HCl (~0.15 ml) and diluted with ~0.4 ml ultra pure Milli-Q water.

5.2.2. Purification and separation of boron

Boron was separated and purified from the samples to avoid isobaric interferences and suppression of the ionization of B species, and to maintain a good vacuum during PTIMS analysis (Aggarwal and Palmer 1995). The sample preparation protocol used follows Wei et al. (2009), which is based on the technique of Lemarchand et al. (2002) and incorporates modifications by Trotter et al. (2011). This method employs two AG50W-X8 cation exchange resin elutions and one Amberlite IRA 743 B-specific resin elution. In the first separation step the dissolved sample is eluted through a column containing 0.5 ml of the cation resin in a 2.5 ml BioSpin column. The purpose of this column is to remove the abundant Ca ions that dominate the coral skeleton and can cause B loss through the

formation of $Ca(OH)_2$ precipitate when the *p*H is raised in subsequent steps (Wei et al. 2009). The eluted sample is adjusted to a *p*H between 7 and 9 using concentrated NH_4OH (Lemarchand et al. 2002). This solution is loaded into a stacked column system, comprising 0.05 ml of the B-specific resin over a second column with 0.05 ml of the cation resin. Boron is strongly immobilized by the Amberlite IRA 743 column. The retention of B in this column increases with the *p*H of the solution. Sample loading is followed by a three step wash; ultrapure H_2O is used first to eliminate residual sample volume, then 0.8M NaCl at *p*H=8 to exchange the anions fixed on the tertiary amine group of the resin with Cl^-, and finally H_2O to eliminate excess Na^+.

The B-specific column Amberlite IRA 743 behaves as an anion exchanger at *p*H values <7 and therefore, to collect B for analysis, the column is eluted with (0.1 ml × 5) 0.1M HCl. The final cation column was added to eliminate any possible contaminants from the elution and washing steps (especially Na from the 0.8 M NaCl washes) that might cause isobaric interferences on Cs_2BO_2. The resin volumes used were smaller than used by Wei et al. (2009) with the purpose of reducing reagent volumes to minimize cost, eluted volume, reagent contamination (blanks) and preparation time. Minimizing evaporation times is particularly significant as some blank contribution is believed to be air-borne (e.g. from the HEPA filters, Foster et al. 2006). CsOH and mannitol are added after collection in 2:1 and 4:3 ratios with respect to the amount of B (Lemarchand et al. 2002). The addition of the mannitol complex prevents the loss of volatile $B(OH)_3$ during evaporation. CsOH is added to the mix to form the complex $Cs_2BO_2^+$. The samples are slowly evaporated on a hot plate or under an infrared lamp at <60°C. They are removed and capped before reaching complete dryness to minimize the potential for B loss or isotopic fractionation through sublimation.

All acids and NH_4OH were prepared using distilled reagents while analytical grade H_2O_2 and mannitol were used. Boron was removed from the Milli-Q system ultrapure water supply using a QGard–Boron (QGARD00B1) cartridge prior to the main de-ionizing cartridge. Small concentrations of B are difficult to measure by PTIMS hence, reagents and complete procedural blanks were measured by G. Mortimer and G. Wei using NTIMS. Measured procedural B blank levels of 10^{-9} g (Wei et al. 2009) compare to sample B

contents of ~10^{-6} g B, indicating blank contributions from reagent and from the procedure are insignificant.

Boron isotope composition was determined by measuring $Cs_2{}^{11}BO_2^+$ and $Cs_2{}^{10}BO_2^+$ using a Finnigan TRITON thermal ionization mass spectrometer (TIMS) in static multi-collecting mode at the Research School of Earth Sciences the Australian National University. This instrument is fit with a double Faraday cup that enables simultaneous static analysis of masses 308 and 309. Samples were loaded onto a degassed single Ta filament to which ~1 µl of graphite-ethanol-water slurry was added. Before the graphite slurry completely dried, the sample was added using 1 µl of 0.1 M HCl as the loading agent to form a sample-graphite slurry and then dried under a ceramic lamp. Samples were then immediately loaded into the mass spectrometer and left for a period, usually over-night, to allow the instrument to reach a working vacuum of <10^{-7} mbar. Filaments were slowly heated to produce an ion current in the range 200 mV to 1000 mV for mass 309, data were collected after reaching this current range.

Each sample analysis comprised one or two blocks of up to 200 three second measurement cycles. Figure 5-1 shows the within-run variability of a typical coral sample. The signal voltage was maintained relatively constant during the run by incrementing the filament current in steps as the signal decayed. The measured $^{11}B/^{10}B$ signal typically increased through a measurement due to an initial contribution on mass 308 from the interfering species $^{308}Cs_2CNO^+$, which is believed to derive from organic material (Wei et al. 2009). This interference is generally exhausted well before the $^{308}Cs_2BO_2^+$ signal such that the measured 309/308 ratio typically plateaus. As described by Wei et al. (2009) $^{301}Cs_2Cl^+$ is also more readily exhausted compared to $^{308}Cs_2BO_2^+$ and is used to monitor $^{308}Cs_2CNO^+$ (Figure 5-1). The final data for the sample analyses was taken from the point where the measured $^{11}B/^{10}B$ first plateaued (Wei et al. 2009).

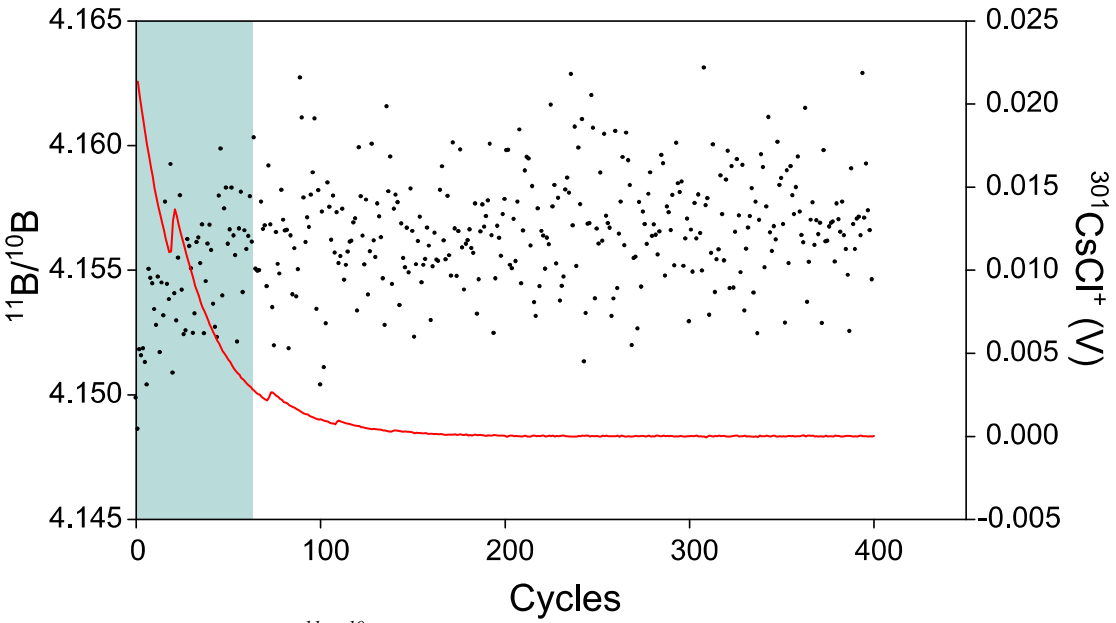

Figure 5-1. *Measured $^{11}B/^{10}B$ ratio during a typical coral sample analysis of 2 blocks of 200 measurement cycles (black circles). The red line shows the variation in signal intensity of mass 302, and the shaded area marks the presence of $^{301}Cs_2Cl^+$, following the exhaustion of which a plateau is established in the $^{11}B/^{10}B$ ratios. Data were collected after the shaded area.*

The B isotope ratio ($^{11}B/^{10}B$) was obtained from measured intensity ratio of $^{309}I/^{308}I$ that has been corrected for a contribution from ^{17}O (Spivack and Edmond 1986):

$$^{11}B/^{10}B = {}^{309}I/{}^{308}I - 0.0007$$

The B isotope compositions ($\delta^{11}B$) are expressed in conventional δ notation corrected to the measured mean value of the NIST SRM 951 standard:

$$\delta^{11}B(‰) = \left[\left({}^{11}B/{}^{10}B \right)_{sample} \Big/ \left({}^{11}B/{}^{10}B \right)_{SRM951} - 1 \right] \times 10^3$$

Over the course of this study, analysis of the directly loaded SRM951 standard yielded a mean value of $\delta^{11}B$ = +0.05‰ relative to a reference value for this standard of 4.054, with an external precision (2σ) of ±0.35‰ (n=43) and an internal precision of ±0.07‰ (Figure 5-2). It is important to note that during a subset of 5 analytical sessions (blue shaded region in Figure 5-2) the standard values obtained were significantly lower than in other sessions. The reason for these low values was carefully scrutinized but no single cause was isolated. Excluding this group of 9 standard measurements results in a mean value for SRM 951 of +0.37‰ with an external precision of ±0.23‰ (2σ, n=39) and an internal precision of ±0.06‰ (2σ). Most of the samples analyzed during the period of low standard values were

from core PAN02 and most of these were subsequently re-analyzed. Measurements of the SRM951 standard that were subject to the column chemistry procedure had a mean value of +0.42‰ with an external reproducibility of ±0.26‰ (2σ, n=9) and an internal precision of ±0.06‰ (2σ). The in-house coral standard NEP-3B returned a mean value of 26.35‰ with an external reproducibility of ±0.44‰ (2σ, n=33) and an internal precision of 0.07‰. Because of the relatively poor external precision obtained for many samples, a large number (~50%) were analyzed twice (about n=20 in the case of HAV06 S3). These repeat analyses had an average reproducibility of ±0.2‰ (2σ).

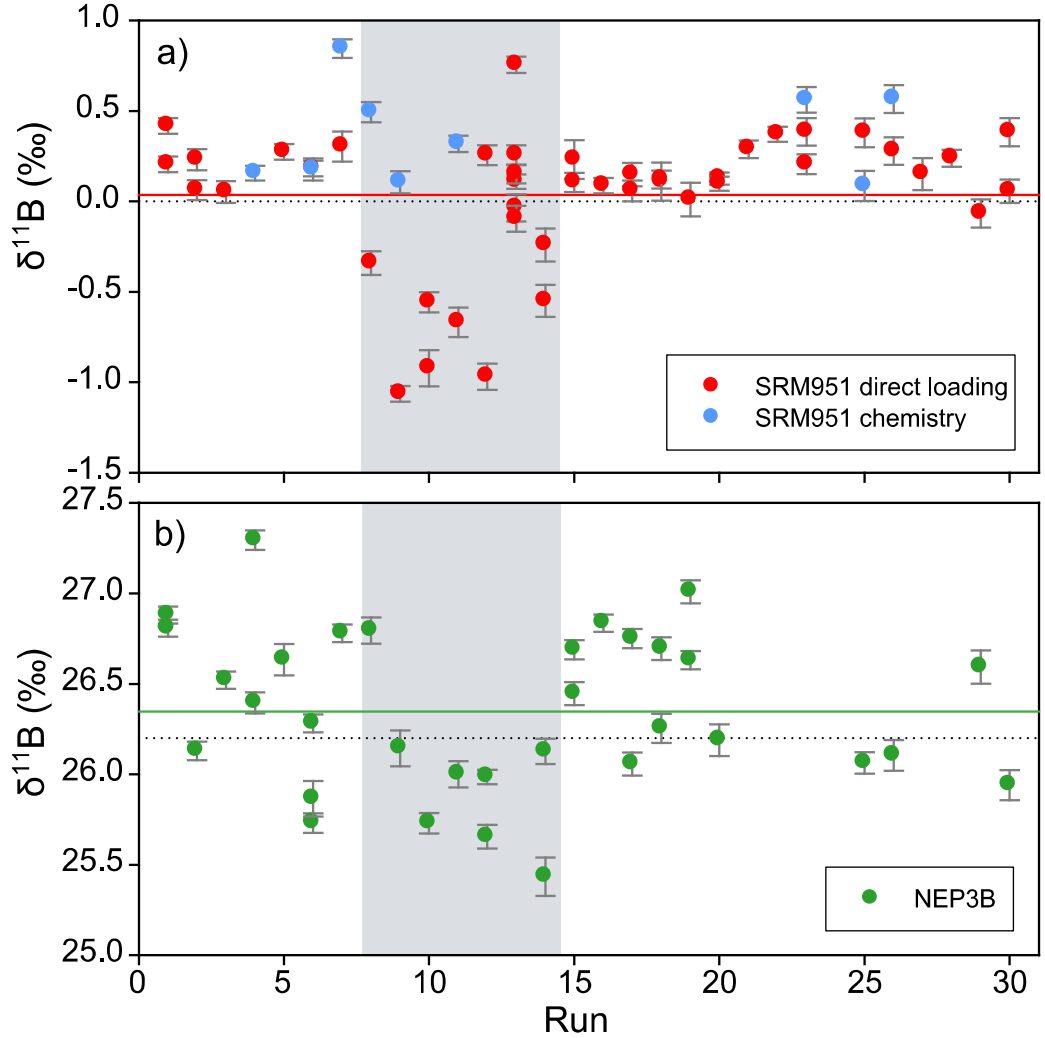

Figure 5-2. *(a) Analyses of directly loaded (red) and chemically processed (blue) NIST SRM951 standard. The solid red line is the long-term mean for the directly loaded SRM951 standard; the dotted line is the reference value. (b) Analyses of the in-house coral standard NEP3B. The solid green line is the long-term mean for the NEP3B standard, the dotted black line is the laboratory long-term average value for the NEP3B standard. The blue shaded area corresponds to a set of 5 analytical sessions during which low $\delta^{11}B$ values where obtained. Error bars represent the ±1SD internal precision.*

Conversion of δ^{11}B to *p*H values was determined through the relationship:

$$pH = pK_B - \log[\frac{\delta^{11}B_{SW} - \delta^{11}B_{Carbonate}}{\alpha_{B3-B4}\delta^{11}B_{Carbonate} - \delta^{11}B_{SW} + 1000(\alpha_{B3-B4} - 1)}$$

where $\delta^{11}B_{sw}$ is the B isotope composition of seawater ($\delta^{11}B_{sw}$= 39.5‰ Spivack and Edmond 1986; Foster 2008) and the B isotope fractionation factor (α_{B3-B4}) is taken from Klochko et al. (2006) as 1.0272. The B dissociation constant (pK_B) was adjusted to the ambient temperature and salinity following Trotter et al. (2011). Since seawater in the inner-shelf reef region is diluted by fresh water during flood events, the associated change in salinity was taken into account in the applied pK_B values. Seasonal variation in salinity was estimated based on the linear relationship observed between the magnitude of past flood events and corresponding salinity values reported by King et al. (2001) and Walker (1981) near the sampled reefs (Figure 5-3). Average annual salinity values were estimated using a mean seawater value of 35.5 and a dilution of this value for a period of two months based on the maximum river discharge in each year using the equation given in Figure 5-3. Despite limitations with this approach, as flood events are spatially and temporally variable (King et al. 2001; Furnas 2003), the effect after correcting the pK_B for salinity and temperature on the estimated seawater *p*H value is small (<~0.01 *p*H units). The external seawater *p*H value was estimated following the method of Trotter et al. (2011) using a *Porites* specific correction factor:

$$p\mathrm{H_{sw}} = (p\mathrm{H_{coral}} - 5.96)/0.32$$

The latter has been calibrated from the results reported by Krief et al. (2010). Reconstructed *p*H values reported are relative to the total *p*H scale.

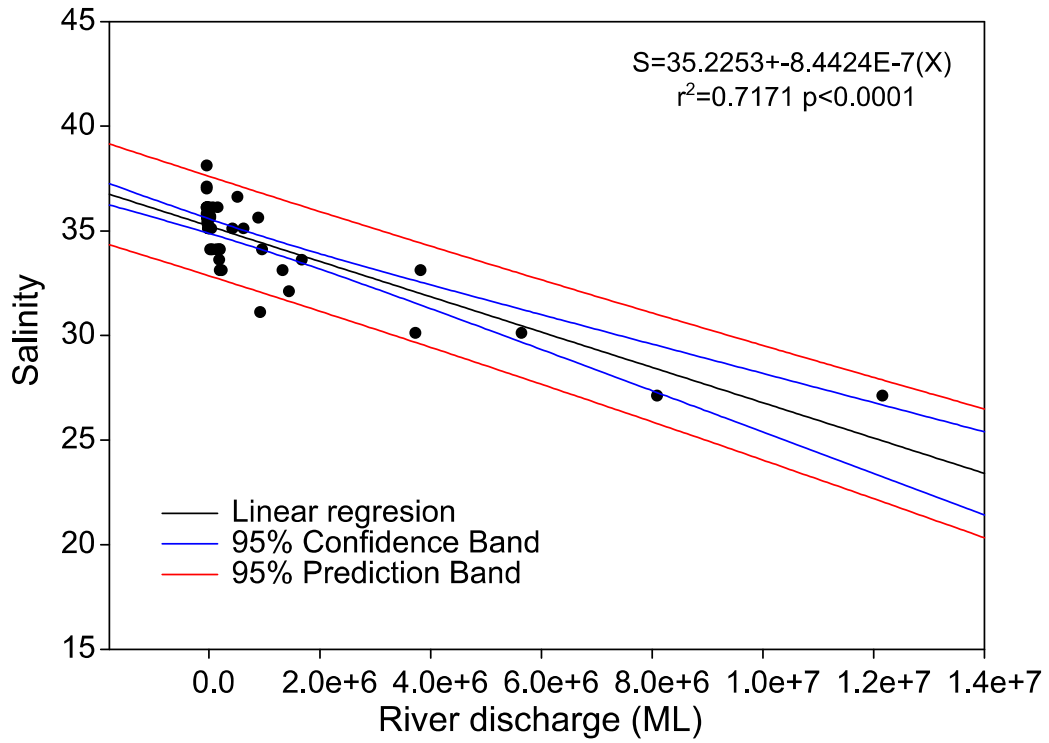

***Figure 5-3**. Comparison of salinity data from King et al. (2001) and Walker (1981) with river runoff of the Burdekin River. The regression line and corresponding equation were used to estimate the dilution from river runoff. The confidence bands indicate the uncertainty associated to the regression lines, while the prediction bands relate to the distribution of values within the 95% probability.*

5.2.3. Water Samples

Water samples were collected to characterize the $\delta^{11}B$ signature of the plume waters in the inner-shelf area during flood events and assist in the interpretation of $\delta^{11}B$ coral signal. In February 2007 a total of 29 water samples were collected by Stephen Lewis from James Cook University (JCU) along a northward transect from the mouth of the Burdekin River to Magnetic Is (Figure 5-4). In February 2009 the author collected water samples from the Burdekin River at the Burdekin Bridge located between the towns of Ayr and Home Hill. Seven seawater samples were also obtained in February 2009 along a northward transect from the mouth of the Burdekin River to Pandora Reef (Figure 5-4). The effect of the river plume was evident at all the sampling sites as colored water. No water sample was collected directly from the river in 2007. After collection, 125 ml of each sample was filtered through 0.45 µm Teflon membrane and acidified using 2-3 drops of ~7 M HNO_3.

Samples were then stored in acid-cleaned, low-density polyethylene bottles in a cool room. Laboratory and refractometer salinity data was provided by S. Lewis (2009).

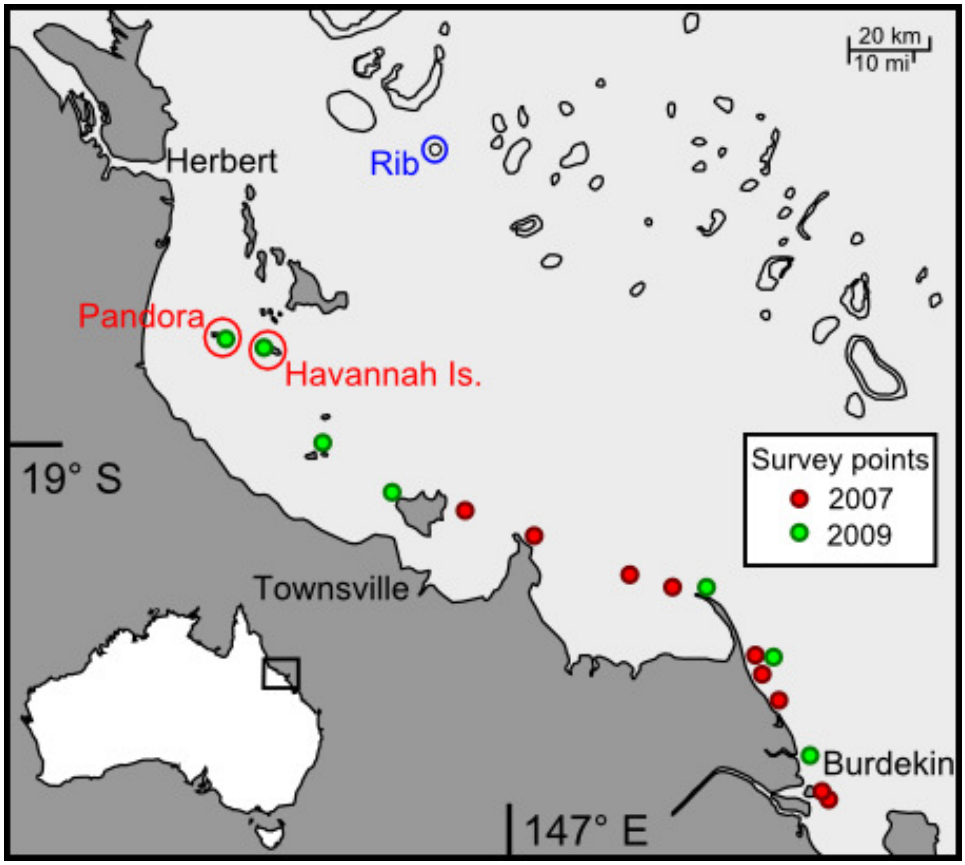

***Figure 5-4**. Map of the central area of the GBR. Coral cores were obtained from Pandora Reef, Havannah Is and Rib Reef. Plume water samples collected during the flood events of 2007 (red) and 2009 (green).*

5.2.4. Solution ICP-MS

Water samples were analyzed for B by solution ICP-MS using a Varian 820 ICP-MS at RSES ANU. A set of standards were prepared with 5 ppb, 50 ppb and 100 ppb of B to obtain a calibration curve (Figure 5-5). A number of the samples were re-analyzed using ^{10}Be as a standard spiked at a concentration of 4 ppb. Water samples were diluted according to their salinity to have a dilution of 1000 times with respect to a seawater salinity of 35. The determined [B] were used to calculate the amount of sample required for δ^{11}B analysis.

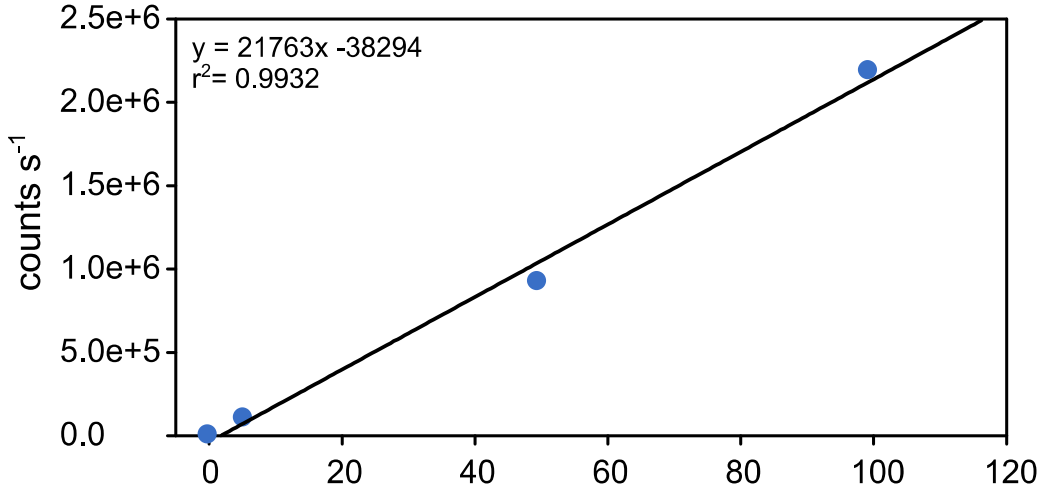

Figure 5-5. *Calibration curve for the B standards used to calculate the [B] in water samples. Data has been corrected for blank levels.*

The $\delta^{11}B$ composition of selected water samples was analyzed by PTIMS following a simplified purification procedure (cf. coral samples), that omitted the H_2O_2 cleaning step and employed a single AGW50-X8 cation column elution followed by an IRA743 column elution (i.e. the final cation column was omitted). The amount of water sample required to extract and purify 1 µg of B was estimated from the relationship between the measured [B] and salinity (S) in the flood plume (B=0.1299(S)+0.1188 and B=0.1302(S)-0.0374; 2007 and 2009, respectively (Figure 5-6).

5.3. Results

5.3.1. Boron concentration and $\delta^{11}B$ ratios in seawater during flood events

Measured [B] and $\delta^{11}B$ plotted against salinity of the water samples collected during the flood events of 2007 and 2009 are presented in Figure 5-6. Lowest salinities with values of 0 were obtained at the river mouth and were highest nearest the reefs, with values of 30 obtained at Havannah Is. and 26.5 at Pandora Reef. Significant correlations ($r=0.9986$; $p<0.0001$; $n=10$ for 2007 and $r^2=0.9917$; $p<0.0001$; $n=8$ for 2009) exists between salinity and [B] concentration during the flood events of 2007 and 2009 consistent with conservative mixing of boron between seawater and flood-waters.

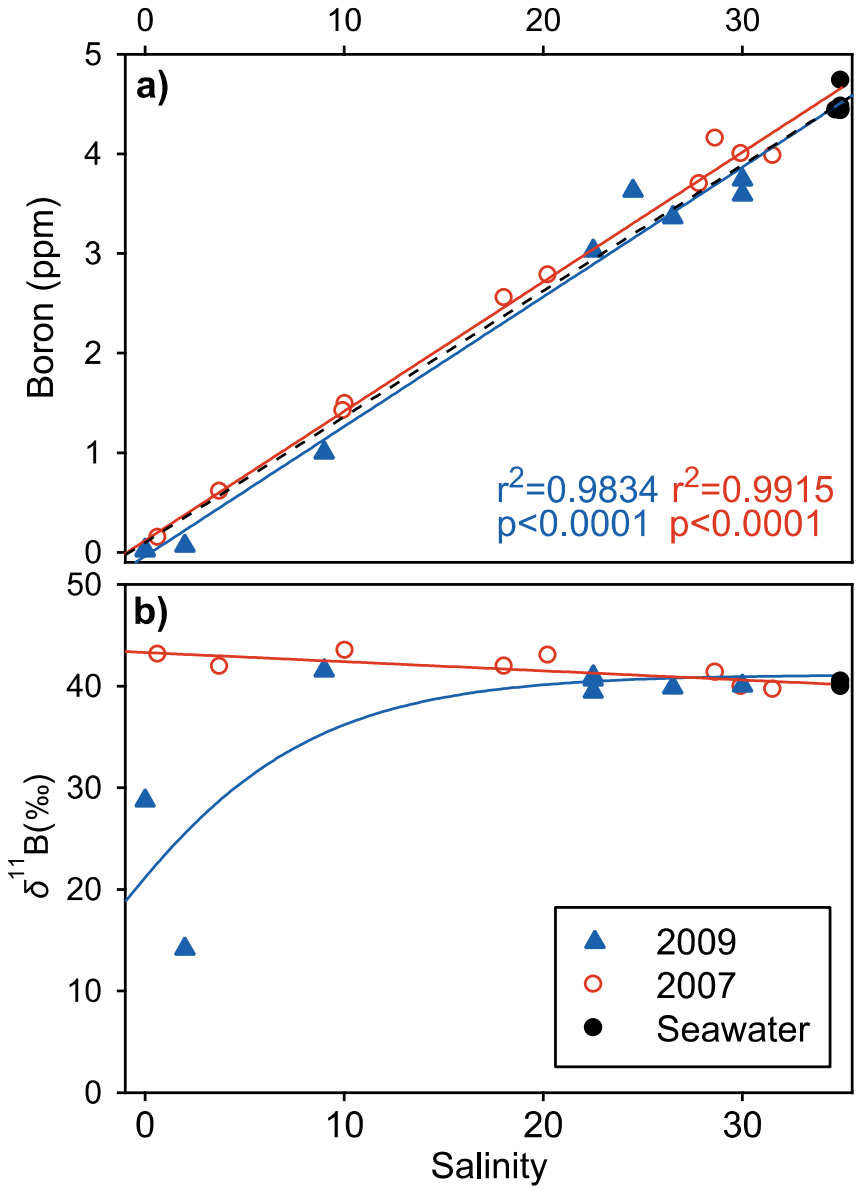

Figure 5-6. *(a) Boron concentration plotted against salinity of waters from the flood events of 2007 and 2009. A linear regression through the data is compared to the theoretical conservative mixing relationship based on a seawater end member with 4.52 µg B/l at S = 35 (black dashed line). (b) Boron isotope composition of waters along salinity transects from the 2007 and 2009 flood events.*

The flood events sampled in 2007 and 2009 show significant differences in the $\delta^{11}B$ of composition of flood-waters that were collected close to the river mouth (Figure 5-6b). The low $\delta^{11}B$ (+15‰) measured during the larger 2009 flood event (Figure 5-7) contrast with the more consistent and higher $\delta^{11}B$ (+42.8‰) of the 2007 flood event. River water collected from the Burdekin River Bridge (23 km upstream from the river mouth) during the 2009 flood event had a $\delta^{11}B$ value of +28‰. Despite the large difference in the $\delta^{11}B$

value of waters from near the mouth in the two flood events, $\delta^{11}B$ of samples taken close to the inner-shelf reefs are very similar, and have an average $\delta^{11}B$ value of 40±0.2‰ (2 S.E. n=2). This value is identical to that of seawater samples from Lady Musgrave Island in the southern GBR ($\delta^{11}B$ v= 39.8±0.37‰; 2 S.E.; n=2) and within previously reported seawater values (summarized by Foster et al. 2010).

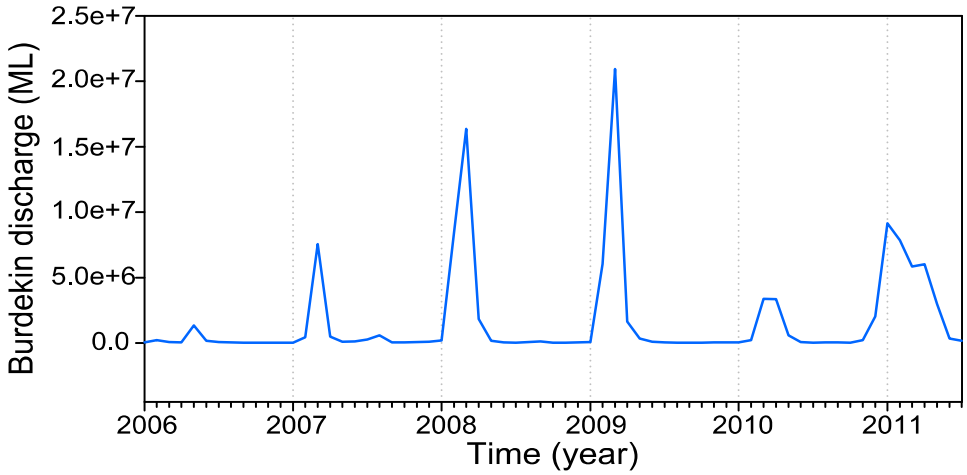

Figure 5-7. *Monthly discharge for the Burdekin River measured at Clare from 2006 to mid 2011. Data obtained from DERM, 2011.*

A binary mixing curve for the flood events (Figure 5-8) was obtained using a river end-member value of from river water collected in 2009 (no river water was collected in 2007) and seawater end-member from seawater samples collected from Lady Musgrave. The same end member value was used for both flood events as no river sample was collected during the 2007 flood event. The binary mixing curve was calculated as follows:

$$\delta^{11}B_{mix} = \left[FB_{sea}\delta^{11}B_{sea} + (1-F)B_{river}\delta^{11}B_{river}\right] / B_{mix}$$

$$B_{mix} = FB_{sea} + (1-F)B_{river}$$

Where $\delta^{11}B_{sea}$, $\delta^{11}B_{river}$, and $\delta^{11}B_{mix}$ are $\delta^{11}B$ values from Lady Musgrave and Burdekin River, respectably, and the mixture and B_{sea}, B_{river}, and B_{mix} are corresponding B concentrations. F is the fraction of seawater components in the mixing. In general 2007 water $\delta^{11}B$ values are higher than in 2009, except for samples collected closest to the reef, which show similar values during both flood events. In a similar way during both flood events samples with salinities higher than ~20 show $\delta^{11}B$ values lay closer to the binary mixing curve obtained for 2009.

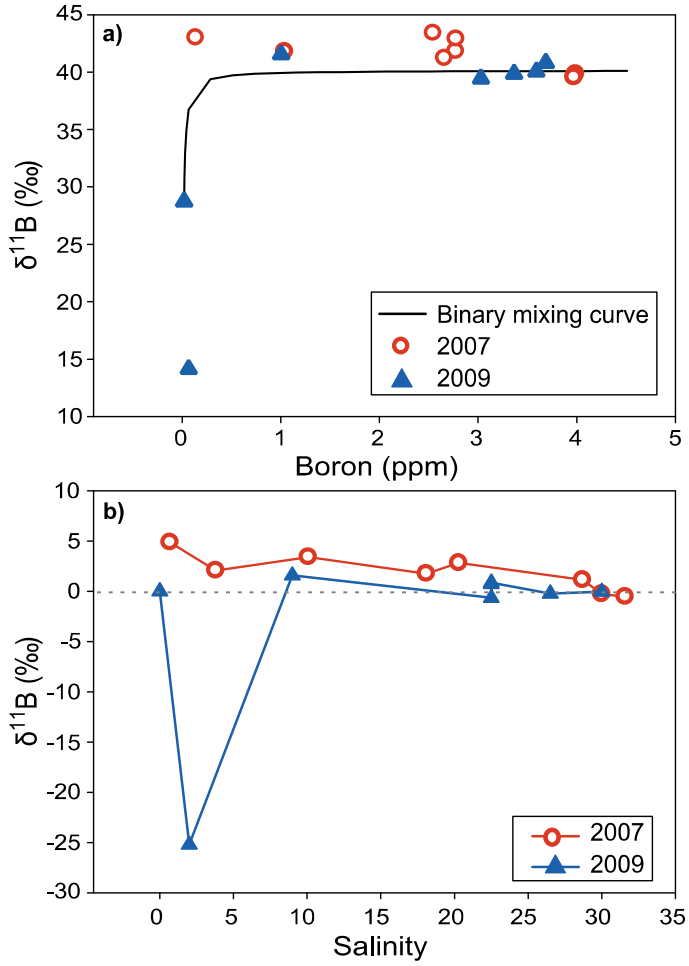

Figure 5-8. *(a) $\delta^{11}B$ vs B concentration in water samples collected during flood events of 2007 and 2009, and the theoretical binary mixing line. (b) Offset between measured $\delta^{11}B$ during the 2007 and 2009 samples and estimated $\delta^{11}B$ mixing line vs salinity.*

5.3.2. Coral $\delta^{11}B$ records

5.3.2.1. Intra-annual variability

The inner-shelf core from Havannah Is. (HAV09_3) and the mid-shelf core from Rib Reef (RIB09_3) show strong seasonal variations in $\delta^{11}B$ being anticorrelated with SST and river discharge/rainfall (Figure 5-9). The $\delta^{11}B$ values translate to a mean seawater *p*H of 7.85 ($1\sigma = 0.14$) for RIB09_3 and 8.08 ($1\sigma = 0.13$) for HAV09_3, with a seasonal range of 0.3 to 0.5 *p*H units. Disruption of the seasonal cycle is apparent during the summer of 1998, where $\delta^{11}B$ values are abnormally high, coinciding with the effects of coral bleaching from the unusually warm SST's. This disruption is most evident in the Havannah Is. coral but is also present at the mid-shelf Rib reef indicating that it is a reef-wide phenomenon.

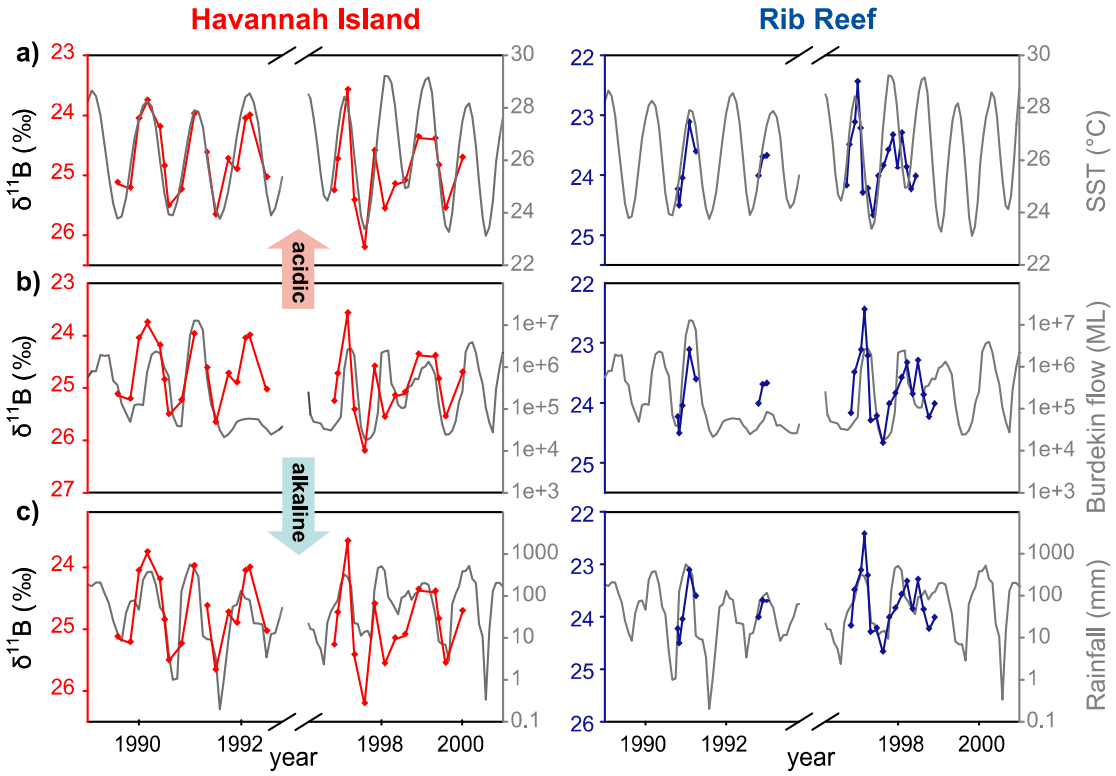

***Figure 5-9**. Intra-annual time-series for coral $\delta^{11}B$ from the inner-shelf reef of Havannah Is. (red) and the mid-shelf reef of Rib (blue). The coral records are compared to (a) instrumental SST, (b) discharge from the Burdekin River and (c) monthly rainfall measured at Townsville. A three-month running average has been applied to the instrumental records to match the resolution of the $\delta^{11}B$ coral data. The $\delta^{11}B$ scale was reversed to facilitate comparisons.*

5.3.2.2. Interannual variability

The boron isotope coral data for annually sampled coral cores over 40-50 years periods from Havannah Is., Pandora Reef and Rib Reef are plotted versus time and compared to river discharge and rainfall data in Figure 5-10. Average $\delta^{11}B$ values for whole cores of 25.23‰ (Havannah Is.), 24.58‰ (Pandora Reef) and 23.87‰ (Rib Reef) are consistent with previously reported values for *Porites* corals (Hönisch et al. 2004; Pelejero et al. 2005; Wei et al. 2009; Krief et al. 2010). The $\delta^{11}B$ values in the inner-shelf corals when de-trended by subtracting the long term linear trend show a slightly larger interannual variability of ±0.11 *p*H units (1σ Havannah Is.) and ±0.14 *p*H units (1σ Pandora Reef) than the mid-shelf coral from Rib Reef (±0.08 *p*H units 1σ). The variability for the inner-shelf $\delta^{11}B$ records is significantly larger in comparison to the mid-shelf Rib Reef record ($p<0000.1$, 1 way ANOVA).

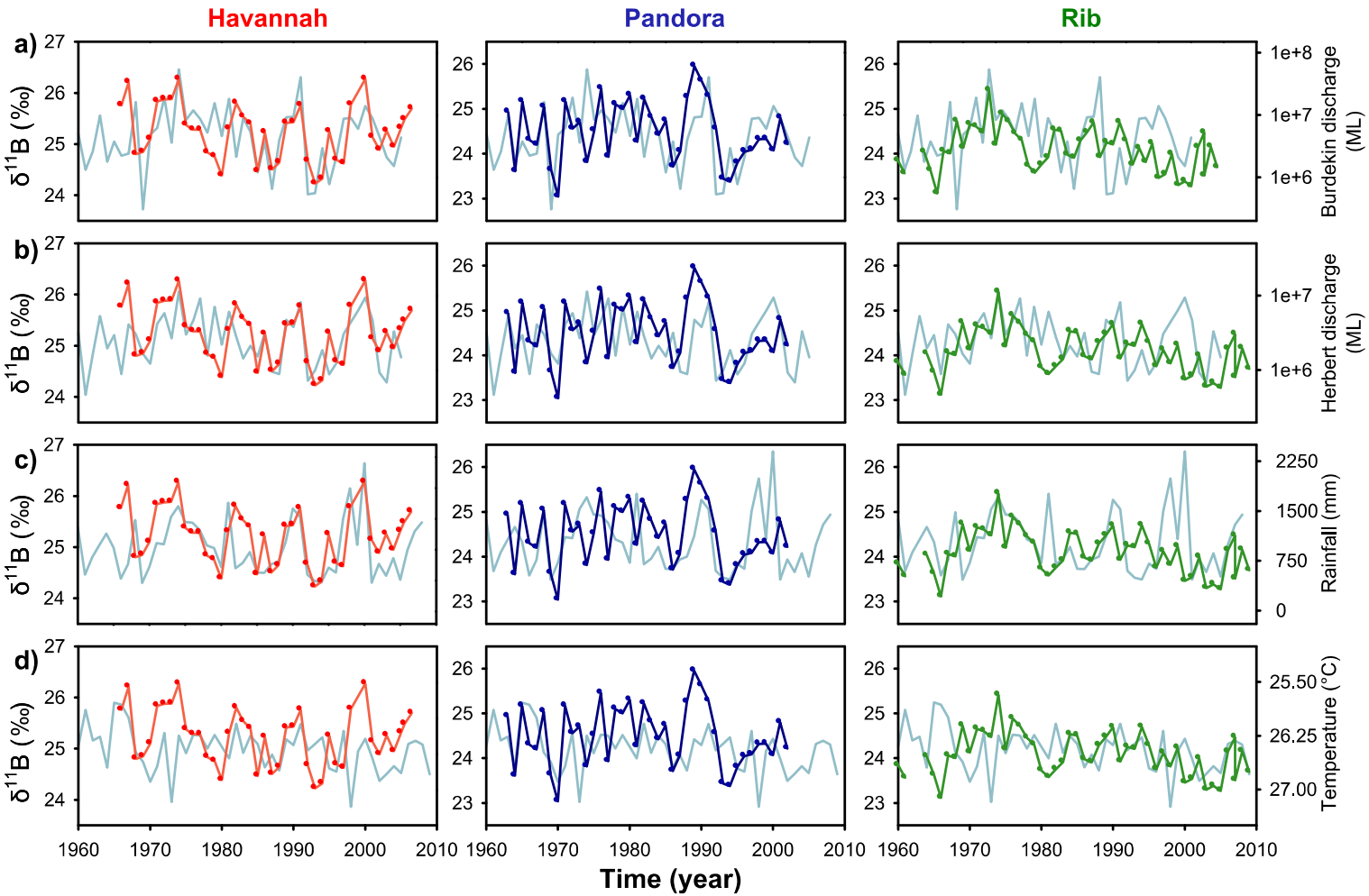

Figure 5-10. *Annual $\delta^{11}B$ time series for two inner-shelf corals from Havannah Is. (red) and Pandora Reef (blue), and one mid-shelf coral from Rib Reef (green) compared to annual discharge from (top) the Burdekin River and the (second) Herbert River, (third) rainfall and (bottom) SST from COADS ERSSTv3b (the temperature axis has been reversed to facilitate comparisons).*

The annual $\delta^{11}B$ data for the inner-shelf coral from Havannah Is. show the highest correlations with river discharge from the Burdekin River and the Herbert River and rainfall (Figure 5-11). The Pandora Reef annual $\delta^{11}B$ results only correlate significantly with SST. The annual $\delta^{11}B$ data for the mid-shelf coral from Rib Reef shows positive correlations with river discharge but these correlations are influenced significantly by a small number of extreme values. No significant correlation was found between the three different $\delta^{11}B$/*p*H coral records (not shown).

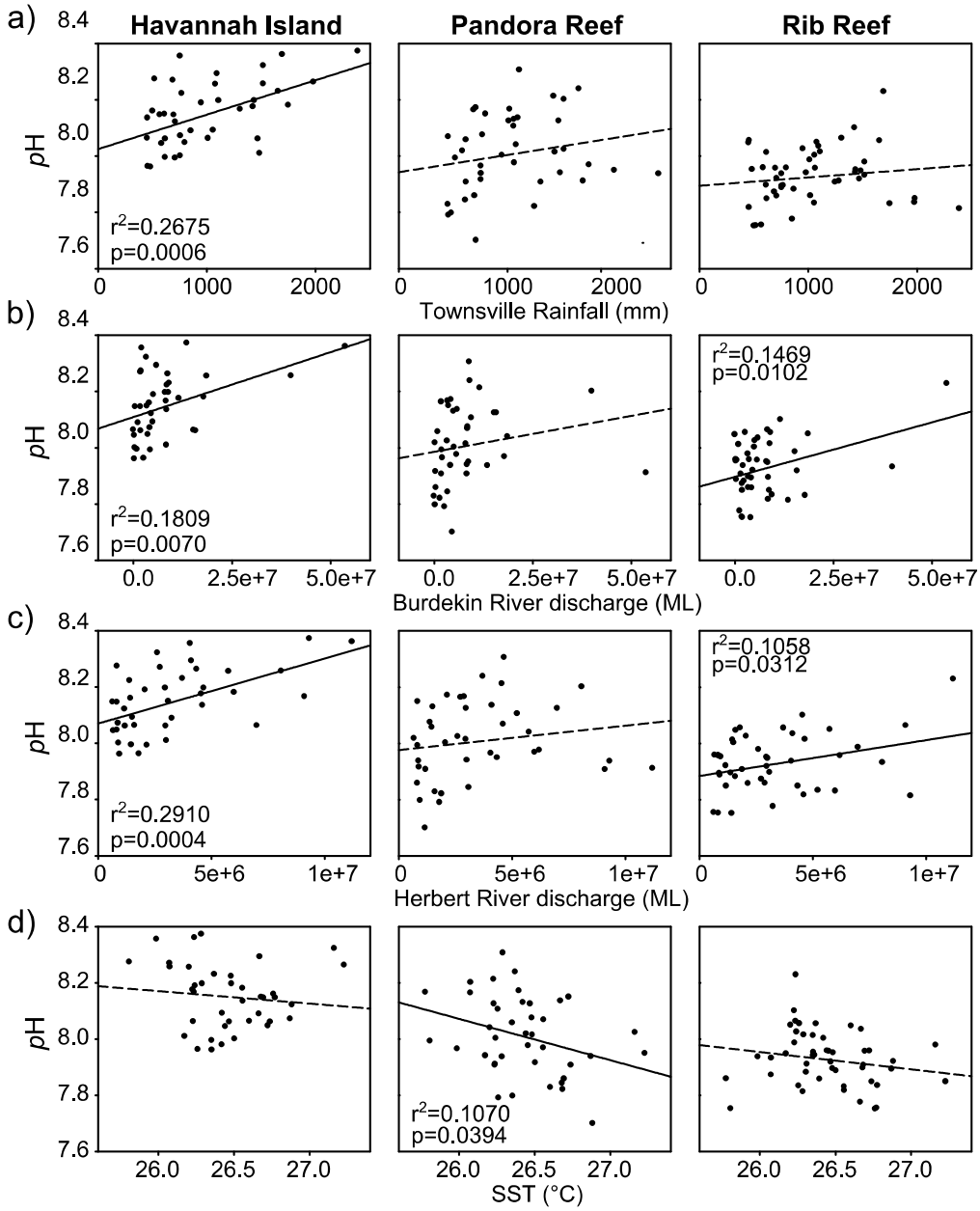

Figure 5-11. *Linear regression for seawater pH reconstructed from coral $\delta^{11}B$ data for Havannah Is., Pandora Reef and Rib Reef against annual records of (a) discharge from the Burdekin River, (b) discharge from the Herbert River, (c) rainfall at Townsville and (d) reconstructed SST from COADS ERSSTv3b. Linear regressions are indicated by a continuous line where significant, dashed lines indicate non-significant relationships. Coefficients of determination and p-values included when significant ($p<0.05$). The seawater pH values were estimated according to Trotter et al. (2011).*

5.3.2.3. Variability over the last 50 years

Linear regressions applied to the reconstructed annual seawater *p*H annual time-series from all three coral records show a decrease that varies from 0.04±0.079 *p*H units at Pandora Reef, 0.115±0.067 *p*H units at Havannah Is. to 0.086±0.052 *p*H units at Rib Reef over the common period of 1966-2002 (Figure 5-12). The average decrease for the master chronology obtained from the three reefs over the common period of 1966-2002 is 0.072±0.041 *p*H units at a rate of 0.020±0.022 *p*H units per decade. This rate is in good agreement with global estimates of 0.017 to 0.020 *p*H units decrease per decade from 1985-2010 based on instrumental data (Pelejero et al. 2010), but lower than the 0.05 *p*H unit decrease per year for the period of 1940-2004 shown by the $\delta^{11}B$ coral record from Arlington Reef (mid-reef) in the Central GBR reported by Wei et al. (2009)

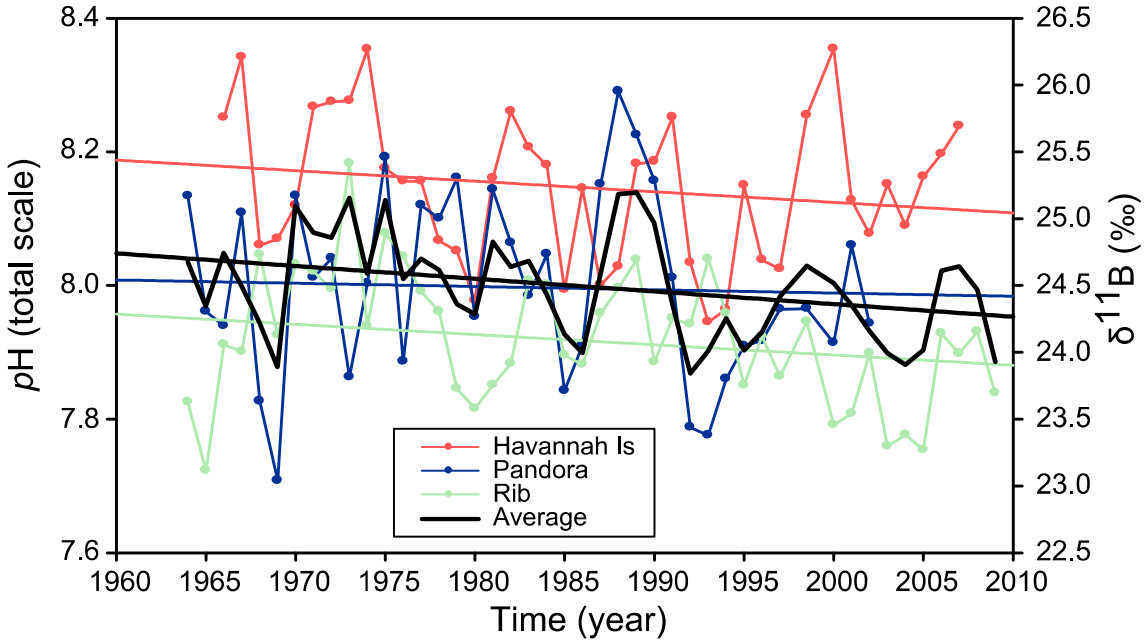

Figure 5-12. *Annual time-series for estimates of seawater pH from coral $\delta^{11}B$ of coral samples from the inner-shelf reefs of Havannah Is. and Pandora Reef, from the mid-shelf reef of Rib and a master chronology for the three records. The master chronology was calculated from normalized data by subtracting the individual mean average over the common period of 1966-2002 for each record, the mean average value for the three records over the same period was added to the master chronology data to preserve the measurement units.*

The 8 year low pass filter applied to the composite seawater *p*H data from the three $\delta^{11}B$ coral records reveals a semi-decadal component of variation in the data (Figure 5-13). Similar variability is observed in inner-shelf coral calcification results where periods of lower calcification coincide with higher terrestrial runoff. It follows that more positive $\delta^{11}B$ (higher *p*H) values coincide with periods of increased river discharge and lower

calcification. Lower solar irradiance coincides with periods of maximum river discharge and wetter periods, and is most likely due to increased cloud cover.

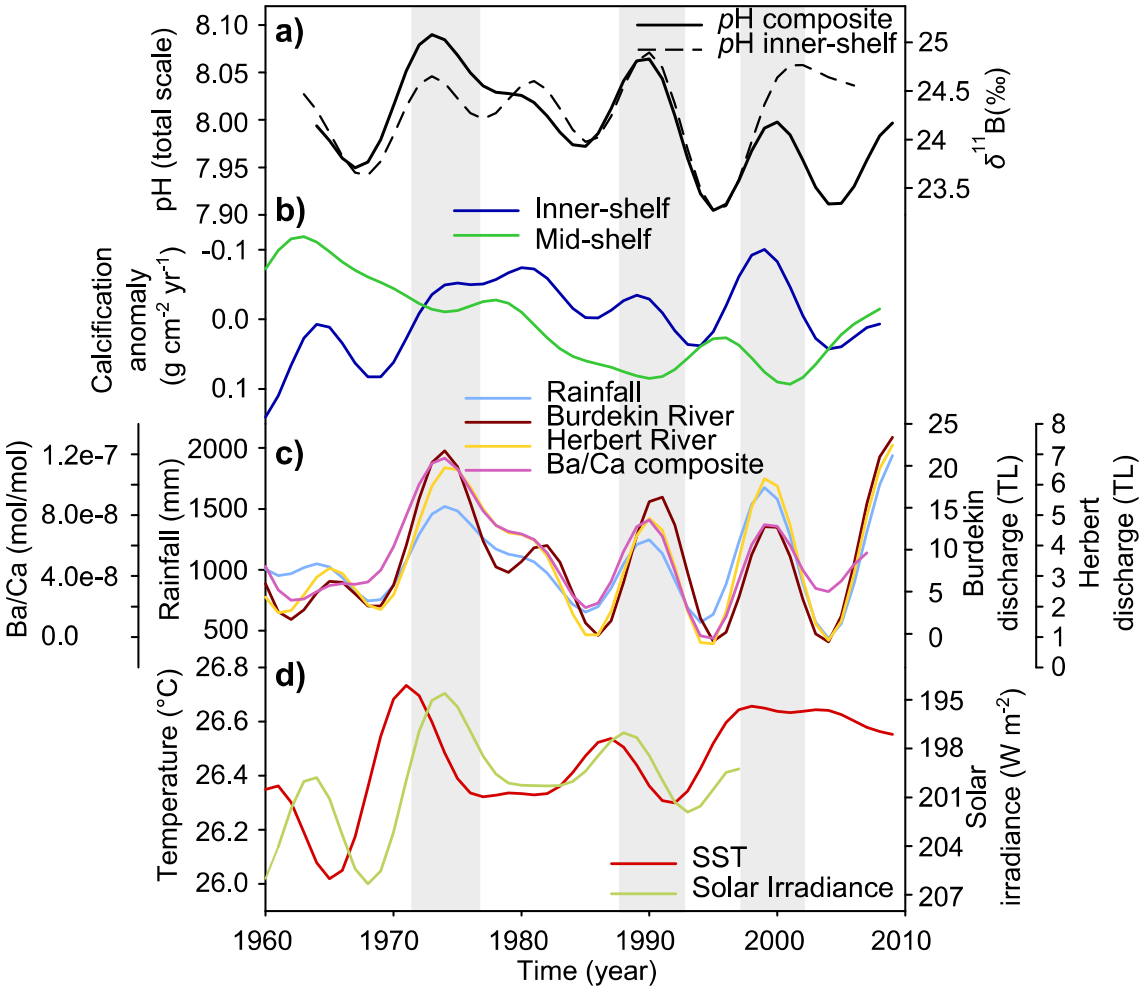

Figure 5-13. *8-year low band pass filter smoothed time-series for: (a) the composite seawater pH reconstruction obtained from all three $\delta^{11}B$ coral records and for the two $\delta^{11}B$ inner-shelf coral records, (b) averaged calcification rates of inner-shelf and mid-shelf reefs in the central GBR (see Chapter 4), (c) terrestrial influx indicated by coral Ba/Ca (see Chapter 3), rainfall at Townsville and discharge from the Burdekin River and Herbert River, and (d) COADS SST from ERSSTv3b 2°x2° and CAYAN Solar irradiance. Shaded areas indicate wetter periods.*

5.4. Discussion

5.4.1. Variations in river and seawater $\delta^{11}B$ during flood events

Historic mean *p*H values of 7.8±0.5 (1SD) for the Burdekin River and 7.1±0.4 (1SD) for the Herbert River (Figure 5-14; data from the Queensland DERM, 2011) indicate that considerably lower *p*H river waters are introduced into the coastal area of the GBR during wet periods. The river *p*H data for the Burdekin River shows significant intra-

annual variability, with a decrease in *p*H during some high discharge events, but there is no consistent seasonal pattern. This indicates that factors other than the amount of rainfall determine the river water *p*H, which could relate to the nature of the material being carried by the river, or the rainfall composition.

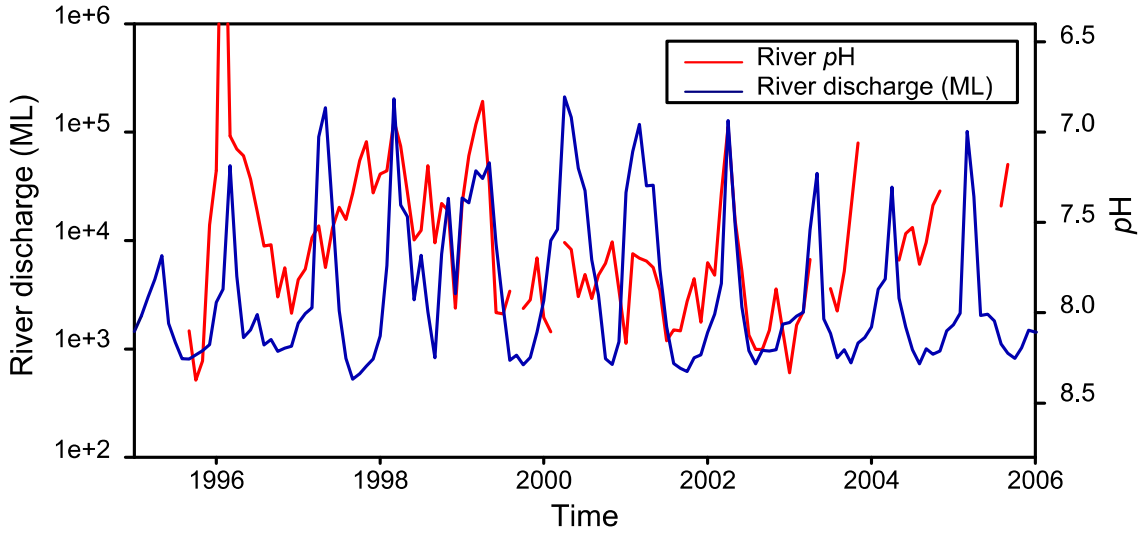

Figure 5-14. *Monthly discharge and pH of the Burdekin River waters (data obtained from Queensland DERM, 2011).*

Boron isotope composition values obtained for flood plume waters from near the mouth of the Burdekin River were noted for being greater during the larger flood event of 2009 (+42.8‰) than during the flood event of 2007 (+15‰). This is opposite to data obtained by Barth (1998) from the Elbe Estuary (Germany), where water samples collected near the Elbe River mouth during a minor flood event had a significantly lower $\delta^{11}B$ value than samples collected during an extreme flood event following intense cyclonic activity. In the case of the Elbe Estuary the heavier $\delta^{11}B$ signal during an extreme flood event is explained by the admixture of a ^{11}B-rich component mainly rainwater (Barth 1998). However, more work is still needed to properly characterize the B dynamics and isotope fractionation mechanisms during flood events, as factors other than rainfall are likely to play an important role in determining the $\delta^{11}B$ signal of river waters. These factors include the type and amount of terrigenous material carried by the river during flood events, and the source of rainfall. Although the $\delta^{11}B$ values show some variation close to the Burdekin River mouth, as shown by the 2007 and 2009 flood events, near the inner-shelf reefs the $\delta^{11}B$ values are still typical of ocean waters (i.e. $\delta^{11}B$ ~40‰).

5.4.2. Intra-annual variability of coral $\delta^{11}B$

The inverse relationship between intra-annual $\delta^{11}B$ coral data and both temperature and terrestrial runoff indicates that more acidic seawater conditions prevail in summer (Figure 5-9). This appears consistent with the expectation that summer should be associated with lower *p*H as temperature has an inverse effect on seawater *p*H. However, since the inner-shelf seasonal SST range is typically 6°C and no more than 9°C, temperature changes can account for a change in seawater *p*H of no more than ~0.12 *p*H units (Figure 5-15). This compares to variations of more than 0.3 *p*H units reconstructed from the $\delta^{11}B$ results. The dilution of seawater from input of freshwater could also explain part of the seasonal *p*H variability, as an additional increase of 0.04 *p*H units could be achieved if salinity drops to a value of 24 as during an extreme flood event (Figure 5-15). This is because increasing temperature or salinity results in an increase of the dissociation constants for carbonic acid in seawater (Zeebe and Wolf-Gladrow 2001). These temperature and salinity changes account for only about half the observed seasonal range and would reflect extreme variations for the central GBR (c.f. most years). Interestingly, seasonal variations in $\delta^{11}B$ (*p*H), equivalent to those during flood years, are observed in the inner-shelf coral during the dry year of 1992. Furthermore, mid-shelf corals not subject to significant salinity changes from flood waters, show seasonal variations in coral $\delta^{11}B$ that are equivalent in magnitude to those observed in the inner-shelf.

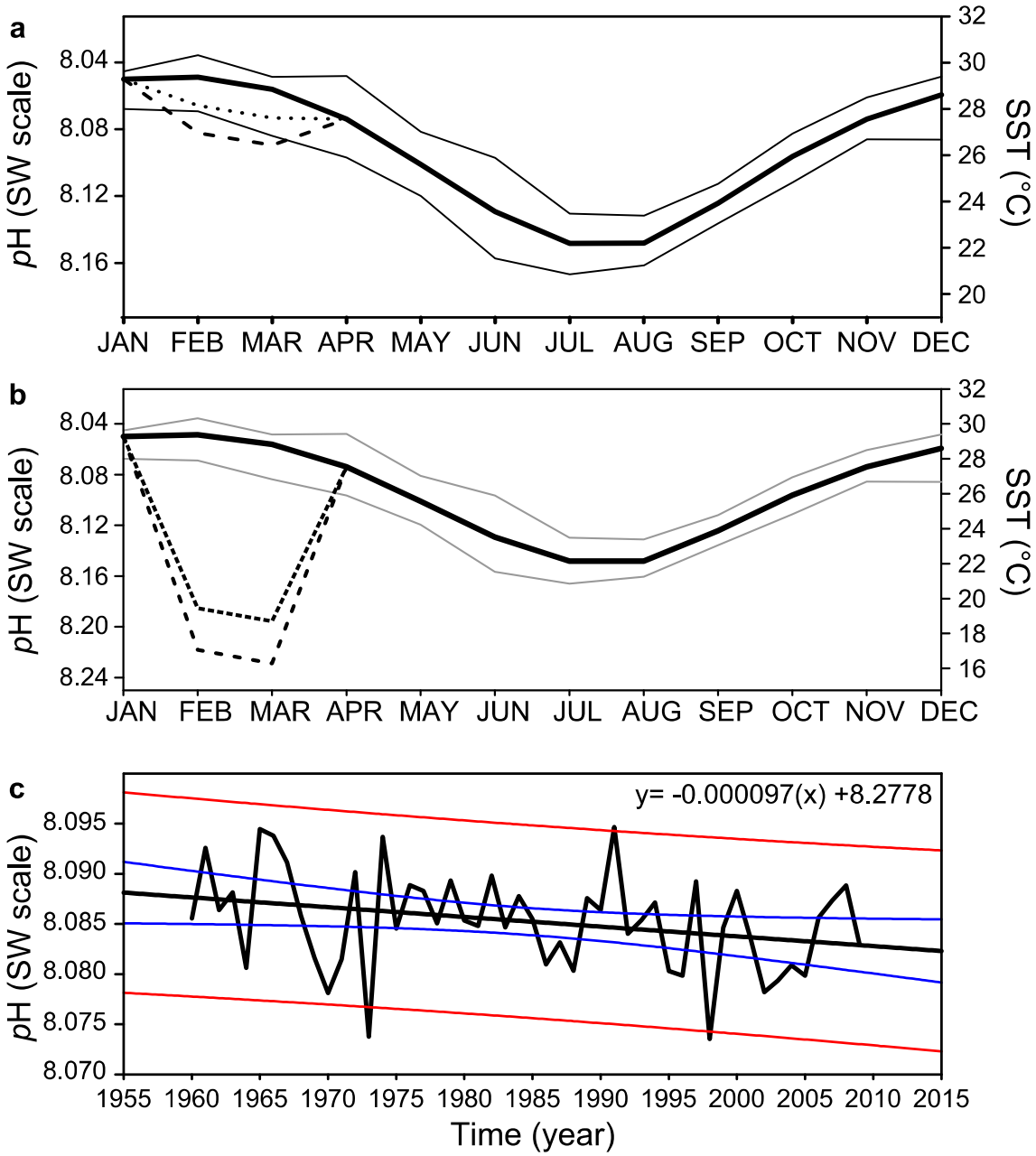

Figure 5-15. ***(a)*** *Estimated seasonal pH changes based on the in situ SST (AIMS) variation. The area between the gray lines shows the range of historic maximum and minimum values for a given month. The associated seawater pH changes related to a hypothetical two month decrease in salinity to values of 30 and 24 due to river discharge are respectively indicated by the dashed and dotted lines.* ***(b)*** *Estimated seasonal pH changes similar as in (a) but in this case calculations include a drawing down in pCO2 of 100 ppm during flood events as a result of an increase in phytoplankton biomass.* ***(c)*** *Estimated annual seawater pH changes based on reconstructed SST (ERSSTv3b) and salinity changes associated with flood events obtained from the equation in Figure 5-3. The confidence bands (blue) indicate the uncertainty associated to the regression lines, while the prediction bands (red) relate to the distribution of values within the 95% probability. Seawater pH values were estimated considering a seawater end member with a TA of 2260 mmol kgsw^{-1} and DIC of 1920 mmol kgsw^{-1} measured by Suzuki et al. (2001) salinity and a river water end member with a of TA 787.7 mmol kgsw^{-1} and DIC of 811.1 mmol kgsw^{-1} estimated from TA and pH data obtained from DERM. Calculations were made using CO_2SYS with carbonate constants K1 and K2 from Merhbach et al. (1973) refit by Dickson and Millero (1987) and for sulfate from Dickson (1990) with atmospheric pressure = 1atm.*

Strong seasonal variation in $\delta^{11}B$ (*p*H) has been previously reported for *Porites* corals from the Western Pacific (Hemming et al. 1998) and the GBR (Pelejero et al. 2005; Jung-Ok Kang, personal communication). Hemming et al. (1998) found higher $\delta^{11}B$ (*p*H) to be associated with high-density bands and attributed this to internal biological processes, mainly to the activity of symbiotic zooxanthellae during periods of high insolation, when increased C fixation by symbionts depletes the DIC pool in CO_2 and results in higher seawater *p*H values. The seasonal variation reported by Hemming et al. (1998) has also been attributed to changes in the carbonate chemistry of seawater caused by biological productivity or a shift in the ocean currents that influence the reef (Hönisch et al. 2004). Pelejero et al. (2005) attributed seasonal *p*H variability to the interaction of physical and biological processes, whereby weaker winds promote CO_2 produced by calcification to buildup in the reef water. As the rate of water renewal slow down, the seawater *p*H values will decrease inside the reef lagoon, on a longer time scale these changes relate to the phases of the Interdecadal Pacific Oscillation (Pelejero et al. 2005). Monitoring studies of inorganic carbon chemistry of coral reefs reveal significant diurnal variations (279-352 ppmv; Kayanne et al. 1995) and seasonal variation (300-550 ppmv; Bates et al. 2010) in pCO_2. These changes are the result of the reef metabolism, and are mainly controlled by the balance between two processes: calcification-dissolution and photosynthesis-respiration (Kayanne 2005; Bates et al. 2010). Therefore the large intra-annual $\delta^{11}B$ (*p*H) variations recorded in the corals are likely to be the combined result of both physical (such as temperature and salinity changes) and biological process (such as photosynthesis respiration and calcification).

5.4.3. Origin of interannual $\delta^{11}B$ variability in corals

The correlations observed in Figure 5-11 indicate a relationship between coral $\delta^{11}B$ and temperature, river discharge and rainfall, particularly for the coral from Havannah Is. However, the interannual variability of ±0.01 *p*H units modeled from temperature and salinity changes due to river run-off (Figure 5-15c) contrasts with the interannual variability of more than ±0.11 *p*H units reconstructed from the $\delta^{11}B$ of the inner-shelf corals and ±0.08 for the mid-shelf coral. This suggests that coral $\delta^{11}B$ is only indirectly related to temperature and terrestrial runoff.

5.4.3.1. Clay adsorption and sediments

A possible explanation for interannual B variations comes from the adsorption of B onto sediments and clays that are delivered to the coastal area by rivers. Clays preferentially remove the lighter isotope ^{10}B from seawater according to the relationship:

$$^{10}B(OH)_3 + \propto -Al_2O_3\,^{11}B(OH)_4^- \leftrightarrow {}^{11}B(OH)_3 + \propto -Al_2O_3\,^{10}B(OH)_4^-$$

(Palmer et al. 1987; Barth 1998). This results in the depletion of marine clays and the enrichment of seawater in ^{11}B, and is the accepted explanation for the heavy isotopic composition of seawater of 39.5‰ relative to average continental crust (Spivack and Edmond 1986; Palmer et al. 1987; Barth 1998). Given the large silt and clay wash load transported from the Burdekin River (Belperio 1979) the fractionation of $\delta^{11}B$ between the dissolved and adsorbed B phases might have a significant effect on the $\delta^{11}B$ of seawater. However, the conservative mixing behavior of B concentration along the salinity transect indicates that boron is not being actively removed by clays from the plume waters (Figure 5-6). This indicates that the clay material is already in equilibrium with the river water before entering the ocean; similar results are reported by Barth (1998) and Xiao et al. (2007). Offset from the binary mixing line to higher $\delta^{11}B$ values for brackish waters could indicate absorption from clays (Figure 5-8). It is important to note that the actual end member value for 2007 is unknown as no sample was collected from the river and a high seasonal variability has been observed in river waters (Lemarchand et al. 2000). Therefore it is not possible to know if the values during this year deviate from the binary mixing line at all. The biggest offset in $\delta^{11}B$ values occurs for the sample collected closest to the river mouth during the 2009 flood event. The river water sample was collected 5 days earlier than the seawater samples and therefore differences could indicate that the $\delta^{11}B$ value of the river water end-member varies as the flood evolves. This large difference may also be the result of processes that modify the $\delta^{11}B$ composition just after the river waters enter the ocean. Nonetheless, the near oceanic $\delta^{11}B$ values near the reefs during flood events and river water low B content suggest that at the reef sites the $\delta^{11}B$ signal is dominated by seawater.

5.4.3.2. Effect of nutrient enrichment and biological productivity on seawater pH

River discharge is an important source of particulate and dissolved nutrients as well as sediments to the inner-shelf area of the GBR (King et al. 2002; Devlin and Brodie 2005), with about 90% of the particulate and dissolved nutrients introduced during flood

events (Mitchell and Bramley 1997; Furnas 2003). Fertilizer use and land clearing since European settlement has increased the amount of nutrients introduced to the GBR by rivers (Figure 5-16; Furnas 2003; Devlin and Brodie 2005). Most particulate matter and sediments are deposited within a few kilometers (~10 km) of river mouths, before reaching a salinity value of 10 (Wolanski and Jones 1981), whereas dissolved nutrients are carried to greater distances, up to about 200 km along the coast (Devlin and Brodie 2005). Once the turbidity drops and light levels are no longer limiting, dissolved nutrients are rapidly taken up by primary producers resulting in phytoplankton blooms (Furnas 2003; Devlin and Brodie 2005). These blooms do not usually develop until the salinity has reached a value of ~25, typically between 50 and 200 km from the river mouth (Devlin and Brodie 2005). These distances correspond to areas where the inner-shelf coral reefs investigated in this study are located.

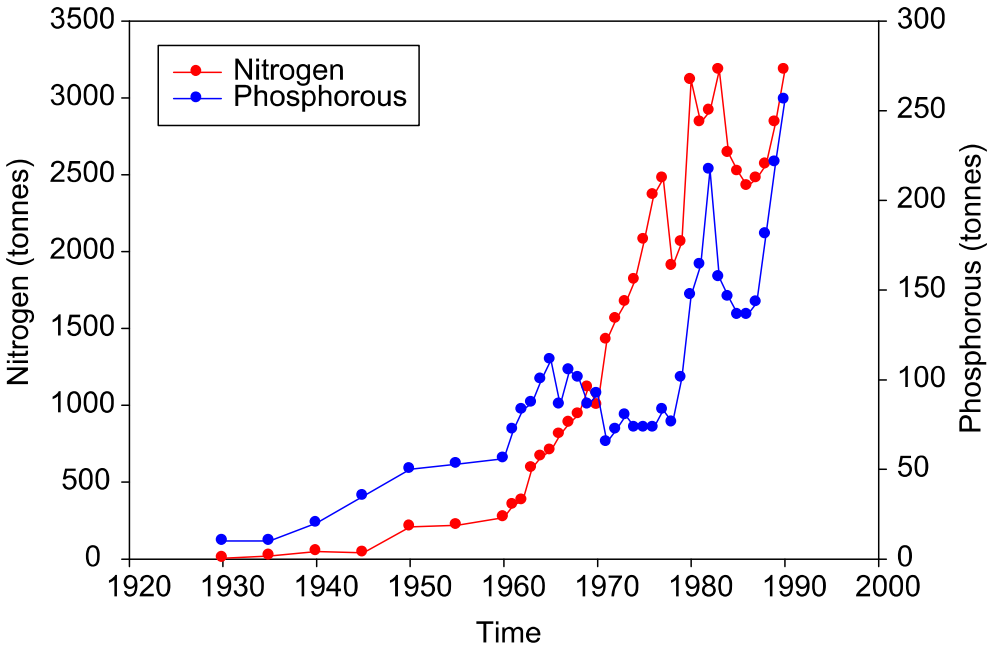

Figure 5-16. *Annual nitrogen and phosphorus fertilizer use in the Burdekin catchment (Pulsford 1996).*

Nitrate (NO_3^-) is the most abundant form of dissolved inorganic nitrogen introduced by runoff into the GBR. The majority of the nitrogen from the Burdekin River enters the GBR as particulate NO_3^- while that from the Herbert River enters as dissolved inorganic nitrate derived from groundwater sources (Furnas 2003). If NO_3^- is the main source of nitrogen to the inner-shelf area of the GBR, plankton productivity can be expressed as:

$$106CO_2+16NO_3^-+HPO_4^{2-}+18H^+ \underset{resp.}{\overset{phot.}{\rightleftharpoons}} C_{106}H_{263}O_{110}N_{16}P+138O_2$$

with the resulting effect being to increase seawater alkalinity by 170 mmol per mole of fixed CO_2 (Gattuso et al. 1999b).

A strong coupling between CO_2 dynamics and large phytoplankton bloom events has been observed at Kane'ohe Bay, Hawaii, that changes the reef system from being a CO_2 source to a CO_2 sink (Drupp et al. 2011). In this case, bloom events are fueled by nutrient inputs following rainfall and terrestrial runoff events. The enhanced productivity is reflected in increased phytoplankton biomass from ~2 to ~6 μg l^{-1} Chl-a which is responsible for drawing down pCO_2 by ~100 ppm (Drupp et al. 2011). Similar large changes in phytoplankton biomass occur in the central GBR, where Chl-a increases from between 0.3 and 0.7 μg l^{-1} Chl-a (Brodie et al. 2007) up to between 1 and 20 μg l^{-1} Chl-a within flood plumes (Devlin and Brodie 2005; Brodie et al. 2010a). Anthony et al. (2011) has recently shown that in a reef environment with a mixture of algae and coral increased productivity removes CO_2 and increases Ω_{arag}. When a decrease in *p*CO2 of 100 ppm is included into the modeled response shown in Figure 5-15 an increase of 0.2 pH units is observed during flood events. In this sense decreased pCO_2 and increased seawater *p*H due to phytoplankton activity would reconcile the higher $\delta^{11}B$ (*p*H) values observed in the corals from these reefs during periods of high river discharge.

Higher *p*H ($\delta^{11}B$) values are found in corals from the inner-shelf compared to the mid-shelf (Figure 5-9, Figure 5-10 and Figure 5-12). It is not surprising to find variations in seawater *p*H values reconstructed from different reefs as significant spatial differences in seawater *p*H have been reported for different habitats in the coral reef systems of the GBR and Ningaloo in Western Australia, with the highest *p*H recorded near filamentous algal beds Gagliano et al. (2010). The lower interannual variation of the coral $\delta^{11}B$ record at Rib Reef compared to Pandora Reef and Havannah Is. could be explained by the decreased influence of river runoff on mid-shelf reefs. Wei et al. (2009) has previously suggested that the greater seawater *p*H variability recorded by the coral $\delta^{11}B$ proxy at Arlington Reef (a mid-shelf reef) compared to Flinders Reef (an open ocean reef) reflects Arlington Reef's location nearer to the coast. The lack of correlation of the Pandora record with the Havannah Is. record and the terrestrial run-off remains unresolved. Low external analytical replication, local variability or unknown biological effects are some of the possible explanations. The remarkably time consuming

methodology involved in the preparation and analysis of $\delta^{11}B$ samples by PTIMS is the main limiting factor that prevented further testing this hypothesis in the current study. Nevertheless, the good agreement of the combined $\delta^{11}B$ coral average with environmental indices is encouraging and suggests that multi-core replication is a key factor to extract meaningful information from this proxy (Lough 2004; Jones et al. 2009). Analysis of other records from the same area should help clarify the uncertainties and improve our understanding of the $\delta^{11}B$ proxy.

5.4.4. Relationship between seawater pH ($\delta^{11}B$) and coral calcification

Calcification rates of inner-shelf corals show a weak long-term decrease over the period from 1960 to 2008 (this study Chapter 4, Lough 2008a), but until now it has not been possible to attribute this decrease to thermal stress, bleaching, eutrophication, seawater acidification or a combination of these factors (Cooper et al. 2008; Lough 2008a; De'ath et al. 2009). The results from this study reveal a decadal-scale wet period and hence increased terrestrial runoff in the central GBR coinciding with periods of reduced inner-shelf coral calcification (see Figure 5-13 and Chapter 4). This is despite $\delta^{11}B$ evidence for concurrent higher seawater *p*H and hence higher seawater carbonate saturation. Given more favorable seawater carbonate chemistry (high *p*H and Ω_{arag}) for coral calcification during wet periods clearly other factors must be responsible for the observed negative calcification response at these times.

Besides high *p*H at the site of calcification other processes involved in promoting aragonite precipitation include the transport of ions to the mineralization site and the synthesis of an organic matrix (Allemand et al. 2004; Venn et al. 2011). Inhibition or reduced activity of these processes has been associated with significant reduction of calcification in other studies (Tambutte et al. 1996; Allemand et al. 1998; Al-Horani et al. 2003; Allemand et al. 2004). The reduction in calcification of inner-shelf coral can be explained by the effects of river discharge that can include increased shading, turbidity, sedimentation or competition for carbon by up-regulated photosynthetic activity of zooxanthella. These external factors can affect enzyme activity or synthesis of the organic matrix involved in the calcification process (Tambutte et al. 1996; Allemand et al. 1998; Al-Horani et al. 2003; Allemand et al. 2004) because energy and DIC required by these processes is reallocated into cleaning or mucus production (Riegl and Branch 1995; Telesnicki and Goldberg 1995; Philipp and Fabricius 2003).

Therefore, it is not surprising to find reduced calcification during wet periods despite higher *p*H and Ω_{arag} conditions.

The $\delta^{11}B$ record of the mid-shelf corals shows a more muted relationship to river discharge than the inner-shelf reefs, consistent with reduced impacts from river flood plumes. Extreme flood events can however occasionally reach the mid-shelf reefs, especially when offshore winds occur (King et al. 2002), as confirmed by the presence of luminescent bands in coral records from Rib Reef that coincide with some large river discharge events. Nevertheless, coral calcification at both mid-shelf and outer-shelf reef locations shows an increase over the last ~50 years that corresponds with the rise in temperature over this period. The moderate positive relationship of $\delta^{11}B$ to increased river-discharge (Figure 5-11) in the mid-shelf region could also be due to increased photosynthesis arising from an increased nutrient supply to the GBR lagoon in these years, occurring at a reduced level that did not compromise coral calcification.

5.4.5. Coral calcification response to bleaching

Aerial surveys in 1998 indicate that in that year more than 60% of inner-shelf corals of the central GBR bleached (Berkelmans 2002). Both higher coral $\delta^{11}B$ values and a partial loss of seasonal $\delta^{11}B$ variability are observed during 1998. This contrasts with a decrease in $\delta^{11}B$ reported by Wei et al. (2009) during the bleaching events of 1998 and 2002 in a *Porites* coral from Arlington Reef (mid-shelf). The year 1998 was not only extremely warm, with average monthly temperatures in the inshore reefs reaching 30.3°C in February, but also coincided with a wet period and hence, sediment and nutrient fluxes to the reef increased. A significant reduction in coral calcification occurred in the inner-shelf area during this year (Lough 2008a, Chapter 4), and in some cases coral extension rates were almost zero although calcification continued (see Carricart-Ganivet 2011). Kayanne (2005) reported a reduction in the reef pCO_2 diel cycle following the 1998 bleaching event as a result of the breakdown of calcification and photosynthetic processes. It follows that the coral $\delta^{11}B$ seasonal cycle could also have been influenced by the dramatic reduction in calcification observed during 1998.

The combination of enhanced community productivity and reduced coral calcification would elevate local surface seawater *p*H values and account for the high coral $\delta^{11}B$ values. This is the opposite response to bleaching observed by Wei et al. (2009). This

could reflect the differing response of individual coral colonies to the bleaching event (it is not known whether any of the analyzed corals in either study bleached or not during these events). Wei et al. (2009) attributed the very low *p*H (<7.6) recorded by coral $\delta^{11}B$ at Arlington Reef to the decrease of internal *p*H at the site of calcification and linked this to the reduction in the rate of calcification. Interestingly, no evidence of flood-plume effects were found at Arlington Reef, in contrast to the reefs analyzed in this study. The very similar response observed in the two intra-annual coral $\delta^{11}B$ records analyzed from Havannah Is. and Rib Reef a indicate a common response of *Porites* corals in the central GBR to the 1998 thermal stress was a reduction in calcification.

5.5. Summary and conclusions

Boron concentration is correlated with the salinity in plume waters from flood events indicating conservative mixing. This and the near oceanic $\delta^{11}B$ of waters close to the reefs suggest that the effect of clay adsorption of B on seawater $\delta^{11}B$ near the reefs is minimal.

Seawater *p*H reconstructions from $\delta^{11}B$ coral records in the central GBR show strong seasonal and interannual variability equivalent to 0.3 to 0.5 *p*H units and 0.08 to 0.14 *p*H units, respectively. These variations cannot be explained by changes in salinity and temperature alone, which account for only ±0.06 *p*H of the observed amplitude at a seasonal scale. Interannual variations in reconstructed seawater *p*H show a positive relationship with regional rainfall and river discharge, opposite to the relationship expected if seawater carbonate chemistry was influenced by the more acidic freshwater input. In addition to the temperature and salinity effects, it is speculated that phytoplankton blooms fueled by increased nutrient inputs from rivers and island mass effects may be responsible for taking up CO_2 and shifting the surface seawater to higher *p*H. The results presented here highlight the importance of coastal and reef processes in controlling seawater *p*H, and support previous results from coral $\delta^{11}B$ studies that show large intra-annual to decadal variability in seawater *p*H in reef systems (Pelejero et al. 2005; Wei et al. 2009).

The long term trend (1960-2008) observed in the three $\delta^{11}B$ coral time-series corresponds to a ~0.02 seawater *p*H unit decrease per decade. This rate is consistent with previous estimates of surface seawater *p*H change and with these coral $\delta^{11}B$

records being influenced by ocean acidification from rising atmospheric pCO_2. These results indicate the value of coral $\delta^{11}B$ as a paleo-proxy for reconstructing past seawater *p*H changes in the absence of instrumental records.

A decrease in calcification of inner-shelf corals is associated with river flood events despite higher seawater *p*H and Ω_{arag} conditions recorded by coral $\delta^{11}B$. This reduction in calcification can be explained by increased shading, turbidity, sedimentation or competition for carbon by up-regulated photosynthetic activity of zooxanthellae. These external factors can affect enzyme activity or synthesis of the organic matrix involved in the calcification process because energy and DIC required by these processes is reallocated into cleaning or mucus production. Although seawater carbonate chemistry plays a fundamental role in coral calcification, no clear effects on calcification can be attributed to ocean acidification in the studied corals. Only inner-shelf corals show a long-term (~60 year) trend of decreasing calcification. While ocean acidification could be the cause of this decrease, evidence suggests it might be equally caused by greater/more frequent thermal stress and/or eutrophication by flood plumes. In contrast, mid-shelf and outer-shelf corals show a long term increase in calcification that can be related to increasing temperature. This could be masking negative effects from ocean acidification

As coral reefs are a net source of CO_2 to the environment, a decrease in coral calcification could partly mitigate the effects of rising atmospheric CO_2. Primary producers may also fix more CO_2 in the presence of extra nutrients and thereby shift the carbonate system equilibrium to higher seawater *p*H. Accordingly, enhanced productivity resulting from both increased nutrient loads and higher DIC due to CO_2 uptake from the atmosphere could lessen the negative effects on coral calcification from ocean acidification (Holcomb et al. 2010; Anthony et al. 2011). Future changes due to increased ocean acidification and eutrophication could result in shifts in coral reef community compositions particularly in coastal ecosystems. Such changes would conceivably lead to competition for space and resources between macroalgae, phytoplankton, corals and filter feeders. Predicting future changes in coral calcification may not be straightforward without considering the combined effects of all these factors and feedback mechanisms between the physical and biological components of the system. The coral $\delta^{11}B$ data presented here indicates that the internal calcifying fluid *p*H is responding to external environmental changes. These changes are mainly controlled

by variations in biological productivity, respiration and calcification that in inner-shelf environments are coupled with terrestrial runoff. *In situ* monitoring of seawater carbon chemistry parameters will enable better prediction of the response of coral calcification to increased atmospheric pCO_2 levels.

6. Summary and conclusions

6.1. Variability in coral calcification across the central GBR

The growth parameters (density, linear extension and calcification rates) of *Porites* sp. corals within the central GBR show some variations according to their location across the shelf. Linear extension rate and density show opposite across-shelf relationships, with higher extension rates (lower density) occurring in inner-shelf corals and lower extension rates (higher density) in outer-shelf corals. Although not statistically significant these trends are consistent with observations from Lough and Barnes (2000) and with the stretch modulation model from Carricart-Ganivet and Merino (2001). Higher calcification rates are associated with the more stable and protected environments within the GBR lagoon. The lower calcification rates but denser skeletons of outer-shelf corals may be an adaptation to more energetic wave action in that environment.

Calcification rates of mid-shelf and outer-shelf corals show a continuous increase of ~11% over 1947-2008 and 1952-2004, respectively, whereas inner shelf corals show a ~5% decline over 1930-2008. The increase in mid-and outer-shelf calcification rates is most likely due to increased SST, but calcification rates of mid-shelf corals have slowed markedly over 1990-2008, possibly indicating that a thermal optimum for calcification has been exceeded. Although average calcification rates of inner-shelf corals are relatively high, they display significantly greater interannual variability, which can be linked to more dynamic coastal processes and enhanced temperature variability. Calcification rates of inner-shelf corals display particularly strong semi-decadal variability over the last ~40 years (~1970-2008) that relates to wet and dry periods evident in river discharge and rainfall data. A severe reduction in calcification and subsequent slow recovery over the period 1998 to 2000 coincides with the 1998 bleaching event, which was caused by unprecedented high temperatures and may have been exacerbated by a wet period prior to the 1998 bleaching event. This may have induced additional stress due to pervasive low salinity plumes and also acted to amplify the summer warming (Marshall and McCulloch 2002). The long-term decline in inner-shelf coral calcification rates could be due to changes in temperature, rainfall and eutrophication, however, it is not possible to discern their respective influences or the extent of interactions between these factors.

6.2. Seawater pH variability in the central GBR over the last 60 years reconstructed from coral $\delta^{11}B$ data

Reconstruction of annual and sub-annual changes in seawater *p*H from the $\delta^{11}B$ composition of coral cores from inner- and mid-shelf environments reveals significant sub-annual variability, with particularly large variability (up to 0.5 *p*H units) evident in inner-shelf corals. Lower $\delta^{11}B$ (seawater *p*H) occurs during summer and can be partially attributed to the effects of increased calcification (a source of CO_2) in response to higher seasonal temperatures. The variability of average annual reconstructed seawater *p*H from inner-shelf corals of ±0.22 (1SD Havannah Island) to ±0.28 *p*H units (1SD Pandora Reef) is slightly greater than the ±0.16 *p*H unit (1SD Rib Reef) variability observed in a mid-shelf coral. Interannual and decadal variations in average annual $\delta^{11}B$ correlate with terrestrial runoff, with higher seawater *p*H occurring in periods of high terrestrial runoff. This is in contrast to expectations based on terrestrial runoff being a source of relatively acidic freshwater, and indicates that coral $\delta^{11}B$ and seawater are responding indirectly to river discharge or rainfall.

Changes in the inorganic carbonate system parameters of seawater due to seasonal temperature variation (±0.42°C 1SD) and salinity (up to 10 units) during flood events cannot account for the observed interannual range of reconstructed seawater *p*H. The near oceanic B composition values in proximity to the inner-shelf reefs indicate that clay adsorption of B is not a dominant process controlling the $\delta^{11}B$ seawater changes recorded in the coral. Reduced coral calcification and a simultaneous increase in productivity associated with the terrestrial input of sediment and nutrients during flood events may explain the observed $\delta^{11}B$ changes. The combined effects of decreased calcification and increased productivity shift the seawater carbonate equilibrium to higher *p*H, as recorded in coral $\delta^{11}B$. A long-term decrease (~50 years) in coral $\delta^{11}B$ reflects a decrease of 0.02 *p*H units per decade, in agreement with global estimates of seawater *p*H changes due to rising CO_2 levels in the atmosphere (e.g. Pelejero et al. 2010). These results highlight the utility of coral $\delta^{11}B$ as a paleo-proxy for reconstructing past seawater *p*H changes in the absence of instrumental records.

This study points to the importance of biologically- and physically-driven changes in the carbonate chemistry and *p*H of coastal waters within the GBR. Proximity to land exposes inner-reef corals to the strong influences of terrestrial freshwater, nutrient and sediment inputs. In the central GBR these inputs are mainly sourced from the runoff of

the Burdekin River. Exposure to these terrestrial derived stressors and the greater environmental variability of inner-shelf reefs makes them more sensitive to environmental changes. By contrast, the more stable and pristine environmental conditions in the mid-shelf area of the central GBR make these regions more robust and less susceptible to the negative effects of ocean warming and acidification.

6.3. What is next?

Coral calcification rates are sensitive to changes in temperature, nutrients, light, sedimentation and seawater *p*H (Ω_{arag}). However, there are significant gaps in our understanding of the complex mechanisms controlling coral calcification in relation to changes in the carbonate chemistry of the reef system. This study highlights the importance of cross-shelf changes in coral calcification, particularly the effects of terrestrial inputs on calcification in inner-shelf reefs. This builds on previous studies, such as that by De'ath et al. (2009) which have developed an overall view of the status of the GBR but which may also be biased from the over-representation of inner-shelf regions. To improve our understanding of the present and future health of corals in the GBR, additional regional-scale studies are required. These studies should focus on changes in calcification in response to the combined effect of environmental variables such as: temperature, *p*H, nutrients, sedimentation and light level. This would help to identify regions that are susceptible to specific environmental changes and could help in the design and implementation of appropriate management plans. Clearly, a study of another cross-shelf transect within the central GBR would help to confirm the results of this study, as well as other regions in the northern and southern GBR, such as the Cape York area and the Capricorn Group in the south. To the north, the shelf width is reduced, reef density increases, terrestrial runoff is more frequent and anthropogenic impacts are reduced, whereas in the south, the shelf is much wider and mid-and outer-shelf reefs are distant from terrestrial inputs. These areas represent markedly different environments from the central GBR, and it follows that our understanding of the GBR would be greatly enhanced by extending research into these regions.

To predict the changes in coral calcification due to ocean acidification it will be important to develop models that consider the complex interactions of the physical and biological components of the reef that affect seawater carbonate chemistry. Measurements of calcification and productivity changes in reef systems in association

with monitoring of water chemistry will help to identify the dynamics and mechanisms that control reef seawater carbonate chemistry. A better understanding of the factors controlling the seawater carbonate chemistry in reef systems will aid in the initial interpretations drawn from paleo-seawater *p*H $\delta^{11}B$ reconstructions made in this study, and also aid our ability to predict the future of the GBR in response to increased CO_2 levels.

The low Ba baseline and variable correlation of the Ba/Ca and $\delta^{11}B$ with terrestrial runoff proxies for the inner-shelf coral cores remains puzzling. A careful identification of samples to species level and comparisons of multiple records from different areas within a same reef would help clarify if the observed differences between coral records are due to species differences, local variability, analysis uncertainty or other unidentified factors. To date, the time consuming methodology involved in the preparation and measurement of $\delta^{11}B$ is the main limiting factor to perform this kind of comparisons. However, new technologies, like solution multicollector ICP-MS, could drastically reduce the time and effort required to prepare samples making this kind of research possible in the near future.

7. References

Abram NJ, Gagan MK, McCulloch MT, Chappell J, Hantoro WS (2003) Coral reef death during the 1997 Indian Ocean Dipole linked to Indonesian wildfires. Science 301:952-955

Aggarwal JK, Palmer MR (1995) Boron isotope analysis - a review. Analyst 120:1301-1307

Al-Horani FA, Al-Moghrabi SM, de Beer D (2003) The mechanism of calcification and its relation to photosynthesis and respiration in the scleractinian coral Galaxea fascicularis. Mar Biol 142:419-426

Al-Rousan S (2012) Skeletal extension rate of the reef building coral *Porites* species from Aqaba and their environmental variables. Natural Science 04:731-739

Al-Rousan SA, Al-Shloul RN, Al-Horani FA, Abu-Hilal AH (2007) Heavy metal contents in growth bands of *Porites* corals: record of anthropogenic and human developments from the Jordanian Gulf of Aqaba. Mar Pollut Bull 54:1912-1922

Albright R, Langdon C, Anthony KRN (2013) Dynamics of seawater carbonate chemistry, production, and calcification of a coral reef flat, Central Great Barrier Reef. Biogeosciences Discussions 10:7641-7676

Alibert C, McCulloch MT (1997) Strontium/calcium ratios in modern *Porites* corals from the Great Barrier Reef as a proxy for sea surface temperature: Calibration of the thermometer and monitoring of ENSO. Paleoceanography 12:345-363

Alibert C, Kinsley L (2008) A 170-year Sr/Ca and Ba/Ca coral record from the western Pacific warm pool: 2. A window into variability of the New Ireland Coastal Undercurrent. J Geophys Res-Oceans 113

Alibert C, Kinsley L, Fallon SJ, McCulloch MT, Berkelmans R, McAllister F (2003) Source of trace element variability in Great Barrier Reef corals affected by the Burdekin flood plumes. Geochim Cosmochim Acta 67:231-246

Allemand D, Tambutt EE, Girard JP, Jaubert J (1998) Organic matrix synthesis in the scleractinian coral *Stylophora pistillata*: role in biomineralization and potential target of the organotin tributyltin. J Exp Biol 201 (Pt 13):2001-2009

Allemand D, Ferrier-Pages C, Furla P, Houlbreque F, Puverel S, Reynaud S, Tambutte E, Tambutte S, Zoccola D (2004) Biomineralisation in reef-building corals: from molecular mechanisms to environmental control. Comptes Rendus Palevol 3:453-467

Allison N, Tudhope AW, Fallick AE (1996) Factors influencing the stable carbon and oxygen isotopic composition of *Porites lutea* coral skeletons from Phuket, South Thailand. Coral Reefs 15:43-57

Andersson AJ, Gledhill D (2013) Ocean acidification and coral reefs: effects on breakdown, dissolution, and net ecosystem calcification. Ann Rev Mar Sci 5:321-348

Andersson AJ, Mackenzie FT, Lerman A (2005) Coastal ocean and carbonate systems in the high CO_2 world of the anthropocene Am J Sci 305:875 - 918

Anthony KRN, Fabricius KE (2000) Shifting roles of heterotrophy and autotrophy in coral energetics under varying turbidity. J Exp Mar Biolo Ecol 252:221 -253

Anthony KRN, Kleypas JA, Gattuso J-P (2011) Coral reefs modify their seawater carbon chemistry - implications for impacts of ocean acidification. Global Change Biol 17:3655-3666

Ashok K, Behera, SK, Rao SA, Weng H, Yamagata T (2007) El Niño Modoki and its possible teleconnection. J Geophys Res Oceans, 112(C11) doi:10.1029/2006JC003798,.

Baker AC, Glynn PW, Riegl B (2008) Climate change and coral reef bleaching: An ecological assessment of long-term impacts, recovery trends and future outlook. Est Coast Shelf S 80:435-471

Baker PA, Weber JN (1975) Coral growth rate: variation with depth. Phys Earth Planet In 10:135-139

Barnes DJ, Taylor DL (1973) *In situ* studies of calcification and photosynthetic carbon fixation in the coral *Montastrea annularis*. HelgoIänder wiss Meeresunters 24:284-291

Barnes DJ, Devereux MJ (1988) Variations in skeletal architecture associated with density banding in the hard coral Porites. J Exp Mar Biolo Ecol 121:37-54

Barnes DJ, Lough JM (1992) Systematic variations in the depth of skeleton occupied by coral tissue in massive colonies of *Porites* from the Great Barrier Reef. J Exp Mar Biolo Ecol 159:113-128

Barnes DJ, Lough JM (1993) On the nature and causes of density banding in massive coral skeletons. J Exp Mar Biolo Ecol 167:91-108

Barnes DJ, Taylor RB (2001) On the nature and causes of luminescent lines and bands in coral skeletons. Coral Reefs 19:221-230

Barnes DJ, Taylor RB (2005) On the nature and causes of luminescent lines and bands in coral skeletons: II. Contribution of skeletal crystals. J Exp Mar Biolo Ecol 322:135-142

Barnes DJ, Taylor RB, Lough JM (2003) Measurement of luminescence in coral skeletons. J Exp Mar Biolo Ecol 295:91-106

Barth S (1993) Boron isotope variations in nature: a synthesis. Geologische Rundschau 82:640-651

Barth S (1998) $^{11}B/^{10}B$ variations of dissolved boron in a freshwater-seawater mixing plume (Elbe Esturary, North Sea). Mar Chem 62:1-14

Bates NR, Amat A, Andersson AJ (2010) Feedbacks and responses of coral calcification on the Bermuda reef system to seasonal changes in biological processes and ocean acidification. Biogeosciences 7:2509-2530

Beck JW, Edwards RL, Ito E, Taylor FW, Recy J, Rougerie F, Joannot P, Henin C (1992) Sea-surface temperature from coral skeletal strontium/calcium ratios. Science 257:644-647

Belperio A (1979) The combined use of wash loads and bed material load rating curves for the calculation of total load: an example from the Burdekin River, Australia. Catena 6:317 - 329

Belperio AP (1983) Terrigenous sedimentation in the Central Great Barrier Reef Lagoon: a model from the Burdekin region. BMR Journal of Australian Geology and Geophysics 8:179-190

Belperio AP, Searle DE (1988) Chapter 5 Terrigenous and carbonate sedimentation in the Great Barrier Reef Province. Developments in Sedimentology 42:143-174

Berkelmans R, Oliver JK (1999) Large scale bleaching of corals on the Great Barrier Reef. Coral Reefs 18:55–60

Berkelmans R (2002) Time-integrated thermal bleaching thresholds of reefs and their variation on the Great Barrier Reef. Mar Ecol-Prog Ser 229:73-82

Berkelmans R, Weeks SJ, Steinberg CR (2010) Upwelling linked to warm summers and bleaching on the Great Barrier Reef. Limnol Oceanogr 55:2634-2644

Berkelmans R, De'ath G, Kininmonth S, Skirving WJ (2004) A comparison of the 1998 and 2002 coral bleaching events on the Great Barrier Reef: spatial correlation, patterns, and predictions. Coral Reefs 23:74-83

Bessat F, Buigues D (2001) Two centuries of variation in coral growth in a massive *Porites* colony from Moorea (French Polynesia): a response of ocean-atmosphere variability from south central Pacific. Palaeogeogr Palaeocl 175:381-392

Bosscher H (1993) Computerized-tomography and skeletal density of coral skeletons. Coral Reefs 12:97-103

Bosscher H, Meesters EH (1993) Depth related changes in the growth rate of *Montastrea annularis*. 7th International Coral Reef Symposium 1:507-512

Boto K, Isdale PJ (1985) Fluorescent bands in massive corals result from terrestrial fulvic inputs to nearshore zone. Nature 315:396-397

Brinkman R, Wolanski E, Deleersnijder E, McAllister F, Skirving W (2002) Oceanic inflow from the Coral Sea into the Great Barrier Reef. Est Coast Shelf S 54:655-668

Brodie J, Waterhouse J (2012) A critical review of environmental management of the 'not so Great' Barrier Reef. Est Coast Shelf S 104-105:1-22

Brodie J, Wolanski E, Lewis S, Bainbridge Z (2012a) An assessment of residence times of land-sourced contaminants in the Great Barrier Reef lagoon and the implications for management and reef recovery. Mar Pollut Bull 65:267-279

Brodie J, Schroeder T, Rohde K, Faithful J, Masters B, Dekker A, Brando V, Maughan M (2010a) Dispersal of suspended sediments and nutrients in the Great Barrier Reef lagoon during river-discharge events: conclusions from satellite remote sensing and concurrent flood-plume sampling. Mar Freshwater Res 61:651-664

Brodie JE, Devlin M, Haynes D, Waterhouse J (2010b) Assessment of the eutrophication status of the Great Barrier Reef lagoon (Australia). Biogeochemistry 106:281-302

Brodie JE, De'ath G, Devlin M, Furnas M, Wright M (2007) Spatial and temporal patterns of near-surface chlorophyll a in the Great Barrier Reef lagoon. Mar Freshwater Res 58:342-353

Brodie JE, Kroon FJ, Schaffelke B, Wolanski EC, Lewis SE, Devlin MJ, Bohnet IC, Bainbridge ZT, Waterhouse J, Davis AM (2012b) Terrestrial pollutant runoff to the Great Barrier Reef: An update of issues, priorities and management responses. Mar Pollut Bull 65:81-100

Brown BE, Le Tissier MDA, Scoffin TP, Tudhope AW (1990) Evaluation of the environmental impact of dredging on intertidial coral reefs at Ko Phuket, Thailand, using ecological and physiological parameters. Mar Ecol Prog Ser 65:273-281

Bucher DJ, Harriott VJ, Roberts LG (1998) Skeletal micro-density, porosity and bulk density of acroporid corals. J Exp Mar Biolo Ecol 228:117-136

Buddemeier RW (1974) Environmental controls over annual and lunar monthly cycles in hermatypic coral calcification. Second International Coral Reef Symposium 2:259-268

Buddemeier RW, Maragos JE, Knutson DW (1974) Radiographic studies of reef coral exoskeletons: rates and patterns of coral growth. J Exp Mar Biolo Ecol 14:179-200

Buddemeier RW, Kleypas JA, Aronson RB (2004) Coral reefs and global climate change: potential contributions of climate change to stresses on coral reef ecosystems. Pew Center on Global Climate Change, Arlington, VA 42

Bull GD (1982) Scleractinian coral communities of two inshore high island fringing reefs at Magnetic Island, north Queensland. Mar Ecol Prog Ser 7:267-272

Canadell JG, Le Quere C, Raupach MR, Field CB, Buitenhuis ET, Ciais P, Conway TJ, Gillett NP, Houghton RA, Marland G (2007) Contributions to accelerating atmospheric CO_2 growth from economic activity, carbon intensity, and efficiency of natural sinks. PNAS USA 104:18866-18870

Cantin NE, Cohen AL, Karnauskas KB, Tarrant AM, McCorkle DC (2010) Ocean warming slows coral growth in the central Red Sea. Science 329:322-325

Carilli JE, Prouty NG, Hughen KA, Norris RD (2009a) Century-scale records of land-based activities recorded in Mesoamerican coral cores. Mar Pollut Bull 58:1835-1842

Carilli JE, Norris RD, Black BA, Walsh SM, McField M (2009b) Local stressors reduce coral resilience to bleaching. PLoS ONE 4:e6324

Carricart-Ganivet JP (2004) Sea surface temperature and the growth of the West Atlantic reef-building coral *Montastraea annularis*. J Exp Mar Biolo Ecol 302:249-260

Carricart-Ganivet JP (2011) Coral skeletal extension rate: An environmental signal or a subject to inaccuracies? J Exp Mar Biolo Ecol 405:73-79

Carricart-Ganivet JP, Merino M (2001) Growth responses of the reef-building coral *Montastraea annularis* along a gradient of continental influence in the southern Gulf of Mexico. Bull Mar Sci 68:133-146

Carricart-Ganivet JP, Barnes DJ (2007) Densitometry from digitized images of X-radiographs: Methodology for measurement of coral skeletal density. J Exp Mar Biolo Ecol 344:67-72

Carricart-Ganivet JP, Lough JM, Barnes DJ (2007) Growth and luminescence characteristics in skeletons of massive *Porites* from a depth gradient in the central Great Barrier Reef. J Exp Mar Biolo Ecol 351:27-36

Carricart-Ganivet JP, Beltran-Torres AU, Merino M, Ruiz-Zarate MA (2000) Skeletal extension density calcification rate of the reef building coral *Montastrea annularis* (Ellis and Solander) in the Mexican Caribbean. Bull Mar Sci 66:215-224

Carricart-Ganivet JP, Cabanillas-Teran N, Cruz-Ortega I, Blanchon P (2012) Sensitivity of calcification to thermal stress varies among genera of massive reef-building corals. PLoS ONE 7:e32859

Carriquiry JD, Horta-Puga G (2010) The Ba/Ca record of corals from the Southern Gulf of Mexico: contributions from land-use changes, fluvial discharge and oil-drilling muds. Mar Pollut Bull 60:1625-1630

Castillo KD, Ries JB, Weiss JM (2011) Declining coral skeletal extension for forereef colonies of *Siderastrea siderea* on the Mesoamerican Barrier Reef System, Southern Belize. PLoS ONE 6:e14615

Castillo KD, Ries JB, Weiss JM, Lima FP (2012) Decline of forereef corals in response to recent warming linked to history of thermal exposure. Nature Climate Change 2:756-760

Catanzaro EJ, Champion CE, Garner EL, Marinenko G, Sappenfield KM, Shields WR (1970) Standard reference materials: boric acid; isotopic and assay standard reference materials. In: Commerce USDo (ed). National Bureau of Standards Special, Washington, D.C. 70

Chalker B, Barnes D (1990) Gamma densitometry for the measurements of skeletal density Coral Reefs 9:11-23

Chalker B, Barnes D, Isdale PJ (1985) Calibration of x-ray densitometry for the measurement of coral skeletal density. Coral Reefs 4:95-100

Cohen AL, McConnaughey TA (2003) Geochemical perspective on coral mineralization. In: Dove PM, Weiner S, deYoreo JJ (eds) Rev Mineral Geochem, pp151-187

Cohen AL, Holcomb M (2009) Why corals care about ocean acidification: uncovering the mechanism. Oceanography 22:118-127

Cohen AL, Gaetani GA (2010) Ion partitioning and the geochemistry of coral skeletons: solving the mystery of the vital effect EMU Notes in Mineralogy, pp377-397

Cohen AL, Owens KE, Layne GD, Shimizu N (2002) The effect of algal symbionts on the accuracy of Sr/Ca paleotemperatures from coral. Science 296:331-333

Cohen AL, McCorkle DC, de Putron S, Gaetani GA, Rose KA (2009) Morphological and compositional changes in the skeletons of new coral recruits reared in acidified seawater: Insights into the biomineralization response to ocean acidification. Geochem, Geophys, Geosys 10: doi:10.1029/2009GC002411

Cole JE (2003) Holocene coral records: Windows on tropical climate variability In Global Change in the Holocene. Arnold, London, pp168-184

Collins JD (1978) A study of the interactive biology of corals. James Cook University, p182

Comeau S, Carpenter RC, Edmunds PJ (2013a) Coral reef calcifiers buffer their response to ocean acidification using both bicarbonate and carbonate. Proceedings Biological sciences. The Royal Society 280:20122374

Comeau S, Edmunds PJ, Spindel NB, Carpenter RC (2013b) The responses of eight coral reef calcifiers to increasing partial pressure of CO_2 do not exhibit a tipping point. Limnol Oceanogr 58:388-398

Cooper TF (2008) Coral bioindicators of environmental conditions on coastal coral reefs. James Cook University, p202

Cooper TF, O'Leary RA, Lough JM (2012) Growth of Western Australian corals in the anthropocene. Science 335:593-596

Cooper TF, De'Ath G, Fabricius KE, Lough JM (2008) Declining coral calcification in massive *Porites* in two nearshore regions of the northern Great Barrier Reef. Global Change Biol 14:529-538

Coplen TB, Bohlke JK, De Bievre P, Ding T, Holden NE, Hopple JA, Krouse HR, Lamberty A, Peiser HS, Revesz K, Rieder SE, Rosman KJR, Roth E, Taylor PDP, Vocke Jr. RD, Xiao YK (2002) Isotope-abundance variations of selected elements. Pure App Chem 74:1987-2017

Corrège T (2006a) Sea surface temperature and salinity reconstruction from coral geochemical tracers. Palaeogeogr Palaeocl 232:408-428

Corrège T (2006b) Monitoring of terrestrial input by massive corals. J Geochem Explor 88:380-383

Crook ED, Cohen AL, Rebolledo-Vieyra M, Hernandez L, Paytan A (2013) Reduced calcification and lack of acclimatization by coral colonies growing in areas of persistent natural acidification. PNAS USA

Cuif JP, Dauphin Y, Freiwald A, Gautret P, Zibrowius H (1999) Biochemical markers of zooxanthellae symbiosis in soluble matrices of skeleton of 24 Scleractinia species. Comp Biochem Phsy A 123:269-278

De'ath G, Lough JM, Fabricius KE (2009) Declining coral calcification on the Great Barrier Reef. Science 323:116-119

De'ath G, Fabricius KE, Sweatman H, Puotinen M (2012) The 27-year decline of coral cover on the Great Barrier Reef and its causes. PNAS USA 109:17995-17999

de Villiers S, Nelson BK, Chivas AR (1995) Biological controls on coral Sr/Ca and $\delta^{18}O$ reconstructions of sea surface temperature. Science 269:1247-1249

Devlin M, Waterhouse J, Taylor J, Brodie J (2001) Flood plumes in the Great Barrier Reef: spatial and temporal patterns in composition and distribution Research publications series no 68. Great Barrier Reef Marine Park Authority, Townsville, Australia

Devlin M, Brodie J, Bainbridge ZT, Lewis SE (2008) Flood plumes in the GBR the Burdekin and Fitzroy flood plumes, 2007/08 case studies for Marine Monitoring Program:63 pp

Devlin MJ, Brodie J (2005) Terrestrial discharge into the Great Barrier Reef Lagoon: nutrient behavior in coastal waters. Mar Pollut Bull 51:9-22

Devlin MJ, McKinna LW, Alvarez-Romero JG, Petus C, Abott B, Harkness P, Brodie J (2012) Mapping the pollutants in surface riverine flood plume waters in the Great Barrier Reef, Australia. Mar Pollut Bull 65:224-235

Dickson AG (1990) Thermodynamics of the dissociation of boric acid in synthetic seawater from 273.15 to 318.15 K. Deep-Sea Research 37:755-766

Dickson AG, Millero FJ (1987) A Comparison of the equilibrium-constants for the dissociation of carbonic-acid in seawater Media. Deep-Sea Res 34:1733-1743

Dodge RE, Lang JC (1983) Environmental correlates of hermatypic coral (*Montastrea annularis*) growth on the East Flower Gardens Bank, northwest Gulf of Mexico. Limnol Oceanogr 28:228-240

Dodge RE, Brass GW (1984) Skeletal extension, density and calcification of the reef coral, *Montastrea annularis*: St. Croix, U.S. Virgin Islands. Bull Mar Sci 34:288-307

Dodge RE, Szmant AM, Garcia R, Swart PK, Swart PK, Forester A, Leder JJ (1992) Skeletal structural basis of density banding in the reef coral *Montastrea annularis*. 7th International Coral Reef Symposium 1:186-195

Dollar SJ (1982) Wave stress and coral community structure in Hawaii. Coral Reefs 1:71-81

Done T (1999) Coral community adaptability to environmental change at the scales of regions, reefs and reef zones. Am Zool 39:66-79

Done TJ (1982) Patterns in the distribution of coral communities across the central Great Barrier Reef. Coral Reefs 1:95-107

Done TJ (1983) Coral zonation, its nature and significance. In: Barnes DJ, Clouston B (eds) Perspectives on coral reefs. Australian Institute of Marine Science 107-147

Done TT (2011) Corals: environmental controls on growth. In: Hopley D (ed) Encyclopedia of Modern Coral Reefs, pp281-293

Doney SC, Fabry VJ, Feely RA, Kleypas JA (2009) Ocean acidification: the other CO_2 problem. Ann Rev Mar Sci 1:169-192

Dore JE, Lukas R, Sadler DW, Church MJ, Karl DM (2009) Physical and biogeochemical modulation of ocean acidification in the central North Pacific. PNAS USA 106:12235-12240

Douville E, Paterne M, Cabioch G, Louvat P, Gaillardet J, Juillet-Leclerc A, Ayliffe L (2010) Abrupt sea surface pH change at the end of the Younger Dryas in the central sub-equatorial Pacific inferred from boron isotope abundance in corals (*Porites*). Biogeosciences 7:2445-2459

Draschba S, Pätzold J, Wefer G (2000) North Atlantic climate variability since AD 1350 recorded in $\delta^{18}O$ and skeletal density of Bermuda corals. International Journal Earth Sciences 88:733-741

Druffel ERM (1997) Geochemistry of corals: Proxies of past ocean chemistry, ocean circulation, and climate PNAS USA 8354-8361

Drupp P, De Carlo EH, Mackenzie FT, Bienfang P, Sabine CL (2011) Nutrient inputs, phytoplankton response, and CO_2 variations in a semi-enclosed subtropical embayment, Kaneohe Bay, Hawaii. Aquat Geochem 17:473-498

Duprey N, Boucher H, Jiménez C (2012) Digital correction of computed X-radiographs for coral densitometry. J Exp Mar Biolo Ecol 438:84-92

Dustan P (1975) Growth and form in the reef-building coral *Montastrea annularis*. Mar Biol 33:101-107

Edinger EN, Limmon GV, Jompa J, Widjatmokos W, Heikoop JM, Risk MJ (2000) Normal coral growth rated on dying reefs: are coral growth rates good indicators of reef health? Mar Pollut Bull 40:404-425

Erez J, Reynaud S, Silverman J, Schneider K, Allemand D (2011) Coral calcification under ocean acidification and global change. In: Dubinsky Z, Stambler N (eds) Coral reefs: An ecosystem in transition Springer Netherlands., pp151-176

Esslemont G, Russell RA, Maher WA (2004) Coral record of harbour dredging: Townsville, Australia. J Marine Syst 52:51-64

Fabricius KE (2005) Effects of terrestrial runoff on the ecology of corals and coral reefs: review and synthesis. Mar Pollut Bull 50:125-146

Fabricius KE (2008) Theme section on "Ocean Acidification and Coral Reefs". Coral Reefs 27:455-457

Fabricius KE, De'ath G, Puotinen ML, Done T, Cooper TF, Burges SC (2008) Disturbance gradients on inshore and offshore coral reefs caused by a severe tropical cyclone. Limnol Oceanogr 53:690-704

Fabry VJ, Seibel BA, Feely RA, Orr JC (2008) Impacts of ocean acidification on marine fauna and ecosystem processes. Ices J Mar Sci 65:414-432

Fallon SJ (2000) Environmental records from corals and coralline sponges. The Australian National University,

Fallon SJ, McCulloch MT, Alibert C (2003) Examining water temperature proxies in *Porites* corals from the Great Barrier Reef: a cross-shelf comparison. Coral Reefs 22:389-404

Fallon SJ, McCulloch MT, van Woesik R, Sinclair DJ (1999) Corals at their latitudinal limits: laser ablation trace element systematics in *Porites* from Shirigai Bay, Japan. Earth Planet Sci Lett 172:221-238

Falter JL, Lowe RJ, Atkinson MJ, Cuet P (2012) Seasonal coupling and de-coupling of net calcification rates from coral reef metabolism and carbonate chemistry at Ningaloo Reef, Western Australia. J Geophys Res-Oceans 117

Feely RA, Sabine CL, Lee K, Berelson W, Kleypas J, Fabry VJ, Millero FJ (2004) Impact of anthropogenic CO_2 on the $CaCO_3$ system in the oceans. Science 305:362-366

Felis T, Patzold J (2004) Climate reconstructions from annually banded corals. In: Shiyomi M (ed) Global Environmental Change in the Ocean and on Land. Terrapub, pp205-227

Fleitmann D, Dunbar RB, McCulloch M, Mudelsee M, Vuille M, McClanahan TR, Cole JE, Eggins S (2007) East African soil erosion recorded in a 300 year old coral colony from Kenya. Geophys Res Lett 34

Foster GL (2008) Seawater pH, pCO_2 and $\left[CO_3^{2-}\right]$ variations in the Caribbean Sea over the last 130 kyr: A boron isotope and B/Ca study of planktic foraminifera. Earth Planet Sci Lett 271:254-266

Foster GL, Pogge von Strandmann PAE, Rae JWB (2010) Boron and magnesium isotopic composition of seawater. Geochem Geophys Geosyst 11

Foster GL, Ni YY, Haley B, Elliott T (2006) Accurate and precise isotopic measurement of sub-nanogram sized samples of foraminiferal hosted boron by total evaporation NTIMS. Chem Geol 230:161-174

Frithsen JB, Keller AA, Pilson MEQ (1985) Effects of inorganic nutrient additions in coastal areas: a mesocosm experiment; data report. Marine Ecosystems Research Laboratory, Graduate School of Oceanography, University of Rhode Island

Furnas M (2003) Catchments and corals: terrestrial runoff to the Great Barrier Reef. Australian Institute of Marine Science and Reef CRC, Townsville, Australia

Furnas M, Mitchell AW (1997) Biological oceanography of the Great Barrier Reef. The Great Barrier Reef: Science, Use and Management: A National Conference Proceedings 1:75-87

Furnas M, Mitchell AW (2001) Runoff of terrestrial sediment and nutrients into the Great Barrier Reef World Heritage Area. In: Wolanski E (ed) Oceanographic Processes of Coral Reefs: Physical and Biological Links in the Great Barrier CRC Press, Boca Raton, pp37-52

Furnas MJ, Mitchell AW (1996) Nutrient inputs into the central great barrier reef (Australia) from subsurface intrusions of coral sea waters: A two-dimensional displacement model. Cont Shelf Res 16:1127-1148
Gaetani G, Cohen A (2006) Element partitioning during precipitation of aragonite from seawater: A framework for understanding paleoproxies. Geochim Cosmochim Acta 70:4617-4634
Gagan MK, Ayliffe LK, Beck JW, Cole JE, Druffel ERM, Dunbar RB, Schrag D (2000) New views of tropical paleoclimates from corals. Quaternary Sci Rev 19:45-64
Gagliano M, McCormick MI, Moore JA, Depczynski M (2010) The basics of acidification: baseline variability of pH on Australian coral reefs. Mar Biol 157:1849-1856
Gaillardet J, Allègre CJ (1995) Boron isotopic compositions of corals: Seawater or diagenesis record? Earth Planet Sci Lett 136:665-676
Gardner TA, Cote IM, Gill JA, Grant A, Watkinson AR (2003) Long-term region-wide declines in Caribbean corals. Science 301:958-960
Gattuso J-P, Allemand D, Frankignoulle M (1999a) Photosynthesis and calcification at cellular, organismal and community levels in coral reefs: A review on interactions and control by carbonate chemistry. Am Zool 39:160-183
Gattuso J-P, Frankignoulle M, Smith SV (1999b) Measurement of community metabolism and significance in the coral reef CO_2 source-sink debate. PNAS USA 96:13017-13022
Gattuso J-P, Pichon M, Frankignoulle M (1995) Biological control of air-sea CO_2 fluxes: Effect of photosynthetic and calcifying marine organisms and ecosystems. Mar Ecol-Prog Ser 129:307-312
Gautret P, Cuif JP, Orsay A, Freiwald A (1997) Composition of soluble mineralization matrices in zooxanthellate and non-zooxanthelate scleractinian corals: Biochemical assessment of photosynthetic metabolism through the study of a skeletal feature. Facies 36:189-194
Gilmour JP, Smith LD, Heyward AJ, Baird AH, Pratchett MS (2013) Recovery of an isolated coral reef system following severe disturbance. Science 340:69-71
Goldenheim WM, Edmunds PJ (2011) Effects of flow and temperature on growth and photophysiology of scleractinian corals in Moorea, French Polynesia. Biol Bull 221:270-279
Goreau TF (1959) The physiology of skeleton formation in corals. I. A method for measuring the rate of calcium deposition by corals under different conditions. Biol Bull 116:59-75
Grigg RW (1982) Darwin Point: a threshold for atoll formation. Coral Reefs 1:29-34
Grigg RW (1998) Holocene coral reef accreation in Hawaii: a function of wave exposure and sea level history. Coral Reefs 17:263-272
Grigg RW (2006) Depth limit for reef building corals in the Au'au Channel, S.E. Hawaii. Coral Reefs 25:77-84
Guzman HM, Burns KA, Jackson JBC (1994) Injury, regeneration and growth of Caribbean reef corals after a major oil spill in Panama. Mar Ecol Prog Ser 105:231-241
Guzman HM, Cipriani R, Jackson JB (2008) Historical decline in coral reef growth after the Panama Canal. Ambio 37:342-346
Hamner WM, Hauri IR (1981) Effects of island mass: Water flow and plankton pattern around a reef in the Great Barrier Reef lagoon, Australia. Limnol Oceanogr 26:1084-1102
Hart SR, Cohen AL (1996) An ion probe study of annual cycles of Sr/Ca and other trace elements in corals. Geochim Cosmochim Acta 60:3075-3084
Haugan PM, Drange H (1996) Effects of CO_2 on the ocean environment. Energy Conversion and Managment 37:1019-1022
Helmle KP, Dodge RE, Swart PK, Gledhill DK, Eakin CM (2011) Growth rates of Florida corals from 1937 to 1996 and their response to climate change. Nature Communications 2:215
Hemming NG, Honisch B (2007) Chapter seventeen boron isotopes in marine carbonate sediments and the pH of the ocean 1:717-734
Hemming NG, Hanson GN (1992) Boron isotopic composition and concentration in modern marine carbonates. Geochim Cosmochim Acta 56:537-543

Hemming NG, Reeder RJ, Hanson GN (1995) Mineral-fluid partitioning and isotopic fractionation of boron in synthetic calcium carbonate. Geochim Cosmochim Acta 59:371-379

Hemming NG, Guilderson TP, Fairbanks RG (1998) Seasonal variations in the boron isotopic composition of coral: A productivity signal? Global Biogeochem Cyc 12:581-586

Henderson GM (2002) New oceanic proxies for paleoclimate. Earth Planet Sci Lett 203:1-13

Hendy EJ (2003) Coral reconstructions of decadal-to-centennial climate variability in the great Barrier Reef since 1565 AD. The Australian National University,

Hendy EJ, Gagan MK, Lough JM (2003) Chronological control of coral records using luminescent lines and evidence for non-stationary ENSO teleconnections in northeast Australia. The Holocene 13:187-199

Hendy EJ, Gagan MK, Alibert CA, McCulloch MT, Lough JM, Isdale PJ (2002) Abrupt decrease in tropical Pacific sea surface salinity at the end of Little Ice Age. Science 295:G1511-1514

Henehan MJ, Rae JWB, Foster GL, Erez J, Prentice KC, Kucera M, Bostock HC, Martínez-Botí MA, Milton JA, Wilson PA, Marshall BJ, Elliott T (2013) Calibration of the boron isotope proxy in the planktonic foraminifera *Globigerinoides ruber* for use in palaeo-CO_2 reconstruction. Earth Planet Sci Lett 364:111-122

Hershey JP, Fernandez M, Milne PJ, Millero FJ (1986) The ionization of boric acid in NaCl, Na-Ca-Cl and Na-Mg-Cl solutions at 25°C. Geochim Cosmochim Acta 50:143-148

Highsmith RC (1979) Coral growth-rates and environmental-control of density banding. J Exp Mar Biolo Ecol 37:105-125

Highsmith RC, Riggs AC, D'Antonio CM (1980) Survival of hurricane-generated coral fragments and a disturbance model of reef calcification. Oecologia 46:322-329

Hinga KR (2002) Effects of pH on coastal marine phytoplankton. Mar Ecol-Prog Ser 238:281-300

Hoegh-Guldberg O, Mumby PJ, Hooten AJ, Steneck RS, Greenfield P, Gomez E, Harvell CD, Sale PF, Edwards AJ, Caldeira K, Knowlton N, Eakin CM, Iglesias-Prieto R, Muthiga N, Bradbury RH, Dubi A, Hatziolos ME (2007) Coral reefs under rapid climate change and ocean acidification. Science 318:1737-1742

Holcomb M, McCorkle DC, Cohen AL (2010) Long-term effects of nutrient and CO_2 enrichment on the temperate coral *Astrangia poculata* (Ellis and Solander, 1786). J Exp Mar Biolo Ecol 386:27-33

Hönisch B, Hemming NG, Archer D, Siddall M, McManus JF (2009) Atmospheric carbon dioxide concentration across the mid-Pleistocene transition. Science 324:1551-1554

Hönisch B, Hemming NG, Grottoli AG, Amat A, Hanson GN, Buma J (2004) Assessing scleractinian corals as recorders for paleo-pH: Empirical calibration and vital effects. Geochim Cosmochim Acta 68:3675-3685

Hönisch B, Bijma J, Russell AD, Spero HJ, Palmer MR, Zeebe RE, Eisenhauer A (2003) The influence of symbiont photosynthesis on the boron isotopic composition of foraminifera shells. Marine Micropaleontology 49:87-96

Hönisch B, Ridgwell A, Schmidt DN, Thomas E, Gibbs SJ, Sluijs A, Zeebe R, Kump L, Martindale RC, Greene SE, Kiessling W, Ries J, Zachos JC, Royer DL, Barker S, Marchitto TM, Jr., Moyer R, Pelejero C, Ziveri P, Foster GL, Williams B (2012) The geological record of ocean acidification. Science 335:1058-1063

Hopley D (1982) The Geomorphology of the Great Barrier Reef: quaternary development of coral reefs. Wiley, New York

Hopley D, Parnell KE, Isdale PJ (1989) The Great Barrier Reef Marine Park: dimensions and regional patterns. Australian Geographical Studies 27:47-66

Hopley D, Smithers SG, Parnell KE (2007) The geomorphology of the Great Barrier Reef: development, diversity and change. Cambridge University Press, Cambridge

Hubbard DK, Scaturo D (1985) Growth rates of seven species of scleractinean corals from Cane Bay and Salt River, St. Croix, USVI. Bull Mar Sci 36:325-338

Hughes TP, Baird AH, Bellwood DR, Card M, Connolly SR, Folke C, Grosberg R, Hoegh-Guldberg O, Jackson JBC, Kleypas J, Lough JM, Marshall P, Nyström M, Palumbi SR, Pandolfi JM, Rosen B, Roughgarden J (2003) Climates change, human impacts, and the resilience of coral reefs. Science 301:929-933

Hughes TP, Graham NA, Jackson JB, Mumby PJ, Steneck RS (2010) Rising to the challenge of sustaining coral reef resilience. Trends in ecology & evolution 25:633-642
Hughes TP, Bellwood DR, Baird AH, Brodie J, Bruno JF, Pandolfi JM (2011) Shifting base-lines, declining coral cover, and the erosion of reef resilience: comment on Sweatman et al. (2011). Coral Reefs 30:653-660
IPCC (2007) The physical science basis. Contribution of working group I to the fourth assessment report of the Intergovernmental Panel on Climate Change, NY, USA
Isdale PJ (1981) Geographical variation in the growth rate of the hermatypic coral *Porites* in the Great Barrier Reef Province, Australia. James Cook University, p135
Isdale PJ (1983) Geographical patterns in coral growth rates on the Great Barrier Reef. Great Barrier Reef Conference:327-330
Isdale PJ (1984) Fluorescent bands in massive corals record centuries of coastal rainfall. Nature 310:578-579
Jokiel PL, Coles SL (1977) Effects of temperature on the mortality and growth of Hawaiian reef corals. Mar Biol 43:201-208
Jokiel PL, Maragos JE, Franzisket L (1978) Coral growth: buoyant weight technique. In: Stoddar DR, Johannes RE (eds) Coral Reefs: Research Methods. UNESCO, pp529-541
Jones PD, Briffa KR, Osborn T, Lough J, van Ommen TD, Vinther BM, Luterbacher J, Wahl ER, Zwiers FW, Mann ME, Schmidt GA, Ammnn CM, Buckley BM, Cobb KM, Esper J, Goosse H, Graham N, Jansen E, Kiefer T, Kull C, Küttel E, Mosley-Thompson E, Overpeck JT, Riedwyl N, Schultz M, Tudhope AW, Villalba R, Wanner H, Wolff E, Xoplaki E (2009) High-resolution palaeoclimatology of the last millennium: a review of current status and future prospects. The Holocene 19:3-49
Jupiter S, Roff G, Marion G, Henderson M, Schrameyer V, McCulloch M, Hoegh-Guldberg O (2008) Linkages between coral assemblages and coral proxies of terrestrial exposure along a cross-shelf gradient on the southern Great Barrier Reef. Coral Reefs 27:887-903
Jury CP, Whitehead RF, Szmant AM (2010) Effects of variations in carbonate chemistry on the calcification rates of *Madracis auretenra* (= *Madracis mirabilis sensu* Wells, 1973): bicarbonate concentrations best predict calcification rates. Global Change Biol 16:1632-1644
Kakihana H, Kotaka M, Satoh S, Nomura M, Okamoto M (1977) Fundamental studies on the ion-exchange separation of boron isotopes. B Chem Soc Jpn 50:158-163
Kayanne H (2005) Seasonal and bleaching-induced changes in coral reef metabolism and CO_2 flux. Global Biogeochem Cyc 19
Kayanne H, Suzuki A, Saito H (1995) Diurnal changes in the partial pressure of carbon dioxide in coral reef water. Science 269:214-216
King B, McAllister F, Done T (2002) Modelling the impact of the Burdekin, Herbert, Tully and Johnstone River plumes on the Central Great Barrier Reef CRC Reef Research Centre Technical Report No 44. CRC Reef Research Centre, Townsville
King B, McAllister F, Wolanski E, Done T, Spagnol S (2001) River plume dynamics in the central Great Barrier Reef. In: Wolanski E (ed) Oceanographic Processes of Coral reefs: Physical and Biological Links in the Great Barrier Reef. CRC Press, Boca Raton, pp145–160
Kitano Y, Okumura M, Idogaki M (1978) Coprecipitation of borate-boron with calcium carbonate. Geochem J 12:183-189
Kleypas JA (1999) Geochemical consequences of increased atmospheric carbon dioxide on coral reefs. Science 284:118-120
Kleypas JA, Langdon C (2000) Overview of CO_2-induced changes in seawater chemistry. 9th Internation Coral Reef Symposium 2:1085-1090
Kleypas JA, Hoegh-Guldberg O (2008) Coral reefs and climate change: Susceptibility and consequences In: Wilkinson C, Souter D (eds) Status of Caribbean coral reefs after bleaching and hurricanes in 2005 Global Coral Reef Monitoring Network and Reef and Rainforest Research Centre Townsville, Qld, Australia pp10
Kleypas JA, Yates KK (2009) Coral reefs and ocean acidification. oceanography 22:108-117
Kleypas JA, McManus JF, Meñez LAB (1999) Environmental limits to coral reef development: where do we draw the line? Am Zool 39:146-159

Kleypas JA, Buddemeier RW, Gattuso JP (2001) The future of coral reefs in an age of global change. Int J Earth Sci 90:426-437

Kleypas JA, Feely RA, Fabry VJ, Langdon C, Sabine CL, Robbins LL (2006) Impacts of ocean acidification on coral reefs and other marine calcifiers: A guide for future research, report of a workshop held 18–20 April 2005. sponsored by NSF, NOAA, and the U.S. Geological Survey, St. Petersburg, FL 88

Klochko K, Kaufman AJ, Yao W, Byrne RH, Tossell JA (2006) Experimental measurement of boron isotope fractionation in seawater. Earth Planet Sci Lett 248:276-285

Klochko K, Cody GD, Tossell JA, Dera P, Kaufman AJ (2009) Re-evaluating boron speciation in biogenic calcite and aragonite using 11B MAS NMR. Geochim Cosmochim Acta 73:1890-1900

Knowlton N (2001) The future of coral reefs. PNAS USA 98:5419-5425

Knutson DW, Buddemeier RW, Smith SV (1972) Coral chronometers: seasonal growth bands in reef corals. Science 177:270-272

Koop K, Booth D, Broadbent A, Brodie J, Bucher D, Capone D, Coll J, Dennison W, Erdmann M, Harrison P, Hoegh-Guldberg O, Hutchings P, Jones GB, Larkum AW, O'Neil J, Steven A, Tentori E, Ward S, Williamson J, Yellowlees D (2001) ENCORE: the effect of nutrient enrichment on coral reefs. Synthesis of results and conclusions. Mar Pollut Bull 42:91-120

Krief S, Hendy EJ, Fine M, Yam R, Meibom A, Foster GL, Shemesh A (2010) Physiological and isotopic responses of scleractinian corals to ocean acidification. Geochim Cosmochim Acta 74:4988-5001

Langdon C, Atkinson MJ (2005) Effect of elevated pCO_2 on photosynthesis and calcification of corals and interactions with seasonal change in temperature/irradiance and nutrient enrichment. J Geophys Res 110:C09S07

Langdon C, Takahashi T, Sweeney C, Chipman D, Goddard J (2000) Effect of calcium carbonate saturation state on the calcification rate of an experimental coral reef. Global Biogeochem Cyc 14:639-654

Le Quéré C, Raupach MR, Canadell JG, Marland G, Raupach MR, Canadell JG, Marland G, Bopp L, Ciais P, Conway TJ, Doney SC, Feely RA, Foster P, Friedlingstein P, Gurney K, Houghton RA, House JI, Huntingford C, Levy PE, Lomas MR, Majkut J, Metzl N, Ometto JP, Peters GP, Prentice IC, Randerson JT, Running SW, Sarmiento JL, Schuster U, Sitch S, Takahashi T, Viovy N, van der Werf GR, Woodward FI (2009) Trends in the sources and sinks of carbon dioxide. Nature Geoscience 2:831-836

Le Tissier MDA, Clayton B, Brown BE, Davis PS (1994) Skeletal correlates of coral density banding and evaluation of radiography as used in sclerochronology. Mar Ecol Prog Ser 119:29-44

Lemarchand D, Gaillardet J, Lewin E, Allègre CJ (2000) The influence of rivers on marne boron isotopes and implications for reconstructing past ocean pH. Nature 408:951-954

Lemarchand D, Gaillardet J, Göpel C, Manhes G (2002) An optimized procedure for boron separation and mass spectrometry analysis for river samples. Chem Geol 182:323-334

Lewis SE, Shields GA, Kamber BS, Lough JM (2007) A multi-trace element coral record of land-use changes in the Burdekin River catchment, NE Australia. Palaeogeogr Palaeocl 246:471-487

Lewis SE, Brodie JE, McCulloch MT, Mallela J, Jupiter SD, Williams HS, Lough JM, Matson EG (2012) An assessment of an environmental gradient using coral geochemical records, Whitsunday Islands, Great Barrier Reef, Australia. Mar Pollut Bull 65:306-319

Liu Y, Liu W, Peng Z, Xiao Y, Wei G, Sun W, He J, Liu G, Chou C-L (2009) Instability of seawater pH in the South China Sea during the mid-late Holocene: Evidence from boron isotopic composition of corals. Geochim Cosmochim Acta 73:1264-1272

Logan A, Anderson IH (1991) Skeletal extension growth-rate assessment in corals, using ct scan imagery. Bull Mar Sci 49:847-850

Lough J (1994) Climate variation and El Nifio-Southern Oscillation events on the Great Barrier Reef: 1958 to 1987. Coral Reefs 13:181-195

Lough J (1999) Sea surface temperatures on the Great Barrier Reef: a contribution to the study of coral bleaching Research Publication no 57 Technical Report. Great Barrier Reef Marine Park Authority, Townsville, Australia

Lough J (2001) Climate variability and change on the Great Barrier Reef. In: Wolanski E (ed) Oceanographic Processes of Coral Reefs: Physical and Biological Links in the Great Barrier Reef. CRC Press, Boca Raton, Florida, pp269-300
Lough JM (2004) A strategy to improve the contribution of coral data to high-resolution paleoclimatology. Palaeogeogr Palaeocl 204:115-143
Lough JM (2007) Tropical river flow and rainfall reconstructions from coral luminescence: Great Barrier Reef, Australia. Paleoceanography 22
Lough JM (2008a) Coral calcification from skeletal records revisited. Mar Ecol Prog Ser 373:257-264
Lough JM (2008b) 10th Anniversary Review: a changing climate for coral reefs. Journal of environmental monitoring : JEM 10:21-29
Lough JM (2011a) Measured coral luminescence as a freshwater proxy: comparison with visual indices and a potential age artefact. Coral Reefs 30:169-182
Lough JM (2011b) Great Barrier Reef coral luminescence reveals rainfall variability over northeastern Australia since the 17th century. Paleoceanography 26:PA2201, doi:10.1029/2010PA002050
Lough JM, Barnes DJ (1990a) Intra-annual timing of density band formation of *Porites* coral from the central Great Barrier Reef. J Exp Mar Biolo Ecol 135:35-57
Lough JM, Barnes DJ (1990b) Possible relationships between environmental variables and skeletal density in a coral colony from the central Great Barrier Reef. J Exp Mar Biolo Ecol 134:221-241
Lough JM, Barnes DJ (1992) Comparisons of skeletal density variations in Porites from the central Great Barrier Reef. J Exp Mar Biolo Ecol 155:1-25
Lough JM, Barnes DJ (1997) Several centuries of variation in skeletal extension, density and calcification in massive Porites colonies from the Great Barrier Reef: A proxy for seawater temperature and a background of variability against which to identify unnatural change. J Exp Mar Biolo Ecol 211:29-67
Lough JM, Barnes DJ (2000) Environmental controls on growth of the massive coral *Porites*. J Exp Mar Bio Ecol 245:225-243
Lough JM, Cooper TF (2011) New insights from coral growth band studies in an era of rapid environmental change. Earth-Sci Rev 108:170-184
Lough JM, Barnes DJ, McAllister FA (2002) Luminescent lines in corals from the Great Barrier Reef provide spatial and temporal records of reefs affected by land runoff. Coral Reefs 21:333-343
Lough JM, Devereux MJ, Barnes DJ (2003) Porites coral growth records from the Arabian Gulf. Australian Institute of Marine Science, Townsville, Australia 55
Lough JM, Barnes DJ, Devereux MJ, Tobin BJ, Tobin S (1999) Variability in growth characteristics of massive *Porites* on the Great Barrier reef. Technical Report No 28. CRC Reef Research Center, Townsville
Loya Y, Rinkevich B (1980) Effects of oil pollution on coral reef communities. Mar Ecol Prog Ser 3:167-180
Lüthi D, Le Floch M, Bereiter B, Blunier T, Barnola JM, Siegenthaler U, Raynaud D, Jouzel J, Fischer H, Kawamura K, Stocker TF (2008) High-resolution carbon dioxide concentration record 650,000-800,000 years before present. Nature 453:379-382
Manzello DP (2010) Coral growth with thermal stress and ocean acidification: lessons from the eastern tropical Pacific. Coral Reefs 29:749-758
Manzello DP, Kleypas JA, Budd DA, Eakin CM, Glynn PW, Langdon C (2008) Poorly cemented coral reefs of the eastern tropical Pacific: possible insights into reef development in a high-CO_2 world. PNAS USA 105:10450-10455
Marshall JF, McCulloch MT (2002) An assessment of the Sr/Ca ratio in shallow water hermatypic corals as a proxy for sea surface temperature. Geochim Cosmochim Acta 66:3263-3280
Marubini F, Davies PS (1996) Nitrate increases zooxanthellae population density and reduces skeletogenesis in corals. Mar Biol 127:319-328
Marubini F, Atkinson MJ (1999) Effects of lowered pH and elevated nitrate on coral calcification. Mar Ecol-Prog Ser 188:117-121

Marubini F, Barnett H, Langdon C, Atkinson MJ (2001) Dependence of calcification on light and carbonate ion concentration for the hermatypic coral *Porites compressa*. Mar Ecol-Prog Ser 220:153-162

Marubini F, Ferrier-Pagès C, Furla P, Allemand D (2008) Coral calcification responds to seawater acidification: a working hypothesis towards a physiological mechanism. Coral Reefs 27:491-499

Mathews E, Heap A, Woods M (2007) Inter-reefal seabed sediments and geomorphology of the Great Barrier Reef, a spatial analysis. Geoscience Australia 140pp

Maynard JA, Anthony KRN, Marshall PA, Masiri I (2008) Major bleaching events can lead to increased thermal tolerance in corals. Mar Biol 155:173-182

McConnaughey TA, Whelan JF (1997) Calcification generates protons for nutrient and bicarbonae uptake. Earth-Sci Rev 42:95-117

McCulloch M, Falter J, Trotter J, Montagna P (2012a) Coral resilience to ocean acidification and global warming through pH up-regulation. Nature Climate Change 2:623-627

McCulloch M, Trotter J, Montagna P, Falter J, Dunbar R, Freiwald A, Försterra G, López Correa M, Maier C, Rüggeberg A, Taviani M (2012b) Resilience of cold-water scleractinian corals to ocean acidification: Boron isotopic systematics of pH and saturation state up-regulation. Geochim Cosmochim Acta 87:21-34

McCulloch MT, Fallon S, Wyndham T, Hendy E, Lough JM, Barnes DJ (2003) Coral record of increased sediment flux to the inner Great Barrier Reef since European settlement. Nature 421:727-730

Meibom A (2003) Monthly Strontium/Calcium oscillations in symbiotic coral aragonite: Biological effects limiting the precision of the paleotemperature proxy. Geophys Res Lett 30

Merhbach C, Culberson CH, Hawley JE, Pytkowicz RM (1973) Measurement of the apparent dissociation constants of carbonic acid in seawater at atmospheric pressure. Limnol Oceanogr 18:897–907

Min GR, Edwards RL, Taylor FW, Recy J, Gallup CD, Beck JW (1995) Annual cycles of U/Ca in coral skeletons and U/Ca thermometry. Geochim Cosmochim Acta 59:2025-2042

Mitchell AW, Bramley RGV (1997) Export of nutrients and suspended sediment from the Herbert river catchment during a flood event associated with cyclone Sadie. Cyclone Sadie Flood Plumes in the GBR lagoon: Composition and Consequences Workshop series. Great Barrier Reef Marine Park Authority. No. 22

Mitsuguchi T, Matsumoto E, Abe O, Uchida T, Isdale PJ (1996) Mg/Ca thermometry in coral skeletons. Science 274:961-963

Morrisey J (1980) Community structure and zonation of macroalgae and hermatypic corals on a fringing reef flat of Magnetic Island (Queensland, Australia). Aquat Bot 8:91-139

Müller A, Gagan MK, McCulloch MT (2001) Early marine diagenesis in corals and geochemical consequences for paleoceanographic reconstructions. Geophys Res Lett 28:4471-4474

Muscatine L (1990) The role of symbiotic algae in carbon and energy flux in coral reefs. In: Dubinsky Z (ed) Ecosystems of the World, 25 Coral Reefs. Elsevier Science Publishing Company, Inc., Amsterdam, The Netherlands, ppp.75-87

Nagtegaal R, Grove CA, Kasper S, Zinke J, Boer W, Brummer G-JA (2012) Spectral luminescence and geochemistry of coral aragonite: Effects of whole-core treatment. Chem Geol 318-319:6-15

Orpin AR, Ridd PV (2012) Exposure of inshore corals to suspended sediments due to wave-resuspension and river plumes in the central Great Barrier Reef: A reappraisal. Cont Shelf Res 47:55-67

Orr JC, Fabry VJ, Aumont O, Bopp L, Doney SC, Feely RA, Gnanadesikan A, Gruber N, Ishida A, Joos F, Key RM, Lindsay K, Maier-Reimer E, Matear R, Monfray P, Mouchet A, Najjar RG, Plattner GK, Rodgers KB, Sabine CL, Sarmiento JL, Schlitzer R, Slater RD, Totterdell IJ, Weirig MF, Yamanaka Y, Yool A (2005) Anthropogenic ocean acidification over the twenty-first century and its impact on calcifying organisms. Nature 437:681-686

Paillard D, Labeyrie L, Yiou P (1996) Macintosh program performs time-series analysis. Eos Trans Amer Geophys Union 77:379-379

Palmer MR, Spivack AJ, Edmond JM (1987) Temperature and pH controls over isotopic fractionation during adsorption of boron on marine clay. Geochim Cosmochim Acta 51:2139-2323

Pastorok RA, Bildyard GR (1985) Effects of sewage pollution on coral-reef communities. Mar Ecol Prog Ser 21:175-189

Pelejero C, Calvo E, Hoegh-Guldberg O (2010) Paleo-perspectives on ocean acidification. Trends in ecology & evolution 25:332-344

Pelejero C, Calvo E, McCulloch MT, Marshall JF, Gagan MK, Lough JM, Opdyke BN (2005) Preindustrial to modern interdecadal variability in coral reef pH. Science 309:2204-2207

Peters GP, Marland G, Le Quéré C, Boden T, Canadell JG, Raupach MR (2011) Rapid growth in CO_2 emissions after the 2008–2009 global financial crisis. Nature Climate Change 2:2-4

Philipp E, Fabricius K (2003) Photophysiological stress in scleractinian corals in response to short-term sedimentation. J Exp Mar Biolo Ecol 287:57-78

Priess K, Thomassin BA, Heiss GA, Dullo WC, Camoin G (1995) Variability in growth-rate of massive *Porites* in the coral reefs of Mayotte island. Comptes Rendus de l'Academie des Sciences-Serie III-Sciences de la Vie 318:1147-1154

Pulsford JS (1996) Historical nutrient usage in coastal Queensland river catchments adjacent to the Great Barrier Reef Marine Park. Research Publication No 40. Great Barrier Reef Marine Park Authority, Townsville 63

Quinn TM, Sampson DE (2002) A multiproxy approach to reconstructing sea surface conditions using coral skeleton geochemistry. Paleoceanography 17:14-11-14-11

Rae JWB, Foster GL, Schmidt DN, Elliott T (2011) Boron isotopes and B/Ca in benthic foraminifera: Proxies for the deep ocean carbonate system. Earth Planet Sci Lett 302:403-413

Redondo-Rodriguez A, Weeks SJ, Berkelmans R, Hoegh-Guldberg O, Lough JM (2012) Climate variability of the Great Barrier Reef in relation to the tropical Pacific and El Niño-Southern Oscillation. Mar Freshwater Res 63:34

Reynaud S, Hemming NG, Juillet-Leclerc A, Gattuso JP (2004) Effect of ρCO_2 and temperature on the boron isotopic composition of the zooxanthellate coral *Acropora sp*. Coral Reefs 23:539-546

Riegl B, Branch GM (1995) Effects of sediment on the energy budgets of four scleractinian (Bourne 1900) and five alcyonacean (Lamouroux 1816) corals. J Exp Mar Biolo Ecol 186:259-275

Ries JB (2011) A physicochemical framework for interpreting the biological calcification response to CO_2-induced ocean acidification. Geochim Cosmochim Acta 75:4053-4064

Ries JB, Cohen AL, McCorkle DC (2009) Marine calcifiers exhibit mixed responses to CO_2-induced ocean acidification. Geology 37:1131-1134

Ries JB, Cohen AL, McCorkle DC (2010) A nonlinear calcification response to CO_2-induced ocean acidification by the coral *Oculina arbuscula*. Coral Reefs 29:661-674

Rinkevich B, Loya Y (1984) Does light enhance calcification in heramtypic corals? Mar Biol 80:1-6

Risk MJ, Sammarco PW (1991) Cross-shelf trends in skeletal density of the massive coral *Porites lobata* from the Great Barrier Reef. Mar Ecol Prog Ser 69:195-200

Rosenfeld M, Yam R, Shemesh A, Loya Y (2003) Implication of water depth on stable isotope composition and skeletal density banding patterns in a *Porites lutea* colony: results from a long-term translocation experiment. Coral Reefs 22:337-345

Runnalls LA, Coleman ML (2003) Record of natural and anthropogenic changes in reef environments (Barbados West Indies) using laser ablation ICP-MS and sclerochronology on coral cores. Coral Reefs 22:416-426

Rustad JR, Bylaska EJ, Jackson VE, Dixon DA (2010) Calculation of boron-isotope fractionation between $B(OH)_3$(aq) and $B(OH)_4^-$(aq). Geochim Cosmochim Acta 74:2843-2850

Sabine CL, Feely RA, Gruber N, Key RM, Lee K, Bullister JL, Wanninkhof R, Wong CS, Wallace DW, Tilbrook B, Millero FJ, Peng TH, Kozyr A, Ono T, Rios AF (2004) The oceanic sink for anthropogenic CO_2. Science 305:367-371

Salisbury J, Green M, Hunt C, Campbell J (2008) Coastal acidification by rivers: a threat to shellfish? EOS 89:513-528
Sanyal A, Hemming NG, Broecker WS, Hanson GN (1997) Changes in pH in the eastern equatorial Pacific across 5-6 boundary based on boron isotopes in foraminifera. Global Biogeochem Cyc 11:125-133
Sayani HR, Cobb KM, Cohen AL, Elliott WC, Nurhati IS, Dunbar RB, Rose KA, Zaunbrecher LK (2011) Effects of diagenesis on paleoclimate reconstructions from modern and young fossil corals. Geochim Cosmochim Acta 75:6361-6373
Schneider K, Erez J (2006) The effect of carbonate chemistry on calcification and photosyntheis in the hermatypic coral *Acropora eurystoma*. Limnol Oceanogr 51:1284-1293
Scoffin TP, Tudhope AW, Brown BE, Chansang H, Cheeney RF (1992) Patterns and possible environmental controls of skeletogenesis of *Porites-lutea*, south Thailand. Coral Reefs 11:1-11
Scott PJB (1990) Chronic pollution recorded in coral skeletons in Hong-Kong. J Exp Mar Biolo Ecol 139:51-64
Sen S, Stebbins JF, Hemming NG, Ghosh B (1994) Coordination enyironments of B impurities in calcite and aragonite polymorphs: A ^{11}B MAS NMR study. Aquat Bot 79:819-825
Shaw EC (2012) Carbonate chemistry variability in the southern Great Barrier Reef: implications for future ocean acidification. The University of New South Wales, p165
Shen GT, Dunbar RB (1995) Environmental controls on uranium in reef corals. Geochim Cosmochim Acta 59:2009-2024
Shen GT, Boyle EA, Lea DW (1987) Cadmium in corals as a tracer of historical upwelling and industrial fallout. Nature 328:794-796
Shen GT, Campbell TM, Dunbar RB, Wellington GM, Colgan MW, Glynn PW (1991) Paleochemistry of manganese in corals from the Galapagos Islands. Coral Reefs 10:91-100
Shi Q, Yu K, Chen T, Zhang H, Zhao M, Yan H (2012) Two centuries-long records of skeletal calcification in massive Porites colonies from Meiji Reef in the southern South China Sea and its responses to atmospheric CO_2 and seawater temperature. Science China Earth Sciences 55:1-12
Shinjo R, Asami R, Huang K-F, You C-F, Iryu Y (2013) Ocean acidification trend in the tropical North Pacific since the mid-20th century reconstructed from a coral archive. Mar Geol
Silverman J, Lazar B, Erez J (2007) Community metabolism of a coral reef exposed to naturally varying dissolved inorganic nutrient loads. Biogeochemistry 84:67-82
Silverman J, Lazar B, Cao L, Caldeira K, Erez J (2009) Coral reefs may start dissolving when atmospheric CO_2doubles. Geophys Res Lett 36
Simpson JJ, Zirino A (1980) Biological-control of pH in the Peruvian coastal upwelling area. Deep-Sea Res 27:733-744
Sinclair DJ (1999) High spatial-resolution analysis of trace elements in corals using laser ablation ICP-MS. The Australian National University,
Sinclair DJ (2005) Non-river flood barium signals in the skeletons of corals from coastal Queensland, Australia. Earth Planet Sci Lett 237:354-369
Sinclair DJ, McCulloch MT (2004) Corals record low mobile barium concentrations in the Burdekin River during the 1974 flood: evidence for limited Ba supply to rivers? Palaeogeogr Palaeocl 214:155-174
Sinclair DJ, Kinsley L, McCulloch M (1998) High resolution analysis of trace elements in corals by laser ablation ICP-MS. Geochim Cosmochim Acta 62:1889-1901
Smith LW, Barshis D, Birkeland C (2007) Phenotypic plasticity for skeletal growth, density and calcification of *Porites lobata* in response to habitat type. Coral Reefs 26:559-567
Smith SV, Buddemeier RW, Redalje RC, Houck JE (1979) Strontium-calcium thermometry in coral skeletons. Science 204:404-407
Royal Society (2005) Ocean acidification due to increasing atmospheric carbon dioxide. The Royal Society, London 57 pp
Spivack AJ, Edmond JM (1986) Determination of boron isotope ratios by thermal ionization mass-spectrometry of the dicesium metaborate cation. Anal Chem 58:31-35

Spivack AJ, Edmond JM (1987) Boron isotope exchange between seawater and the oceanic-crust. Geochim Cosmochim Acta 51:1033-1043
Spivack AJ, You CF, Smith HJ (1993) Foraminiferal boron isotope ratios as a proxy for surface ocean pH over the past 21-Myr. Nature 363:149-151
Steinberg C (2007) Impacts of climate change on the physical oceanography of the Great Barrier Reef. In: Johnson JE, Marshall PA (eds) Climate change and the Great Barrier Reef, Great Barrier Reef Marine Park Authority and Australian Greenhouse Office, Townsville, pp51–74
Sturman A, Tapper N (1996) The weather and climate of Australia and New Zealand. Oxford Univ. Press, New York
Suzuki A, Kawahata H, Ayukai T, Goto K (2001) The oceanic CO_2 system and carbon budget in the Great Barrier Reef, Australia. Geophys Res Lett 28:1243-1246
Suzuki A, Gagan MK, Fabricius K, Isdale PJ, Yukino I, Kawahata H (2003) Skeletal isotope microprofiles of growth perturbations in *Porites* corals during the 1997?1998 mass bleaching event. Coral Reefs 22:357-369
Sweatman H, Syms C (2011) Assessing loss of coral cover on the Great Barrier Reef: A response to Hughes et al. (2011). Coral Reefs 30:661-664
Sweatman H, Delean S, Syms C (2011) Assessing loss of coral cover on Australia's Great Barrier Reef over two decades, with implications for longer-term trends. Coral Reefs 30:521-531
Tambutte E, Allemand D, Mueller E, Jaubert J (1996) A compartmental appproach to the mechanism of calcification in hermatypic corals. J Exp Biol 199:1029-1041
Tanzil JTI, Brown BE, Tudhope AW, Dunne RP (2009) Decline in skeletal growth of the coral *Porites lutea* from the Andaman Sea, South Thailand between 1984 and 2005. Coral Reefs 28:519-528
Telesnicki GJ, Goldberg WM (1995) Effects of turbidity on the photosynthesis and respiration of two south Florida Reef coral species. Bull Mar Sci 57:527-539
Tomascik T, Sander F (1985) Effects of eutrophication on reef-building corals 1. Growth-rate of the reef-building coral *Montastrea-annularis*. Mar Biol 87:143-155
Tossell J (2006) Boric acid adsorption on humic acids: Ab initio calculation of structures, stabilities, ^{11}B NMR and ^{11}B,^{10}B isotopic fractionations of surface complexes. Geochim Cosmochim Acta 70:5089-5103
Trotter J, Montagna P, McCulloch M, Silenzi S, Reynaud S, Mortimer G, Martin S, Ferrier-Pagès C, Gattuso J-P, Rodolfo-Metalpa R (2011) Quantifying the pH 'vital effect' in the temperate zooxanthellate coral *Cladocora caespitosa*: Validation of the boron seawater pH proxy. Earth Planet Sci Lett 303:163-173
Tudhope AW, Lea DW, Shimmield GB, Chilcott CP, Head S (1996) Monsoon climate and Arabian Sea coastal upwelling recorded in massive corlas from southern Oman. PALAIOS 11:347-361
Tyrrell T (2008) Calcium carbonate cycling in future oceans and its influence on future climates. J Plankton Res 30:141-156
Vengosh A, Kolodny Y, Starinsky A, Chivas AR, McCulloch MT (1991) Coprecipitation and isotopic fractionation of boron in modern biogenic carbonates. Geochim Cosmochim Acta 55:2901-2910
Venn A, Tambutte E, Holcomb M, Allemand D, Tambutte S (2011) Live tissue imaging shows reef corals elevate pH under their calcifying tissue relative to seawater. PLoS ONE 6:e20013
Venn AA, Tambutte E, Holcomb M, Laurent J, Allemand D, Tambutte S (2013) Impact of seawater acidification on pH at the tissue-skeleton interface and calcification in reef corals. PNAS USA 110:1634-1639
Veron JEN (2000) Corals of the World. Australian Institute of Marine Science, Townsville, Australia
Veron JEN (2011) Corals and coral reefs. In: Hopley D (ed) Encyclopedia of modern coral reefs: structure, form and process, pp198-206
Vézina AF, Hoegh-Guldberg O (2008) Effects of ocean acidification on marine ecosystems. Mar Ecol Prog Ser 373:199-201

Walker T (1981) Seasonal salinity variations in Cleveland Bay, northern Queensland. Aust J Mar Fresh Res 32:143-149
Weber JN, White EW (1974) Activation energy fo skeletal aragonite deposited by the hermatypic coral Platgyra spp. Mar Biol 26:353-359
Weber JN, Deines P, White EW, Weber PH (1975) Seasonal high and low-density bands in reef coral skeletons. Nature 255:697-698
Weber JN, White EW (1977) Caribbean reef corals *Montastrea annularis* and *Montastrea cavernosa*— long-term growth data as determined by skeletal X-radiography. Am. Assoc Pet Geol 4:171–179.
Wei G, Sun M, Li X, Nie B (2000) Mg/Ca, Sr/Ca and U/Ca ratios of a porites coral from Sanya Bay, Hainan Island, South China Sea and their relationships to sea surface temperature. Palaeogeogr Palaeocl 162:59-74
Wei G, McCulloch MT, Mortimer G, Deng W, Xie L (2009) Evidence for ocean acidification in the Great Barrier Reef of Australia. Geochim Cosmochim Acta 73:2332-2346
Weiner S, Dove PM (2003) An overview of biomineralization processes and the problem of the vital effect. Rev Mineral Geochem 54:1-29
Wolanski E (1994) Physical oceanographic processes of the Great Barrier Reef. CRC Press, Boca Raton, Fl
Wolanski E (2001) Physics-biology links in the Great Barrier Reef. In: Wolanski E (ed) Oceanographic processes of coral reefs: Physical and biological links in the Great Barrier Reef. CRC Press, Boca Raton, Florida, pp7-18
Wolanski E, Jones M (1981) Physical properties of the Great Barrier Reef lagoon waters near Townsville. I effects of Burdekin River floods. Aust J Mar Fresh Res 32:305-319
Wolanski E, Pickard GL (1983) Upweilling by internal tides and kelvin waves at the continental shelf break on the Great Barrier Reef. Aust J Mar Fresh Res 34:65-80
Wolanski E, Hamner WM (1988) Topographically controlled fronts in the ocean and their biological influence. Science 241:177-181
Wolanski EC, Pickard GL (1985) Long-term observations of currents on the central Great Barrier Reef continental shelf. Coral Reefs 4:47-57
Wooldridge S, Brodie J, Furnas M (2006) Exposure of inner-shelf reefs to nutrient enriched runoff entering the Great Barrier Reef Lagoon: post-European changes and the design of water quality targets. Mar Pollut Bull 52:1467-1479
Wooldridge SA (2009) Water quality and coral bleaching thresholds: formalising the linkage for the inshore reefs of the Great Barrier Reef, Australia. Mar Pollut Bull 58:745-751
Xiao Y, Liao B, Wang Z, Wei H, Zhao Z (2007) Isotopic composition of dissolved boron and its geochemical behavior in a freshwater-seawater mixture at the estuary of the Changjiang (Yangtze) River. Chinese Journal of Geochemistry 26:105-113
Zeebe R (2005) Stable boron isotope fractionation between dissolved B(OH) and B(OH). Geochim Cosmochim Acta 69:2753-2766
Zeebe RE, Wolf-Gladrow DA (2001) CO_2 in seawater: equilibrium, kinetics, isotopes. Elsevier, Amsterdam
Zeebe RE, Sanyal A, Ortiz JD, Wolf-Gladrow DA (2001) A theoretical study of the kinetics of the boric acid–borate equilibrium in seawater. Mar Chem 73:113-124

8. Appendix

The contents of chapter 4 have been published as:

D'Olivo JP, McCulloch MT, Judd K (2013) Long-term records of coral calcification across the central Great Barrier Reef: assessing the impacts of river runoff and climate change. Coral Reefs 32: 999-1012.

A copy of the publication is included at the end of this thesis.

The CD attached to the back cover contains all seawater and coral geochemical data, and raw coral growth parameters.